

Magnetic Assistance in Laser Powder Directed Energy Deposition

Peter Harry Smith, MEng

Submitted October 2021

To fulfil the degree of Doctor of Philosophy.

Department of Mechanical, Materials and Manufacturing Engineering.

University of Nottingham

Abstract

Directed energy deposition is an additive manufacturing process characterised by the concurrent delivery of material and energy in order to consolidate material into a desirable component geometry. The process is useful as a coating technique to improve wear and chemical resistance in the nuclear industry; it is used to repair worn dies in the automotive industry, and is also used for the near-net shape manufacturing of large components in the aerospace industry. The material deposition efficiency, and particularly the powder catchment efficiency (the ratio of consolidated powder to total powder input) is critical to both the cost-effectiveness of the process, and its overall accuracy. Loss of this powder into the surrounding environment can also be hazardous. To tackle these issues, this work uses magnetic fields to improve the level of control over powder flow and improve catchment efficiency in laser powder directed energy deposition.

Magnetic control of powder flow has potential to be a practically implementable technique to precisely change the quantity and direction of powder entering the melt pool in laser directed energy deposition (LDED). This work demonstrates the use of magnetic assistance, and examines how different directed energy deposition parameters, such as the powder feed rate, laser power and scanning speed affect the efficacy of magnetic assistance. In addition, the dependence of process performance on magnetic parameters including the size, strength and placement of magnetic fields, is also determined and discussed. Hardness, surface roughness, composition and porosity are also examined. Magnetic fields are shown to provide a 50.8 % improvement in catchment efficiency, increasing the width of tracks by at least 25%, whilst also reducing the dilution in depositions made using ferromagnetic powders. An improved powder catchment efficiency has potential to drastically reduce the cost of manufacturing, especially considering the large size of components which can be manufactured using this technology and the high cost of powder (which can easily be above £400 per kg).

Furthermore, magnetic field strength is shown to have a positive relationship with track size, suggesting that altering magnetic field strength may allow magnetic assistance to be used in a discrete fashion. The technique is also proposed and examined for its potential as a new control method, by varying the placement and dynamically changing magnetic fields during deposition. Similar geometric outcomes were achievable over specific portions of the deposition, when switching magnetic fields dynamically, suggesting that magnetic assistance is an effective dynamic control technique. It is currently difficult to alter track dimensions

during operation, therefore this technique has the potential to give the technology significant greater potential.

The fundamental mechanism of magnetic assistance is also examined and discussed in detail, by comparing the effects of magnetic powder pre-loading over a large magnetic field in contrast to feeding powder over a smaller coaxial magnetic field.

This work acts as the first in this field, thus considers the potential future of magnetic assistance in three dimensional additive manufacturing, though it is limited to two dimensional tracks in this work, due to the magnetic field being located beneath the substrate. To develop the technique in a greater range of materials demonstration of enhanced deposition through magnetic assistance of more complex alloy systems, in particular those that are not entirely ferromagnetic is also performed, using composite bespoke powder systems. Further to improving the materials efficiency; in future, the technique has potential for use as an adaptive control technique, to vary the powder catchment efficiency in process, dynamically altering the dilution into the substrate and the track geometry as is necessary, though currently it is mainly restricted to ferromagnetic alloys, or those with a significant component.

Preface

This thesis is submitted to the University of Nottingham for the degree of Doctor of Philosophy. The research, carried out over three years, was supervised by Professor Adam Clare, Dr Joel Segal and Dr James Murray in the department of Mechanical, Materials and Manufacturing Engineering.

Publications

During the production of this work the following list of publications have been published.

Presented in this thesis:

- P.H. Smith, J.W. Murray, D.O. Jones, J. Segal, A.T. Clare, Magnetically assisted directed energy deposition. *Journal of Materials Processing Technology*. 288 (2021) 11682. <https://doi.org/10.1016/j.jmatprotec.2020.116892>
- P.H. Smith, J.W. Murray, A. Jackson-Crisp, J. Segal, A.T. Clare, Magnetic manipulation in directed energy deposition using a programmable solenoid. *Journal of Materials Processing Technology*. 299 (2022) 117342. <https://doi.org/10.1016/j.jmatprotec.2021.117342>

Not presented in this thesis:

- S. Sanchez, P.H. Smith, Z. Xu, G. Gaspard, C.J. Hyde, W.W. Wits, I.A. Ashcroft, H. Chen, A.T. Clare, Powder bed fusion of nickel-based superalloys: A review. *International Journal of Machine Tools and Manufacture*. 165 (2021) 103729. <https://doi.org/10.1016/j.ijmachtools.2021.103729>
- J.W. Murray, A. Spiedel, A. Jackson-Crisp, P.H. Smith, H. Constantin, A.T. Clare, Unprocessed machining chips as a practical feedstock in directed energy deposition. *International Journal of Machine Tools and Manufacture*. 169 (2021) 103803. <https://doi.org/10.1016/j.ijmachtools.2021.103803>
- P.H. Smith, A.T. Clare, J. Segal, Magnetic directed energy deposition: Assessment for microgravity. *Proceedings: Additive Manufacturing Turkey Conference*. 1 (2019) 128.

Covid-19 Impact Statement

The Covid-19 pandemic has had some negative effects on my ability to conduct research during the course of my PhD. This has been mitigated wherever possible, although mitigation has been not always been possible during an experimental degree. Foremost, the pandemic and subsequent restrictions inhibited my ability to use laboratories. This means that access to equipment was limited, the consequence of this is that the number and variety of experimental trials was reduced. This issue was further exaggerated as the time which could be devoted to characterising and analysing the outcomes of experiments was also limited. As an additional consequence, colleagues such as technicians and support staff also could not enter laboratories to maintain equipment and waiting times to use equipment were extended. This meant that even when equipment was available it was sometimes out of order. Other staff and I having to self-isolate continued to exacerbate these issues. Uncertainty over when and how much access to laboratories could be provided worsened this impact, due to the short notice in changes to regulations and self-isolation. Regulations also limited my ability to attend academic conferences to broaden my understanding of the field, this was mitigated primarily through further reading.

These impacts have been alleviated wherever possible, leading to the completion of this thesis. When equipment could not be used, these periods were used to write-up and plan experiments. Mitigation via computer modelling was also considered.

Despite these challenges this work includes comprehensive description and analysis of the areas investigated, minor additional data collection was not always possible, however this has not significantly impeded the value of the work as a whole.

Acknowledgements

Thanks goes to my supervisory team, led by Prof Adam Clare, whose continued advice and guidance has led to an improvement in my work, time after time. Thank you to Prof Joel Segal who has supported and encouraged me throughout my higher education experience. Likewise, Dr James Murray's contributions to my progress have been invaluable and his pragmatic advice has always served me well.

The gracious patronage of Dr Neville Rieger facilitated this work, for which I am very grateful, particularly alongside the opportunity to conceive my own topic.

The problem-solving expertise of Mr Alexander Jackson-Crisp have repeatedly helped me to overcome both practical and technical hurdles, for which I am thankful. Thanks also to Mr Stuart Branston for his knowledge and experience in the use of laser equipment and to Dr Elisabeth Steer and Dr Hannah Constantin for their aid with analysis equipment. Thank you also to all those colleagues who have kindly supported me throughout my PhD studies with their experiences and personal advice.

My gratitude goes to Ms. Camilla Woodrow-Hill for her unwavering support and her knowledge of cross-disciplinary data visualization.

Finally, a special thanks to my parents whose support and well-wishes have always been the most encouraging.

Contents

Abstract.....	2
Preface.....	4
Publications	4
Covid-19 Impact Statement.....	5
Acknowledgements	6
Contents	7
Table of Figures	11
List of Tables.....	16
1 Introduction	17
1.1 Research Aims.....	19
1.2 Thesis Overview.....	20
2 Literature Review	22
2.1 Introduction to Laser Directed Energy Deposition	22
2.2 Process Systems	23
2.2.1 Definition of a Laser	23
2.2.2 Powder Feeding	25
2.2.3 Coaxial Powder Nozzle Designs.....	29
2.2.4 Wire Feeding.....	32
2.2.5 Adaptive Control Techniques	33
2.2.6 Summary of Process Systems	35
2.3 Mechanisms of Material Deposition	35
2.3.1 Laser Melting & Solidification	35
2.3.2 Laser Attenuation.....	36
2.3.3 Laser Power Distributions.....	38
2.3.4 Powder Distributions in Coaxial Nozzles	40
2.3.5 Powder Entrapment.....	43

2.3.6	Melt Pool Dynamics	45
2.3.7	Powder Rheology	47
2.3.8	Powder Mixtures	50
2.3.9	Summary of Mechanisms of Material Deposition	52
2.4	Physical & Processing Quality in DED Products.....	52
2.4.1	External Track Geometry	52
2.4.2	Skewness.....	56
2.4.3	Dilution	57
2.4.4	Track Porosity	59
2.4.5	Surface Quality	60
2.4.6	Catchment Efficiency.....	62
2.4.7	Summary of Physical & Processing Quality in DED Products	64
2.5	Materials Properties of LDED Products	65
2.5.1	Properties of ferromagnetic steels.....	66
2.5.2	Nickel Alloys	69
2.5.3	Summary of LDED Material Properties	71
2.6	Fundamentals of Magnetic Attraction.....	71
2.6.1	Summary of Magnetic Attraction	73
2.7	Effect of Magnetic Fields on Metal Processing	74
2.7.1	Summary of Effect of Magnetic Fields on Metal Processing	77
2.8	Literature Review Summary and Research Gaps.....	77
3	Experimental.....	81
3.1	Experimental Setup for LDED Experiments.....	81
3.1.1	Laser.....	82
3.1.2	Powder Feeder	83
3.1.3	Coaxial Nozzle.....	84
3.1.4	Computer Numerical Control	84

3.2	Characterisation Techniques	85
3.2.1	Characterisation and Preparation of Inputs	85
3.2.2	Deposition and track characterisation	85
3.3	Materials Used.....	87
3.3.1	AISI 4340 Powder.....	87
3.3.2	Nickel Powder.....	89
3.3.3	Chromium powder	90
3.3.4	Nichrome powder.....	91
3.3.5	Substrates	92
4	Feasibility of Magnetically Assisted LDED.....	93
4.1	Introduction	93
4.2	Experimental	95
4.2.1	Materials	95
4.2.2	Experimental Setup.....	96
4.3	Results	97
4.3.1	Material catchment.....	97
4.3.2	Effect of field line position	99
4.3.3	Track dilution.....	100
4.3.4	Effect of inclination	102
4.3.5	Roughness & Geometry	105
4.3.6	Hardness.....	107
4.4	Discussion	108
4.5	Conclusions	113
5	Investigation of Electromagnetic LDED	115
5.1	Introduction	115
5.2	Experimental	116
5.3	Results	119

5.3.1	Magnetic field strength	120
5.3.2	Role of laser power with magnetic assistance	121
5.3.3	Powder flow rate and traverse speed in the presence of a magnetic field	123
5.3.4	Solenoid position	125
5.3.5	Hardness.....	126
5.4	Discussion	127
5.5	Conclusions	132
6	Expanding the Applications of Magnetic Assistance	133
6.1	Introduction	133
6.2	Experimental	134
6.3	Results	138
6.3.1	Solenoid switching.....	138
6.3.2	Thick walls & meandering toolpaths	140
6.3.3	Nickel powder.....	141
6.4	Discussion	143
6.5	Conclusions	146
7	Manufacturing Non-Magnetic Alloys using Magnetic Assistance.....	148
7.1	Introduction	148
7.2	Experimental	150
7.2.1	Powder manufacturing	152
7.3	Results	157
7.3.1	Deposition Geometry	157
7.3.2	Deposition Composition	158
7.4	Discussion	160
7.5	Conclusions	164
8	Overall Discussion.....	166
9	Overall Conclusions & Future Work.....	170

9.1	Future Work	171
10	References	173

Table of Figures

Figure 1-1	Flow of experimental chapters conducted for this thesis.	20
Figure 2-1	Principle of photon emission in lasers.....	24
Figure 2-2	Typical DED Powder Feed Systems	25
Figure 2-3	Alternative designs to pneumatic powder feeding [6].	28
Figure 2-4	Typical different nozzle designs as discussed by Lamikiz et al.[32].	30
Figure 2-5	Common laser intensity distributions in LDED.....	39
Figure 2-6	Collimated powder stream from a discrete coaxial nozzle. Processed image from Fearon & Watkins [76].	41
Figure 2-7	Powder concentrations with distance from the nozzle tip; a) showing powder concentration at various points, b) shows a luminance image from the cone tip. From Pinkerton and Li [34].	42
Figure 2-8	Powder Absorption in DED [83].	44
Figure 2-9	Particle Entrainment Via Laser Due to Powder Vaporisation [14].	45
Figure 2-10	Fluid flow due to Marangoni convection; a) and b) from a CFD model of copper, c) showing the grain structure which sometimes occurs as a result. Adapted from Khamidullin et al. [87].	46
Figure 2-11	Schematic of measurements of track geometry. Where h is the deposition height, θ are the wetting angles of either side of the track, A is the area of the track cross-section, w is the track width and d is the depth of the dilution zone.	53
Figure 2-12	Retained austenite in LDED 4340 [127].	66
Figure 2-13	Hardness of AISI 4340 with distance from the substrate. This indicates that hardness is greater at the top layer, where the phase is untempered martensite and has not undergone thermal cycling [127].	67
Figure 2-14	Equilibrium phase diagram for Fe-C AISI 4340, as marked by the arrow [127]. A represents the ferrite phase and γ represents the austenite phase.	68
Figure 2-15	Magnetic hysteresis loop for cold rolled carbon steel sheets with different percentage strains, B is replaced with J here [154].	72
Figure 2-16	Hardness in 316 steel when deposited using different fields. SE - static electric field. RE - rotating electric field. SM - static magnetic field. RM - rotating magnetic field.	

SEM - static electric and magnetic fields. REM - rotating electric and magnet fields.

Magnetic field strength 62.5 mT. Electric field strength 1209.3 V/m [165]. 74

Figure 3-1 LDED system used throughout this work 82

Figure 3-2 Powder feeder disk speed and resultant feed rates. Showing 95% confidence intervals. Root mean square error is 1.26. 84

Figure 3-3 AISI 4340 powder particle size distribution as measured using Malvern Mastersizer 3000 instrument. 88

Figure 3-4 AISI 4340 powder showing high sphericity and few satellites. 89

Figure 3-5 Nickel powder particle size distribution. 90

Figure 3-6 Particle size distribution of chromium powder. 91

Figure 3-7 Powder size distribution of pre-alloyed nichrome powder. 91

Figure 4-1 Experimental Setup (a) shows 0° tracks and magnetic flux density, (b) shows 45° tracks 96

Figure 4-2 Direction of tracks with magnetic flux, (a) showing track direction and (b) showing the magnetic flux lines. 96

Figure 4-3 Effect of magnetic assistance with increasing powder flow rate on track mass per unit length, for tracks in both orientations and magnetic states for (a) mild steel and (b) stainless steel substrates. 98

Figure 4-4 Powder catchment efficiency with increasing powder flow rate for tracks in both orientations and magnetic states for (a) mild steel and (b) stainless steel substrates. 98

Figure 4-5 3D images of example track sections at points of magnetic field intersection using mild steel substrates, demonstrating the effect of magnetic assistance on increased track size. 99

Figure 4-6 Effect of magnet on cross-sectional area at field line intersection points (in pink), compared to average cross-sectional areas of tracks. 100

Figure 4-7 Cross-sectional optical images of tracks on mild steel (a) without and (b) with magnetic assistance, showing the effect of magnetic field on track size and dilution zone. . 101

Figure 4-8 Effect of magnet on % dilution at two different powder flow rates on a 0° on mild steel. The magnet reduces the proportion significantly at low flow rates. This reduction is less at the high flow rate. 101

Figure 4-9 Effect of inclination angle on powder catchment efficiency for mild steel, using two different parameter sets, with magnetic assistance turned on and off. 103

Figure 4-10 a) Shows how skewness is measured by calculating the difference in cross-sectional areas either side of the track centre, as a percentage of the total area. Microscope

images b) and c) show representative (at 200 mm/min, 13.1 g/min) track morphologies in cross-sections of two tracks. The skewness was measured as 10.46% and 6.46% respectively. 104

Figure 4-11 Magnetic assistance reduces cross-sectional skewness in inclined tracks, at high inclination angles, in the case of mild steel. 105

Figure 4-12 Effect of magnetic assistance on track surface roughness at 0 and 90° orientations to field lines for (a) Mild steel and (b) Stainless steel. (c) and (d) show the height/cross-sectional area ratios of tracks for mild and stainless steel respectively. 106

Figure 4-13 Microhardness of tracks produced with and without magnetic assistance along the track length..... 107

Figure 4-14 Schematic of enhanced deposition behaviour using magnetic assistance with deposition at (b) 90° to magnets and (c) 0° to magnets, in comparison to (a) without magnets. 109

Figure 5-1 Experimental setup and toolpaths. Shown in (a) for fundamental experiments, on the effects of electromagnetic field strength, laser power, powder feed rate and traverse speed with a coaxial solenoid. The magnetic flux around the solenoid is shown in (b). The different positions of the solenoid are shown for the solenoid position experiment (c)..... 117

Figure 5-2 Effect of magnetic field strength on track properties, demonstrating that increased magnetic field strength leads to improved catchment efficiency, whilst dilution is reduced. (a) Catchment efficiency (b) track width (c) cross sectional area (d) dilution is reduced. (a) Catchment efficiency (b) track width (c) cross sectional area (d) dilution area. Error bars indicate standard deviation. 121

Figure 5-3 Effect of laser power and magnetic assistance on (a) cross sectional track area (b) track width (c) height and (d) area of dilution zone. Cross-sectional area increases due to magnetic assistance whilst height and the area of the dilution zone decrease. Error bars indicate standard deviation. 123

Figure 5-4 Effect of powder flow rate and scan speed on (a), (c), cross-sectional area and (b), (d) track width. The effects of magnetic assistance are consistent with regard to scan speed, but vary with flow rate. Asterisk (*) indicates powder flow rate calculated from mass of control tracks. Error bars indicate standard deviations. 124

Figure 5-5 Effect of magnetic preloading on track geometry, (a) cross-sectional area, (b) track height at the preloading positions. A significant increase in track cross-sectional area and height occurs when using magnetic assistance in the preloading condition compared to where the solenoid is coaxially aligned to the laser..... 125

Figure 5-6 Hardness of cross-sections produced at different magnetic field strengths with the magnetic field coaxially aligned.	126
Figure 5-7 Images of the powder stream exiting the nozzle without an incident laser; (a) shows with no magnetic assistance, (b) shows with 93.5 mT magnetic assistance after the magnet had been switched on for 0.12 s. The brightness of these images was measured across the nozzle width to generate (c)-(e). The 3d plot of pixel brightness (c) demonstrates that the powder converges from a bimodal to a gaussian distribution, whilst (d) shows a slice of the distributions at the orifice as the powder exits the nozzle and (e) shows the distributions 5mm after exiting the nozzle.	128
Figure 5-8 Mechanisms of powder capture via magnetic assistance, (a) where preloading is eliminated via a coaxial aligned solenoid. (b) Where preloading is encouraged using a solenoid in a fixed position relative to the substrate. Both have been shown to increase the dimensions of tracks.	131
Figure 6-1 Setup of experiments used in this chapter. (a) shows the physical setup, (b) shows the magnetic field, whilst (c) - (f) show the toolpaths, magnetic and feedstock parameters used.	136
Figure 6-2 Effect of dynamic magnetic switching on track morphology. The magnetic field was reduced to zero halfway along the track; starting with 32.2 mT of magnetic assistance (left), before being switched to 0 mT (right). The mean (averaged in the y direction) cross-section of the box indicated in (a) is shown in (b), this shows how the peak height changed in one example across the transition. All dimensions are taken from the mean profiles in FVM measurements. Experiment conducted at 600 W, 500 mm/min, 19.4 g/min.	139
Figure 6-3 Dimensional changes in bulk depositions due to magnetic assistance. (a) shows an FVM render of the sample with magnetic assistance, in (b) the effect on dimensions are shown. Both samples were produced with 1.20 mm stepover.	140
Figure 6-4 Meandering toolpaths with magnetic assistance. FVM height colour map (a) without magnetic assistance and (b) with 93.5 mT magnetic assistance, (c) shows the difference in catchment efficiency. The meandering toolpath is overlaid on (a) and (b).	141
Figure 6-5 The role of magnetic assistance when using pure nickel powder on different substrate materials. (a) shows an image of a nickel track with an inconsistent surface, produced on a mild steel substrate, (b) catchment efficiency with magnetic assistance using different substrates. The magnetic field was measured as 79.6 mT whilst through the MS substrate this was measured as 109.1 mT. 500 W laser power was used for the nickel powder and 900 W for the 4340 powder.	142

Figure 6-6 Demonstration of switching magnetic assistance, showing cross-sections of while magnetic assistance was applied (a) and when this was switched off (c). A render of the centre section of a switched track is shown in (b). 144

Figure 7-1 Hypothesis of magnetically assisted DED using satellited powder. 148

Figure 7-2 Powder manufacturing and analysis process. Initial powder composition was chosen based on a nichrome 80:20 and the powder diameters described in the literature [179]. 152

Figure 7-3 Improved powder satelliting manufacturing process flow as determined by SEM. 153

Figure 7-4 SEM/EDX images showing the effect of increasing binder quantity on satellited powder; a) and b) showing 0.04 wt. % binder solution; c) and d) showing with 0.07 wt. % binder solution. 154

Figure 7-5 Powder size distributions of the constituent powders and the satellite powder used in LDED experiments. 156

Figure 7-6 Results from satellited material experiments. showing a) powder catchment efficiency, b) cross-sectional area above the substrate, c) percentage porosity and d) the area of the cross-sectional dilution zone..... 158

Figure 7-7 Compositions of satellited and pre-alloyed nichrome tracks. Showing EDX maps of the chromium and nickel content in tracks produced with magnetic assistance in a) a satellited powder track and d) a pre-alloyed nichrome track. Also shown is the composition of these cross-sections b) and d) at the locations marked in black. The white marks indicate additional compositional measurements. The colour strength of the nickel is reduced 50 % here compared to in Figure 7-4 to show the difference in chromium more effectively. 160

Figure 7-8 Percentage volume of chromium content with parent particle diameter. Showing that as the diameter of the parent particle increases the percentage volume of the coating material declines. 163

Figure 7-9 Small particles deflected by the vapour plume without magnetic assistance in a) these particles are retained by the magnetic field shown in b). 164

List of Tables

Table 3-1 Particle size distribution (μm) of AISI 4340 as measured using different methods.	88
Table 3-2 Composition of AISI 4340 powder by different methods (wt.%).	89
Table 3-3 Nickel powder particle size distribution (μm).	89
Table 3-4 Composition of nickel powder (wt. %) according to manufacturer's data.	90
Table 3-5 Particle size distribution of chromium powder.....	90
Table 3-6 Composition of chromium powder by wt. % as given by the manufacturer's data.	91
Table 3-7 Pre-alloyed nichrome powder size distribution.	91
Table 3-8 Composition (wt. %) of nichrome powder as given by manufacturer's analysis....	92
Table 4-1 Parameters used for experiments in this chapter.	97
Table 5-1 Summary of experimental parameters used. Field strengths are those measured on the surface of substrates.	119
Table 6-1 Composition of materials used in Chapter 6 (wt. %).	135
Table 6-2 Magnetic and material properties of materials used in this study [148,177]. The magnetic field strength, measured at the substrate surface, is shown for comparison.	137
Table 6-3 LDED parameters used in each experiment conducted in this chapter (Chapter 6).	138
Table 7-1 Powder compositions used in this section (wt. %).	151
Table 7-2 Experimental parameters used for satellited powder experiments.	152
Table 7-3 Powder size distribution of powders used in this section (μm) as measured by laser diffractometry [102].	156
Table 7-4 Powder flow rates using standardised test methods.....	156

1 Introduction

The laser directed energy deposition process is both a coating and near-net shape additive manufacturing technique which is seeing expanding use due to its process flexibility and the ability to conduct the manufacturing process in a range of different setups (e.g. 3 axes, rotary or robot kinematic systems). Process parameters can be optimised to reduce the dilution of the cladding material (by reducing laser power) which limits the changes to the body material; or the process may be operated as an additive manufacturing process with high dilution being used to ensure subsequent layers are well bonded to each other. Material feed rates may also be altered significantly, so that the process can be used to manufacture large structures relatively quickly, or to create more precise near-net shape components with reduced machining being required. However, the current inability to change powder catchment (except in one work using a solenoid valve) during manufacturing reduces the process flexibility and consistency.

The process, it is still under-utilised in industry, the inefficient use of expensive powder materials means that the processing route is considered more often for high-cost, low volume manufacturing. As powder material is pneumatically delivered much of it is not consolidated into the final component, hence powder catchment efficiencies could be improved, which would lead to significant reductions in processing costs. Configuring the large number of parameters correctly is also complex and means that the final products must undergo rigorous inspection procedures in order to qualify them. Adaptive control techniques have been developed to attempt to reduce the variability of these parameters, with some success. Particularly, adaptive control over laser power has been shown to improve track consistency and dimensions, but powder input is more difficult to adaptively control than other parameters and thus is not of primary consideration. The use of body forces produced via magnetic fields has the potential to alter and control the trajectory of powder in-flight, to increase powder catchment efficiency and improve the ability to dynamically control the behaviour of powder between the nozzle and the melt pool. Previously, changes to the nozzle design, laser mode and parameter optimisation have improved catchment efficiency, but this could be improved further using more novel techniques. To date the use of magnetic fields has not been seriously considered within the laser directed energy deposition process, because of the challenges in modelling such an approach, while it may be limited to specific groups of materials. A challenge of this work is to show that the use of magnetic fields can be applied as widely as conventional methods. This thesis instead examines various methods of

using magnetic fields to change powder delivery and alter the geometry and properties of the resulting depositions experimentally.

1.1 Research Aims

The overall aim of this thesis is to: improve and understand material efficiency and deposition geometry in the laser directed energy deposition process, via the use of magnetic assistance. This aim can be broken down into the following objectives:

1. Establish if magnetic fields may be used to improve powder catchment efficiency by modifying the trajectory of powder streams. Magnetic fields may represent a new way to change the deposition process in a reliable manner.
2. This new method could help to avoid the lengthy process of parameter optimisation to improve catchment efficiency which is currently required.
3. Further examination will reveal the effect of changing laser power and powder feed rate on track geometry with the application of magnetic assistance. Relationships between magnetic field strength, track width, track height and catchment efficiency should be established. This is required to understand the scope of the new process addition and to begin to understand how magnetic assistance may be used and to begin to determine a processing window.
4. Establish and quantify the relationship between magnetic field strength and any improvement in powder catchment efficiency, including on an inclined substrate.
5. Ascertain the underlying mechanisms through which the established relationships occur.
6. Develop and improve equipment which enables magnetic fields to be used to control powder trajectory and track geometry and identify technological barriers.
7. Identify and assess the methods through which magnetically assisted DED may be utilised, particularly for adaptive control.
8. Determine the effect and potential of different material compositions on the magnetically assisted process. Establish whether the magnetic permeability of the powder or substrate material have a meaningful effect on track geometry or powder catchment efficiency. Furthermore, invent new methods to advantageously tailor materials to suit magnetic assistance in LDED.
9. Understand the effect of magnetic assistance on the microstructural phases and mechanical properties produced. Though the primary focus of this work is to investigate magnetic fields for their usefulness as a manufacturing process tool, effects on the material and microstructural properties should be assessed to ensure the

process can create useful products. This has never been attempted when using ferromagnetic materials and hence represents a new area of research.

Upon completion of these objectives an understanding of whether and how this new technique can be used will be gained. This research aims to uncover the fundamentals of this process, to inform future work which will be conducted in this area.

1.2 Thesis Overview

Relevant existing research on and around the topic of magnetic assistance in directed energy deposition is examined in Chapter 2. Discussion is made of the sub-systems and the different phenomena which amalgamate to produce the overall LDED manufacturing tool. This includes the mechanisms of material addition and the phenomena which occur around and inside the molten pool. Further to this, the state-of-the-art of LDED material deposition and control is also characterised. The use of magnetic fields in material melting and their potential in particulate processing is also discussed, though these works have different aims to the research conducted here. From this literature review, the research gaps needs are identified. The prominent research gaps identified for investigation are: the need for more material efficient systems and the development of more advanced control techniques, magnetic assistance is identified as a possible remedy for these gaps.

Chapter 3 describes the methods, systems and materials which were used in experiments and the subsequent analysis in this thesis. Four core research chapters present new experimental research into various aspects of magnetic assistance in LDED, these chapters were developed in the order of the aims in Section 1.1 and the flow of these is detailed in Figure 1-1.

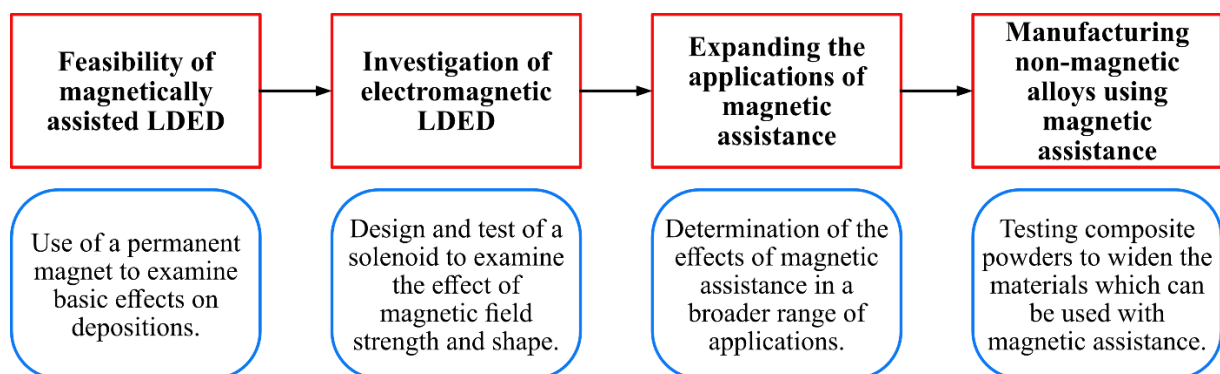


Figure 1-1 Flow of experimental chapters conducted for this thesis.

In Chapter 4 the feasibility of using commercially available permanent magnet tools is assessed and the effect on the process is examined. This study formed the foundation for the following three sections, by evaluating whether magnetic fields of this strength could be used

to change the geometry and surface characteristics of depositions. The design of the experiments and the equipment used reflects this aim.

In Chapter 5, equipment is developed to allow greater manipulation of parameters. An electromagnet is used to give control over the strength and size of the magnetic field. This allows a more refined examination of the parameters and their effects on tracks, also allowing determination of which of the mechanisms theorised in Chapter 4 are most impactful.

Chapter 6 uses the same equipment to examine different, novel techniques which could be used to: improve control over the LDED process, determine the capability of magnetic assistance in a greater range of possible use cases, and use a different ferromagnetic powder.

Chapter 7, the final experimental chapter includes further development of powder feedstocks for magnetically assisted LDED, to expand the range of materials which can be used with magnetic assistance. This will allow more complex alloys to be used in the process and hence widen the usefulness of the magnetic assistance. This work investigates whether alloying composite powders, in-situ, is an effective method to combine the benefits of magnetic assistance with the material properties of using non-magnetic alloys.

Chapter **Error! Reference source not found.** summarises the overall conclusions of the thesis. This chapter presents some of the potential impacts of this work's findings and details a number of suggestions for future work which build upon the conclusions made here.

2 Literature Review

2.1 Introduction to Laser Directed Energy Deposition

Powder directed energy distribution (DED) additive manufacturing has its roots in the laser cladding of components to improve their hardness [1] or corrosion resistance [2]. More recently, this process has been developed into a flexible additive manufacturing process by building successive layers of cladding material into near-net-shape component geometries. DED refers to any process where “focused thermal energy is used to fuse materials by melting as they are being deposited” [3]. This means that the energy source is not required to be a laser, plasma arcs and electron beams are also commonly researched [4], but are beyond the scope of this thesis. In this work the terms DED and LDED have been used in preference to laser cladding in spite of the two-dimensional nature of the experiments because the long term goal of this work is to improve the additive manufacturing process where this term is more commonly used. There are many embodiments of laser DED (LDED), though fundamentally the process uses a laser beam to melt an input material (normally wire or powder, though pastes have been used too [5]). An automated kinematic system is used to move either the nozzle or the workpiece, so that tracks can be produced in a defined path. The tracks produced are built in successive layers to produce 3d components. An inert gas is normally required to convey powder and shield the melt pool from oxidation [6]. Unlike other additive manufacturing processes, localised (rather than enclosed) shielding means that large components can be made, whilst the process does not always need to be operated with the layers being added in the vertical direction [7–9] (depending on the kinematic system), allowing complex geometries to be produced without support materials.

The LDED process is commonly used in manufacturing, to repair mould tools [4] and in the energy industry [10] whilst uptake is growing for use in aerospace components, including for aerofoils and high temperature rocket nozzle components [11]. DED is useful when manufacturing large, complex components with tall, thin walls as it is easily scaled to large volumes using kinematic robotic arms [6,12,13]. It is also advantageous due to the range of materials which can be used and blended, [14] and the mechanical properties which can result. These properties include the ability to functionally grade materials, particularly layer by layer [6]. Compared to conventional subtractive manufacturing, DED is also useful to reduce design complexity, as assemblies can often be combined into a single component using additive manufacturing, this is especially useful in the aerospace industry to reduce the total mass of parts [15,16].

A large range of process parameters can be used in powder LDED depending on the application. The parameters may be balanced at different levels, for example if very high throughput is required, feed rates up to 48.3 g/min have been demonstrated, although feed rates as low as 6.8 g/min [17] are more common. Naturally, there is a trade off in terms of track quality such as crack density at such high speeds. DED is well known to have higher deposition rates than other metal AM processes, especially when using a wire feedstock. Post-process machining is normally required, especially when using wire feeding [13]. In the following literature review the various sub-systems required in LDED are first elucidated. Following this, the precise nature of material is explained according to the state-of-the-art. Linked to these mechanisms are the properties that tracks and components in DED are measured by, and how these products may be improved against these metrics, which are discussed in the context of their geometric and material properties. The final sections of the literature review will then describe the fundamentals of magnetic materials and how magnetic fields have been used to alter the process. The literature review then concludes with a summary of gaps in the research in this field, some of which are examined by the research chapters in this thesis.

2.2 Process Systems

Laser blown powder DED is fundamentally a dynamic process, due to the number of time dependant interactions which are acting simultaneously. Originally, DED comes from laser welding, in which a high-power laser is directed onto the material. Different interactions between substrate and laser are possible depending on the energy density per unit time. The addition of blown powder and the high velocity shielding gas which accompanies this powder results in further variation sensitive dynamic phenomena. These elements interact with one another, meaning they should sometimes be considered holistically, particularly when considering powder catchment efficiency, and material and mechanical properties. In general, the LDED systems described in this work consist of a laser to supply the energy source and a pneumatic feeding system to convey the feedstock material and provide local shielding. In this section, different manifestations of the process are also described.

2.2.1 Definition of a Laser

Laser stands for light amplification by the stimulated emission of radiation. Lasers are commonly used where high energy density is required, such as in the precise manufacturing or cutting of metals. Lasers operate via electron excitation. When energy is introduced to an atomic electron it can move to a higher energy orbit (shown in Figure 2-1) and is described as

being in an “excited state”. This higher orbit is not stable, so the electron will quickly decay, into a lower energy metastable orbit. When this occurs for many electrons it is called “population inversion” and the electrons will remain in this metastable state for a short amount of time (around 10^{-3} s) [5]. After this time some electrons will decay further, moving back to the ground state, causing the spontaneous emission of a photon. If this photon goes on to interact with other electrons in the metastable state these electrons decay into their ground state, stimulating a cascade of photon emissions. As these electrons have moved from the same energy levels, the energy of the resulting photons is identical, this causes the light emitted to be monochromatic (deviating little in wavelength) and coherent (in phase) [5]. These two principles make lasers different from other electromagnetic radiation.

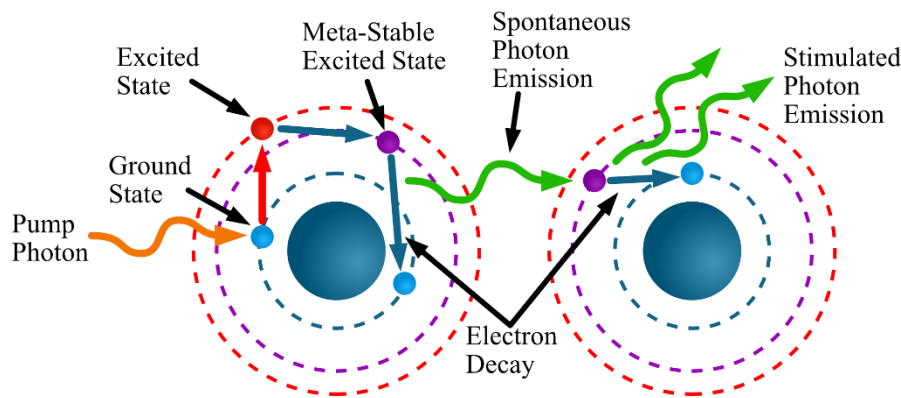


Figure 2-1 Principle of photon emission in lasers.

When the laser medium (normally a gas or crystal) is placed between two mirrors in an optical resonator cavity, the photons reflect internally, increasing the possibility of interactions, leading to greater light output. The mirror on one side is not completely reflective and allows some light to pass through an aperture. This light consists of the laser beam, the useful output. The energy and wavelength of the laser therefore fundamentally depends on the laser medium which is used.

Lasers with a CO₂ medium have historically been used for LDED, however modern developments in laser technology means that the use of lasers with a fibre source (such as Ytterbium) are now commonly used. These lasers offer numerous advantages over CO₂ lasers. The primary advantages in LDED are that they are more readily absorbed by metals and they can be delivered by total internal reflection through optical fibres [5]. This means that there is greater flexibility in the design of laser systems and lower power lasers can be used to produce the same heat input. Fibre lasers may also be pumped by diodes, simplifying the design of the laser system and reducing costs.

When the laser is incident on a surface a portion its energy is absorbed, heating the material. This is the interaction which is used to melt materials in LDED.

2.2.2 Powder Feeding

The powder feed system is generally composed of 3 sub-systems, powder conveyance, powder metering unit, and powder delivery system. A typical configuration is shown diagrammatically in Figure 2-2. The conveyance system is required to push the powder onwards. The metering unit to ensure a controlled feed rate is used, before the delivery system introduces the powder to the energy beam via the nozzle.

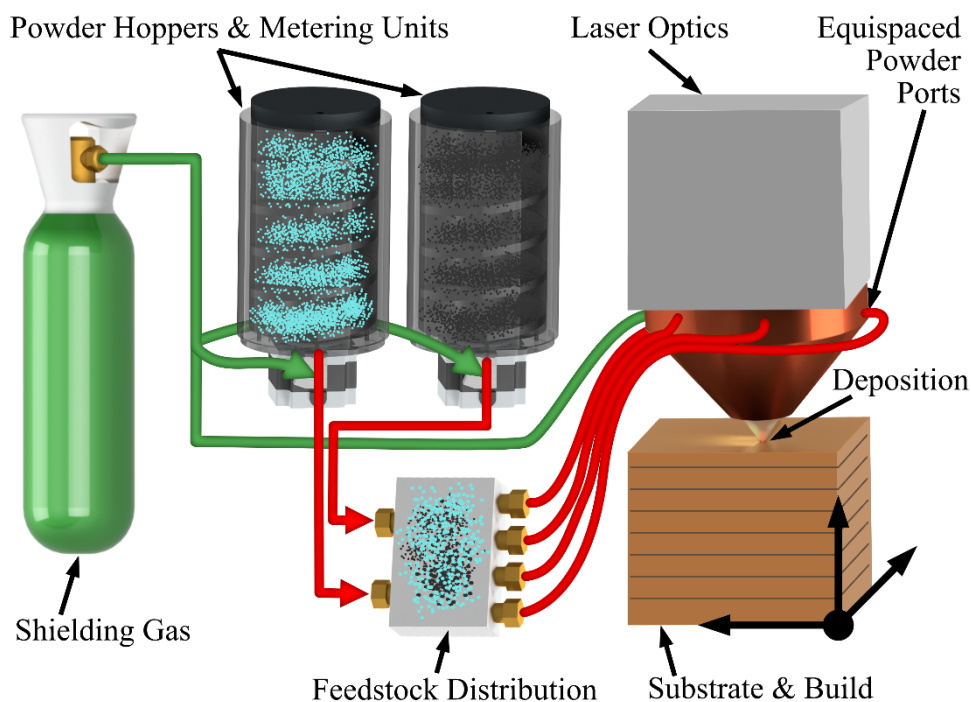


Figure 2-2 Typical DED Powder Feed Systems

Feeder designs are generally evaluated based on a few key principles: the stability, repeatability and consistency of flow; the responsiveness to allowing dynamic control over powder feed rate; the particle feed velocity; the availability and need for carrier gas; the ability to introduce multiple materials in a controlled manner; and the compatibility of the feeder with certain nozzle designs.

Stable flow is extremely important in powder DED, to ensure that the process may create tracks of consistent, known dimensions, as well as producing known material and mechanical properties. The powder feed rate also affects the thermal history and crystal structure of the component. Flow rate is often determined over a short test of around 1 min duration when using a new material or powder size distribution. This has been shown to not necessarily be

accurate, as flow rate may take time to stabilise over longer periods of around 20 mins as shown by Steen & Lin for a screw feeder [18].

Various feeders have been designed and tested including: gravity-based; mechanical wheel [6]; fluidised bed; vibration and ultrasonic [19]. The success of each design of feeder depends on the particle size distribution, material density and flow properties including powder geometry. It is well understood that, for good flowability, powders should have high sphericity and that when powders with similar densities are mixed to produce functionally graded materials (FGM), they should have similar diameters [20], be smooth and have few satellites [21]. Therefore, gas atomised powders are the most widely used.

However, stable powder feeding remains an issue when using open-loop controlled powder feeding. For example, Whiting et al. measured a 10% deviation in flow rate when using a constant feeder disk rotation speed and have developed an acoustic emission device to measure the powder feed rate in real-time [22]. A few other researchers have suggested using optical detectors or lasers to monitor powder feed rates [23], so that powder feed rate can be made more consistent. But, acceleration and deceleration of the motion system means that consistent flow does not necessarily lead to a track with consistent height. Vibration and the jerk in the process can cause powder to be jetted from the nozzle inconsistently. Tang et al. showed that this can lead to variable powder capture and feed-forward control systems (where measurements and simulation are used to alter parameters in real-time) are being developed to improve track consistency further [24]. However, varying powder feed rates alone can lead to increased variation in track dilution and therefore, coupling the variable flow rate to variable laser power has been suggested, further complicating the system.

Where the use of multiple powders has been researched, it is common to premix these powders in a simple manner to obtain the intended composition [20], however this does not enable the functional grading of parts. An alternative to this is to use multiple feeders, so that the powder ratios can be dynamically controlled and functionally graded parts or accurate alloys can be produced in-situ. Jeng et al. were one of the first to do this, noting that improvement to powder feeding was needed to improve the process [25]. Naturally, any longer-term issues with powder feeding will be further exaggerated when using multiple feeders, even if consistency is good over short time periods. This makes producing alloys with small quantities of alloying elements (such as modern nickel super-alloys or HSLA steel) more difficult.

A further issue with conventional blown powder feeders is the inability to effectively pause powder feeding. A gate valve is ineffective due to the build-up of powder and subsequent over-expulsion that would be produced when restarting the process. The effect of gravity when gas flow is turned off would also lead to further inconsistencies in powder flow. To remedy these issues, gravity, vibration and ultrasonic piezo feeders have been tested without carrier gas. Sometimes very high powder catchment efficiencies have been demonstrated using these methods, for example Wang and Li suggested they could achieve close to full powder catchment efficiency using an ultrasonic powder feeder [19]. Some of these possible configurations are shown in Figure 2-3, as reviewed by Singh et al., these methods are not as well developed as gas-feed LDED, but have scope for future development [6].

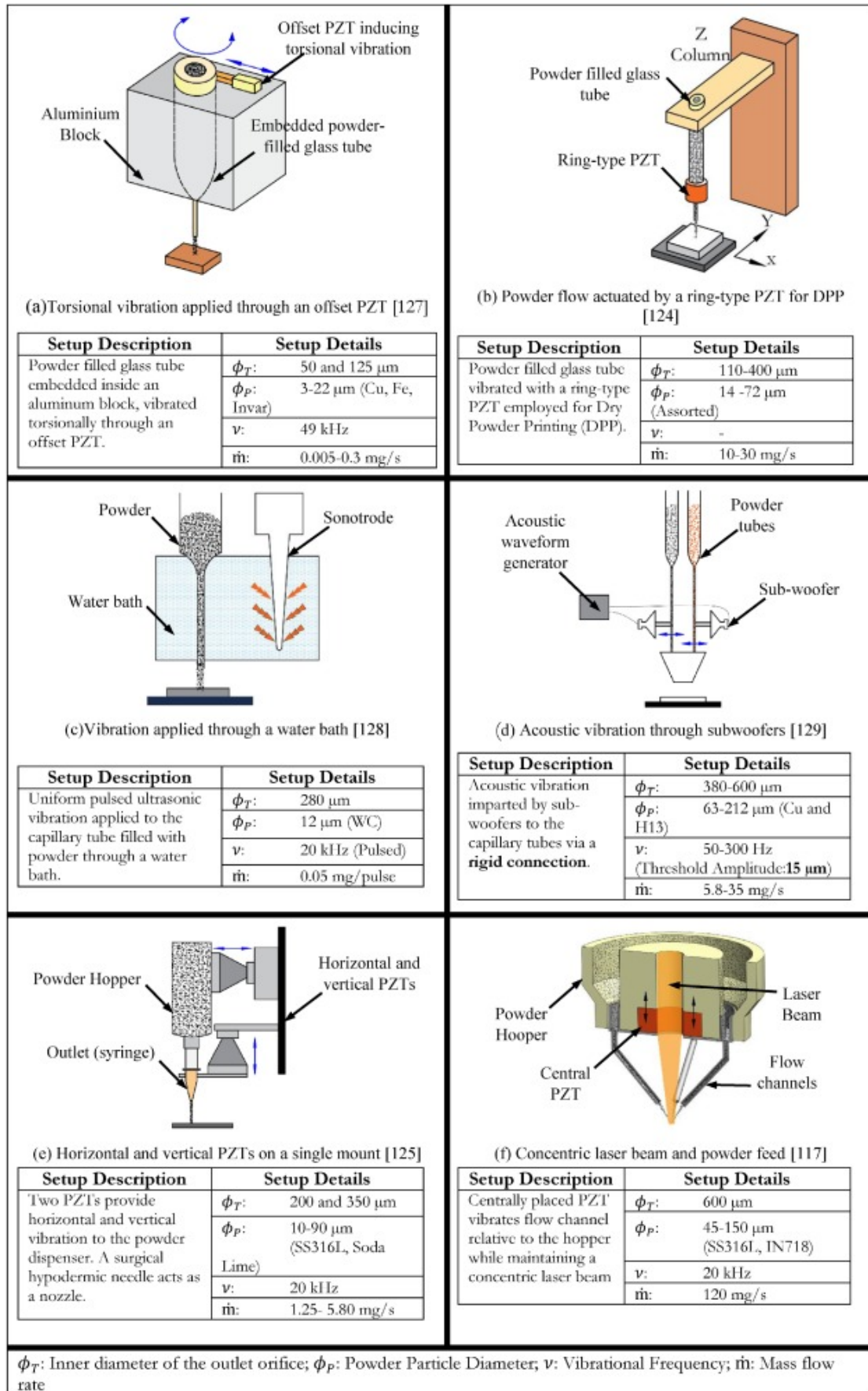


Figure 2-3 Alternative designs to pneumatic powder feeding [6].

The alternatives to pneumatic powder feeding are generally only used experimentally; either to investigate whether these powder feeding techniques can be used successfully, as demonstrated by Wang and Li [19], or to simplify the process so that, for example it can be examined via X-ray imaging to better understand process mechanics [26]. Three different vibrational feeding mechanisms have been identified. The “sealskin” mechanism is where the coefficient of friction is reduced for powder travelling forwards compared to that holding it in place, hence vibration moves it forwards. The “jerk” mechanism moves backwards more slowly than it moves forwards, causing powder to move forwards [27]. More recent research has investigated the use of combined radial and jerk vibration. This is done by using radial vibration to lift the powder away from the conveyance surface while it is moving backwards [28], but this has not yet been examined in relation to DED. The most notable research in this area is from Wang and Li, who demonstrated coaxial vibrational feeding leading to a very high deposition rate and excellent catchment efficiency (reportedly close to 100%) [19]. Chen et al. used a vibrational system to better understand the melt pool dynamics, although they suggested that it did not allow sufficient powder velocity for material to enter the melt pool [29]. Vibrational feeding is therefore a research area which requires significantly more investigation, given the success of the few studies which have examined it.

It is clear that current open-loop solutions to gas fed powder DED require further development, making closed loop solutions a popular research area, whilst vibration and gas-free solutions show promise [6]. Thus far, controlling powder after it has left the nozzle annulus has not been attempted, therefore this is an area of possible future interest.

2.2.3 Coaxial Powder Nozzle Designs

Coaxial nozzles are more commonly used in industry than lateral (or side feeding) nozzles as, unlike in lateral nozzles, deposition is consistent in any direction within the XY plane, offering higher versatility. Side feeding nozzles have been shown to cause asymmetry in depositions when powder velocity is high [30]. The powder feed direction and strategy is also important in side feeding nozzles, whereas coaxial nozzles are omnidirectional and hence are more useful to industry [6]. Moreover, powder catchment efficiency in side feed nozzles is also reduced (by around 15%) [31]. Hence this work mainly focusses on coaxial nozzle designs.

There are several different designs of blown powder coaxial nozzles which are used in both industry and research. Aitzol et al. summarised these designs into two categories, namely discrete coaxial and continuous coaxial and discussed the differences in patents in this area in

2011 [32]. Discrete coaxial nozzles are those which use several separate orifices to deploy the powder, these nozzles are commonly referred to as LENS (Laser Engineered Net Shaping) in the research community. The different nozzle designs are shown schematically in Figure 2-4. Continuous coaxial nozzles are those that use a single orifice which surrounds the energy source. Discrete nozzles are considered to be cheaper, whilst coaxial nozzles are more complex, but offer greater powder concentration and therefore greater powder catchment efficiency (60.1% in discrete nozzles compared to 85.4% in continuous ones, according to Ramiro-Castro et al.) though discrete nozzles are not susceptible to catchment efficiency reduction when tilting the nozzle [33].

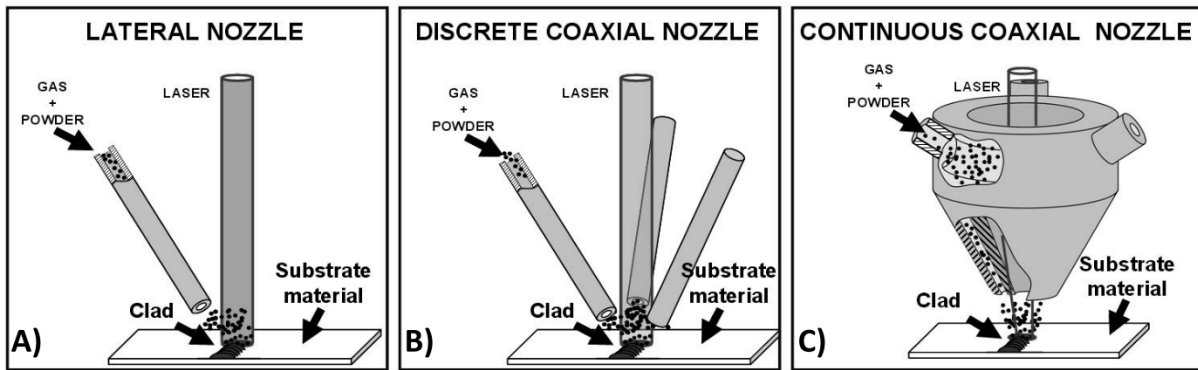


Figure 2-4 Typical different nozzle designs as discussed by Lamikiz et al.[32].

Within the field of continuous coaxial nozzles designs generally alter either the cooling, the outlet angle and concentration of powder, or the use of shielding gas to redirect powder outside the nozzle [32]. The most common design of continuous coaxial nozzle uses a pair of nested coaxial cones. These cones must withstand high temperatures without melting or deforming, they must also exhibit wear resistance to ensure the flow of powder does not erode the nozzle geometry. The nested cones are used to focus the powder stream at a focal point. Ideally the focal point of the powder will be at the melt pool (on the substrate surface). Varying the angle of the inner and outer cones changes the distance at which this focal point occurs [6]. The gap between the two nozzles (annulus distance) is also important, a gap distance between 0.5 mm and 1.5 mm is common. A larger gap reduces the chance of blockage, whilst a narrower gap ensures a narrower powder concentration distribution as described by Pinkerton et al using the equation [34]:

Equation 2-1
$$\omega = \frac{2(r_o - r_i) \tan \theta}{r_o + r_i} z$$

Where ω is the stream width, θ is the cone angle, z is the stand-off distance and $r_o - r_i$ is the gap width. As a narrower powder focus is associated with improved catchment efficiency this dimension is critical in the design of nozzles.

Some works have associated stand-off distance with powder catchment efficiency directly, whereas a better approach is to consider the powder feed angle and stand-off distance together as shown by Pinkerton et al. [35]. Otherwise the analysis will only capture relationships for the specific system which cannot necessarily be extended to other nozzles. Eisenbarth et al. showed this best by examining the powder capture in a pinhole using two different nozzles with varied stand-off distances [36], also developing a simple technique to assess powder focus.

Several modelling methods have been used to determine how nozzle design can be improved by modelling the outcomes of nozzles. Zekovic et al. proved the importance of gas flow as a protection mechanism for lenses [37], though this has been used for some time. Additional shroud gas flow channels have been theorised to compress the powder stream and many patents have been published which include this feature [32], though it is primarily intended to ensure that deposition takes place totally inside inert gas [6]. The use of powder guiding features such as channels has been shown to improve the powder trajectory and catchment efficiency in continuous coaxial nozzles (the necessity of these channels is discussed further in 2.3.4) [32].

A new innovation from Kuznetsov et al. proposed a coaxial laser with axial powder feeding. Using this method, the laser is directed from around the central axis, whilst the powder is fed directly along the central axis. Theoretically, this means that a much higher proportion of the powder will be directed into the melt pool [38]. Later work has shown that catchment efficiencies over 80% are achievable using this technique [39]. Crucially, this method improves upon existing technology by achieving good bonding at the clad edges without compromising on powder catchment efficiency. This works lay the foundation for a new design of nozzles which may make significant improvements on those which currently exist, though more work is required to fully understand and characterise how this may change depositions.

Clearly much attention has been given to the nozzle design to improve catchment efficiency and track geometry, with recent innovations such as coaxial lasers being particularly successful. However, even with exceptional nozzle design there is still inconsistency in track

geometry and catchment efficiency can still be improved. One method to improve upon these metrics is using adaptive control, this will enable more controllable deposition.

2.2.4 Wire Feeding

Though not the primary focus of this work, wire fed LDED is a common and useful alternative to using powder feedstock. Wire feeding is advantageous when high machine productivity is required, enabled because material deposition rates in wire feeding are typically greater than in powder feed systems (up to 48.0 g/min [40] compared to 19.2 g/min in a high throughput powder feed system [41]). Therefore, wire feeding is often used to make very large components, where using powder feed would take a prohibitively long time. The surface roughness is also generally improved because all of the feedstock is entirely melted, whereas poor surface roughness is caused by partially melted powder attaching to the surface of tracks in powder DED, though re-melting has been shown to improve surface finish both by re-melting partially melted powder and reducing stair step effects [42]. In wire LDED the material utilisation is also considerably improved, with catchment efficiency being close to 100% whilst material is often cheaper in wire form and easier to handle even in difficult environments, as discussed by Watson et al. [43]. However, these advantages are accompanied with a loss in resolution, because tracks created using wire LDED are typically much larger than those produced using powder. Fundamentally the geometry of the track is entirely limited by the size of the wire. This disadvantage is often considered to outweigh many of the advantages of wire feeding as fine features may not be produced and significant post machining will be required [40]. Demir used wires with a diameter down to 0.3 mm to reduce the layer heights from 2 – 19 mm to 0.3 mm, thereby significantly improving process resolution, but this is dependent on using wires which have high stiffness [44].

Like in powder LDED there are a number of methods for feeding the wire into the melt pool, with both side feed and coaxial methods being possible. As in powder feeding the side feeding direction changes the process characteristics in wire LDED. Feeding from the front of the melt pool has been shown to allow a greater wire feed rate to be used and is more common, whereas feeding the wire into the back of the melt pool is sometimes more stable. Ding et al. conclude, from a review of the literature, that the stability under different wire orientations depends on the material of the wire [40]. This is in part because the wire tip should remain in constant contact with the same region of the melt pool and if this changes during deposition the mechanism of droplet transfer can change significantly, this in turn changes the track quality. Closed loop or hybrid solutions, such as resistive wire heating have

been suggested as solutions [45]. Coaxial wire feeding is also becoming more common as the technology improves. This requires complex beam shaping in order to surround the wire with the laser beam, allowing material to be deposited independently to the direction of travel without the use of complex control algorithms [46]. Due to the limited resolution and high distortion in laser wire DED the process is mainly limited to creating components which are near-net shape, but may require significant machining.

The process advantages mean that wire LDED heads are widely available, but the component quality issues mean powder LDED is more common. There are many potential avenues of research in laser wire DED as a result. Hybrid systems have been proposed to improve component quality by machining between layers [47] and early research into closed loop control over parameters has shown that this can improve the consistency of the process [40]. Combining powder and wire DED has also proved to have potential uses for creating novel materials [48]. However, in general, methods such as wire arc additive manufacturing (WAAM) improve upon the advantages of wire LDED by having even greater deposition rates [49] and are now used to make large components; whereas powder additive manufacturing methods have much greater resolution. By better controlling the flow of powder in laser powder directed energy deposition, it may be possible to improve both powder catchment efficiency and improve the process resolution. This would bring together many of the advantages of different DED processes.

2.2.5 Adaptive Control Techniques

Wang et al. recently contributed a comprehensive review of adaptive control techniques in the deposition of both powder and wire DED. In this review it is suggested that more widespread use of LDED has been impeded by the lack of geometric consistency within the process [50]. Adaptive control is generally used to improve the process stability, this is normally done by monitoring the process and predicting the outcomes based on the measurements of either the process outputs or measurement of the inputs. Parameters may then be adjusted to improve or change the outcomes to achieve the desired outcome in a stable manner. Fundamentally, adaptive control requires a quantitative understanding of the effects of parameters on the physical properties in LDED; these are discussed further in Sections 2.3.8 and 2.4.6. Laser power has been determined to be the most influential parameter on LDED geometry, in full factorial experiments [30], and especially as it can be altered rapidly, meaning it is one of the most commonly controlled parameters [50]. This has been shown to be effective by Miyagi et al. who used adaptive control of the laser power to

reduce inconsistencies in width by 51%, when combined with measurement of the thermal radiation [51]. Adapting the scan speed based on the clad height has also been reported as a faster response method of adaptive control, with Fathi et al. using this method to deposit tracks which have greater dimensional accuracy [52]. These semi-empirical feedforward models predict future outcomes based on those that have previously been observed to reduce overshoot and improve response time [53]. However, Haley et al. state that passive stability can be achieved by selecting the correct working parameters and that a greater powder density can passively correct deviations in geometry more effectively [54]. Fathi et al. showed that the use of a feed forward PID controller can be further advantageous, by manufacturing tracks with consistent heights even when the substrate was uneven [52]. Depositing onto uneven surfaces is useful, particularly because thermally induced stress can cause significant distortion in substrates during manufacture. In these works, the scanning speed is reduced to effectively allow control of the quantity of powder which is delivered over a unit length. However, powder feeding has been shown to have independent effects, such as on the depth of dilution meaning altering scan speed may not be the best method to control track stability.

Closed loop powder feeding has been used since the 1990s to ensure that powder feed rates remain stable, [18] leading to a process which is more consistent. However, adaptive control of powder feed rates is less common due to slow response time and lag caused by the length of feeding. A few works have sought to remedy this, as powder feed rate has been shown to affect the geometry of depositions. Most commonly this is done by adapting build parameters based on the expected geometry, for example reducing feed rate at a corner where build up may otherwise occur, as demonstrated by Ding et al. [55], whilst similar models have been used to vary the width of tracks based on geometry using laser power as the input parameter [56]. The powder feed rate can also be adaptively controlled close to the nozzle (to avoid delay issues) using a fast acting solenoid valve to discretely change powder feed rate by sending extra powder to a separate bin [57]. Arrizubieta et al. demonstrated that this method can be used to both effectively stop powder mid-flow and reduce build up when direction is changed. Work in adapting powder flow rate or controlling the powder stream is generally limited however, especially in the case of online adaptive control rather than using expected outcomes based on geometry. Using dynamically altered magnetic fields represents a new method to change the powder flow rate and capture which is as yet untested.

2.2.6 Summary of Process Systems

- Lasers used as the heat source by directing them onto a suitable substrate, this interaction creates the melt pool.
- Most commonly powder is metered and fed using a pressurised inert gas. Though some research has used alternative methods such as vibration feeders. This gas also serves to shield the melt pool from contamination.
- Stable powder flow is important for the process to produce consistent geometry.
- Discrete coaxial, continuous coaxial and lateral powder feeding may be used, only coaxial nozzles offer true directional flexibility. Discrete nozzles may be tilted without issue, but continuous ones offer better catchment efficiency.
- Wire feeding may also be used for higher deposition rates, but with lower resolution.
- Adaptive control mainly focuses on varying laser power, whereas varying material feed rate may be more effective.

2.3 Mechanisms of Material Deposition

To improve the LDED process the fundamental mechanisms of material incorporation and bonding must be well understood. The interactions of the different factors and how they lead to a usable product is described here, so that changes to the process can be understood in context.

2.3.1 Laser Melting & Solidification

When a laser is directed into a solid, a portion of the laser is reflected and some is absorbed by the material (laser energy distribution and attenuation is discussed in Section 2.3.2). This imparts energy as heat into the object in a concentrated area. When the substrate is heated in this manner the heat will conduct through the workpiece in a hemispherical shape, this forms the basis of the melt pool as the matter changes state. Upon melting, fluid convection begins to take place in the melt pool, which has been shown to cause the deepest part of the melt pool to be at the back of the melt pool when the laser source is moving [58].

As the power of the laser is increased and the resulting temperature of a metal increases so will its absorptivity as its conductivity decreases and an oxide layer forms [59]. Trapp et al. showed that powder material more readily absorbs laser radiation [60], whilst Clare et al. showed that powder may be modified to further increase its absorptivity [61]. It is well understood, from laser welding, that when lasers interact with a solid metal there are two primary modes of penetration depending on the energy density used and the interaction time.

Conduction mode takes place when power density at the material is low (under $\sim 10^9$ W/m²), allowing the heat to be conducted to the surrounding material. In the keyhole mode, which is much more efficient, higher energy densities are used (greater than 10^{10} W/m²) this causes a deep weld where material vaporisation occurs, and a cavity forms. This vaporisation and the resulting gas can lead to the production of pores in the material as it solidifies. In keyhole mode the vapour pressure also leads to the expulsion of material [62], this has been shown to be greater at higher energy densities and is undesirable in LDED, as it reduces material efficiency and promotes inconsistent geometry. Pores can reduce the structural integrity of the fabricated component and are therefore undesirable. LDED is therefore performed in the laser conduction mode, with lower energy densities and large spot sizes as compared to other metal laser processing techniques.

After the material has melted the laser heat source is removed (traverses past the region of interest). As the heat is highly concentrated in laser material processing, the thermal gradients are high, and the heat will begin to dissipate quickly, mainly conducting into the surrounding material. The presence of material surrounding the melt pool and its temperature largely govern the cooling rate. Pinkerton et al. showed that Rosenthal's equations can be used to model this conductive heat loss in LDED, showing that this can be used to develop predictive models [35]. As the material cools it will begin to recrystallise. The cooling rate will dictate the material phases which are present in the material as various phases solidify at different temperatures. Directional solidification occurring in the direction of the thermal gradients means that columnar or dendritic crystals forming in the vertical direction are common in the LDED of steels [63] (discussed further in Section 2.5).

The overall mechanisms at play when a bead, and following this a track, are formed are complex and dynamic due to the fast-moving nature of heat and mass transfer during the process. These interactions including their effects on track geometry and properties are discussed further in the following sections.

2.3.2 Laser Attenuation

Where suspended powder intersects the laser beam an attenuating effect occurs, whereby some of the energy in the beam is absorbed by the particles. This effect was long theorised in laser cladding, and comprehensively proven by Gedda et al. [64]. The amount of attenuation is often determined simply by the size of the shadow which a particle casts on the clad zone, therefore it is commonly referred to as laser shadowing. Greater laser shadowing therefore occurs when denser powder streams and larger powder particles are presented.

This shadowing effect can cause the melt pool to stabilise, thus reducing the porosity caused by material vaporisation in keyhole mode. However, the opposite is also true in LDED. High velocity powders entering the melt pool can lead to an increase in gas entrapment, in turn increasing porosity, as has been observed using in-situ X-ray imaging [26]. This introduction of matter and gas means that the melt pool in DED is inherently less stable than in processes such as laser welding, hence the melt pool dynamics in DED can be aggressive, especially when penetration depth is high in keyhole mode.

Gedda et al. measured the energy redistribution in laser-powder DED, showing that when using stainless steel and a CO₂ laser, 10% of the total laser energy is reflected by the powder cloud [64]. The proportion of this energy which is wasted depends on the powder catchment efficiency, as less of this energy is lost when more of the heated particles enter clad. Other factors which play a key role in laser attenuation by the powder cloud include: the particle diameter, with bigger particles absorbing more energy, but less energy compared to their mass; the absorptance of the powder; the wavelength (and therefore source) of the laser [65] and the mode in which melting takes place [61].

Molten workpiece reflectance is also dependant on a myriad of different factors. With some alloys, such as steels exhibiting higher absorptivity at greater temperatures, whilst the opposite is true of aluminium. The thickness of the oxide layer can also increase the absorptivity, meaning that absorptivity is greater when laser power is high, with higher laser power, but reduced with greater scanning speed [66]. Absorptivity naturally increases with greater substrate roughness, as internal reflectance within pits causes absorptivity to approach that of a black body [67] (a theoretical material with complete absorptivity), hence it is common to grit blast substrates before they are used. A small quantity of energy is also lost to convection of the melt pool to surrounding gases, depending on shielding gas parameters which lead to greater or lesser forced convection depending on the flow rate. Although the role of forced convection is sometimes disputed, Gouge et al. showed that when it is included in modelling the accuracy of models is improved [68].

After accounting for all losses, as little as 40% of the original laser power may be used in heating the substrate (much of which will be conducted outside the clad zone) and only 10% may be used to melt the cladding material. Although, absorption values for CO₂ lasers appear to exaggerate the effects of reflective losses when compared to modern fibre lasers with much shorter wavelengths [69]. The distribution of this energy is therefore of critical importance to achieving geometrically accurate depositions. Changes to laser shadowing caused by

differences in the powder flow change the energy provided to the melt pool, hence the consistency of powder flow is important to energy absorption. The effect of changing the powder distribution and flow rate on laser absorptivity has not been well researched, hence this is an area of potential future research.

2.3.3 Laser Power Distributions

Historically, CO₂ lasers have been common in LDED due to the high energy density that they can provide. But fibre lasers have become much more common as they are more efficient than CO₂ lasers at melting metals. The ability to carry the beam via a fibre optic in fibre lasers also enables more system flexibility. The efficiency improvement comes from the difference in wavelength. A CO₂ laser operates at a wavelength of around 10.64 μm, whilst Nd:YAG lasers have wavelengths around 1.06 μm which is absorbed much more readily by metals [5].

The effect of laser power distributions on the quality of LDED depositions has received an increasing level of attention recently. Toyserkani, suggested that circular beams with a uniform (tophat) power distribution may be better for laser cladding using pre-placed powder, as this allows a consistent amount of energy to be deployed to the powder [5]. This is in contrast to with coaxial blown powder, in this case a Gaussian power distribution is normally used. This is because the blown powder commonly has a Gaussian concentration distribution, so using a matching laser power intensity means that the power level is suitable for the amount of powder which is present radially away from the centre. Although in practice the diameters of the laser spot and powder distribution may be different, meaning the difference in distribution does not have the expected effect. This theory appears not to have been rigorously proven, but is commonly applied as is discussed below.

In general, three different laser power distributions are used in coaxially blown powder LDED. Power distributions are classified by their transverse electromagnetic (TEM) mode. These TEM modes apply to cylindrical laser beams and low order modes are generally used in LDED. TEM₀₀ refers to a power distribution which has a greater power intensity at the centre of the beam, these are normally Gaussian in intensity as shown in Figure 2-5. In contrast a TEM₀₁ refers to a power distribution which has its greatest intensity in a ring around the centre of the beam, commonly referred to as donut or ring lasers [70]. The third type of laser power intensity commonly used in LDED, is the tophat power distribution [71]. This distribution is still described as being TEM₀₀, but the intensity drops off much more quickly with radial distance from the centre. A perfect tophat laser beam is one which has a

uniform intensity across the spot, however in practice this is not possible using conventional optics which focus the beam via lenses [72]. In LDED, where highly coherent laser beams are used a diffractive optical element (DOE) is often used to shape the beam into a tophat profile. The beam quality parameter (M^2) is used to assess the drop in intensity, with a value close to 1 indicating that the beam is Gaussian, with a M^2 approaching infinity suggesting that the beam is operating with a tophat distribution.

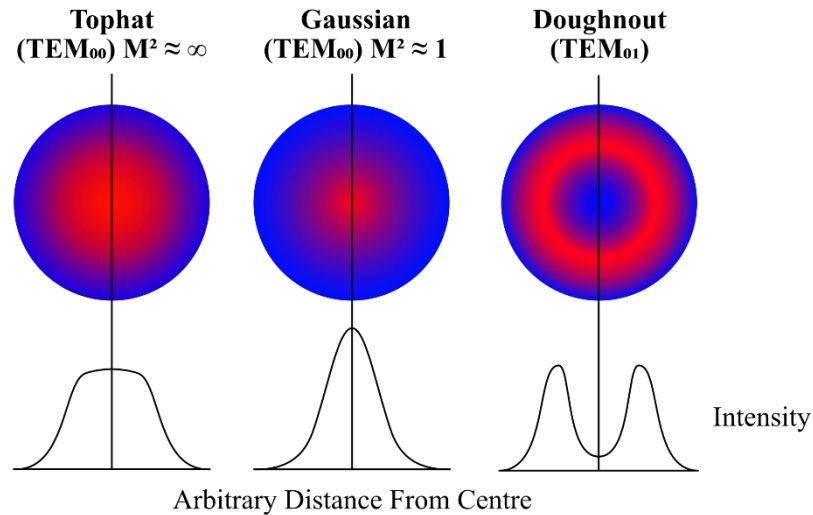


Figure 2-5 Common laser intensity distributions in LDED.

Experimentally, works using the different laser beam intensity distributions in Figure 2-5 show that there is little change in the external (above substrate) geometry due to the power distribution of the beam. Bax et al. showed that fundamental parameter relationships do not change the external geometry with the beam profile when analysing data from the literature [71]. This consistency is likely due to heat transfer causing the melt pool to remain the same shape and the powder being introduced similarly even when different TEM modes are used. On the other hand, the geometry of the dilution zone can change considerably. Goodarzi et al. showed that with a symmetrical Gaussian laser distribution the dilution zone is deep in the centre [30] with many other works suggesting that the deposit may be poorly bonded at the edge of the melt pool [38], although the amount and velocity of incoming powder can also be the cause of inconsistent and asymmetric dilution [30]. It is therefore sometimes preferred to operate the laser out-of-focus to achieve a doughnut shape laser distribution, as is suggested in ASTM F3187 [73]. The effect of these various laser beam TEMs has been confirmed even in axially fed powder with a coaxial (annular) laser beams [39]. In the case of annular beams, it

was also suggested that a distribution between Gaussian and doughnut may be the best solution, particularly as it did not result in a plasma plume, which can deflect incoming powder.

Gibson et al. take this idea further, suggesting that even with uniform energy distribution, as in a tophat beam, an undesirable thermal history can be produced [72]. This is because a circular profile means that the centre of the deposition will receive energy input for a longer duration, leading to a slower cooling rate in the centre and hence larger grains. They also suggest that modifying the energy distribution so that less energy is input at the centre will reduce the doming of beads, meaning less overlap would be required to manufacture thick walls, also potentially improving layer stacking, and reducing the side surface roughness of walls. They used a diffractive optical element was used to generate a beam profile which is square, with much higher intensity on two opposing edges, and a minimum intensity along the centreline between these edges. This was successful in producing tracks which were less domed, and squarer shaped by reducing convective flow within the melt pool. This experiment was done using pre-placed powder to eliminate the effect of using Gaussian blown powder distributions. A few other works have attempted to change the external geometry of laser clad beads by altering the laser beam intensity profile more significantly. Liu et al. used a diode laser to produce a wide laser beam (14 mm x 2.5 mm) which is rectangular in shape [74]. This produced short, wide depositions which would be suitable when applying coatings over a large surface.

To truly take advantage of this new beam profile and create tracks with binary, rectangular cross-sections the powder distribution must be altered. By delivering more powder at the edges of the melt pool it may be possible to create tracks which have still steeper sides and require minimum overlapping. This will reduce processing time and increase productivity whilst also reducing wall roughness and therefore move LDED closer to being a net-shape process.

2.3.4 Powder Distributions in Coaxial Nozzles

Many works have discussed the powder distribution of continuous and discrete coaxial nozzles and how this effects the geometry and properties of LDED tracks. Older lateral feeding nozzles produced a diverging powder trajectory which was not conducive to good powder catchment efficiency (as low as 10% to 40%) as shown by Partes [75]. In discrete coaxial nozzles the many orifices are designed at such an angle so that the powder jets meet at a specified focal distance, this creates a column of high powder concentration which is around 1.6 mm in height (in the case of Zekovic et al.) [37], this is shown in Figure 2-6. In this converged column a Gaussian concentration distribution of powder is apparent. The long focal area created using this method has been proven to allow passive stability in laser

cladding, even when the programmed layer height does not exactly correlate to the actual layer height [54]. Though use of discrete nozzles has been shown reduce powder catchment efficiency compared to continuous nozzles [33], this may be because the powder is more dispersed, although Singh et al. suggested it is due to the greater particle velocity in continuous nozzles [6].

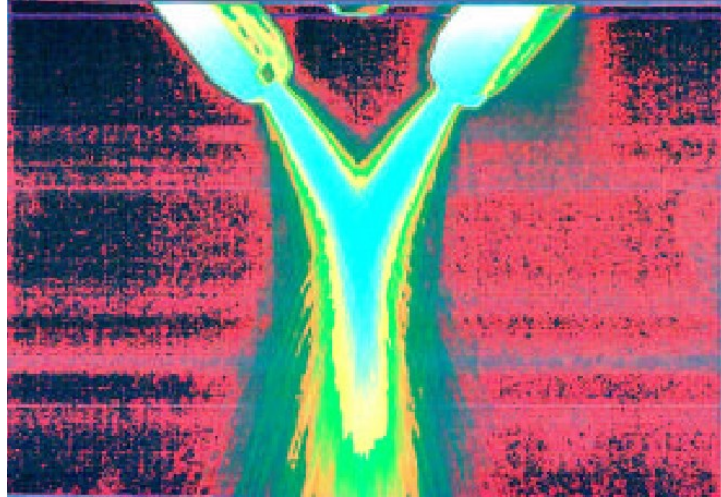


Figure 2-6 Collimated powder stream from a discrete coaxial nozzle. Processed image from Fearon & Watkins [76].

The concentric cones in continuous coaxial nozzles have been shown to result in a consistent convergent trajectory. Powder exits the aperture between the cones in a converging cone shaped stream with a void in the centre. The powder converges into a round spot at a distance from the nozzle. The concentration of the powder at this powder focal point is Gaussian, with the greatest amount being on the central axis. Pinkerton and Li used a geometric-numerical model to correctly predict the distributions at various points along the central axis [34], this is in agreement with similar work conducted by Eisenbarth et al. [36] and is shown schematically in Figure 2-7.

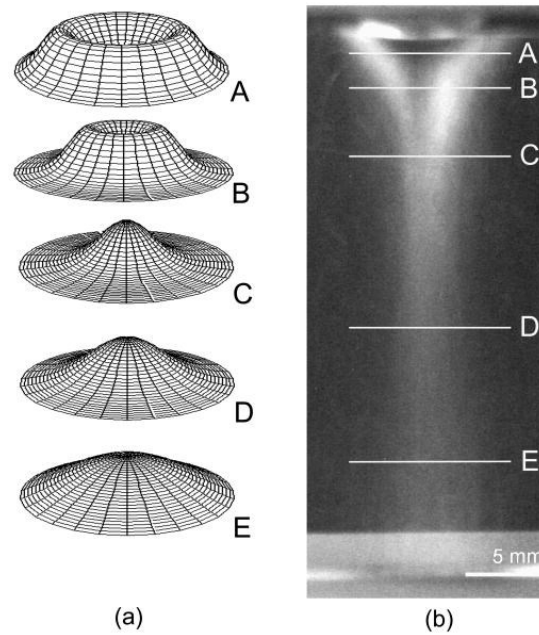


Figure 2-7 Powder concentrations with distance from the nozzle tip; a) showing powder concentration at various points, b) shows a luminance image from the cone tip. From Pinkerton and Li [34].

Naturally, the powder catchment efficiency would be greatest when the powder is concentrated into the melt pool at the powder focal distance (C in Figure 2-7) assuming the ratio of the melt pool diameter to powder focus diameter approaches 1 [77]. Modifying the angle of the powder nozzles alters the powder focal distance, with a steeper angle of injection leading to an increase in the powder focal distance [34]. Arrizubieta et al suggested that powder will only converge in this manner if there are guiding features in the nozzle [78], and a similar effect was observed by Medina et al. [79], but this is likely because a very steep injection angle was used in their work. Consensus suggests that these powder guiding channels are not required to produce a convergent stream, and this has been shown by imaging the powder stream. Takemura et al. used CFD modelling to suggest that the powder focal distance should be shorter than the laser focal distance to improve catchment efficiency, as this will produce an advantageous power distribution. It is well known that operating the laser out of focus can improve deposition [73], though this is often done beyond the laser focal point rather than before it [80].

Notably, many works, such as Fearon & Watkins [76], which use imaging to analyse the powder stream use the light reflected from the powder to quantify powder concentration. However, this may neglect any small particles fractions which cannot be seen due to the difference in brightness between these and the denser parts of the powder stream. This means that the powder distribution is only comparable in terms of brightness and does not account

for rogue particles which will be included in calculations of powder catchment efficiency based on mass.

Modifying the powder trajectory after it has left the nozzle has sometimes been attempted using a secondary gas feed around the edge of the annulus [32] with few results published. Otherwise, no attempt has been made to modify the powder trajectory after it has left the nozzle. Doing so would enable a significant improvement in LDED as the stand-off distance may be changed to match the desired laser characteristics and build up of powder at different locations could be better controlled. This would lead to surface quality improvements which are similar, but more precise than those demonstrated by He et al., where powder flow rate was increased at the edge of bulk depositions to improve the sidewall surface roughness [81].

2.3.5 Powder Entrapment

Following the powder exiting the nozzle and being distributed as discussed in the previous section it should become trapped in the melt pool in order for the powder to be included in the deposition.

Particle entrapment in blown powder DED can occur in three different scenarios:

1. When solid powder is travelling at sufficiently high velocity, it breaks through the surface tension of the melt pool and is absorbed by the melt pool, where it is melted by the heat present there.
2. Particles which interacted with the laser beam before getting to the melt pool and have become molten or partially molten are absorbed on impact with the melt pool, or bond to solid metal upon impact [82].
3. Solid particles with insufficient velocity to break into the melt pool can be captured on the surface of the melt pool [83] (as shown in Figure 2-8).

Naturally, where solid particles strike a cold solid surface no entrapment takes place.

Material with sufficient kinetic energy will ricochet, whilst slower moving particles may stay where they fall, without bonding. Other grains, which are travelling too slowly to overcome vapour plumes given off by the melt pool will be deflected before reaching the melt pool, as shown by Wolff et al. in X-ray imaging [26].

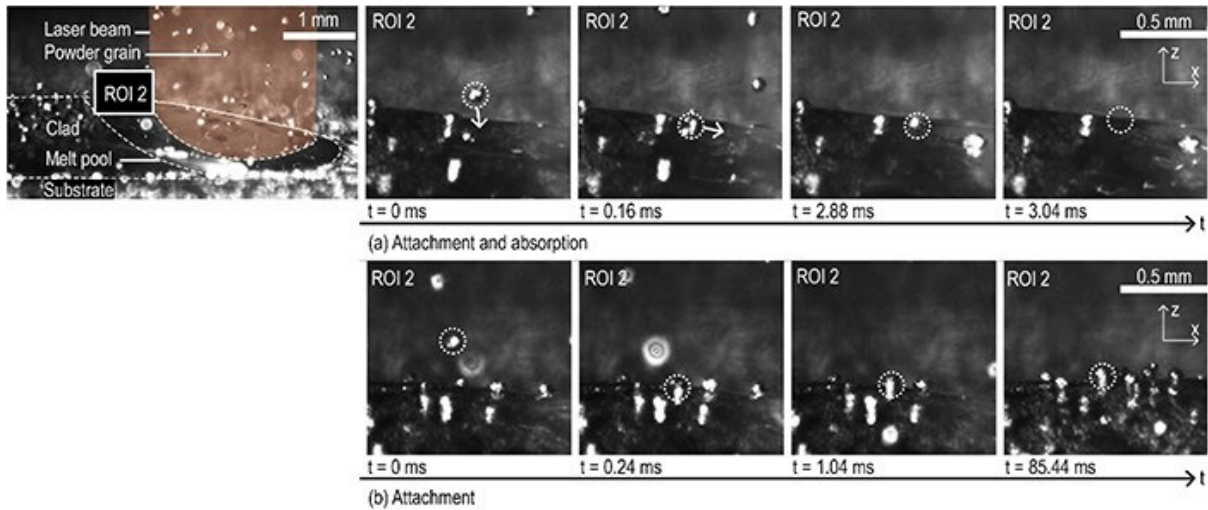


Figure 2-8 Powder Absorption in DED [83].

Particles travelling at a velocity of up to 0.6m/s have been observed to be deflected before reaching the melt pool [26], whilst particles travelling more quickly, at around 1 m/s, successfully enter the melt pool [84]. This necessitates the powder to be fed into the melt pool at speed. This is normally done through the use of an inert carrier gas, although some gravity/ultrasonic vibration feeding has been demonstrated successfully using high powder feed rates [19]. Normally, the effect of gravity on powder momentum is considered negligible when the particles are travelling at least 1 m/s [82], due to the velocity of particles due to carrier gas being significantly greater (commonly quoted as around 2-5 m/s [83]).

Aside from the pressure supplied by the shielding gas, pressure also plays a key role in particle entrapment in DED, vapour plumes have been shown to push molten material out of the melt pool [62], particularly when higher laser powers are used. This vapour plume can also have detrimental effects on powder entrapment, causing particles up to 1mm away from the melt pool, on a collision path to be absorbed to be deflected. The reverse is also true, where particles interact with the laser beam before a subsection of the particles on the “bright side” can be vaporised, with the pressure of this vaporisation propelling the particles into the melt pool at increased velocities (as shown in Figure 2-9), aiding powder catchment [26]. In contrast, when shielding gas is travelling very rapidly hot particles have been observed to ricochet from solid surfaces much more readily [77], the difference between these phenomena is that increasing gas flow also causes the powder stream to diverge, whereas the opposite has been observed when partial vaporisation occurs.

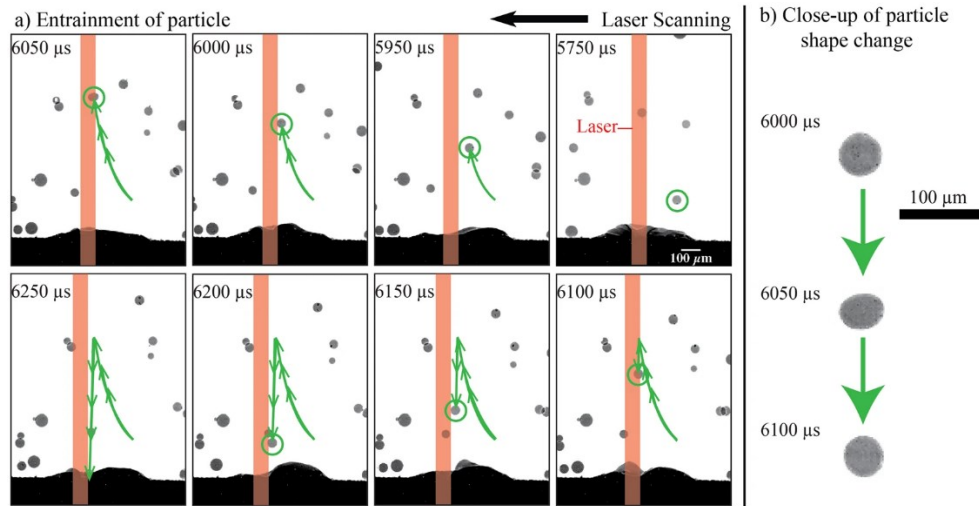


Figure 2-9 Particle Entrainment Via Laser Due to Powder Vaporisation [14].

Those particles that reach the melt pool are all absorbed, previously particles have been theorised to ricochet off the melt pool surface [77], Kovalenko et al. therefore suggests that reducing powder velocity therefore increases catchment [85]. However, high speed cameras have shown that particles which impact the melt pool are readily absorbed [83], more likely a reduction in powder velocity reduces the powder stream diameter improving catchment. Using a bigger melt pool results in the same effect, of increasing powder catchment [76], particularly if this melt pool is larger than the powder cloud at the substrate. A larger pool simply means more of the width of the powder stream will be into the molten pool. Upon being captured by the melt pool, powder grains continue to be affected by the new forces which are present there, as discussed in the following section.

The mechanics of powder entrapment must be well understood in order to effectively modify and improve powder catchment efficiency, as the ratio of powder which is integrated is dependent on the mechanisms of how this takes place. New methods of powder entrapment may be required to continue to improve catchment efficiency, for example by manipulating powder velocity and trajectory as it approaches the melt pool using field forces.

2.3.6 Melt Pool Dynamics

Within the melt pool, motion occurs mainly due to convective forces. The effects of Marangoni convection on melt pool dynamics, motion and cooling has achieved much attention, due to its complex, dynamic nature.

Prasad et al. used a high speed camera to determine how melt pool turbulence affects the motion of particles trapped on the melt pool surface [83]. They suggested that particles

trapped on the melt pool surface will either be quickly accepted into the melt pool after floating on the oxide layer; or the particles form aggregates after moving together, before being incorporated. Some particles were also observed to remain trapped on the surface of the melt pool oxide layer, forming surface roughness. This lends credibility to the theory that particles require sufficient momentum to impinge on the melt pool, especially as those are incorporated in a mean of only 2.97 ms. It was also suggested that particles move at around 0.52 m/s along the melt pool surface, towards the centre of the laser spot, with those that are added at the front of the melt pool always then being incorporated. This suggests that the position of particles when entering the melt pool also affects whether it is absorbed in addition to its momentum and size. The flow patterns are captured when the melt pool solidifies and can be observed in cross-sections of clads readily [86]. It is evident from these patterns, and the theory of surface tension in different alloys, that the flow depends on both the temperature and composition of the alloy being used, although generally similar melt pool geometry can be expected, especially among similar alloys and energies [58].

Marangoni convection is often discussed in relation to LDED. This fluid flow phenomenon occurs when there is a thermal gradient through the melt pool. The central region will be hotter, with decreasing temperature towards the melt pool edge and the solid boundary. This thermal gradient means that there is greater viscosity and higher surface tension at the edge of the melt pool. While the higher temperature in the centre causes this region to expand. The edge of the melt pool therefore exerts an outward force on the central region. As the material is forced outwards it begins to cool, and sink causing a turbulent region to form towards the edges of the melt pool. This is best shown in images from modelling done by Khamidullin in Figure 2-10 [87].

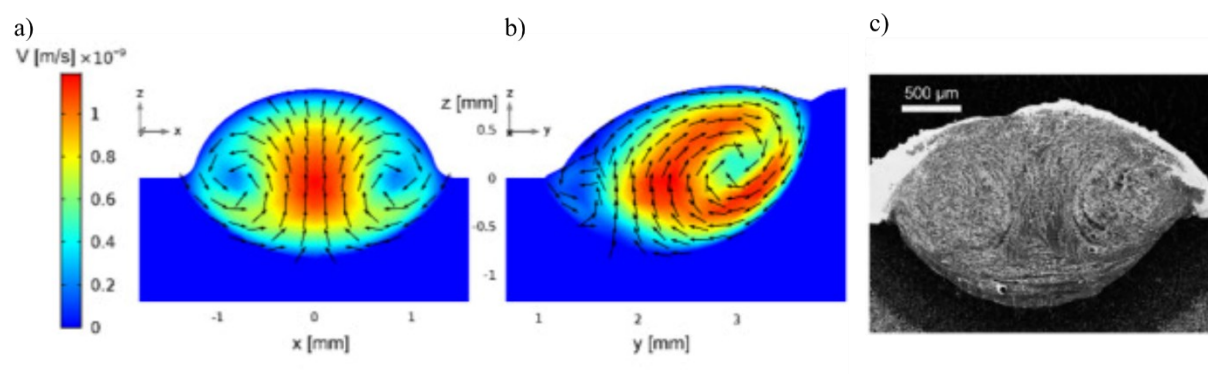


Figure 2-10 Fluid flow due to Marangoni convection; a) and b) from a CFD model of copper, c) showing the grain structure which sometimes occurs as a result. Adapted from Khamidullin et al. [87].

Gan et al. used simulation to suggest how increasing powder flow rate can influence Marangoni flow, changing the geometry of the dilution zone. When powder flow rate is reduced the energy available is distributed over a smaller mass, the temperature and surface tension gradients are greater and hence there is more turbulent flow. Increasing powder flow rate caused the flow direction to switch from an inwards to outwards, leading to a uniform convex dilution zone rather than deeper penetration in the centre. This effect was also observed when altering the energy input accordingly. The change in flow pattern was also shown to alter the sulphur content across the height of the track, where increased Marangoni convection meant more sulphur from the substrate was carried higher into the bead [88]. Recirculation does little to normalise the cooling rates in the melt pool as it happens for such a short time before solidification begins to occur. Hence in single tracks the grain morphology is often inconsistent, as shown in Figure 2-10c. These flows clearly affect the grain morphology in the melt pool in other ways and have been confirmed to increase dendrite spacing in super-nickel alloys [89].

Work by Bachman et al. used a combination of electric and magnetic fields to disrupt the normal fluid flow present in laser welding, showing that the motion of fluid could be retarded and the temperature distribution could be disrupted [90]. This was consistent with CFD modelling they produced. By using Lorentz forces to slow the flow in the molten pool they showed that spatter could be reduced and reduced workpiece deformation. The potential to manipulate the formation of grains in LDED and thereby improve the mechanical properties could be extremely beneficial to the process, therefore this is an area of research which should be explored further.

2.3.7 Powder Rheology

Several works have examined the effect of powder size, quality, recycling and manufacturing method on the directed energy deposition process. These studies have revealed that the morphology of powder can have a significant impact on the end products.

Gas atomised powders are most commonly used in LDED because they are both spherical and cheaper than using other alternatives. In gas atomisation molten material is dripped from a crucible and a stream of gas is used to break the molten stream into droplets and cool the material. The quality of powders is often determined by a few factors: powder porosity, powder sphericity and the satellites present (globules on the particles surface) [91]. Porosity is caused by the presence of the atomising gas in the powder particles and can lead to defects in the manufactured component. Whereas poor sphericity and a high number of satellites

cause poor powder flowability as the particles may mechanically interlock, causing jams [92]. Powder flowability is generally measured using the Hall flow rate, where the time taken for 50 g of powder to run through an orifice with a known geometry. Other test methods have also been developed, though they normally rely on the same principle [93]. This includes the Carney flow method, where a larger orifice is used to measure the flow rate of powders with poor flowability [94]. Water atomised particles can be used in LDED, though generally this is avoided because these powders are plate like in shape and are generally expected to have poor flowability. Though Pinkerton et al. showed that the other characteristics of water atomisation, such as high laser absorptivity, mean that layers bond together better and the microstructure can be more refined [95]. In contrast, plasma atomised powders are highly spherical, but are only available for some materials [91].

Particles between 50 – 150 μm are normally used for LDED [6]; smaller particles (100 μm compared to 160 μm) have been shown to reduce voids and crack initiation [96], likely due to a reduction in gas entrapment. Though conversely, sometimes it has been suggested that too small powders do not have enough momentum to enter the melt pool [97] and therefore reduce catchment efficiency. Smaller particles are often associated with agglomeration, which can cause inconsistent powder flow in the process, forces which have only minimal effects on large particles, such as those caused by electrostatics, have a proportionally greater effect on smaller particles. Whereas larger particles are considered to have better flowability and therefore lead to more consistent geometry. Therefore, selecting the correct size powder is important to the LDED process. Although the size and shape of powders required for directed energy deposition is generally not as constrictive as it is for other metal additive manufacturing techniques, such as PBF the process. LDED is more resilient to poor packing densities and larger powders can be used.

Provided effective powder recycling is possible, improvements to catchment efficiency become less important, as the cost of materials is not truly wasted. A few works have examined the use of recycled materials in LDED, normally this includes powder which passed through the nozzle, but was not consolidated. This powder is then collected and reused. Recycling powder has produced variable results, some indicate that it does not affect the deposition [97], whilst others imply that it is severely detrimental [21]. This has sometimes been reported even in the same material (SS 316L), therefore it is important that the relevant application limiting property is measured directly as although the deposition may appear not have any more defects properties such as elongation failure may be greatly

reduced. Currently, the literature does not reach an adequate consensus on this topic, though it is clear that powders reused up to 10 times can often still be used in both LDED [98] and powder bed fusion processes [99], great care must be taken if the components will be operating in critical applications, because an apparent lack of defects may not mean the performance is equivalent. Most studies do agree that if the powder passes through the nozzle (close to the heat source) then the powder may agglomerate and change shape, reducing the flow rates. But, this is not the case if powder simply goes through the system up to the nozzle [57]. More guidelines on how powder can be recycled must be developed across alloys in order to properly qualify recycled powder for critical applications. It is important that the amount of powder which is utilised and can be recycled is not overstated, resulting in green washing [100]. Therefore, there is still great potential for further research in this area.

Meisnar et al. summarised some of the key metrics and measurement methods which can be used to identify the quality of powder for additive manufacturing [101]. This includes standard test methods and more novel ones. Particle size distribution is the most common measurement done on powders; more recent works normally involves laser diffractometry to determine the percentage volume density of different powder diameters. This is governed by BS EN ISO 8130 the light scattered by a sample of powder is detected by a multi array detector, this is then mathematically converted into a volumetric proportion [102]. This method is advantageous as it can take place in a matter of minutes, using off the shelf apparatus and only 3 – 5 g of powder is required. Laser diffractometry is a useful method as common metrics can be used. The diameter of powder which is at 10% (D10), 50% (D50) and 90% (D90) of the volumetric distribution is normally quoted. This allows for effective comparison between powder sizes provided the distribution of diameters is similar (normally Gaussian). Sieving analysis should be conducted according to BS EN ISO 4497 for spherical metallic powders. When laser diffractometry is not available particle size analysis may be done using this simple powder sieving method. This data is often provided by manufacturers as it requires the least costly equipment. This test requires that 100 g of powder is sieved through successively smaller aperture sizes, the weight of powder which is retained by each sieve is measured [103]. This method makes particle size comparison more difficult because different sized sieves are used depending on the manufacturer. Further techniques for particle size analysis use microscopy, BS 3406 suggests standardised test methods using optical microscopy [104], but in practice SEM is now more common. Meisnar et al. suggest that SEM is the most accurate method of measuring particle size, however the amount of time

taken to measure the particle sizes is prohibitive [101]. Though use of image analysis software can significantly expedite this task. This method also allows standardised proportions to be used (D10, D50, D90), but without mathematical manipulation these will be given as numerical proportions instead of volumetric ones. Therefore, the PSD will be skewed towards smaller particles.

Powder shape, size and the resulting flowability are clearly important factors in DED. As they can change both the materials and processing properties of the technology. Though powder recycling has received some attention, this requires more work to be properly understood. Alternatively powder utilisation efficiency (and therefore powder catchment efficiency) could be improved to eliminate waste before it is allowed to accrue. This may also avoid some of the cost and complexity of qualifying components made from recycled powder.

2.3.8 Powder Mixtures

The ability to change the properties of materials locally was recognised as an advantage of additive manufacturing almost from its conception and has been suggested as a method to create components which have enhanced material properties [69]. Powder directed energy deposition is one of the most promising methods to do this, because the material is fed into the process at the time of deposition.

Several methods have been examined to mix materials in-process. The most common method used is to use multiple powder feeders which feed into a single nozzle, and by changing the quantity of powder fed from each hopper the composition of the feed material can be varied across and within layers [6]. This method has been shown to be effective in grading material compositions gradually between Ti6Al4V and AlSi10Mg, leading to an even distribution when changing the composition in a layer wise fashion [105]. The hardness of the samples was also shown to vary following the grading, showing that the phases and resultant mechanical properties change as expected. This has great potential for uses when different properties are required throughout a material or as bonding layers in weld joints of dissimilar materials. However, additive manufacturing already requires a greater level of evaluation of components than conventional ones [106] and functional grading requires further qualification.

Bespoke alloys may also be created by mixing together powder without functionally grading them. It is relatively common in research to pre-mix powders, so that the desired alloy is formed in the melt pool itself.

Li et al. demonstrated that choosing the correct particle size is important to obtain a well-mixed powder during deposition. When a poorly optimised mixture of powder size distributions was used, separation occurred, but this was mitigated by selecting particles with an optimised diameter. For mixtures of two powders the Equation 2-2 can be used to choose powders which will not separate during deposition [20].

Equation 2-2
$$\frac{d_1}{d_2} = \sqrt{\frac{\rho_1}{\rho_2}}$$

Where d_1 and d_2 represent the powder diameters and ρ_1 and ρ_2 represent their densities.

However, the option of optimising particle diameters is not always possible. When only a low volume fraction of one element is required, obtaining a mix of powders which have compatible diameters but still allow homogenous melting is difficult. This is because if the powder wt.% in the mixture is low, but large particles are required to avoid separation (due difference in material density) then the melt pool will sometimes receive no particles and an inhomogeneous material will be made. When this is the case composite powders may be used. The use of composite powders, which have two materials bonded together avoids problems of powder separation but comes with additional powder preparation steps. Li et al. demonstrated this concept using nano TiB_2 particles in an AlSi10Mg matrix, but a complex and expensive process of alloying and gas atomisation was required [107]. This led to the SLM processed material having an improved tensile strength of 530 MPa. By using a simpler process Tan et al. showed that they could use LDED to similar effect [108]. The process known as powder satelliting involves using an aerosolised binder to bond a small TiB_2 satellite particle ($<3 \mu\text{m}$) to a larger AlSi10Mg parent particle (15-45 μm). When depositing using this technique a uniform distribution of TiB_2 was produced and the strength of the material was increased. Powder satelliting has seen limited further applications in research. Some of the notable findings from this work includes creating titanium aluminides, resulting in a 40% material cost reduction as compared to purchasing the equivalent alloy powder [48]; and to determine that iron can be used as a grain refiner in Ti6Al4V manufactured by SLM [109]. A similar satellite powder feedstock has been made by ball milling a parent particle of Ti6Al4V with 5 wt.% B_4C for two hours, these powders were shown to have reduced

flowability compared to the parent powder, mechanical interlocking of satellites was suggested as the reason for this [92].

The potential benefits of satellites allowing small volume fractions to be mixed into alloys whilst retaining material homogeneity have been elucidated. Various satelliting processes are therefore beginning to be understood, however much more work is required to properly characterise the effects of using satellite powders on additive manufacturing processes and compare these methods. Properties of satellite powders, such as flowability, have not been systematically characterised, meaning this process has not yet been adopted widely.

2.3.9 Summary of Mechanisms of Material Deposition

- The substrate acts as a heat sink, therefore cooling rates in LDED are typically high. LDED should take place with the laser in conduction mode.
- Only a small portion of the laser energy melts the input material due to attenuation from the powder cloud and the reflectance of the material.
- Laser power is commonly Gaussian in distribution, though donut lasers may give better dilution at the edges of depositions. Sometimes lasers are operated outside of the focal distance to achieve this.
- Powder distribution is also Gaussian in distribution from coaxial nozzles and converges at a focal distance.
- Either the powder or the substrate must be molten for powder to become trapped. The speed of powder and carrier gas flow rate must be optimised to ensure entrapment.
- Marangoni flow occurs in the melt pool, this may be retarded by electric/magnetic fields.
- Powders should be spherical and be between 50 – 150 μm to achieve high flowability.
- Both the density and diameter of powders determines whether mixtures will segregate, satelliting may be used to mix incompatible powders.

2.4 Physical & Processing Quality in DED Products

2.4.1 External Track Geometry

Many works exist which link the geometry of tracks to specific parameters in the LDED process. However, these are commonly inconsistent, and it has been suggested that this may depend on the specific design of the machine being used. Though some works have made generalised statements based on the available literature [71]. Figure 2-11 shows some commonly used measures of track geometry.

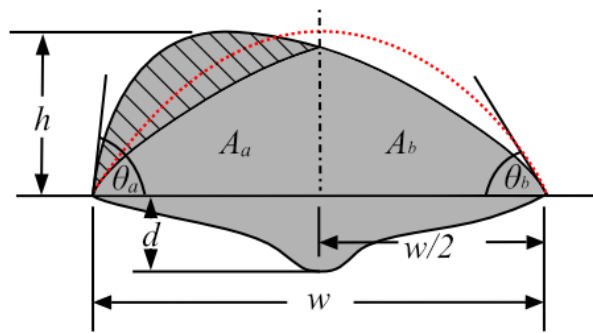


Figure 2-11 Schematic of measurements of track geometry. Where h is the deposition height, θ are the wetting angles of either side of the track, A is the area of the track cross-section, w is the track width and d is the depth of the dilution zone.

The literature is generally in agreement that an increase in the laser power or laser spot size leads to an increase in the width of tracks produced [110–114]. This is due to the increase in available energy creating a larger area which is at high enough temperature to melt material. The track bead spreads to the width of this melt pool due to gravitational pressure. The increase in power also increases the size of the dilution zone, as more energy being available naturally leads to an increase in both the depth [111] and width of the melt pool below the substrate surface. More energy is available to melt the substrate even if some proportion is absorbed by the incoming powder. This means that slower scanning speed can also increase the width of tracks, but instead of increasing the energy available, the time that the energy is supplied is reduced when scanning speed is reduced. This results in greater energy per unit length and hence a wider track [71]. Given this fact, a larger laser spot size causes a larger melt pool to form, this also increases track width [113].

The effect of laser power on the height of depositions is more ambiguous. Sreekanth et al. reported that laser power had no significant impact on the height of depositions at two different stand-off distances [111]. Zhong et al. suggest that height actually decreases with an increase in laser power, however their results suggest only a slight change in track height [110]. In contrast to this, Jinoop et al. suggest that when laser power is increased, then the height of tracks also increases [114], this is similar to Zhang et al. who suggested that increasing both laser power and spot size increases track height [112]. This discrepancy may be explained by Ansari et al., who showed that there are parameter regions where power has a greater influence and those where it is less influential on track height [115]. When looking at the literature as a whole, this appears to be true. Works which use high laser powers (around 1 kW or higher) tend to suggest that laser power has little influence on track height. Whereas

those which use lower laser powers (<1 kW), suggest that increasing laser power leads to a large increase in track height. This is most obvious in work from Zhang et al. where at some spot sizes the effect of laser power on height appears to reach an upper limit [112]. This difference is due to the deposition rates at which the effects are studied. LDED is sometimes split into two categories: high deposition rate (HDR) and low deposition rate (LDR <0.5 kg/hr or 8 g/min). The process is often expected to behave differently depending on the deposition rate, although there is sometimes overlap between the two, as such power has a much greater effect on track height in LDR. In general experiments in HDR do not show that laser power has a large effect on track height. Instead powder feed rate (\dot{m}) is considered to have the greatest effect on height [71].

Scan speed (v) is also considered to be an important factor. As both feed rate and scan speed are time dependent, the combined parameter of line mass (\dot{m}/v) can be used to better predict the height of tracks [75,111]. Line mass is therefore the quantity of powder which is deposited over a given length. Using line mass allows comparisons to be made when both scanning speed and powder flow rate are varied. Conversely it also allows line mass to be kept constant while one of the constituent parameters (e.g. powder flow rate) is varied, to ensure that the same quantity of powder is deposited at different scanning speeds.

In contrast to in other laser additive manufacturing processes simple measures of volumetric energy density such as global energy density (GED) is not considered to be a good predictor of melt pool dimensions [116]. This is because laser power and powder flow rate have different types of relationship (linearly increasing vs exponentially decreasing) with melt pool dimensions. Unlike in other additive manufacturing processes, the effects of laser attenuation in the powder cloud the variations in powder density therein mean these make GED a bad indicator of melt pool geometry.

Other combined parameters exist, such as $P \cdot v^{-\frac{1}{2}}$ which can be used to predict track width [71]. These other combined parameters are not in common usage, but can be useful for predicting track geometries. In addition to track width and height, the aspect ratio of tracks is sometimes used to compare the size and shape of tracks [33]. This is generally only useful for comparative purposes, as the factors which change these variables differ.

Apart from the height and width, the shape of tracks is particularly important to ensure that when successive tracks are overlapped voids between them are minimised and the bulk product is fully dense and well bonded. Wetting angle has commonly been used to assess the

shape of tracks [5]. The wetting angle is defined as the angle between the substrate (horizontal) surface and the angle tangential to the side of the track. This is shown schematically in Figure 2-11 and is commonly referred to as θ . Some works have successfully linked wetting angle to parameters or a combination of parameters. In their foundational work Toyserkani et al. suggest that the wetting angle is related to the interfacial surface tensions which are present around the melt pool. Changes to the balance of these surface tensions are expected to cause greater or lesser spreading of the melt pool and hence change the wetting angle [5]. However, in practice this relationship is not generally considered in research because the temperature of the melt pool, the materials and oxides present will considerably alter the substrate wetting. As each machine and process parameter will differ based on the specific use case, study of the interfacial energies is rarely applied practically. Instead, the wetting angle is more readily modelled by linking it to combined parameters [117]. In experimental research it has been shown that an increase in the laser power or scanning speed will reduce the wetting angle of the track, and an increase in the powder flow rate will increase the wetting angle. This is because any increase in the power will increase the size of the melt pool, allowing the melted powder to spread over a wider area, whereas any increase in the line mass will cause more powder to be present over the same melt pool area, causing the track to bulge upward [110]. Hence, the wetting angle is best described using the combined parameter $P^1V^{-1}F^{1/2}$ and a linear regression model [115]. Wetting angles can be optimised to reduce issues with defects when overlapping tracks, the optimum angle is between 30 – 70°. However, as stated by Bax et al. in practice the wetting angle is a poor measure of track geometry [71]. This is because wetting angles are often inconsistent and can be much more ambiguous than when shown schematically. Furthermore, equations which are sometimes used to determine the wetting angle (such as Equation 2-3) assume the track is round instead of measuring the angle, comparison between measured and calculated wetting angles is less meaningful. The wetting angle also does not qualify the overall shape of the track, only the angle of the edges. Therefore, Bax et al. suggest an alternate combined measurement of w_s^2/A_c where w_s is the width of the contact of the track with the substrate and A_c is the proportion of area occupied by a cross-section of a track in a square. Where the square is defined with w_s as the bottom side. The larger this measurement the less chance of defects, although a value of 3.5 is suggested as a good compromise between track size and shape. This parameter is a useful measure of the track shape, but is difficult to comprehend without extensive analysis and experience, so has not yet been fully accepted into the literature.

Equation 2-3 $\theta = \arcsin\left(\frac{H}{\sqrt{W^2+H^2}}\right)$ [118]

The measurements discussed above are generally considered to describe the external geometry of LDED clad tracks. These will be the initial considerations where external geometry is discussed throughout this work. Some works also discuss the skewness of tracks which is dependent largely on other factors and is discussed in Section 2.4.2. Furthermore, there are a few other measures which are used to characterise other aspects of depositions, these are described further in the following sections.

2.4.2 Skewness

The skewness of a DED track refers to how symmetrical the track is along its length. If a track is skewed the cross-section will show that there is more material on one side of the centreline. Skewness is rarely studied directly, however a few examples of this measure being used exist in the literature. The measure is important for a few reasons. Firstly, if a track is significantly skewed to one side of the centre then as successive overlapping tracks are added there will be greater build up on one side [36] and voids may be expected on the opposite side. Also, as skewed tracks are stacked to create thin (or thick) wall structures the sidewall surfaces will be poor [81] and the successive layers may not bond together properly, there will also be a loss in the accuracy of the wall and the side wall surface will not be smooth.

Skewness has mainly been investigated for tracks on inclined surfaces. However, Eisenbarth et al. showed that if the coaxial flow of powder is not well aligned to the laser beam skewed tracks will be manufactured [36]. To improve the laser-powder alignment a simple method to determine the alignment was realised using a small orifice and a load cell. In the Standard Guide for Directed Energy Deposition of Metals (ASTM F3187) [73] the importance of nozzle alignment is also discussed, showing its importance. Most nozzles allow some change to their alignment, so provided alignment is systematically checked this should be easily achievable.

Aligning the powder flow with the laser beam over inclined angles is more difficult. When using continuous coaxial nozzles the powder stream has been shown to become skewed when tilting the head, whereas Ramiro-Castro et al. showed that this is not a problem with discrete nozzles [33]. Lin and Hwang also showed this by measuring the luminance of the powder streams at different inclination angles, they showed that at an angle of 60° the peak luminance shifted by up to 0.8 mm [9]. 0.8 mm is a significant margin when laser spot sizes can be in the order of magnitude ~1 mm. Various studies have shown that tilting the nozzle

causes a skewed track to be produced at varying inclination [7,8,119]. However, the track skewness is often blamed upon the effect of gravity on the molten pool. Even though the pool is only molten for a very short duration. Some works have suggested that gravity effects the balance of surface tension in this pool, causing the skewness [7]. But, changing the powder concentration has been shown to change the track geometry [81]. Decoupling the two effects has not been attempted for an inclined substrate, this is therefore an area of potential future work.

Different measures of track skewness are used, the most common of these is to take the cross-section of the track and measure the distance between the centre of the track and the peak [8,120]. Though Lin and Hwang use a slightly altered method, where rather than measuring the offset from the centreline, the distance from the peak is measured (D) and the total width (w), they then calculated an offset factor (D/w) [9]. These methods are not very robust, because there is significant variation in the peak placement even on flat surfaces, also they do not properly identify the volume of material which is asymmetric, just the area in one slice. Localised deviations can play a large part in these measures. Alya et al. used a more robust measure, where percentage skewness is determined by calculating the percentage of the total cross-sectional area either side of the centreline, thereby considering all the material not only local peaks [7]. However, all of these methods use slices of the track only, so there is potential for the data to be unreliable unless a very large number of slices are used.

2.4.3 Dilution

The geometric definition of track dilution is the material added which is below the surface of the substrate in the first layer. The optimum dilution depends on the use case, in traditional laser cladding where coatings are required, generally low dilution is required so that both the coating and the substrate material remain compositionally independent. This is desired because the coatings are required to have different properties to the bulk material. In contrast, in additive manufacturing a greater level of dilution is normally intended, this indicates that the track is well bonded to the substrate. Also, greater dilution implies that successive layers will be well bonded, thus improving mechanical properties in the direction of the build [5]. There is no standardised measurement for dilution zone size or shape. Depth of the dilution is commonly used, this is useful in that it gives some indication of how well bonded the track is to the surface, but reduced dilution is common at the edges of clad tracks [121] especially when using common gaussian laser distributions [38]. Therefore, it is more helpful to use the area of the dilution zone to determine the bonding, this is a better measure than depth,

because where there is deep dilution only in the centre of the clad tracks this will be better reflected [30]. Sometimes the dilution zone area as a proportion of the total track cross-sectional area is also used, this helps quantify whether adequate dilution has been achieved considering the overall size of the track [121]. Ideally the optimum shape of dilution zone is one which exhibits uniform depth across the width of the track. However, in practice this is unlikely, because surface tension and convection currents in the melt pool dictate the melt pool shape along with the laser power distribution. Therefore, even when using donut laser distributions, greater dilution still occurs in the centre of the track [6]. Defects with the dilution zone often refer to the shape rather than the size. Lange et al. characterised the different dilution zone shapes and which of these may be preferred. Four types of dilution zone were identified: limited dilution, where the track appears to sit on the substrate surface; symmetrical burn in, with a deeper dilution zone in the centre; double peak dilution, where there is a maximal dilution size either side of the centre; and asymmetric dilution, where the peak is greatly offset to one side of the centre [80]. Lange et al. suggest that asymmetry is caused by the high powder velocity of side feeding nozzles causing an increase in pressure and pushing the dilution zone away from the nozzle. Goodzari et al. suggest that Marangoni convection is the cause of the double burn in shape and is dependent on the size of the melt pool and the laser power [30]. Many works have shown that laser power is mainly responsible for the size of the dilution zone, with a few suggesting that there is a more complex interaction at play. Power appears to be the dominating factor; however line power and powder feed rate also reduce the dilution size when reduced. A greater velocity (and resulting momentum) of the powder has been shown to increase the depth of the dilution zone [6]. This has also been shown for off-axis powder feeding, where side feeding causes an increase in the dilution zone opposite the nozzle [30].

If the distribution and velocity of powder could be controlled in a more deliberate way, it may be possible to alter the size and shape of the dilution zone. Making it closer to the ideal shape by manipulating pressures in the melt pool. If convective flows and surface tension could be controlled this may be possible, or if the speed of powder could be increased at the edges a then more consistent dilution may be achieved. A force field may be capable of doing this given the correct parameters. This is a niche area of research which is not well documented, this is discussed further in Section 2.6.

Despite laser power having the greatest effect on dilution size and layer bonding. Practitioners should be wary of simply increasing laser power to attempt to improve

intralayer fusion. Increasing the specific energy can cause the process to operate in keyhole mode, this increases the chance of defects such as keyhole pores which weakens the bond in the build direction. A balance must be found, as keyhole pores have been observed when dilution area increases above 30%, whilst lack of fusion can occur when dilution is under 10% [45] (in the limited dilution case). By dynamically changing laser power and powder feed rate together it may be possible to manipulate dilution more deliberately, allowing practitioners to control the geometry and dilution of tracks throughout a build or change the dilution in a more precisely controlled manner. The use of force fields is an area of future research which may help to achieve this.

2.4.4 Track Porosity

Porosity is a common defect in components manufactured by DED. Porosity is potentially problematic because pores can act as stress risers, encouraging crack formation and propagation. Therefore, it is important to understand how porosity occurs in the process, as well as to understand how pores can be quantified and mitigated.

Studies often quote that builds are “fully dense” this implies that there are no pores or voids in the manufactured track or component [37,95,112]. This description is used to suggest that LDED components are equivalent to cast components and can be treated with a high level of confidence. In truth the presence of pores is highly dependent on the material being used and the processing parameters. Fujishima et al. noted some of the mechanisms of pore initiation in Inconel 625 [122]. They determined that adjusting parameters can often reduce porosity by acting on these mechanisms. It is suggested that incomplete powder melting causes pores to form and therefore increasing laser power can reduce porosity. Furthermore, this relates to the balance of energy and mass, as reducing the powder flow rate has the same effect. They also conclude that an increase in the gas flow rate can increase porosity via gas entrapment. Kuriya et al. suggest that an increase in the solidification time is responsible for this, as it allows gas to rise to the surface and be released [123]. Keyholing should be avoided however, as Webster et al. suggested that increasing the combined parameter of global energy density will also increase porosity [124]. Tan et al. also suggest that gas entrapment from moisture evaporating may be a cause of circular pores in stainless steel [125] and noted that most pores are present closer to the top of multi-layer depositions, suggesting that re-melting aids void removal.

Common engineering steels and nickel superalloys have their composition adjusted to reduce pore formation and growth. For example, even commercially pure nickel alloys contain 1.5%

aluminium and up to 3.5% titanium to restrict pore formation through the formation of solid oxides when used in welding [126]. This is due to nitrogen and oxygen having low solubility in nickel, but the addition of aluminium and titanium improves this, allowing the nitrogen to form a solid solution. Alloys in more common usage include other components which reduce porosity further. High porosity is not generally expected in the deposition of high toughness steels which frequently used in this work, with porosity of below 0.4% being produced when using parameters which are not significantly optimised [70,127].

Khanzadeh et al. used in-situ imaging to determine the shape and cause of pores and help to predict when they will appear [128]. They propose using porosity prediction based on melt pool temperature and shape monitoring instead of through destructive testing or time consuming X-CT. Importantly, the study identifies that porosity can be reduced through parameter optimisation without online monitoring. They noted some major pore contributors including: lack of fusion due to insufficient track overlap, and keyhole porosity where deep melting causes vaporised elements to become trapped. Hosseini et al. showed that pore size and shape depends on its formation process, they show that gas pores can form at high cooling rates as gas does not have time to escape the solid lattice. Shrinkage cooling is also shown to be a factor, where different cooling rates cause different shrinkage rates in certain phases, leading to voids [129]. In the alloy used (LM13) higher cooling rates (5 – 50 °C/s) produced a 0.8% area fraction reduction in porosity. They suggest this is because the grains produced at higher cooling rates are smaller, leading to fewer shrinkage pores. The samples with fewer pores demonstrated a higher tensile strength, showing the importance of manufacturing fully dense components.

Going beyond parameter optimisation, novel research from Zhang et al. has shown that the use of electric and magnetic fields can change the percentage porosity and distribution in DED tracks [130]. By using these fields, a force is exerted on the gas in the melt pool. This is then used to either retain the pores or force them out of the molten pool depending on the field orientation. With a current of 120 A the porosity could be reduced by 65% or increased by 144% which also increased track height. There is potential that this method could be used to produce porous structures using DED, a potential area of future research.

2.4.5 Surface Quality

Surface roughness analysis is not normally of primary interest in the literature on LDED, this is because the process is generally considered to be near-net-shape, meaning final machining will be required, which will produce the final surfaces. This is primarily because the large

layer size and use of powders with large diameters results in both high waviness and roughness compared to other metal manufacturing methods [11]. Study of surface quality in DED is therefore performed either to help to understand the underlying mechanisms better, or to push the process towards net shape capability.

In powder LDED surface roughness is attributed to partially melted particles being present on the surface of the tracks. The mechanism by which this takes place has been assumed [131] for some time, but was confirmed by high speed imaging by Prasad et al.. They confirmed that when powder is captured by the hot (but not molten) part of the track behind the melt pool it may sinter to the track surface, causing local roughness [83]. Therefore, carefully controlling the powder trajectory could have beneficial effect on surface roughness, but no study has specifically investigated this. This would represent a logical and novel approach to measure the efficacy of such methods, whilst potentially reducing the requirement for post-machining.

Chen et al. show that the average roughness (R_a) is generally poor in LDED and they measured it as at least 100 μm on the surface of tracks [29]. This was shown to increase to 150 μm when process conditions are sub-optimal, in-situ X-ray imaging suggested that this was due to irregular melting and the flow within the melt pool. Higher laser power, traverse speed, or a reduced powder feed rate all improved the surface roughness of tracks, due to the increase in line energy. They suggest that perturbations are larger when the powder feed rate is greater than the capacity of the melt pool, as this increases turbulence in the melt pool. Importantly, this showed that roughness was a metric for other aspects of the process which are harder to quantify, such as melt pool turbulence.

When producing overlapping tracks for bulk deposition there are some common issues which affect AM widely, DED is not immune to these issues. As each track has a round upper surface, when these are combined together, even with carefully selected overlap proportions, the surface will exhibit waviness transverse to the direction of deposition. Ocelík et al. showed that by increasing the overlap ratio to as much as 80% of the track width the absolute waviness could be reduced from 0.316 to 0.249. However, increasing overlap ratio also increased the height of deposition by 3-4 times, reducing the vertical resolution [132]. Similarly, when creating components which have sloped (rather than vertical) surfaces the stair step effect means that surfaces are wavy along the slope, this becomes worse at shallower slope angles. Rombouts et al. proved that by re-melting the top surface of flat component the waviness could be dramatically reduced [42], as the individual tracks merged

into one cohesive surface. Using this method, the waviness in the direction transverse to the deposition direction could be reduced from over 30 μm (R_t) to around 4 μm , whilst along the scanning direction roughness was reduced from 20 μm to around 2 μm . However, re-melting does reduce the process productivity.

He et al. showed that the powder distribution plays an important role in the sidewall surface finish in LDED. They reason that in the centre of objects the accumulation of material from overlapping tracks means that there is more material there. Whereas, at the edge of components less material is available, leading to an inconsistent amount of powder causing roughness of around 30 μm (R_a). By increasing the powder feed rate by 1.2 times the roughness was reduced to around 20 μm [81].

Innovations in improving the surface roughness in DED products mean that the process is moving closer to being one which is considered to produce net-shape components. Current methods of roughness measurement are not designed for AM processes which have such significant directional differences in roughness. New areal measurements of roughness have been developed, however these have not generally been used in DED, using these new measurement techniques may reveal more about the mechanisms at play in AM and allow surfaces to be more readily related to parameters [133].

2.4.6 Catchment Efficiency

Catchment efficiency is defined as the mass of powder consolidated in the deposition as a proportion of the total mass of powder fed into the system. There is consensus that catchment efficiency is one of the most important processing characteristics in LDED, with it often being suggested that it is the primary characteristic to optimise parameters for. This is because catchment efficiency is a significant driver of cost. A kilogram of unusual powder can be 250 €/kg for industrial customers [98] and Inconel powders are commonly quoted at up to 400 £/kg. With LDED being used to make metre scale near-net shape components [11] this cost quickly accumulates. By improving catchment efficiency and reducing powder wastage the manufacturing and environmental costs can be significantly reduced.

Improvements in catchment efficiency have a potentially significant impact on costs. When a comparatively small 10kg component could have material costs of £5,700 with high powder catchment efficiency (70%) or £20,000 at lower efficiencies (20%).

In addition, Ocelik et al. noted that catchment efficiency fundamentally effects the geometry of tracks to the point where it defines whether the deposition will be stable or unstable [132];

whilst Lin et al. state that poor catchment efficiency is one of the main problems in DED [134]. In addition to governing process stability, track geometry, and quality; catchment efficiency is one of the primary drivers of cost. Especially when expensive materials such as nickel superalloys are used, powder wastage exacerbates existing problems with poor buy-to-fly ratios, because catchment efficiency is often reported to be as low as 30% [6]. Powder recycling is also uncertain, and its efficacy depends on deposition parameters, the material, and its use. Saboori et al reported a 50% reduction in elongation failure when using recycled 316L powder [21] whilst Terassa et al. suggested that the build properties and number of defects were unchanged when recycling the same material [97]. In any case it would be better for powder reprocessing to be avoided and catchment efficiency to be improved. Especially because extra non-destructive testing which may be required when using non-virgin powders is prohibitively expensive [106].

A simple model of powder catchment efficiency was developed by Lin in 1999 [77]. Lin showed that increasing the stand-off distance, or the powder stream velocity reduces the catchment efficiency [135]. Since then, many studies have used parameter optimisation to improve catchment efficiency. Fearon & Watkins showed that catchment efficiency could be optimised by ensuring the standoff distance placed the densest concentration of powder into the melt pool [76]. On the other hand, Eisenbarth et al. showed that too small stand-off can lead to unstable deposition [36]. Fearon & Watkins also investigated the effect of particle velocity on powder catchment efficiency, a topic which is often debated [6]. The effect of powder velocity on entrapment is discussed in Section 2.3.5. Particles that move either too slowly or too quickly are likely to not be integrated into the melt pool. Commonly carrier gas with a velocity between 2 – 5 m/s is used to convey the particles with sufficient velocity [83]. This means that the conveyance gas is supplied at 3 – 10 l/min [76]. Takemura et al. used CFD simulation to show that using a lower gas flow rate (4 l/min) will reduce the powder focal distance by reducing powder velocity. Therefore to ensure stand-off distance remains minimised, lower gas flow rates should be used, leading to an improved catchment efficiency (66%) [136]. Nagulin et al. also showed that higher gas flow rates (above 10 l/min) can lead to turbulent powder feeding which defocusses the powder stream and reduces catchment efficiency [137]. Another parameter which effects powder catchment efficiency significantly is the powder feed rate, increasing the feed rate clearly leads to an increase in track mass [77]. However, this increase in feed rate does not always correlate to an increase in catchment efficiency. Work by both Dias da Silva et al. [31] and Lee [138] suggests that catchment

efficiency does not vary significantly with changing powder feed rate. However, the ratio of laser power to line mass has been shown to do this [121]. This is an expected result, because the balance of scan speed and power change the melt pool size and larger melt pools have been shown to improve catchment efficiency. Saturating the melt pool with an excess of material would also be expected to reduce catchment efficiency and the size of the melt pool, but the introduction of increased laser power alleviates this. In practice, using too great a powder feed rate leads to tracks being improperly bonded, causing them to peel from the substrate, therefore this is easily noticed and eliminated [71,139]. The effect of laser power on powder catchment is twofold, as the increase in power also increases the melt pool size. An alternative is to use novel meandering or trochoidal overlapping toolpaths to increase the heat input, melt pool size and cooling rates, in turn improving powder catchment by 15% [140]. Toyserkani stated this basic concept succinctly as “minimising impact between the solid particles and solid surfaces” [5]; the inverse is also true, by maximising the solid-liquid impact catchment efficiency is optimised.

Using parameter optimisation alone has capped deposition efficiency in conventional nozzle designs to around 55% - 70% [141], whilst this is often as low as 30% [6]. Therefore, some works have attempted to improve the nozzle design in minor or more significant ways, as discussed in Section 2.2.3. The most notable works are those which use a coaxial laser beam with centrally fed powder, leading to catchment efficiency of around 80% [38,39]. However, methods which require complex and expensive laser optics have not been significantly studied yet.

An alternative solution is to change the manner in which powder is directed, this has been done using alternatives to gas feeding with catchment efficiency reportedly up to 100% using vibration feeding [28]. Whilst others have suggested that vibration feeding does not give particles the necessary velocity to enter the melt pool [26]. Further study of novel new technologies is therefore required to improve catchment efficiency further. Manipulating the powder stream so that it is compressed and catchment efficiency improves is an interesting avenue which has been attempted by adding gas flows [32], but future research should find other methods to do this which are more effective and easier to dynamically control.

2.4.7 Summary of Physical & Processing Quality in DED Products

- The width of tracks is mainly determined by the laser power, whereas the effect of power on track height depends also on the deposition rate.

- There are a number of methods to measure skewness, the area each side of the centreline is more reliable than some others.
- LDED can produce fully dense products, though porosity can form in certain alloys or with some parameter combinations.
- The rough surfaces produced by LDED is due to partially melted powder and stair stepping, re-melting may reduce this roughness.
- The size and power of the laser spot greatly influence catchment efficiency. Optimising stand-off distance can help to improve catchment efficiency, though improving nozzle design has also demonstrated this.
- Catchment efficiencies have peaked at around 60 – 70 % in most cases, new methods must be used to further improve this issue.

2.5 Materials Properties of LDED Products

The research gaps highlighted so far show that manipulation of the powder prior to entering the melt pool has a significant effect on the LDED process, though the use of traditional methods of changing this via gas flow has mainly been studied. Novel methods have been proposed here that use magnetic fields to control the trajectory of powder instead.

In this initial work on magnetic control of powder trajectories two classes of alloy are the clear candidates for experimentation. These materials include those that are naturally ferromagnetic, meaning a force may be readily applied to them via a magnetic field. These materials are also widely used in applications which LDED is a contending process for manufacturing. Steel was chosen as the primary research material because it is the most widely manufactured metal and ferromagnetic phases such as the ferritic phase are useful in a broad spectrum of applications. The second class of alloys consists of those which are based on nickel. Nickel is also ferromagnetic and super-nickel alloys are used in high value components such as in turbine engines. Though many of these alloys are not ferromagnetic, this provides an additional avenue of exploration. As LDED is most applicable to low volume, high value production such as for large turbine components, this provides a suitable secondary alloy class to examine. Hence, these two alloy materials will be considered here in this review.

2.5.1 Properties of ferromagnetic steels

2.5.1.1 Material Properties and grain morphology

High strength low alloy (HSLA) steel is used in the nuclear and aerospace industry for its high toughness properties and resistance to fatigue at high temperatures [70]. AISI 4340 steel in particular has been investigated thoroughly in recent years due to its utility and availability. Contributions such as those made particularly from the University of Michigan [70,127,142] have shown that the material is suitable for processing via LDED and the resulting products have been well characterised. 4340 is also a ferromagnetic alloy which has had its magnetic properties somewhat characterised in regards to phases [143]. These studies, and its large range of applications, means that AISI 4340 is a material which is well suited for use in new innovative processes as the results can be compared to pre-existing literature. Other designations for AISI 4340 exist (such as UNS G43400), though the material will be referred to as 4340 here.

From LDED manufacturing of 4340, Bhattacharya et al. showed that the phases consist of Ferrite (α), martensite (γ), and cementite (Fe_3C), with retained austenite being present at the grain boundaries (Figure 2-12) [127]. In Figure 2-12 the martensite appears to mainly have a lath morphology, though plate martensite was also present in the samples.

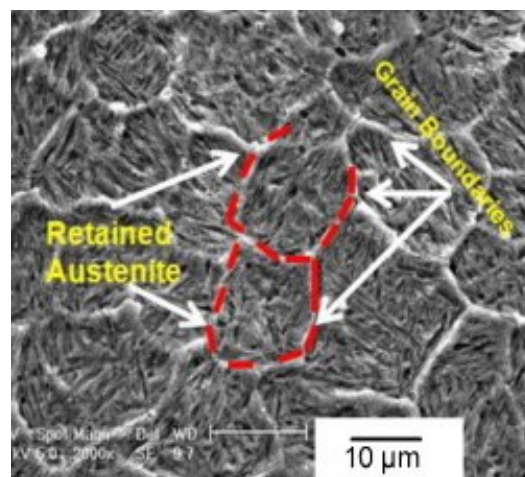


Figure 2-12 Retained austenite in LDED 4340 [127].

The rapid cooling in LDED, due to the small thermal mass under the laser and surrounding material acting as a heat sink, means that metastable phases such as martensite are to be expected. They show that needle shaped martensite is present at the top layer, with rounded, tempered (plate) martensite being present in the lower layers due to thermal cycling.

Hardness was shown to decrease (from 681 Hv to 480 Hv) in the lower layers due to this tempering effect (as shown in Figure 2-13). The high hardness of 4340 produced by LDED is

generally attributed to the presence of brittle martensite formed at high cooling rates [144]. XRD did not reveal the presence of retained austenite, however this is frequently reported as being present, particularly at grain boundaries and in the heat affected zone and is clear in Figure 2-12 [17,70,127,142,145].

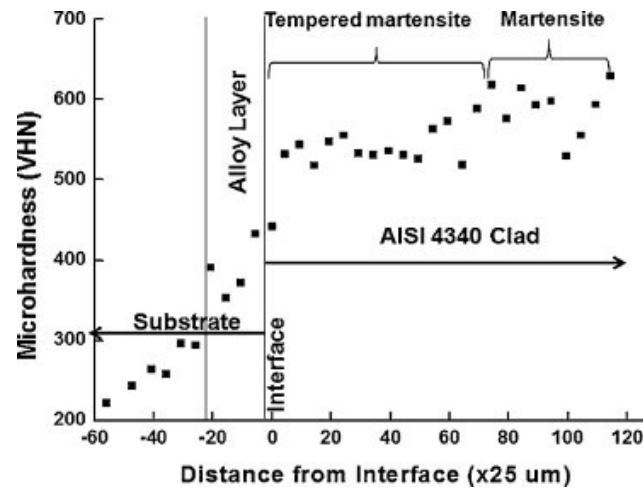


Figure 2-13 Hardness of AISI 4340 with distance from the substrate. This indicates that hardness is greater at the top layer, where the phase is untempered martensite and has not undergone thermal cycling [127].

Subsequent work from Sun et al. investigated how altering the processing parameters in LDED changes the grain morphology [70]. It is noted that the clad is free from defects such as cracks and pores. In this work, samples were produced at a high feed rate (45 g/min) with higher scanning speed (1100 mm/min) and laser power (3.2 kW); and with low power (1.4 kW), speed (600 mm/min) and powder feed rate (22 g/min). The lower power experiment also used a smaller spot size. Previous tracks are said to have a preheating effect on subsequent ones which are close by, reducing the cooling rate this leads to an increase in the amount of retained austenite, tempered martensite, and carbides. The specific energy (energy density divided by scanning speed) is lower for the specimens produced at higher parameter settings, this increased the cooling rate in this specimen, and also led to an increase in the amount of austenite present. From this research it is clear that the specific energy and scanning pattern can alter the allotropes present in LDED 4340 samples. Substrate preheating has also been shown to reduce the number of defects, such as cracks and pores, when cladding Stellite 1 onto 4340 [146].

AISI 4340 manufactured by LDED is also of interest because the mechanical properties have been shown to be improved by heat treatment, meaning products manufactured using this method are more versatile. G. Sun et al. used a furnace treatment to relieve the residual stress

directions [145]. Whereas, lenticular and cellular structures tend to exist in higher layers, as preheating of the layer by previous depositions and subsequent thermal cycling reduces the effect of directional solidification [127].

2.5.1.2 Magnetic properties

The magnetic properties must also have been characterised for the chosen materials in order to suggest they may be used as representatives for a class of alloys in a new process. Few works have investigated the magnetic properties of 4340 specifically. This is because 4340 is not an alloy which is particularly designed for any magnetic purpose and the relationship between material composition and magnetic properties is generally well understood. Ferrite and martensite are ferromagnetic phases (magnetic permeability above 1) and therefore will permeate a magnetic field. Austenite on the other hand, is paramagnetic and is therefore not readily magnetised [147]. Alloys which are designed to be primarily austenitic, such as common stainless steels, are therefore paramagnetic. As such these common stainless steels (304, 304L, 316) all have a relative magnetic permeability (μ_r) of approximately only 1.02 [148].

AISI 4340 has been suggested for use when materials are required which are magnetically soft, have higher strength and are cheaper than maraging steels. Ajus et al. showed that using different heat treatments effects the saturation magnetism in 4340, using this to quantify the presence of the austenite phase in the material. To maximise saturation magnetism austenite was transformed into bainite by quenching between 860 °C and 960 °C, then tempering at 300 °C [143]. Tempering at temperatures at or below 200 °C significantly reduced the saturation magnetisation in samples which were quenched at or above 1060 °C, whilst those which were quenched at lower temperatures (860 °C and 960°C) demonstrated high saturation magnetisation (above 205 Am²/kg) even when tempered.

Though the properties of LDED deposited 4340 have been extensively investigated in the literature, no work has explored the effect of magnetic fields on the material properties of this material during processing (as discussed in Section 2.6). Indeed, unlike in paramagnetic alloys, no work has investigated the effects of magnetic fields on the properties of any ferromagnetic material manufactured via LDED under a magnetic field.

2.5.2 Nickel Alloys

Elemental nickel is also ferromagnetic and is used in high value, critical applications such as in the nuclear industry and in alloys in turbine engines. Therefore, this material is also of

interest to the application and development of the proposed magnet based studies. Two nickel alloys are considered in this work, the aerospace alloy Inconel 625 and the common heating element nichrome (80 wt.% nickel 20 wt.% chromium). Broadly, and particularly in terms of magnetic properties, Inconel 625 is representative of many super-nickel alloys. Whereas nichrome is commonly used as a heating element in electrical applications. Nichrome is mainly considered for its similarity to Inconel 625 in composition, both being nickel mainly alloyed with chromium. Both of these alloys are paramagnetic due the presence of chromium, which causes solid solution strengthening creating dislocations, which break up the magnetic domains [149].

Many works have considered the laser directed energy deposition of Inconel 625 whereas none have investigated nichrome. Clearly this disparity is due to the plethora of high-value use cases for Inconel 625 whereas there are few for nichrome at the component scale. In this work nichrome is used to demonstrate the feasibility of using a novel satellited feedstock to create alloys using the developed process, due to the simplified composition.

Paul et al. initially showed that Inconel 625 could be deposited into a bulk product without major defects using mid-range parameters (7.6 g/min powder feed rate, 500 mm/min scan speed, 1.5 kW CO₂ laser power) [150]. They showed that depositions of this nature manufactured products with few pores, which they suggest are caused by trapped gases. Also having a primarily dendritic microstructure in the direction of deposition, with some cellular microstructures occurring due to the reduced cooling rates in multi-layer depositions. High hardness was found to be due to the rapid cooling rate in LDED, as confirmed by the reduction in hardness after annealing. The study suggests that Inconel 625 manufactured by LDED had improved tensile and elongation properties as compared with conventionally manufactured samples, whilst having similar toughness. Lia et al. confirmed that the grain morphology was dendritic along the deposition direction and showed that increasing the energy density increased the cooling rate [151]. Unlike Inconel, nichrome is not designed for its mechanical properties, hence grain boundary sliding means that nichrome is ductile and susceptible to creep, with deformation being difficult to predict [152]. This is because nichrome lacks the alloying elements which give Inconel its high strength and resistance to creep. Although chromium will add some solid solution strengthening to the product, without the addition of aluminium, titanium or niobium no precipitates of the geometrically closed packed intermetallic γ' (Ni₃Al) phase or γ'' (Ni₃Nb) phases form. This means that there is no

precipitation strengthening in nichrome. Without precipitates dislocation motion is uninhibited and resistance to creep is therefore limited.

Studies have considered in-situ alloying of Inconel in additive manufacturing [153] previously due to the potential for additive manufacturing to be used in aerospace manufacturing. The use of nichrome as a simplified material to examine manufacturing processes may be a novel method to expedite the development of in-situ alloying in additive manufacturing.

2.5.3 Summary of LDED Material Properties

- The high cooling rates in LDED mean that the grains often align with the build direction (normally vertically). Grain size and shape can vary throughout a single layer.
- In AISI 4340 mainly ferritic phases are produced, though some martensite and retained austenite may sometimes be present.
- The magnetic properties of the material depend on its phase and the ability to form magnetic domains.

2.6 Fundamentals of Magnetic Attraction

This work presents a novel solution to improve the catchment efficiency and track geometry in LDED, by using magnetic fields to alter powder trajectories. Magnetically manipulating the trajectory of ferromagnetic powder particles is theorised due to the principles of magnetic attraction as described here.

The magnetic properties of materials depend on a large number of different factors, including the composition, stress, thermal history, grain morphology and orientation [149]. The strength of a magnetic field is known as the magnetic flux density (B), this is commonly represented by the density of flux lines which pass through a given region of interest. Ferromagnetic materials require an external magnetic field to magnetise the material, this magnetic field strength, H is known as the magnetising field strength. Magnetic permeability is the ability of a material to sustain a magnetic field when an external one is applied. Thus permeability (μ) is defined: $\mu = B/H$. As B and H both have the same units (T) permeability is unitless. The strength of the induced field depends on the strength of the magnetising field; therefore it is often useful to plot the B - H curve. The maximum strength of field which can be induced in a given material is described as the saturation induction (B_s). When the applied magnetic field (H) is increased the induced field (B) will increase following the B - H curve,

when this external field is then reduced there is a lag in the reduction of the induced (B) field. This is known as magnetic hysteresis, [149] the magnetic hysteresis curve of cold rolled carbon steels with different levels of plastic strain are shown in Figure 2-15. This work is primarily interested in materials which represent either high permeability which are classed as ferromagnetic (permeability greater than 1.1), and materials which display negligible permeability (approximately <1.1). Due to the B - H curve described above, the permeability depends on the strength of the applied (H) field.

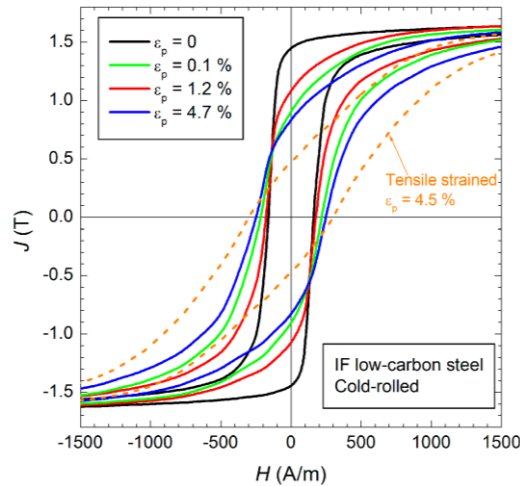


Figure 2-15 Magnetic hysteresis loop for cold rolled carbon steel sheets with different percentage strains, B is replaced with J here [154].

Domain theory governs whether a given material is ferromagnetic, paramagnetic or otherwise. This is the idea that materials consist of many atomic scale dipoles, which align to form magnetic domains. When these domains are aligned this causes the material to have bulk magnetic properties. Ferromagnetic materials may not have bulk magnetic properties in their natural state as the domains are randomly orientated, meaning the net magnetisation is zero. Applying a magnetic field to a ferromagnetic material causes the domains to orientate in the direction of the magnetising field, inducing a net magnetisation according to the hysteresis loop. In iron magnetisation can be induced most easily along the direction of the cubic axes (100) in the crystals, whereas in nickel this occurs in the most diagonal directions (111). These domains can align either by rotating or by changing in volume when a magnetic field is applied [155]. In iron and steel the γ FCC (austenite) phase is paramagnetic whilst the BCC α phase (ferrite) is ferromagnetic due to the quantum property spin [156]. This is in contrast to nickel, where the FCC phase is ferromagnetic. This relationship between crystal structure and magnetic domains means that both strain, composition and heat treatment can have significant effects on magnetic properties including permeability. For example, with

decreasing carbon content the packing of ferrite BCC crystals becomes more distorted. This lattice distortion reduces the alignment of the grains, meaning that the magnetic permeability is reduced. Nickel acts as an austenite stabiliser in steel, which causes many grades of stainless steel to be paramagnetic. Small concentrations of impurities, such as oxygen carbon and sulphur, can also have a detrimental effect on permeability. Whereas annealing may increase permeability. Indeed, in a very regular lattice even changing the measurement direction can appear to change the permeability [149].

When a ferromagnetic material is magnetised, the domains are aligned with the magnetising field. The ferromagnetic material will therefore be attracted to the magnetising field. This means that a torque and force will be applied to the magnetically charged material. This force can be modelled using the Biot-Savart law [157]. Even static magnetic fields can therefore be used to control the path of ferromagnetic bodies in free space. Some work has therefore been conducted on the manipulation of small bodies such as micro-bots using magnetic fields. Abbott et al. developed a simple model to predict this movement using the principles of magnetisation and the resultant forces and torques on ellipsoid bodies [158]. This work clearly demonstrates that the acceleration and the path divergence of magnetic materials depends on the different gradients of fields present. This has also been demonstrated practically in particles as small as 4 μm for biomedical research, allowing researchers to sort particles [159]. Methods similar to this one are commonly used to sort particles [160] and droplets [161] electrostatically, but research using magnetic fields is less common. Therefore, the use of magnetic fields to control additive manufacturing processes is not a widely considered concept. The use of magnetic fields to control levitated substrates has been proposed [162] and simulated [163] very recently, but has never been attempted in practice. Here it is suggested that instead of using magnetic fields to control the motion of substrates, it may instead be used to control the velocity and acceleration of metal particles. The use of magnetic fields in additive manufacturing is a burgeoning field to affect the material properties that emerge as the melt pool solidifies, as described in the following chapter. However, it has not been examined in terms of particle trajectory and control as the fundamentals of ferromagnetism allow.

2.6.1 Summary of Magnetic Attraction

- Magnetic attraction relies on ferromagnetic materials becoming magnetised and being drawn to the magnetic source along the gradient of increasing magnetic field strength.

- Magnetic permeability and the resulting magnetic hysteresis governs how strong a ferromagnetic material is magnetised.
- Magnetic fields have been used to control both small ferromagnetic objects and substrates in additive manufacturing, but not experimentally on powder.

2.7 Effect of Magnetic Fields on Metal Processing

Several works have investigated the effects of different types of fields on various melting phenomena in LDED. These primarily focus on the effect of magnetic and electrostatic fields on the melt pool, how this results in changes to grain morphology, porosity and mechanical properties. The first study on the effect of magnetic fields on deposition in LDED was conducted in 1997. Kovalenko et al. used an alternating electromagnetic field to agitate the melt pool [164]. The fluid motion in the melt pool was reportedly increased in an alloy steel, changing the residual stress and increasing the wear resistance of coatings.

Lu et al. investigated the effect of using electric and magnetic fields on the cooling of austenitic steel in LDED [165].

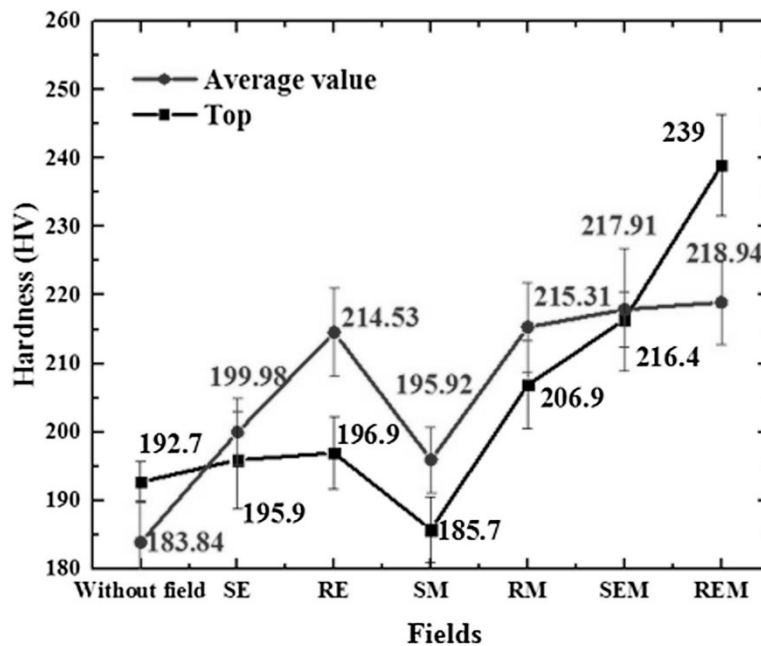


Figure 2-16 Hardness in 316 steel when deposited using different fields. SE - static electric field. RE - rotating electric field. SM - static magnetic field. RM - rotating magnetic field. SEM - static electric and magnetic fields. REM - rotating electric and magnet fields. Magnetic field strength 62.5 mT. Electric field strength 1209.3 V/m [165].

They found that that a static magnetic field of only 62.5 mT could constrain the plasma produced in the deposition process, as determined by imaging of the process. It is suggested that the plasma containment reduced heat loss, which increased the melt pool size and the

average hardness in the track. In contrast to this, the authors suggest that a rotating field had the opposite effect, causing the plasma to be disturbed, increasing cooling time. The effect of cooling time on the phases present is suggested as a reason for the change in hardness, with reduced cooling time leading to more austenitic material than mixed austenitic-ferritic as in the case of the slowly cooled static magnetic field. Longer cooling speed was expected to produce harder materials, but it is suggested that a reduction in tensile residual stress caused hardness to increase when static fields were used (as shown in Figure 2-16). Use of an infrared pyrometer confirmed the thermal history of the materials.

Together Bachman et al. [90] and Du et al. [89] showed static magnetic fields can be used to slow fluid motion in the localised melting of aluminium and Inconel 718 respectively. This is because the applied magnetic field induces electric currents and Lorentz forces which act in the opposite direction to Marangoni flow. This was shown to make the weld bead smaller and reduce spatter in keyhole laser welding and reduced the spacing of dendrites in LDED of nickel superalloys. Though in both cases the effect on material properties were not investigated. With more study this technique may lead to beneficial material properties in material consolidation, widening the applications of laser processes.

To date only two works have only simulated the use of magnetic fields for particle control in additive manufacturing and these have been published only in the thesis repository of the University of Waterloo. Therefore, there is scope for significantly more work in this area. As a chapter of his PhD thesis, Yuze simulated using magnetic fields to induce Lorentz forces and narrow the powder stream in DED when considering non-magnetic particles. The modelling suggested that using strong electromagnetic fields ($\sim 1 - 1.5$ T) could be used to concentrate large particles with radii (300 – 1000 μm) using this a Halbach arrays of permanent magnets [166]. The reduction in magnetic field strength towards the centre of the Halbach arrays combined with the magnetic fields induced in the particles by Lorentz forces means that the particles are repelled from the edge of the magnetic field and concentrate towards the centre of the Halbach array. However, Yuze states that particles with a diameter smaller than 200 μm cannot be concentrated using this method, due to eddy currents having been limited by the available space. Therefore, they conclude that using permanent magnet Halbach arrays cannot be used to concentrate non-magnetic particles in LDED as they are too small. No analysis is made of either ferromagnetic particles or other types of magnetic sources.

The other study suggested that this may be possible when using ferromagnetic particles. Dombroski stated that a combination of square and round neodymium magnets may be able to move a particle by up to 1 mm, increasing powder concentration in DED [167]. Dombrowski used two distinct methods to analyse the problem, using a mathematical geometric model in MATLAB and finite element analysis in COMSOL Multi-physics to determine the forces on and displacement of ferromagnetic particles due to magnetic fields. This work suggests that using either solenoids or a combination of permanent magnets, a lensing effect could be produced to focus powder into a narrower distribution and hence improve catchment efficiency. The study suggests that particles will be drawn to the centre axis of the field to a greater extent with increasing distance from the central axis. It was shown that larger particles would also be more affected by the field, the study concludes that 125 μm particles could be altered by up to 1 mm by the correct arrangement of permanent magnets, where a small cylindrical permanent magnet was stacked upon a larger one. Although the study is an effective feasibility study it is fundamentally limited for the following reasons: the study was entirely theoretical with no experimental work; it was assumed that particles would be 125 μm in diameter which is at the upper limit of what can be used in LDED (the normal range is from 5 – 150 μm); only the path divergence of particles was considered, without consideration of particle collision with each other, the melt pool or thermal/melting effects; only soft iron particles were considered which have much greater magnetic permeability than most functional alloys; finally iron core solenoids were not included in the analysis. This work is useful in suggesting that “ferromagnetic path divergence” is likely to be possible under the correct conditions though. Experimental study using real conditions must be carried out to determine whether any change to LDED can be affected by using magnetic fields. Both of the works investigating magnetic control of powders are available in theses only, with the investigation not being very comprehensive. There is therefore significant scope to uncover whether these methods can practically be used in DED. There is still much more scope for the development of these methods, even basic use of iron core solenoids has not been examined. The investigation is also limited by the suggested potential applications and outcomes. Examination of whether using magnetic fields may change track geometry or whether it could be used dynamically as an adaptive control technique were not conceived or discussed. The simulations are also limited to considering particle trajectories, without being applied to melt pool dynamics, or mechanical properties and the unintended consequences and other mechanisms which using magnetic fields are not discussed. This technique has the potential to change concentration and operation of DED

significantly, by offering improvements to catchment efficiency and powder stream concentration, therefore needs much greater consideration.

2.7.1 Summary of Effect of Magnetic Fields on Metal Processing

- Magnetic fields can change the hardness of LDED samples, likely by increasing the compressive residual stress.
- Combined magnetic and electric fields can also be used to reduce liquid flow in the melt pool.
- Some simulation has been carried out to suggest that magnetic fields may be able to alter the trajectory of particles in LDED, but this is incomprehensive and only simulation was used.

2.8 Literature Review Summary and Research Gaps

The fundamentals of the LDED have been discussed here to determine the research gaps and present the current state-of-the-art. Each aspect of the laser system has been explained in terms of the holistic process. The advantages of modern fibre lasers have been described, including that their wavelength means less radiation is reflected and flexibility in delivery is enabled. The introduction of material as powder has also been explained, powder is generally metered and delivered pneumatically, using an inert gas. The addition of powder at the correct speed and distribution is important to the process stability and catchment efficiency. With stable flow being more difficult to achieve than is sometimes imagined, the use of closed loop control is beginning in LDED and has the benefit of improving track consistency. But this requires further development to resolve some of the issues with powder feeding. Other methods of adapting the process dynamically to improve performance are more common as they are easier to adjust with low latency, hence power adjustment has shown some positive results in improving track consistency. Many different nozzle designs have been attempted, but generally only slightly alter the concentration of powder from coaxial nozzles. To further improve powder concentrations, this area has become saturated resulting in diminishing returns in terms of catchment efficiency improvements and new methods must be examined. Though recent developments using coaxial laser delivery with axial powder injection show promise in improving catchment efficiency more significantly.

Developments in the precise mechanisms which take place at the melt pool have also been examined, showing their importance in the development of mechanical properties and how

magnetic fields may alter the normal behaviour. The shape of the melt pool and the resulting track geometry has already undergone some study, though this mainly affects the dilution zone. To further improve the capability of the process in terms of resolution and productive manufacturing, advancements in the precise delivery of powder concentrations are required, with their influence on outcomes being categorised. Generally, both energy distribution and powder distribution are commonly Gaussian, with the designed stand-off distance and powder injection angle having the greatest effect on the distance of the powder focus from the nozzle tip. Modifying powder concentration is normally done by changing the nozzle design, but altering the concentration after it has left the nozzle has not been attempted except through the use of additional gas flow. Many other factors affect powder entrapment, though at least one component must be molten for powder to be consolidated. The velocity of powder is important to trapping powder in the melt pool, with lower velocity powder being deflected by gas plumes. Altering the powder velocity and trajectory after leaving the nozzle may therefore also change powder entrapment mechanisms and would benefit from further study. The most dynamic effect in the resulting melt pool is Marangoni convection which can cause changes to the grain morphology in the products of LDED and is clearly observable. Some research has studied whether magnetic and electric fields can change the flow inside the melt pool. Experimental work on how this may affect mechanical properties is missing, however.

The quality of the powder input to the process does affect the outcome. Powder size, shape and sphericity all affect the powder flow, whilst porosity in the powder can lead to defects in the component. Whether recycled powder may be used depends on the application the product will be used in, and the material it consists of, more research is required in order to fully characterise this across materials. When mixing feedstocks, powders with matching diameter-density ratios should be selected to avoid segregation. Where this is not possible satelliting is a novel method to obtaining these composition combinations and represents a novel new method, which is not widely used.

Tracks are generally geometrically characterised by their height and width, with track width being most associated with laser power. Combined parameters such as line energy are better parameters to determine the expected geometry given the complex interactions in the process. Furthermore, robust metrics for track geometry have only just been developed and the continued improvement in characterisation techniques is vital to further process control. Controlling porosity and dilution are intertwined by the parameter which has the greatest

effect on them, laser power must be balanced so that high dilution with low porosity is achieved. An ideal dilution zone size which avoids porosity, whilst ensuring track bonding is about 20% of the total volume of the track. Increasing dilution and track bonding can lead to porosity, making this a difficult balancing act. Some works have used force fields to control porosity directly, and with further development this may allow the processing zone to be expanded.

Powder catchment efficiency is of vital importance in LDED, generally this is governed by the ratio of the powder focus diameter and the melt pool diameter. Though surface quality would be expected to vary with the same ratio, this has not been investigated yet. The overall distribution of powder is also important and changes to nozzle design have intended to improve this. Improvements to catchment efficiency have stagnated (at around 60% - 70%) in recent years, as these nozzle designs have become well developed. Further improvement may now be made using more novel approaches, which should be researched further. This work proposes the use of magnetic fields to control the velocity and distribution of powder entering the melt pool, though many other methods, such as using vibrational or gravity feeding are also beginning to be examined.

The grain morphology of components processed by LDED depends on the thermal history, which in turn affects both the magnetic and mechanical properties. Bulk defects are generally the greatest impediment to LDED products, with heat treatments generally giving defect free depositions similar properties to wrought products. This is particularly true if re-melting occurs. The mechanical properties of LDED products may be anisotropic in bulk products, due to differences in grain morphology and layer bonding/pores. Magnetic fields have been examined to change the porosity and grain morphology in paramagnetic materials. It has been shown that the magnetic field can retain or remove pores and change the thermal history. This has only been considered in a few select cases and materials, and requires further investigation, particularly in ferromagnetic materials. This is also true of particle trajectory diversion, which has only been studied theoretically and so is not well understood within the myriad of factors in LDED.

Of the gaps in research which have been described thus far, the use of magnetic fields is the least well researched and therefore the area which has the greatest scope for future development. This is particularly true because even in the few works where magnetic fields have been used the works are by no means all encompassing. Works on materials affects have not considered mechanical properties, whilst those which examine powder trajectories are

entirely theoretical without any experimental comparison or much consideration of the wide-ranging implications of such technology. There is therefore significant scope for magnetic fields to be used in connection with LDED. Magnetic fields should be investigated in regard to LDED in the following areas:

- Powder stream concentration modification, to improve the focus of powder trajectories, particularly to increase the powder catchment efficiency.
- The modification of powder trajectory and its effect on track geometry, including the above surface track geometry, dilution, and surface roughness.
- Investigation into magnetic fields in relation to porosity, especially in materials which generally exhibit high porosity and are difficult to process.
- Examination of whether magnetic fields may be used to decouple substrate inclination effects, including determining the cause of asymmetry of tracks produced on inclined surfaces.
- Development of equipment, processes and parameters which enable and optimise magnetic particle trajectory modification. As well as understanding the technological barriers which may exist.
- Determination of the effects of magnetic fields on fluid motion in the melt pool in a larger range of materials and the affect this has on grain morphology and mechanical properties of the products.
- The use of magnetic fields as an adaptive control technique.

The following work will systematically investigate these areas, to determine the potential for magnetic fields in LDED. This work will inform researchers of whether this avenue is worthwhile of future exploration.

3 Experimental

This chapter describes the equipment and materials used for the experiments in this work, including the experimental, measurement and analytical techniques used. LDED depositions were made onto sheet metal substrates using a continuous coaxial nozzle in this work. The magnetic source, placed below these substrates provided the novel change to this apparatus. Following deposition, full geometric characterisation of tracks was performed using a range of techniques, including focus variation microscopy to generate 3d images for measurement, cross sections for metallography and mass measurements to quantify powder catchment efficiency. This combination of techniques was used in order to gain a complete understanding of the products produced using the magnetic assistance in LDED, including the external, internal and processing characteristic of the tracks. More detail on each section of the equipment and characterisation techniques is given in this chapter, discussion of the magnetic devices used is given in the Sections 4.2.2 & 5.2 as these were altered significantly.

3.1 Experimental Setup for LDED Experiments

The LDED system which was used in this work consists of a CNC bed, a laser, powder feeder and deposition nozzle. The different possible configurations which are sometimes used are described in Section 2.2. The embodiment of LDED which is used during experiments conducted for this work is described in greater detail in the following sections and is shown in Figure 3-1.

As this work aims to improve catchment efficiency using a time effective method, lengthy parameter optimisation for catchment efficiency was not conducted prior to investigations, as this would undermine the purpose of the method. Baseline experiments (without magnetic assistance) were therefore conducted based on parameters which are given in the literature; although these may not be as effective due to slight differences in the experimental setup.

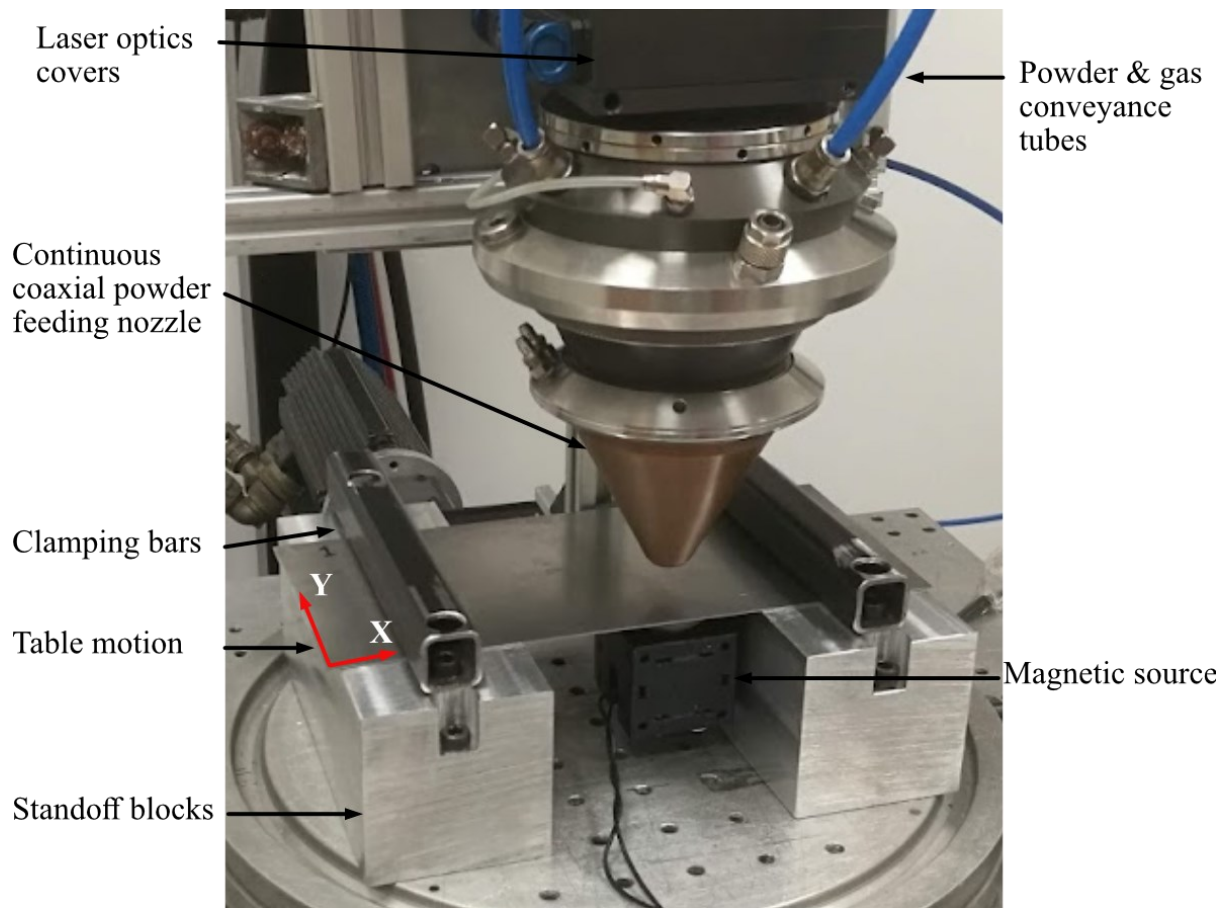


Figure 3-1 LDED system used throughout this work

A one variable at a time (OVAT) approach was taken to experiments because the use of magnetic fields is a new field of investigation, therefore the fundamental relationships must be determined before statistical methods can be properly utilised. These statistical approaches are better suited to well-developed processes which are known to be commercially viable.

3.1.1 Laser

The laser used in this work consists of a 2kW Ytterbium fibre laser. The YLR-2000 laser manufactured by IPG Photonics has a wavelength of 1070 ± 6 nm. The laser source has a diameter of 100 μm and the laser beam is delivered to the nozzle via glass fibre by total internal reflection. The laser, power and activation are controlled independently to the CNC table using the LaserNET software (IPG photonics). A collimating lens is coupled with a focusing lens to produce the desire spot size of 1.4 mm at this focal distance. The laser is operated at a focal distance of 186 mm. A further window is used to protect the lens from hot gases and powder during deposition. A camera feed coaxial to the laser beam can be used to monitor the process in real-time whilst another camera is also used to monitor the deposition process from the side. During this work the laser was operated in the power range of 400 –

1200 W with a gaussian beam profile (TEM_{00}) as measured by Laser Trader (UK). This analysis suggested that the reported power was approximately 88 % of the power input from the software. In this work, laser power is plotted directly rather than using global energy density, as this combined parameter has been shown not to be a useful predictor of melt pool characteristics in LDED as discussed in Section 2.4.1 [116].

3.1.2 Powder Feeder

Powder was fed and metred using the blown powder method (as discussed in Section 2.2.2). In this case a rotating disk type feeder was used (TAFA Model 1264), from Praxair Surface Technologies (USA). In this type of feeder the powder is placed in a hopper with gravity allowing the powder to fall towards a rotating disk, with orifices which allow the powder to pass through. The speed that the disk is rotated and the size of the orifices determines the rate of powder feeding. After the powder passes through the disk pressurised gas conveys the powder to the nozzle. The disk used here has orifices of 1.5 mm in diameter spaced 1.9 mm apart. The powder hopper is placed at an angle of 45° to ensure powder gathers at the disk. The feeder features a heat blanket to pre-heat powder and is pressurised using argon to transport the powder through the disk and provide an inert atmosphere. The powder feeder is controlled independently of the CNC table and laser systems. In this work powder was allowed to pre-heat for 20 min before beginning deposition experiments. In all experiments using this apparatus argon flow rate was set at 10 l/min, this is based on a common level used in literature and extensively proven with this setup.

The powder feeder used is known to have a linear relationship between disk speed and feed rate. This was not tested explicitly, but disk speeds and powder feed rates were collected for experiments produced here, this data is plotted in Figure 3-2, showing that there is a linear relationship between disk speed and powder feed rate when using the same material (AISI 4340). Due to the variation in powder feed rates present at identical disk speeds the feed rate as measured immediately before the experiments is quoted here. To measure the powder feed rates powder was fed into a container and the difference in mass of the container was measured, powder feed rates were then calculated. In this work powder was fed for 2 mins to measure the feed rate. In this work, powder feed rates are primarily used in the LDR mode, which is more relevant to the manufacture of high value near-net components (which is the eventual intended use case for the technology) rather than HDR which is more commonly used in coatings applications.

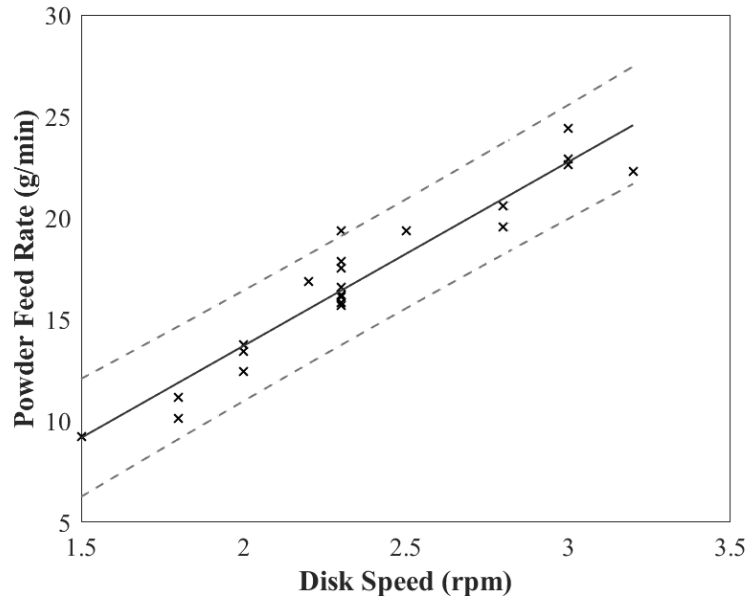


Figure 3-2 Powder feeder disk speed and resultant feed rates. Showing 95% confidence intervals. Root mean square error is 1.26.

3.1.3 Coaxial Nozzle

During coaxial powder feeding experiments the Precitec (Germany) YC 50 cladding head was used. The argon carried powder is separated into four outlets before arriving at the nozzle, the powder is then fed into the nozzle via four ports which are evenly spaced around the circumference. This is a continuous coaxial nozzle, where the powder all passes through one orifice which is coaxial to the laser which is along the central axis. As in many nozzles of this type, this orifice is between two copper cones. The gap between these cones can be varied using different nozzles, in this work the gap was selected as 0.75 mm to allow the powder to flow freely whilst minimising dispersion. This nozzle feeds powder at an angle of 60° relative to horizontal. This produces a gaussian distribution of powder coaxial to the laser beam. The nozzle equipment is operated with the nozzle tip 10 mm from the substrate surface, at the laser focal distance. The nozzle can be moved in the vertical (Z axis) direction using the CNC control discussed in the following section. Once set the nozzle was kept stationary during experiments. The nozzle is fixed in the horizontal direction (X and Y axes), but can be rotated around the Y axis to alter the nozzle inclination angle. The nozzle may be inclined from the vertical up to 45° .

3.1.4 Computer Numerical Control

Motion of the system is provided using a cartesian CNC system. This consists of a Talmont Control Systems LTD (UK) CNC table and an ECS 1400 D controller. The table can be

moved in the X and Y axes using G code programmed either manually or from an inserted disk. In this work, bed velocities between 200 mm/min and 900 mm/min were used. Substrates were clamped to the bed using bars screwed to the CNC bed, or in early chapters by a bolted connection through the corners of the substrates. This clamping is used to ensure minimal substrate distortion during laser operation whilst enabling a fast changeover of substrates to allow repeats to be carried in close succession.

3.2 Characterisation Techniques

3.2.1 Characterisation and Preparation of Inputs

The primary material inputs to the LDED process are the powder material and the substrates which are used. Powder was acquired which was determined to be suitable for LDED from the supplier's data. This means that matrix powders (those not used as satellite powders) must have a particle size distribution (PSD) between 50 – 150 μm as discussed in Section 2.3.7. Where possible, powder was obtained where the PSD had already been measured by the supplier using laser diffraction, where this was not available conventional sieve analysis was used. The PSD was then measured in-house using laser diffraction (Malvern Mastersizer 3000 particle size distribution measurement machine in “general purpose mode”) to ensure the powder was within the specified range. Matrix powders are also required to be spherical, therefore only powders which manufacturers stated were spherical were purchased [73]. Matrix powder manufactured via gas atomisation was therefore preferred when this was available. The sphericity of powders was then checked using scanning electron microscopy (Quanta 600 by FEI) at 20 kV electron acceleration and a spot size of 4 mm. The requirements for the satellite powders used in Chapter 7 were not as strict - here powders which were between 2 – 15 μm diameter were acceptable and the sphericity was not as important.

Hall and Carney flow measurements were taken according to the standards ASTM B213 and ASTM B964 [94] using 50 g of each powder. These methods are commonly used in both industry and the scientific community, with Carney flow generally being used to measure the flowability of powders which are not free flowing and the Hall test for those that are. The size morphology and flow rate of the powders used in this work are discussed in Section 3.3.

3.2.2 Deposition and track characterisation

The simplest and most commonly used metric of powder catchment efficiency is through the change in mass. Each substrate was measured before and after depositions with a known

length. The difference in mass was used to calculate powder catchment efficiency using the equation:

Equation 3-1 $\eta = \Delta m v / l f$

Where η is catchment efficiency, Δm is the change in mass (g), v is the traverse speed (mm/min), l is the length of the track (mm) and f is the flow rate (g/min). The change in mass could be easily quantified through the mass of the tracks, as is commonly used in the literature [75]. Whilst the total mass which leaves the nozzle is calculated through values was first calibrated by measuring the flow rate and then calculated based on the actual length of track which the laser operated over, which could be directly controlled.

Geometric data was obtained by scanning 1.5 mm (minimum) samples of each track using focus variation microscopy (FVM) (Infinite Focus Alicona G4 at 20x magnification), these samples were taken where the deposition was stable - 20 mm from the start of each track. The length of track scanned was consistent for each study. For the measurements taken of stable regions, mean profiles were taken from these sections to remove the effect of local deviation. Geometric measurements (height, width, area, skewness, roughness) were then made, after first removing any tilt angle present in the sample (MountainsMap 7.4 Digital Surf [168]). To obtain robust geometric data from these mean profiles the mean measurement of each condition was calculated. Where additional geometric data was required (e.g. where magnetic switching occurred) additional scans were made of each region of interest (e.g. before and after the magnetic state was changed). To examine dynamic changes along the track length, longer scans of 20 mm were taken at 10x magnification over the dynamically changing sections.

Roughness analysis was conducted on the upper 30% of the FVM track of scans at 20x magnification. The data was filtered by form (F-operator) using a second-order polynomial filter and Gaussian S (short-scale) and L (long-scale) filters of 25 μm and 0.8 mm respectively in order to produce areal roughness measurements. This is in accordance with ISO 25178 [169].

A sample of the tracks produced in each condition was transversely sectioned, mounted in resin, ground, (according to ASTM E3-11 [170]) polished (with 6 μm and 1 μm diamond paste) and etched by swabbing 1% Nital Solution over the sample for 20 s or 2% Nital for 12 s (for steel samples), then examined using optical microscopy. This revealed the dilution zone and grain structure. Marbles etchant was used for nickel (and its alloys) samples. Image

analysis software (ImageJ [171]) was used to determine the area of the dilution zones in these samples and confirm the accuracy of focus variation measurements.

Vickers hardness was measured using a microhardness test machine with a 500 gf.

Measurements were taken on one sample with the magnet on and one with the magnet off to examine whether large changes in hardness occurred. Then the mean was taken from rows and columns of indentations. Indentations were taken at a distance of at least 2x the width of the indentations apart.

3.3 Materials Used

The materials used in experiments in this work include powder feedstocks and sheet metal substrates. The powder material was characterised using standard test methods discussed below. These include, flowability tests, such as Hall flow, particle size measurement and microscopy, including EDX. This is because, the size of particles is not the only important metric in additive manufacturing. In DED the shape of particles is also important for flowability, this is why it is common to do microscopy on powders. This range of techniques was chosen in order to fully characterise the full range of powder properties relevant to each experiment, as shape, flowability and composition can all have a significant effect on the LDED process.

Primarily ferrous materials are used in this work, either for their ferromagnetic properties, which were required for magnetic assistance to function, or as comparisons to demonstrate the effect of changes to magnetic permeability.

The feedstocks and substrates which were used in this work are detailed below. In Chapter 7 alternative feedstocks are created; the compositions and constituents of these materials are discussed there.

3.3.1 AISI 4340 Powder

The 4340 powder was supplied by Sandvik Osprey (UK), who also supplied compositional, hall flow and tap density data. The Hall flow is given as 21.0 s / 50g. The tap density of the powder is 4.7 g/cc. The manufacturer used sieve and laser light diffraction to give indications of the particle size distribution, sieve analysis is given as >75 μm 0.8%, 32 – 75 μm 96.9%, <32 μm 2.3%. Since the powder was used throughout this work, the particle size distribution was also measured using the SEM micrograph and the particle number method and using laser diffraction using a Malvern Mastersizer 3000 particle size distribution measurement machine. ImageJ software was used to manually measure the size of 200 particles in SEM

images. Particle size distribution measurements are shown in Table 3-1. The size distribution as measured in-house is shown in Figure 3-3.

Table 3-1 Particle size distribution (μm) of AISI 4340 as measured using different methods.

Measurement Method	D10	D50	D90
Manufacturer's data	34.3	51.9	76.9
Laser diffraction	35.9	52.2	75.9
SEM particle count	1.9	4.4	43

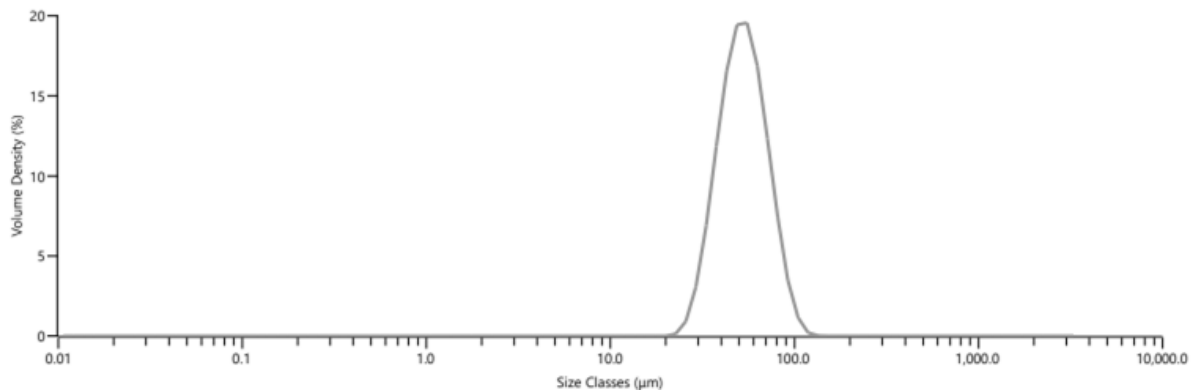


Figure 3-3 AISI 4340 powder particle size distribution as measured using Malvern Mastersizer 3000 instrument.

This indicates that there is little difference (up to $1.6 \mu\text{m}$) between the particle diameters as measured by the manufacturers and in-house using laser diffraction. However, using the number of particles present in an SEM image gave very different results (up to $47.5 \mu\text{m}$ difference compared to manufacturer's data). The units should be carefully considered when comparing different methods as suggested by Meisnar et al. [101] particle counts skew size distributions towards smaller sizes compared to volume density distribution. In Meisnar et al.'s work SEM imaging is described as the "ideal tool for particle morphology studies". However, it is also noted that this method is severely time consuming as compared to laser diffractometry.

The composition of the 4340 powder was given by the manufacturer, whilst also being measured via EDX. The powder compositions are given in Table 3-2. EDX is unlikely to give an accurate representation of the true composition, especially for carbon, this is given for comparison with the samples produced.

Table 3-2 Composition of AISI 4340 powder by different methods (wt.%).

Measurement Method	Ni	Cr	Mn	C	Mo	Si	P	S	Fe
Standard [172]	1.7-2.0	0.70-0.90	0.70-0.90	0.37-0.43	0.20-0.30	0.150-0.30	<0.035	<0.040	95.2-96.3
Manufacturer	2.0%	0.92	0.79	0.38	0.29	0.23	–	–	Bal

This powder was manufactured by gas atomisation and is highly spherical with few satellites, as determined by SEM shown in Figure 3-4. The high quality of the powder makes this material a good baseline material for experiments.

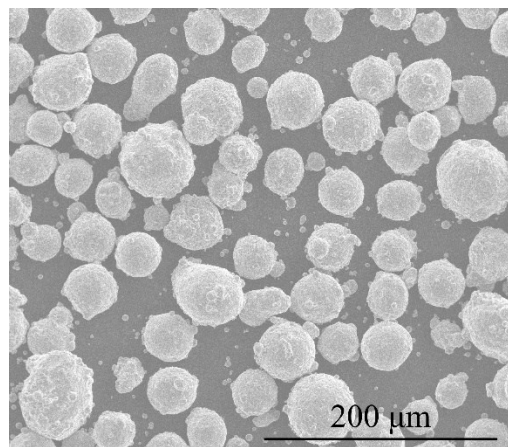


Figure 3-4 AISI 4340 powder showing high sphericity and few satellites.

3.3.2 Nickel Powder

Commercially pure nickel powder is used for the investigations described in Chapters 5 and 7. This powder was supplied by Alfa Aesar (USA). The manufacturer’s sieve analysis shows that 93% of the powder is between 74 μm and 89 μm. No other particle size distribution, tap density or Hall flow data was provided by the manufacturer. The particle size distribution was once again measured via laser diffraction and is given in Table 3-3 and Figure 3-5. In house Hall and Carney flow measurements were 22.1 s / 50 g and 3.0 s / 50 g respectively.

Table 3-3 Nickel powder particle size distribution (μm).

Measurement method	D10	D50	D90
Laser diffraction	88.4	102	117

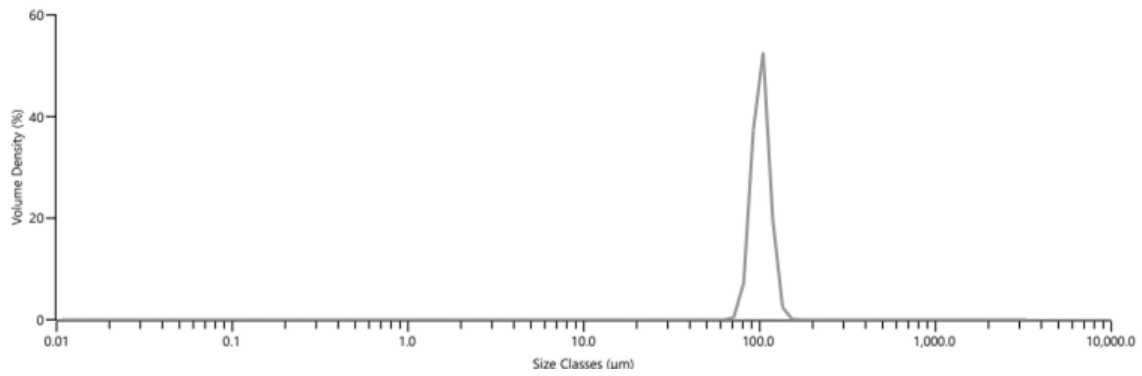


Figure 3-5 Nickel powder particle size distribution.

This powder was intended to be as pure as reasonably possible, so that it could be used to create alloys without contamination leading to unintended compositions. The composition of this powder as given by the manufacturer is shown below.

Table 3-4 Composition of nickel powder (wt. %) according to manufacturer’s data.

Measurement method	Ni	Co	Fe	Cu	C	S
Manufacturer	99.9	0.08	<0.01	<0.01	<0.01	0.03

Scanning electron microscopy of this powder revealed that it was highly spherical, but had many satellite particles and an uneven surface as discussed in Chapter 7.

3.3.3 Chromium powder

Chromium powder with a smaller particle size distribution is used in Chapter 7, as the satellite (coating) powder on a nickel parent particle. The particle size distribution of this powder is shown in Figure 3-6 and Table 3-5. The composition of this batch of chromium powder (as described by the manufacturer) is given in Table 3-6. This powder was supplied by Alfa Aesar (UK).

Table 3-5 Particle size distribution of chromium powder.

Measurement method	D10	D50	D90
Laser diffraction	2.26	3.97	6.77
Manufacturer	-	4.41	9.99

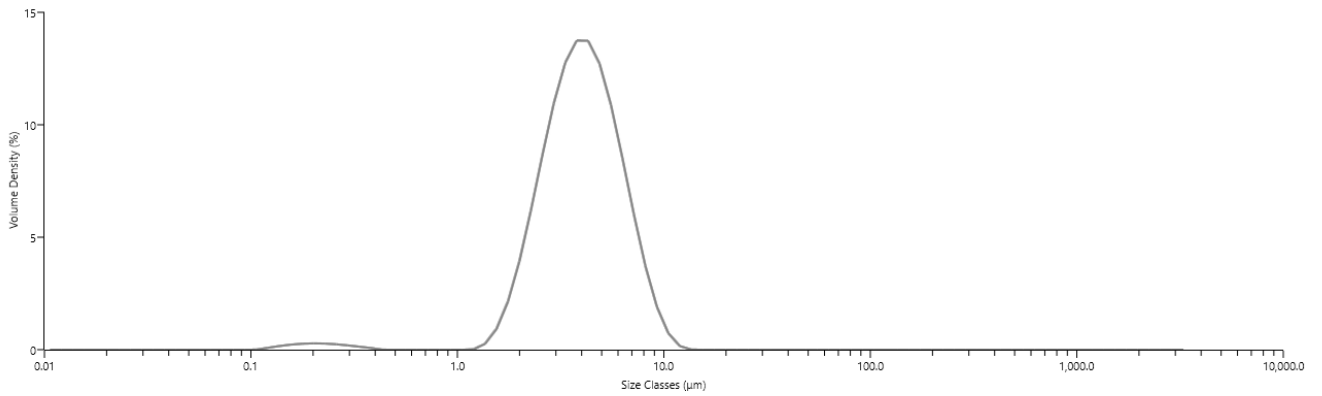


Figure 3-6 Particle size distribution of chromium powder.

Table 3-6 Composition of chromium powder by wt. % as given by the manufacturer's data.

Cr	Fe	Al	Si	C	S
99.6	0.31	0.003	0.009	0.018	0.02

3.3.4 Nichrome powder

Pre-alloyed nichrome powder is used in Chapter 7 as the control to compare to satellited powder. The particle size distribution of this powder is shown in Table 3-7 and Figure 3-7. The composition of this batch of nichrome powder (as described by the manufacturer) is given in Table 3-8. This powder was supplied by Alfa Aesar (UK).

Table 3-7 Pre-alloyed nichrome powder size distribution.

Measurement method	D10	D50	D90
Laser diffraction	52.9	85.7	135

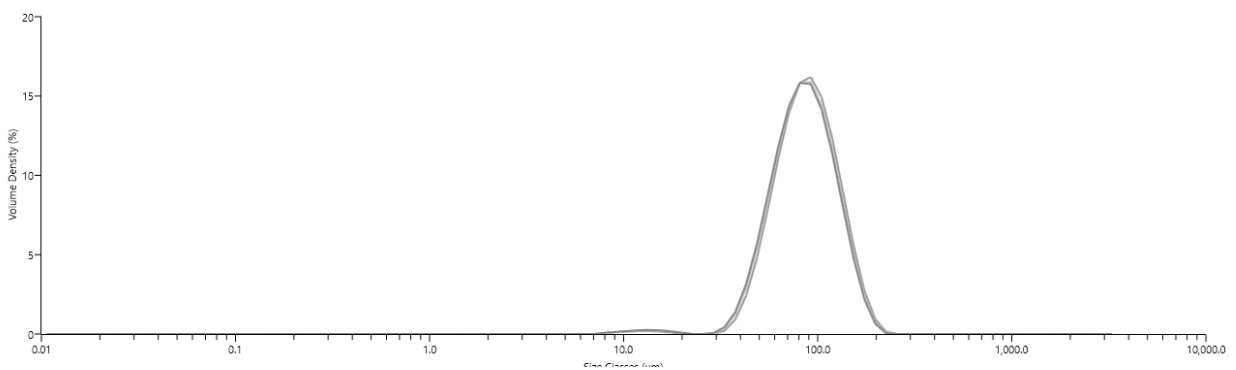


Figure 3-7 Powder size distribution of pre-alloyed nichrome powder.

Table 3-8 Composition (wt. %) of nichrome powder as given by manufacturer's analysis.

Ni	Cr	Si	Fe	C	Mn	S
79.25	19.44	0.97	0.53	0.016	0.03	0.004

3.3.5 Substrates

Only substrates with precise thickness were used in this work, to ensure that thermal and magnetic effects were kept constant. All substrates were therefore measured using digital Vernier callipers, those which deviated by more than ± 0.3 mm from the mean thickness were discarded. Substrates were cleaned with isopropyl alcohol on both sides before use. Except where otherwise discussed, substrates were not ground or grit blasted prior to use, as this was found to cause distortion in the substrates. Stainless steel, mild steel and pure nickel substrates of different thickness were used in the various chapters of this work, the dimensions and properties of each is presented in the relevant chapters.

4 Feasibility of Magnetically Assisted LDED

4.1 Introduction

To achieve an improved level of material and energy efficiency in LDED, understanding and measuring the powder catchment efficiency and track symmetry are critical. This is especially important when material cost is high or supply is limited, and when high accuracy tracks are required, such as in on-site repair or potentially for manufacturing in difficult environments such as space. Powder catchment efficiency is also important to avoid recycling powder, given the correlation between powder reuse and formation of defects in AM parts [173] and the need to sieve and dry powder prior to re-use as identified in Section 2.3.7.

Powder catchment efficiency have been a major subject of research work in the field of LDED. In spite of this, until recently catchment efficiencies around 40-65% were considered good [36], depending on nozzle design and deposition parameters as discussed in Section 2.4.6. Previously, design changes and parameter optimisation have been made to try and improve this. Wang & Li implemented a piezo sonic based delivery system for full powder catchment efficiency when using nickel alloys, with an added benefit of reducing pore density in the final part [19]. This system also principally relies on gravity to drive powder flow; therefore it is likely that this process will be significantly less efficient on inclined planes. Axial powder feeding with annular lasers has also been shown to improve powder catchment significantly compared to side and coaxial feeding, providing excellent efficiencies of up to 80% [39]. These promising new technologies (which are further discussed in Section 2.2.3) will certainly improve LDED processing efficiency as they are more widely adopted and developed, but the capital investment required is significant. Although significantly greater efficiencies have been reported, using novel techniques, this low level of efficiency (around 40%) is still common in industry. Furthermore, the process of parameter optimisation is time consuming and therefore costly. This work aims to find efficiency gains using a method which avoids this time consuming process. Hence, the baseline catchment efficiencies remain lower than the quoted optimised ones.

For advancement of LDED to produce tracks and parts on tilted surfaces, for example as part of a 5-axis system or on location with vertical substrates [120], it is important to understand the effect of inclined deposition on LDED processing, track quality and catchment efficiency.

It has been shown that LDED on inclined planes does not change the mechanical properties of the tracks produced using a stainless steel [8], however it is widely agreed that track height decreases with greater inclined angles [119], whilst track width is only slightly affected. Powder catchment efficiency has been shown to drop markedly at inclined angles, dropping from 66% at 0° to only 19% at 75° inclination [7]. Alya et al. suggest that simply increasing the flow rate to compensate for the drop in catchment efficiency is an effective measure, however this further contributes to waste and could cause unpredictable track geometry. The symmetry of the track cross-section produced on inclined planes is another critical metric for LDED and has also been subject to investigation. Zhu et al. showed that the track becomes slightly skewed at higher angles, whilst Alya et al. demonstrated that skewness can increase quite significantly at higher flow rates on inclined planes. He et al. also show that peak displacement offset, a form of skewness, increases at higher flow rates. [9] measured luminance from powder stream images, showing that the powder concentration distribution is diverted at inclined angles, explaining the mechanism of increased skewness and reduced catchment efficiency. Alya et al. noted that small measured skewness is due to reduced track volume at higher angles, and therefore introducing more powder may not be an effective remedy.

This study investigates how a magnetic field can be used to manipulate, and compensate for poor catchment efficiency, as well as other track characteristics including skewness and other geometrical properties.

Some research in this area has been done to investigate the effect of magnetic fields on mechanical properties, as discussed in Section 2.7. Despite this, there has been little study so far, to investigate the influence of magnetic fields during LDED on the powder catchment and track geometry. Such a study is critical to the advancement of the process, improving material and energy efficiency whilst increasing our ability to accurately control powder placement, aiding its use in the manufacture of complex components.

This study systematically investigates the impact of magnetic field manipulation during DED on the deposition of a common ferromagnetic powder feedstock – 4340 steel. AISI 4340 has been subject to significant research work as a feedstock for laser deposition, and its microstructural [127], fatigue [142] and defect [17] properties have been well characterised. It is an industrially useful material given its use in fatigue critical applications [142] and its soft ferromagnetic properties [143]. Previously, the effect of substrate material on dilution has been investigated, showing that this depends both on the specific alloys present and

thermal properties of the materials [5], with 4340 deposition on mild steel being demonstrated by Bhattacharya et al. [127].

The effects of the different magnetic properties of substrates, is investigated here via the use of a magnetic mild steel, and a paramagnetic stainless steel. The effect of plane inclination, powder flow rate and traverse speed are also investigated.

Using an off-the-shelf work-holding magnet, commonly used in subtractive manufacturing processes the fundamental effects of magnetic assistance could be investigated quickly, whilst demonstrating the use of such a simple setup for industry.

4.2 Experimental

4.2.1 Materials

The ferromagnetic AISI 4340 (approximate melting temperature, T_m , 1427°C) powder was used as the feedstock material for experiments in this chapter, this feedstock is described in Section 3.3.1. The mean thickness of substrates was measured as 1.0 mm and 1.2 mm for the mild steel (T_m , 1480) and AISI 304 (T_m , 1450°C (ASM International, 2002)) stainless steel substrates respectively.

A magnetic work holding chuck was used to deliver the magnetic field. This device allows a magnetic field to be switched “on” or “off” by moving an array of neodymium magnets inside the device (Figure 4-1a). Similar chucks are described in detail by Wahab et al, with reference to operation, manufacture and magnetic arrangement [174]. The chuck supplies a theoretical 100 N/cm² at its surface. When viewed through a magnetic viewing film with the chuck in the on position the lines of dense magnetic flux can be observed on the surface of the substrate along the width of the device. On a mild steel substrate these lines are approximately 1.8 mm wide. In the case of the stainless-steel substrate, accurate measurement of line width proved difficult, due to the indistinct edge of the lines. The magnetic field was measured, using a PCE-MFM 3000 Gauss Meter, as having a maximum magnetic field strength of 27 mT when used through a mild steel substrate. The field strength was shown to have a maximum strength within ± 3 mT on each line of dense magnetic flux, regardless of the position of the line in relation to the magnetic chuck.

4.2.2 Experimental Setup

Schematics of the experimental setup are shown in Figure 4-1.

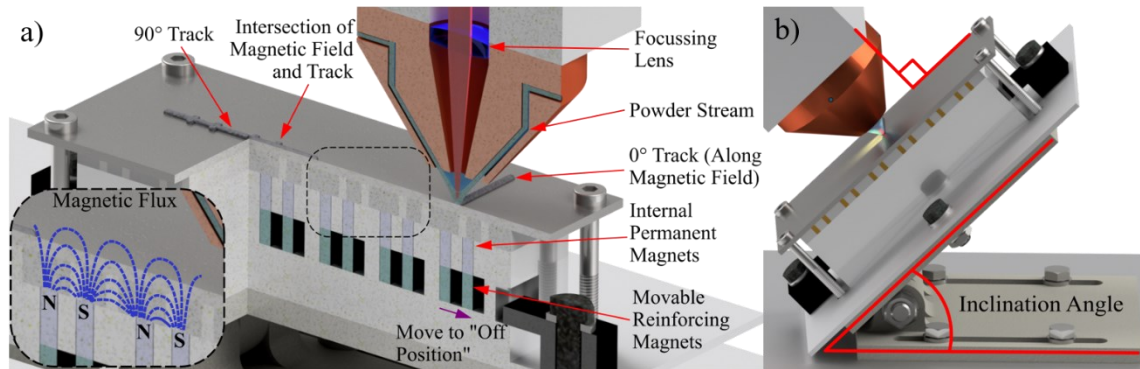


Figure 4-1 Experimental Setup (a) shows 0° tracks and magnetic flux density, (b) shows 45° tracks

0° and 90° tracks are shown along and perpendicular, respectively, to the magnetic field lines. This is shown in Figure 4-2 below.

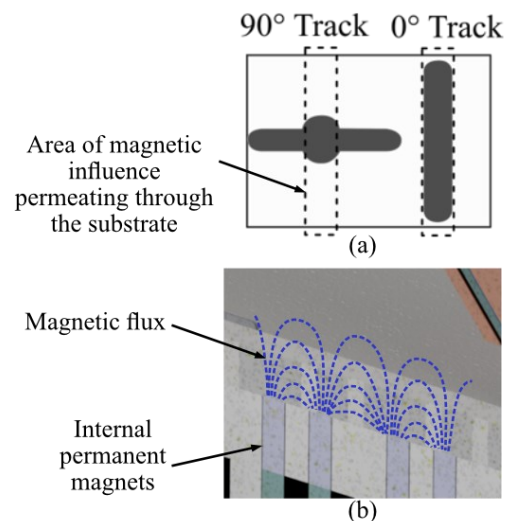


Figure 4-2 Direction of tracks with magnetic flux, (a) showing track direction and (b) showing the magnetic flux lines.

In the inclined plane tests, the laser was rotated at the same angle to maintain a right angle with the substrate. Each experiment was conducted with the magnetic field in the on and off positions, with a laser power of 600W. Parameters which were varied are shown in Table 4-1. These parameters were chosen to produce high quality deposits based on preliminary trials, in which powder flow rate and laser power were varied over larger ranges (500 W – 1 kW and 9 – 30 g/min) to determine a suitable parameter range. These preliminary trials were based on commonly used parameters in the literature for 4340 steel powder [127]. Parameters were

then optimised to produce large tracks as it has been suggested that effects of angle on skewness are greatest when tracks are larger [9]. Where incline angle was zero, tracks were produced perpendicular and in-line with the magnetic field lines, whereas only in-line (Figure 4-1) tracks were produced in incline experiments. The same disk speeds were used for all of the experiments with the resulting powder feed rates being measured immediately prior to each experiment. Powder feed rate was measured over a 3 minute time interval to reduce the effect of fluctuations in powder supply which can occur when the powder begins being supplied.

Table 4-1 Parameters used for experiments in this chapter.

Experiment #	Incline Angle (°)	Substrate Material	Powder Feed Rates (g/min)	Traverse Speed (mm/min)
1	0	Mild Steel	9.2-23.0	500
2	0	304	9.6-22.51	500
3	0-45	Mild Steel	10.6 & 13.1	200500

Tracks were characterised by their mass, by FVM, cross-sectional microscopy and hardness as discussed in Chapter 3.

4.3 Results

4.3.1 Material catchment

Figure 4-3 shows the results of track mass per unit length using both mild and stainless steel substrates. Results are shown for tracks along the magnetic field (0°) and perpendicular to the field (90°), with magnets both on and off. The powder catchment efficiencies relating to these results are shown in Figure 4-4. In this chapter baseline results are shown in both directions because changes in direction has been shown to effect powder catchment in some nozzles. In addition, the laminated surface of the magnetic chuck could have a directional effect on deposition.

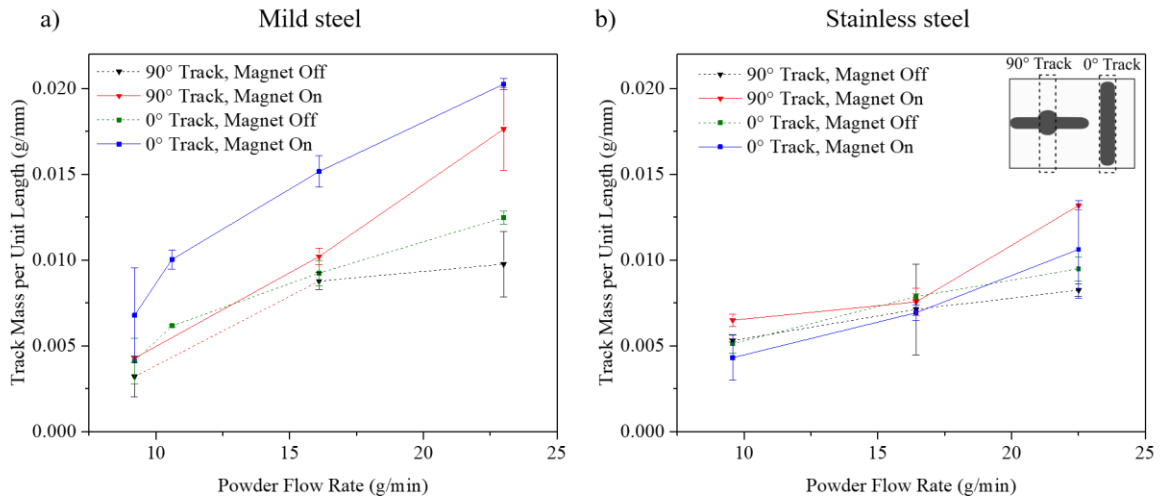


Figure 4-3 Effect of magnetic assistance with increasing powder flow rate on track mass per unit length, for tracks in both orientations and magnetic states for (a) mild steel and (b) stainless steel substrates.

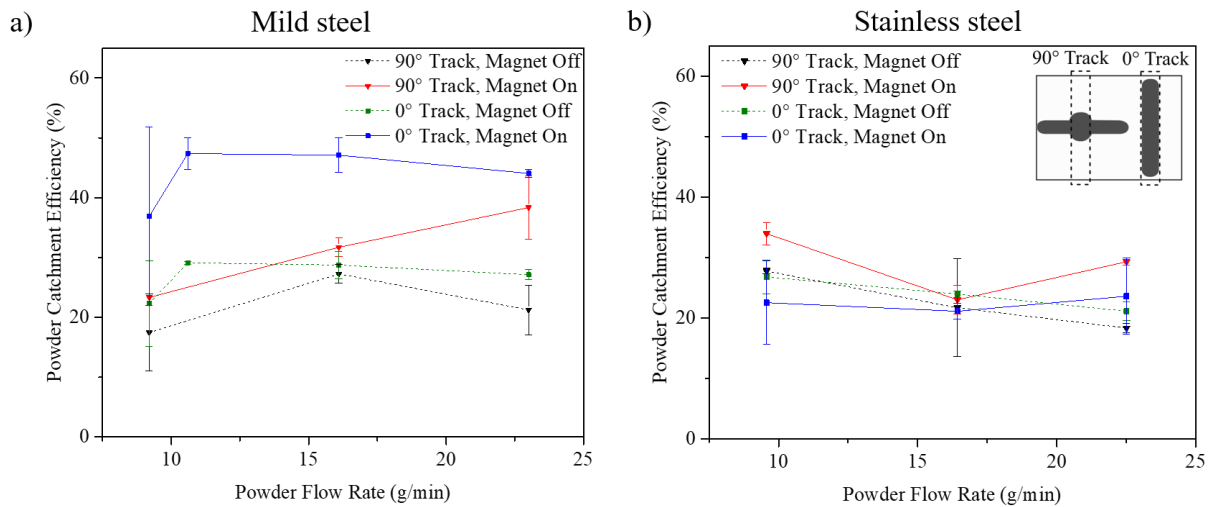


Figure 4-4 Powder catchment efficiency with increasing powder flow rate for tracks in both orientations and magnetic states for (a) mild steel and (b) stainless steel substrates.

In the case of the mild steel substrate, the tracks at 0° with the magnet on, showed the highest track mass per unit length and powder catchment efficiency for all powder flow rates. The percentage catchment efficiency reaches close to 50% at 0° with the magnet off for the mild steel substrate, and is slightly reduced with increasing flow rate. This can be compared to a maximum of 30% reached without use of the magnet. The 90° tracks with magnet on yielded higher mass and catchment efficiencies than the same tracks with the magnet off, although

this increase was lower than for the 0° tracks. No significant difference in deposition based on direction can be observed here.

In the case of the stainless steel, the magnet showed less of an effect on powder catchment, however the 90° track with the magnet on was still the highest at low and high flow rates, considering error. This increase was not as clear at the medium flow rate. However, the results demonstrate that, generally on the stainless steel substrate, the magnetic field appears to have less of an influence on powder catchment as shown in Figure 4-3 and Figure 4-4.

4.3.2 Effect of field line position

Where the 90° tracks intersect the magnetic field, localised increases in width and height were seen. These regions were measured separately by FVM. The effect of the magnetic field on this behaviour can be seen in the 3D images in Figure 4-5.

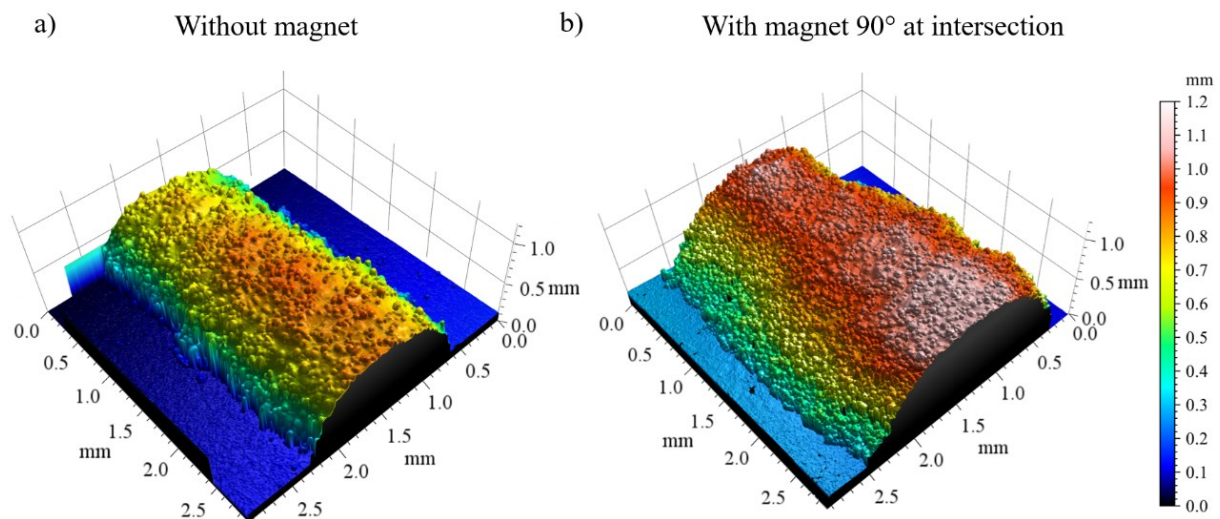


Figure 4-5 3D images of example track sections at points of magnetic field intersection using mild steel substrates, demonstrating the effect of magnetic assistance on increased track size.

In Figure 4-5 (b), an increase in overall size of the track is shown when magnetic assistance is used, in the location of field line intersection, can be clearly seen. Width in this example increases to ~2.2 mm, compared to 1.6 mm without the magnet. The height is also approximately 20% higher, reaching ~1.0 mm in height at regions of intersection.

Given direct weight measurement of small sections of track is not possible, powder catchment in these areas was assessed via cross-sectional area data measured by FVM. This data is presented in the graphs in Figure 4-6.

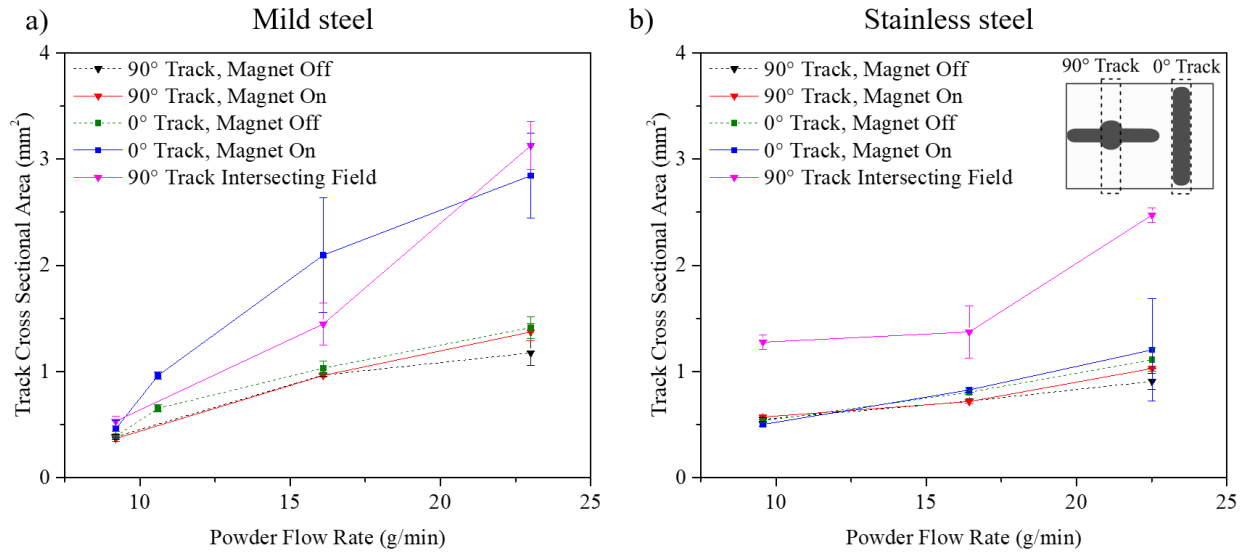


Figure 4-6 Effect of magnet on cross-sectional area at field line intersection points (in pink), compared to average cross-sectional areas of tracks.

When considering the directly comparable experiments, for 90° axis tracks with magnet on (i.e. pink and red in the graphs), it is clear that the magnetic field yielded increases in cross-sectional area which were particularly localised to regions of magnetic field intersection. In the case of the mild steel, the areas at points of intersection match closely, considering error, with the overall average cross-sectional areas of the 0° tracks, with magnets turned on. In the case of the stainless steel, the intersection points yielded larger cross-sectional areas, than the other results. Once again, the general trend of cross-sectional area of the tracks at intersection points is upwards with powder flow rate, reflecting the trend of all powder catchment and area data so far. It can also be noted that the heights and widths of the equivalent data points in the area graphs in Figure 4-6 were measured and followed the trend seen here very closely, however were not included for sake of redundancy.

4.3.3 Track dilution

Given the stronger effect of the magnetic field on deposition when the mild steel substrate is used, tracks were cross-sectioned and imaged on this substrate material. 0° tracks cross-sectioned here, and representative cross-sectional images are shown in Figure 4-7.

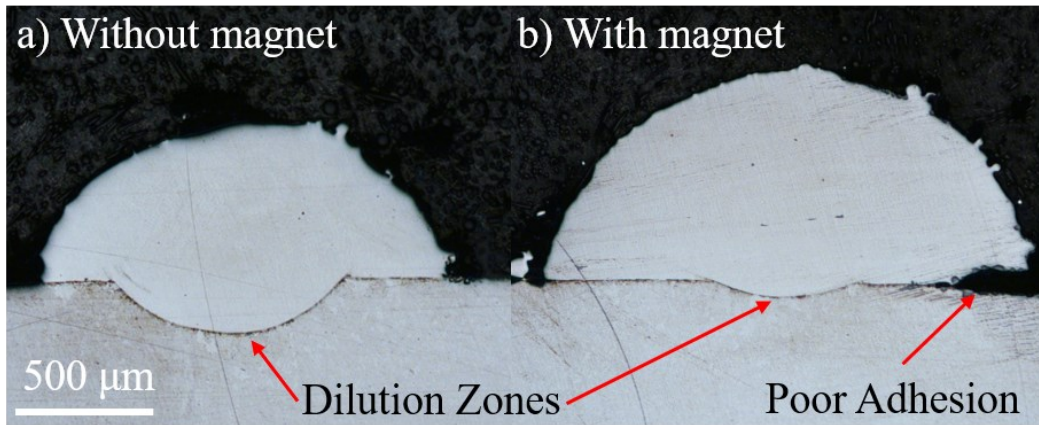


Figure 4-7 Cross-sectional optical images of tracks on mild steel (a) without and (b) with magnetic assistance, showing the effect of magnetic field on track size and dilution zone.

Considering the representative images in Figure 4-7, it is clear that although cross-sectional areas of the tracks, and overall catchment efficiency is increased with magnetic assistance, absolute and proportion of dilution area is reduced. The difference in dilution zone sizes as a percentage of the total cross-sectional area of representative tracks, for two different flow rates on mild steel is shown in Figure 4-8.

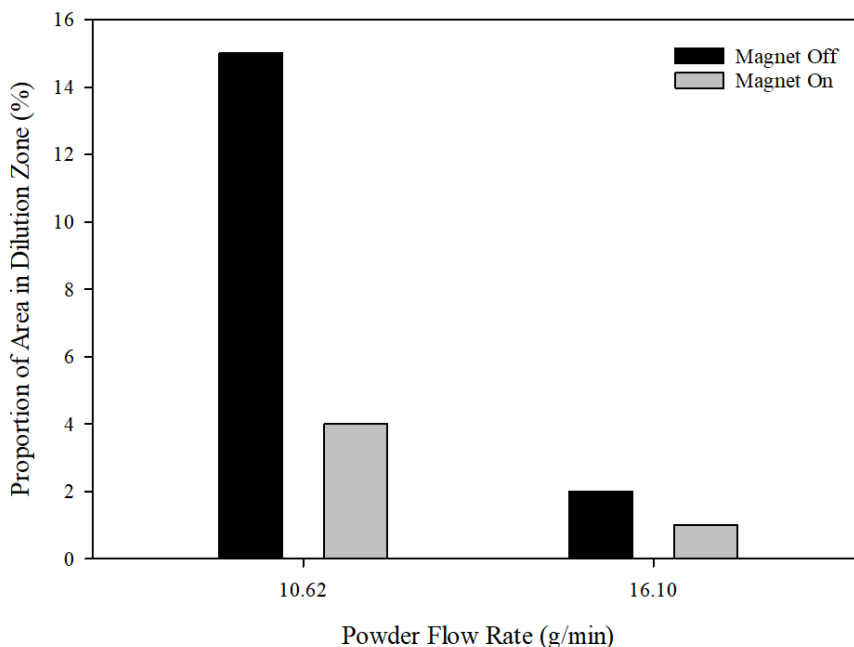


Figure 4-8 Effect of magnet on % dilution at two different powder flow rates on a 0° on mild steel. The magnet reduces the proportion significantly at low flow rates. This reduction is less at the high flow rate.

At both powder flow rates, % dilution was significantly reduced when magnetic assistance was used. This reduction is much greater in the case of the lower flow rate, reducing by almost a factor of 4, compared to the higher flow rate, at which dilution was approximately halved. It can also be noted that increasing powder flow rate significantly reduces track dilution. When dilution zone area is considered as a proportion of total track cross-sectional area, dilution zones were proportionally equal in size, although further experimentation may be required to definitively confirm this.

4.3.4 Effect of inclination

To gauge the potential use of magnetic assistance in DED for assisting more complex arrangements, and to determine if the effects of inclination can be compensated for, tracks were prepared using magnetic assistance on plane inclination angles of up to 45°. The effect of plane inclination on powder catchment efficiency is shown in Figure 4-9 for the mild steel substrate. Both powder flow rate and traverse speed were changed to produce highly different mass per unit length of delivery, in order to better understand skewness, as suggested in the literature [8]. In Figure 4-9 mass deposited per unit length is used. This is calculated from the traverse speed and powder feed rates in Table 4-1, and allows for more effective comparisons when powder deposition is altered in this manner.

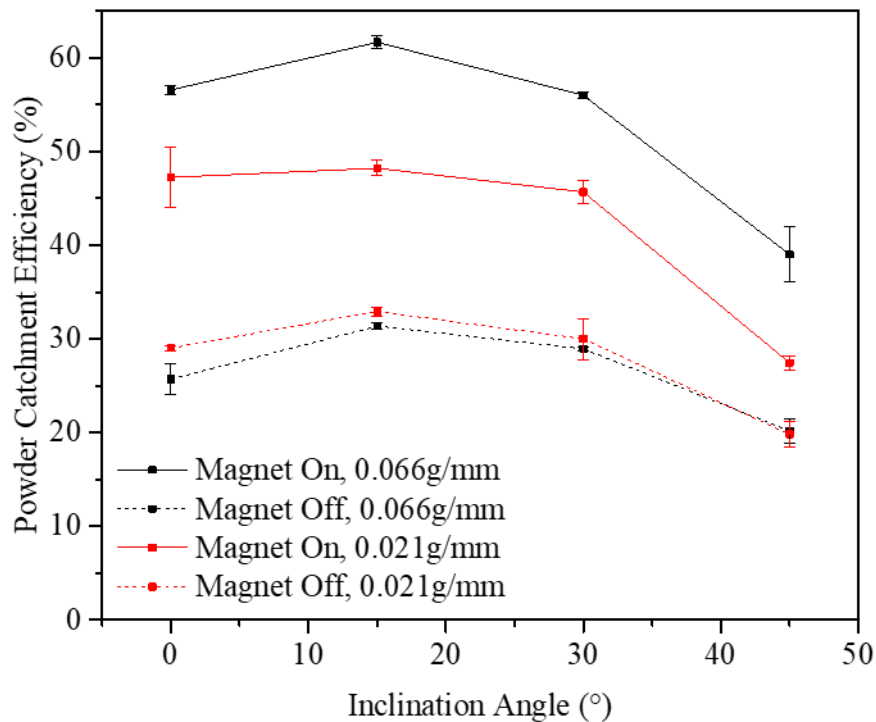


Figure 4-9 Effect of inclination angle on powder catchment efficiency for mild steel, using two different parameter sets, with magnetic assistance turned on and off.

In all cases, the addition of the magnetic field improved powder catchment efficiency. In the case of the higher deposition parameters, the improvement to catchment efficiency was greater. With increasing angle to 15°, efficiency increased slightly for all parameters, beyond which, the efficiency dropped. After 30°, the magnet assisted experiments showed absolute drop in efficiency than the non-magnet assisted experiments. At the highest inclination angle of 45°, magnetic assistance still showed a significant improvement in efficiency over the tracks produced without magnets.

The tracks made using low traverse speed and high powder feed rate [8] parameters were chosen in order to measure track symmetry, via skewness. Based on previous work in the literature, skewness is measured using the area method developed by Alya et al. [7] with the exception that data originated from FVM. Areas were measured either side of the centreline and the difference, as a proportion of the total cross-sectional area is used to calculate percentage skewness. This method is described in Figure 4-10. The results are shown in Figure 4-11.

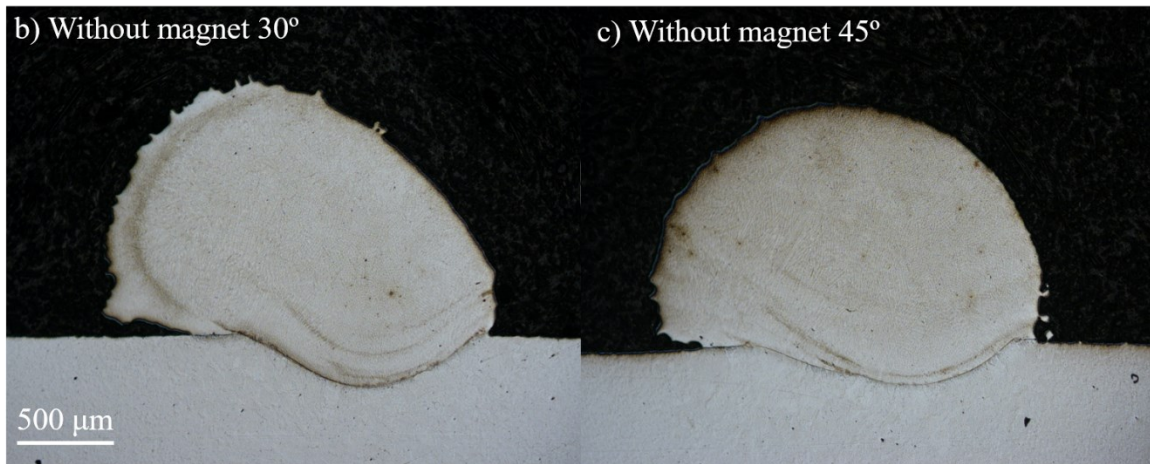
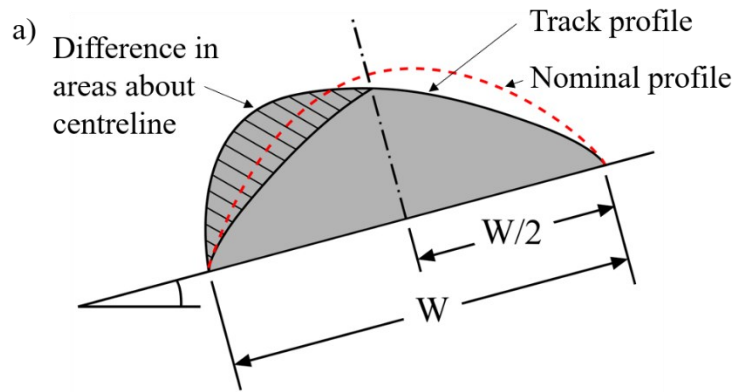


Figure 4-10 a) Shows how skewness is measured by calculating the difference in cross-sectional areas either side of the track centre, as a percentage of the total area. Microscope images b) and c) show representative (at 200 mm/min, 13.1 g/min) track morphologies in cross-sections of two tracks. The skewness was measured as 10.46% and 6.46% respectively.

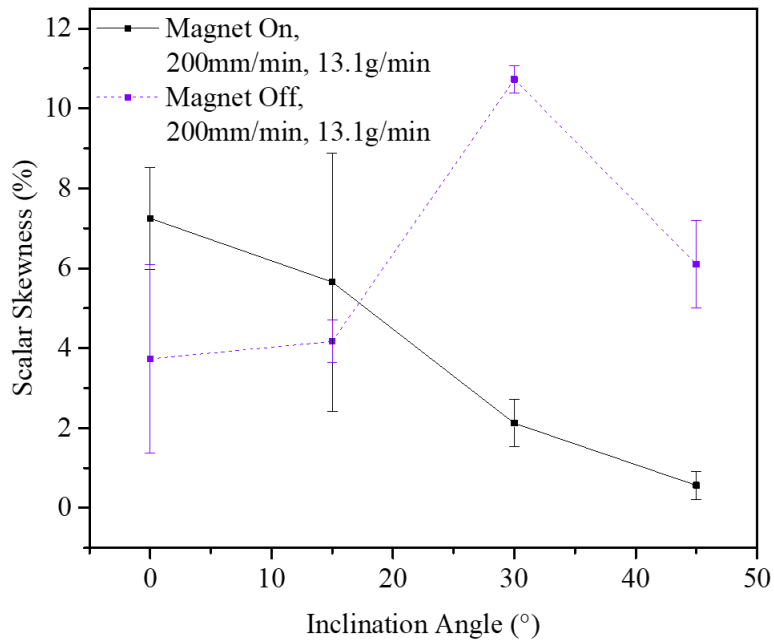


Figure 4-11 Magnetic assistance reduces cross-sectional skewness in inclined tracks, at high inclination angles, in the case of mild steel.

It is clear that the results for some measurements have a large range, represented in Figure 4-11 by standard deviation. However, despite this, there is a clear trend of decreasing skewness of the tracks with increasing inclination angle, when the magnet is switched on. This trend is opposite to that when the magnet is off, whereby the skewness increases notably at 30°, and then falls at 45°, this can be clearly seen in Figure 4-10b and Figure 4-10c in comparison to the flat plate shown in Figure 4-7. It can be said therefore that magnetic assistance of the deposition process plays a key role in track skewness.

4.3.5 Roughness & Geometry

To understand the effect of magnetic assistance on track surface properties, and to gain insight from surface data on deposition behaviour, areal Sa roughness measurements were taken from the tops of tracks and the data from this measurement is shown in Figure 4-12. The process of roughness analysis is described in Section 3.2.2.

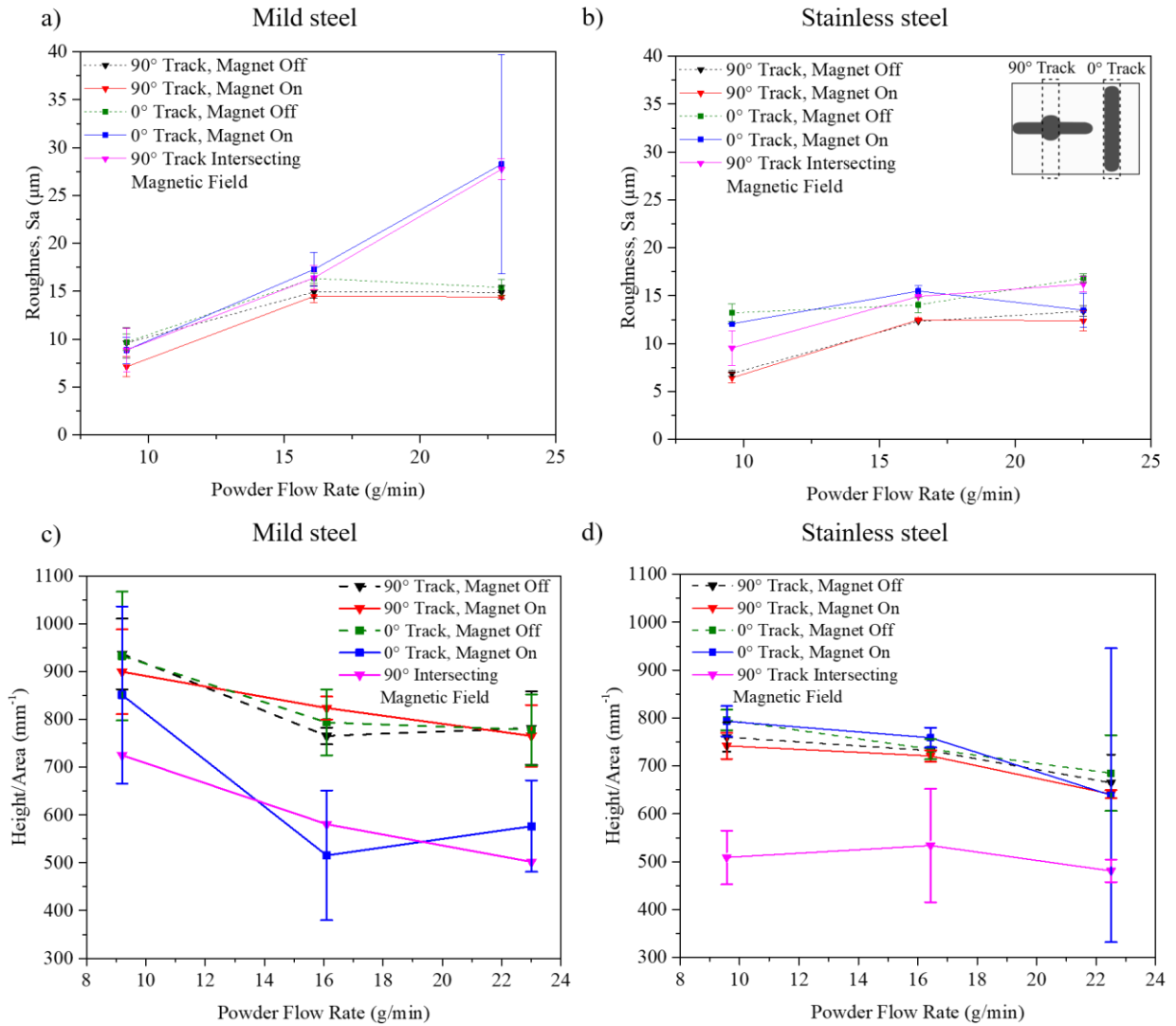


Figure 4-12 Effect of magnetic assistance on track surface roughness at 0 and 90° orientations to field lines for (a) Mild steel and (b) Stainless steel. (c) and (d) show the height/cross-sectional area ratios of tracks for mild and stainless steel respectively.

In the case of the stainless steel substrate, there is no clear trend of roughness according to having the magnet on and off. There is only a slight increase in mean Sa roughness with increasing powder flow rate, but considering errors it is difficult to draw this conclusion. In the case of the mild steel substrate, at the highest flow rate the 0° tracks, as well as the 90° tracks at points of intersection yielded a similar, notably higher roughness value than the rest of the parameters. However, in the case of the 0° track, the standard deviation of the mean roughness was much higher than from any other parameter.

Height/cross-sectional area ratios were also calculated for all tracks with and without magnets at both orientations, for both mild and stainless steel. In the case of the mild steel, both the 0° and 90° tracks at intersection points showed a reduced height/cross-sectional area implying a flatter geometry, when a magnet was used. The stainless steel showed a notably lower height/area ratio at the 90° intersections points with magnetic assistance; however no trend was seen for any other parameter for this material. Large roughness variation can be observed at the highest flow rate with the magnet engaged and at the process limits for height/area. The compounding of standard deviations in the case of height/area measurements due to the nature of the calculation, means the method obtaining these data should be considered when considering these results.

4.3.6 Hardness

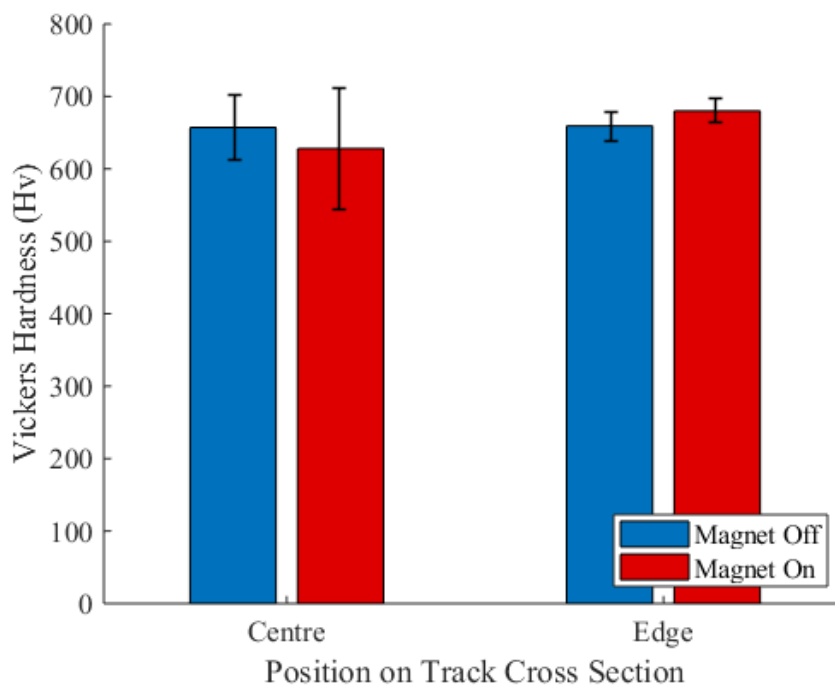


Figure 4-13 Microhardness of tracks produced with and without magnetic assistance along the track length.

The mean hardness of the two samples is shown in Figure 4-13, at both the centre and the edge of cross sections. Without a magnetic field, the centre of the track had a hardness of 647 Hv and 628 Hv with magnetic assistance. Standard deviations of between 17 and 83 Hv were noted. No statistically significant difference in hardness was noted when the hardness results were compared averaged by position.

4.4 Discussion

Magnetic assistance improved both overall material catchment and powder catchment efficiency using an approach which can be easily and economically replicated, as can be seen in Figure 4-1, Figure 4-3 and Figure 4-4. Where tracks were placed along the magnetic field (0°) and using a mild steel substrate the improvement in powder catchment efficiency due to magnetic assistance remained between 14-18%. This is in contrast to in stainless steel where no notable improvement in powder catchment was seen at 0° . With tracks at 90° to the magnets, increases in catchment were particularly concentrated at intersections between track and magnet. This was performed with minimum previous parameter optimisation, demonstrating that magnetic assistance has potential as a simple add-on which can be used to improve catchment efficiency in a time effective manner. However, it is unclear whether powder catchment efficiency could be expected to make improvements in a setup which had previously had parameters optimised, given that more of the powder would be caught in this scenario it is likely that magnetic enhancement in efficiency may be reduced. Given the complex nature of magnetic assisted DED, comprising nozzle based powder delivery, a high energy laser beam and magnetic attraction of particles, a schematic is shown in Figure 4-14 to illustrate the proposed phenomena taking place during deposition.

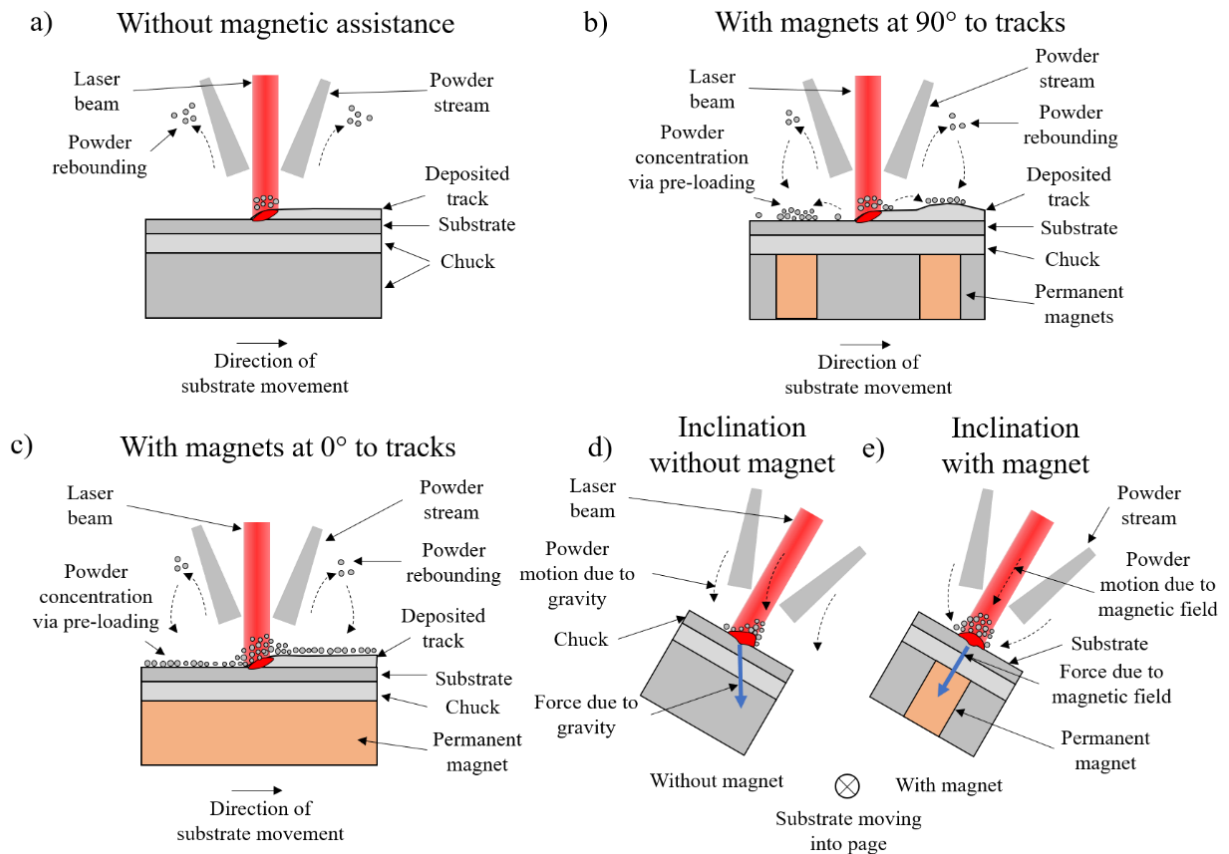


Figure 4-14 Schematic of enhanced deposition behaviour using magnetic assistance with deposition at (b) 90° to magnets and (c) 0° to magnets, in comparison to (a) without magnets.

In Figure 4-14 (a) a typical powder fed DED situation can be seen. Here, there is a concentration of powder based on the nozzle delivery beneath the laser beam and this material is melted and forms a track. Material not melted is thought to rebound away from the deposition zone and to not contribute further deposition. In (b), the same deposition scenario is shown, however with permanent magnets placed at 90° to the track direction. Here, additional concentration of powder takes place when the laser beam intersects the position of a magnet. In addition, the pre-loading of powder, whereby rebounded powder is attracted to positions above the locations of magnets, also contributes to additional material catchment. This results in an increased track size, i.e. increased powder catchment, at regions where the track intersects with the positions of the magnets.

In Figure 4-14(c), deposition takes place in an orientation in-line with the directions of the magnets. Here, a generally increased track size is produced, as powder is attracted to the positions of the magnet, which is always under the laser beam. Due to lower latency between powder leaving the nozzle and powder reaching the position of the underlying magnet, there

is in effect, less time for a more substantial build-up of magnetically pre-loaded powder, in comparison to the scenario in (b), where pre-loading at intersections is more prominent.

Figure 4-14(d) and (e) show the effect of inclination angle on powder catchment and skewness. In (d) the force on the powder due to gravity causes the track to become skewed to the downhill side, in agreement with Lin & Hwang [9]. The influence of the magnetic field is shown in (e), the force draws the powder towards the centre of the track path where the field is strongest. The mechanisms described above, and the general trend of improved catchment was seen mainly in the case of the mild steel substrate, and not generally for the stainless steel. This is explained by the ferritic structure and resulting ferromagnetic properties of mild steel. These properties cause the substrate itself to become magnetised and the powder to therefore be more strongly attracted. On the other hand, the significantly weaker paramagnetic properties, with around three orders of magnitude lower relative magnetic permeability of austenitic stainless steel [148] means it effectively does not contribute to the magnetic field strength in the vicinity of the track, and can be theoretically considered an air gap. In this scenario, the magnetic field strength is weakened with distance more greatly in accordance with Coulomb's inverse square law.

It is proposed that pre-loading of powder plays a role in overall catchment as shown in Figure 4-14 (b) and (c). The majority of powder which built up in the preloading effect is likely that which was dispersed in the air as a result of not being constrained in the melt pool. These particles have low velocity relative to those exiting the nozzle, and so are more greatly affected by the magnetic field. This effect occurs more strongly on the 90° tracks, where the nozzle alternates between close and far from the magnetic field. The preloading effect would explain why 90° tracks had greater powder catchment in the case of stainless steel, where the limited field strength had a reduced effect on fast moving particles directly under the nozzle, but slow moving, dispersed particles are affected similarly to the case of the mild steel. This is in contrast to the 0° tracks on stainless steel, where effectively no significant catchment improvement was seen. Particles which would be deflected by the vapour plume above the track may also retain their trajectory, also contributing to the increase in powder catchment efficiency.

In general, the preloading effect may be most desirable in practical situations only where an equilibrium between pre-loading of powder delivered from a nozzle can be achieved, avoiding a net build-up of unpredictable levels of powder. This unpredictability could be

potentially debilitating, by causing components to have unpredictable geometry. However, the concentration of powder beneath the nozzle via magnetic assistance would be considered to be a desirable outcome in most situations. Alternatively, pre-loading may be deliberately used in certain areas of a component by placing magnets in these positions, although future work would be required to investigate this further.

Magnetic assistance at 0° to magnet orientation once again showed an improvement to powder catchment when inclined angles were used. At all inclination angles, the improvement to powder catchment efficiency via use of a magnet, was greatest at the lower traverse speed, and higher powder flow rates. In other words, when more powder is supplied to an area per unit length, magnetic assistance has a greater effect on powder catchment efficiency. This implies that the effectiveness of magnetic assistance, depends on amount of powder reaching the workpiece. With increasing inclination angle, all results followed the same trend, with a slight increase in efficiency at 15° , and a large drop at 45° . At 45° , the impact of the magnet is lower than at 0° , for both parameter sets. This supports the previous statement, whereby effectively less powder reaching the deposition area reduced the efficacy of the magnet. This is because the usual effects of inclination are still taking place, the magnet will only capture a greater percentage of the powder nearby and cannot capture that which is already lost further from the magnetic field.

The percentage skewness being lower at higher inclination angles with the magnet on, and greater than the skewness without the magnet at smaller angles is explained by the difference in track volume, given skewness has previously been shown to negatively correlate with track volume [7]. With magnetic assistance the track volume is initially very large, but catchment efficiency reduces with greater inclination angle and the skewness decreases as a result. The turning point for skewness, at 45° when the magnet is off, is also likely to be as a result of this reduction in track size.

Without the magnet, powder is drawn preferentially to the lower side by gravity, leading to a skewed track. Whereas the magnetic field means the powder is both preloaded and focused onto, the centre of the track (as shown in Figure 4-14 (e)), especially as the field is stronger in the middle of the path.

It was also shown that despite yielding increased powder catchment efficiency, the level of dilution of material into the substrate was reduced. This is expected and can be explained by

the divergence of laser energy into the increased level of powder material in the vicinity of and above the melt pool. Therefore, this factor should be carefully considered in work aiming to produce increased dilution deposits. A reduction in dilution could be used as a beneficial method to minimise dilution in coatings applications, where the coating is not intended to affect the base material. However, in additive manufacturing this reduction in dilution would be expected to reduce layer adhesion. Future work should therefore examine whether an increase in laser power has the usual effect of increasing dilution depth and reducing the negative effect.

To further understand powder catchment behaviour in magnetically assisted LDED, roughness measurements of track surfaces were taken. Interestingly, only at the highest flow rates, and only for mild steel, did the magnetic assistance yield a statistically higher S_a roughness value. This may be explained by the higher flow rates increasing the likelihood of catchment of powder onto the cooling track, meaning there is more partially melted powder attached to the track surface and greater roughness. It is suggested that further work is conducted to characterise the near surface of these tracks to understand this behaviour to confirm this. Large variation in roughness was observed, primarily at the edges of the process window. The large variation observed at the highest flow rate in mild steel is likely due to instability caused by the increase in powder catchment, particularly without the typical practical increase in laser power to effectively melt this amount of powder fully. This factor in combination with the magnet potentially attracting powder to the partially molten pool, being dependent on the amount of powder dispersed in the atmosphere, explains this behaviour. Height/cross-sectional area data was also taken to understand the effect of magnetic assistance on the aspect ratio of the tracks. In mild steel, height/area ratio was notably lower with magnet assistance at 0° and 90° orientations. This effect was only seen at the intersection points at 90° orientation for the stainless steel. This gives some evidence that despite enhancing overall catchment, magnetic assistance also compresses the tracks somewhat, and therefore has the potential to manipulate track geometry as well as overall catchment.

No significant change in the hardness of materials was noted within this experiment. Previous work on austenitic steel has shown that static magnetic fields as weak as 62.5 mT may have led to a slight increase in hardness due to an increase in compressive residual stress, however as in this work the difference was within the expected margin of error [165]. Other magnetic

and electric fields have been shown to change the hardness of depositions produced via LDED, so more extensive work is required to determine the effect of static magnetic fields on the microstructure and hardness of steels. Determination of the strength, direction and type of magnetic field required to begin to alter track hardness must be identified.

4.5 Conclusions

This work has demonstrated for the first time that beneath-workpiece magnet placement is a simple and effective method for manipulating ferromagnetic feedstock powders used in DED. The following conclusions can be made from this study.

- Using magnetic assistance can increase powder catchment efficiency of ferromagnetic powder to a value of 56% on a horizontal plane, compared to a maximum of 26% without use of magnets. This shows that considerable efficiency improvements are possible using this novel method.
- The increase in powder catchment is due to both the increased concentration of powder directly beneath the nozzle, as well as pre-loading of powder over the positions of high magnetic flux density.
- Substrate material type plays a key role in the effectiveness of the magnet for powder catchment. Ferromagnetic mild steel yielded greater magnetic manipulation of powder and higher powder catchment. Whereas paramagnetic stainless steel, having much less magnetic permeability, only showed a significant effect on catchment at intersections of concentrated magnetic flux, suggesting that the magnetic pre-loading mechanism is dominant when the magnetic field is weak.
- Magnetic assistance can mitigate the decrease in powder catchment when an inclined workpiece angle of 45° is used, from 20% to 39% at higher flow rates.
- At lower traverse speeds, and higher powder flow rates, magnetic assistance has a greater effect on powder catchment.
- There is evidence that magnetic assistance can increase the aspect ratio, compressing tracks.
- The track skewness reduced with increasing inclination angle when a magnet was used. This may be explained by the reduced powder catchment at higher inclination angles and by the magnet aligning powder along the centre of the track.

- The level of dilution significantly decreased when using a magnet, particularly at lower powder flow rates. This is explained by the greater divergence of laser energy when the magnetic field is present.

In work beyond this thesis more advanced placement of permanent magnets should also be considered to manufacture complex 3D parts and coatings. Future work within this thesis investigates the use of more precise manipulation of magnetic fields to better control powder movement to achieve uniform increases in powder catchment while varying process parameters, also determining the extent to which magnetic preloading is the primary mechanism at work.

5 Investigation of Electromagnetic LDED

5.1 Introduction

As discussed in the literature review (Section 2.3.4) The ability to focus the powder stream is vital in reducing the feature size which may be produced [111], thereby expanding potential applications. Melt pools larger than the powder focus diameter, and high laser powers, are required to efficiently melt the material over the whole width of the powder focus diameter [6]. But, the high energy input required has also been shown to result in broader tracks [113]. Improving the convergence of powder streams is therefore critical to allowing narrower tracks to be produced, due to both the smaller powder stream as well as allowing smaller laser spot sizes and reduced powers to be used as a result.

Bax et al. summarised a number of parametric studies on DED, contributing a statistical process map to convincingly suggest generic relationships between input parameters and their effects on tracks, [71] allowing track geometry to be optimised. As discussed previously (Section 2.3.7) catchment efficiency is one of the main drivers of cost in LDED. Although some powders may be reused, [97] this generally results in poor resource efficiency and inflates process cost [100]. It is known that catchment efficiency is strongly dependent on stand-off distance, laser power and laser spot size, [36] because high catchment efficiency occurs when the powder stream is focused within the melt pool [6]. Changes to both material and method of laser delivery have been used to improve both catchment efficiency and the process resolution. Rapid development in nozzle design [32] means improvements in this area are ongoing, leading to significant improvements in catchment efficiency, as shown by Takemura et al. [136]. Though even in state-of-the-art nozzles catchment efficiency is generally limited to around 60 - 70% [6]. Ideally a large laser spot [76] will be used with a narrow powder focus [77], to ensure the maximum quantity of powder is directed into the melt pool. Govekar et al. showed that delivering powder with an annular laser is an effective method to do this, and can increase powder catchment efficiency to around 80% [39]. A recent review from Singh et al. also promoted the use of vibrational feeding methods as an alternative to conventional blown powder methods, giving the user more flexibility to quickly change the feed rate [6]. Wang et al. also showed that this can be used to create narrower powder streams [19].

Track resolution and powder catchment however are fundamentally in opposition, as higher laser power and stand-off distance optimised for better catchment efficiency both tend to lead

to an increase in the width of the tracks produced. A choice is therefore often made between an efficient process and one which produces a high-resolution product. New methods which address either of these factors must be developed so that parameters may be better optimised for the other.

Sometimes magnetic fields have been used in conjunction with LDED as discussed in Section 2.7. Zhou et al. for example showed that by magnetically stirring the melt pool they could increase the hardness of a magnesium alloy by refining the grain structure [175]. This study uses a new approach, where the effect of a magnetic field on the macroscopic morphology and track geometry in ferromagnetic materials is assessed.

In this chapter a new method of magnetic assistance is demonstrated, this represents a step change in the ability to control magnetic assistance. By using a solenoid coaxially aligned to the laser, magnetic fields may be created which eliminate the magnetic preloading effect which was suggested to be problematic in the previous chapter. The relationships between the strength supplied by this magnetic field and geometric properties may also be assessed for the first time, along with the effect of this new type of magnetic assistance on both geometry and hardness.

5.2 Experimental

Commercially available 12 V solenoids were used to provide the magnetic fields used here. Frustum cones were used to focus the magnetic field into a smaller area, so that the powder would be drawn towards the laser spot. The diameter of the base of the cone was equal to the core diameter of the solenoids. This frustum cone was placed underneath the substrate with the tip in contact with the underside of the substrate and the base on the solenoid core. Using this method, the diameter of the magnetic field through the substrate (when measured using magnetic viewing film and Vernier callipers) was reduced from 24 mm in diameter to approximately 4 mm. Further reduction in the diameter of the cone tip resulted in a drastic reduction in the strength of the magnetic field (using a 3 mm diameter tip resulted in the magnetic field strength dropping to approximately one third of that when 4 mm tip was used). This setup is shown schematically in Figure 5-1. Pulse width modulation (PWM) was used to control the magnetic field strength and an Arduino Mega (Arduino, Italy) was used to automate control of this magnetic field. This solenoid setup allows more advanced control over the magnetic field and restricts the size of the field, meaning magnetic placement can be varied precisely. The magnetic field strength was measured using a PCE-MFM 3000 Gauss metre (PCE instruments, UK) and was found to vary by only 0.5 mT within the effective

diameter. Only normal background magnetic field strength was detected outside the area measured using magnetic viewing film. Using the setup shown in Figure 5-1 magnetic assistance was used in single-layer depositions.

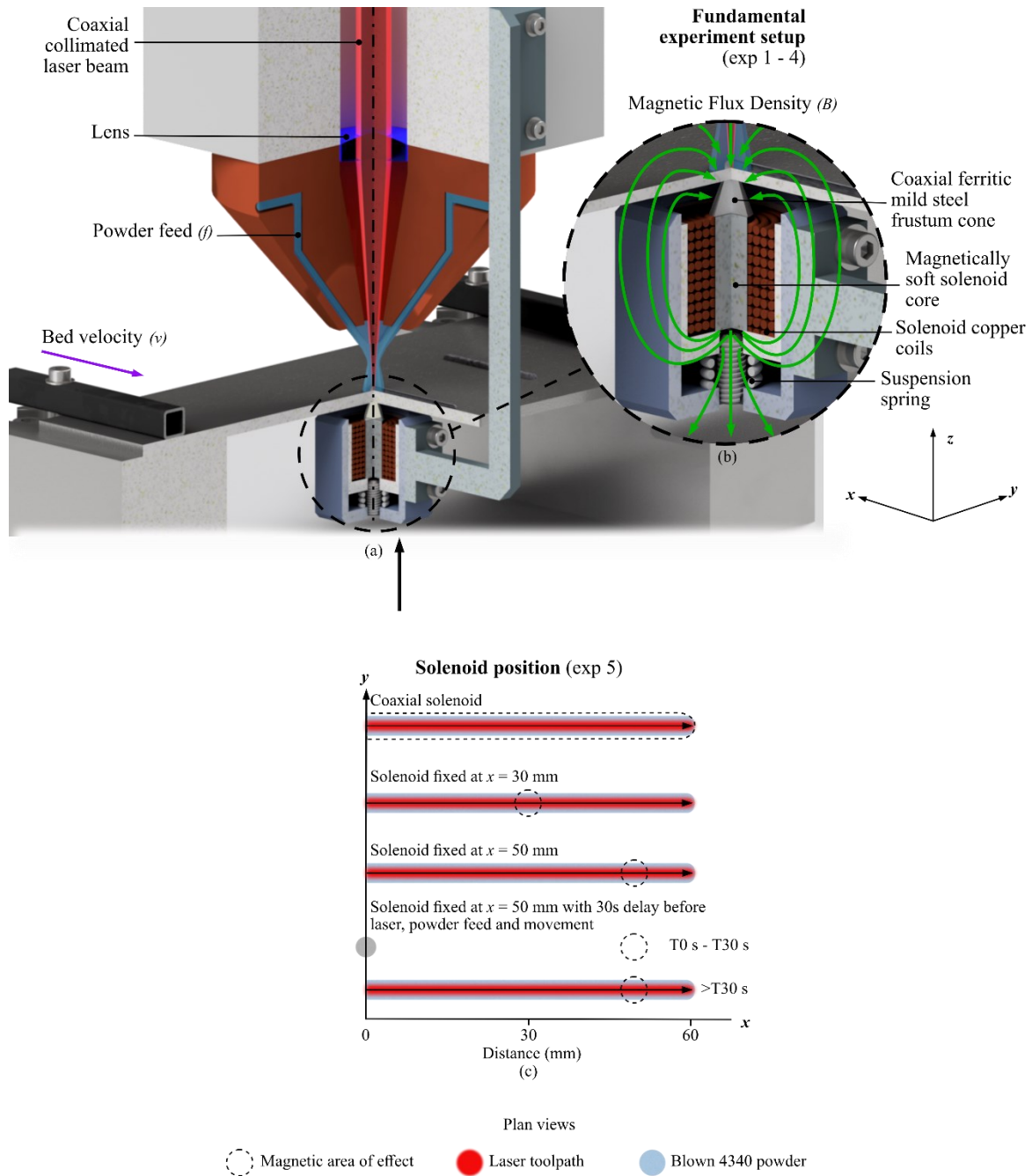


Figure 5-1 Experimental setup and toolpaths. Shown in (a) for fundamental experiments, on the effects of electromagnetic field strength, laser power, powder feed rate and traverse speed with a coaxial solenoid. The magnetic flux around the solenoid is shown in (b). The different positions of the solenoid are shown for the solenoid position experiment (c).

AISI 4340 (Sandvik Osprey) powder was used to examine the effects of the magnetic field on various parameters. This is a low alloy steel [143] and is used in the aviation and nuclear

industries. Powder size distributions were measured using a Malvern Mastersizer 3000 and are available in Table 5-1, chemical composition is available in Table 3-2. Rolled mild steel (MS) substrates were used in all experiments in this chapter, these had a thickness of 0.8 mm as discussed in Section 3.3.5. Thin ferromagnetic substrates were used so that the magnetic field from the solenoid could be induced locally in the substrate and to avoid magnetic shielding. The real measured magnetic field strength at the substrate surface is given for each of these materials, in Table 5-1, when using the setup described above. Magnetic field strength was reduced in some experiments as the increased material present can cause tracks to peel from the substrate, similar to when high powder feed rates are used.

Experimental parameters were chosen to characterise the effects of different process parameters and variables on MADED. Different parameter sets and variables were therefore used in this study, with parameters outlined in Table 5-1. As parameter interactions are not yet fully understood in MADED a one variable at a time (OVAT) approach was used to characterise geometry before moving on to investigate novel uses of magnetic assistance.

Table 5-1 Summary of experimental parameters used. Field strengths are those measured on the surface of substrates.

#	Investigated Variable	Solenoid Placement	Flow Rates (g/min)	Laser Powers (W)	Field Strengths (mT)	Scan Speeds (mm/min)	Powder Material	Substrate Material
1	Magnetic field strength	Coaxially aligned to laser	15.7	900	0-93.5	500	AISI 4340	0.8mm ± 0.09 0 Mild Steel
2	Laser power	“	16.6	600-1000	0 & 32.2	500	“	“
3	Powder feed rate	“	10.1-20.6	600	“	500	“	“
4	Traverse speed	“	13.0*	600	“	200-650	“	“
5	Solenoid position (magnetic preloading)	Static 30 mm, & 50mm from track start.	17.5	900	0 & 93.5	500	“	“

When investigating the effect of magnetic placement (exp 5) the solenoid was fixed to the moving bed, so that only one portion of the track would be affected by the magnetic field, as shown in Figure 5-1(c). This was done to examine the difference between using a coaxial magnetic field and a fixed magnetic field, where the powder is allowed to accumulate (or magnetically preload) on the magnetic field ahead of deposition. Build duration was expected to play a role in the quantity of powder which would be attracted to the solenoid position throughout the course of a build. Therefore, the magnet was placed 30 & 50 mm from the beginning of the track; in an additional condition, powder was deposited with the laser inactive over the track start point and with the bed stationary ($x = 0$) for 30 s before beginning track consolidation. This was done to simulate a longer build. In the delayed condition the solenoid was also placed 50 mm from the track start to maximise the preloading time.

5.3 Results

The experiments in this section were used to determine the fundamental behaviour of the process of magnetic assistance. Therefore, the effects of magnetic field strength, laser power,

traverse speed and powder feed rate on track geometry and powder catchment efficiency were examined.

5.3.1 Magnetic field strength

The magnetic field strength experiment was designed to determine whether a coaxially aligned magnetic field (rather than one which covers the whole or a specific part of the track) could be used to change track geometry and improve powder catchment efficiency and investigate how the strength of such a field affects catchment efficiency and track geometry. The 12 V input was reduced, by 5% increments of pulse width, to determine whether a weaker field resulted in more significant changes.

The improvement in catchment efficiency with increased magnetic field strength is shown in Figure 5-2(a), with catchment efficiency improving with greater magnetic field strengths. In the region between 0 mT and 10.1 mT the substrate shielded the magnetic field from the solenoid so that the flux was dispersed through the substrate, the laser could not be accurately aligned with the magnetic field using magnetic viewing film, hence no experiments were conducted in this range. A substantial increase in track width occurred when magnetic assistance is used even at the lowest strength of 19.9 mT as shown in Figure 5-2(b), this is then followed by a linear region of increase from 19.9 mT to 93.5 mT. Over the range tested there is a proportional increase in track cross sectional area as magnetic field strength increases as demonstrated in Figure 5-2(c) in contrast to the jump in track width when the magnet is switched on. This increase in cross sectional area is accompanied by a reduction in the cross-sectional area of the dilution zone (Figure 5-2(d)). Some representative examples of the dilution zones are shown to permit comparison, though as the error bars suggest this large change did not always occur. It is unclear whether the magnetic field causes a change to the deviation in results, with error bars indicating that this may be the case. The standard deviation in a few field strengths for dilution results is much greater than in other cases, as single slices must be used to measure this, whilst longer FVM sections were used for the above substrate morphology.

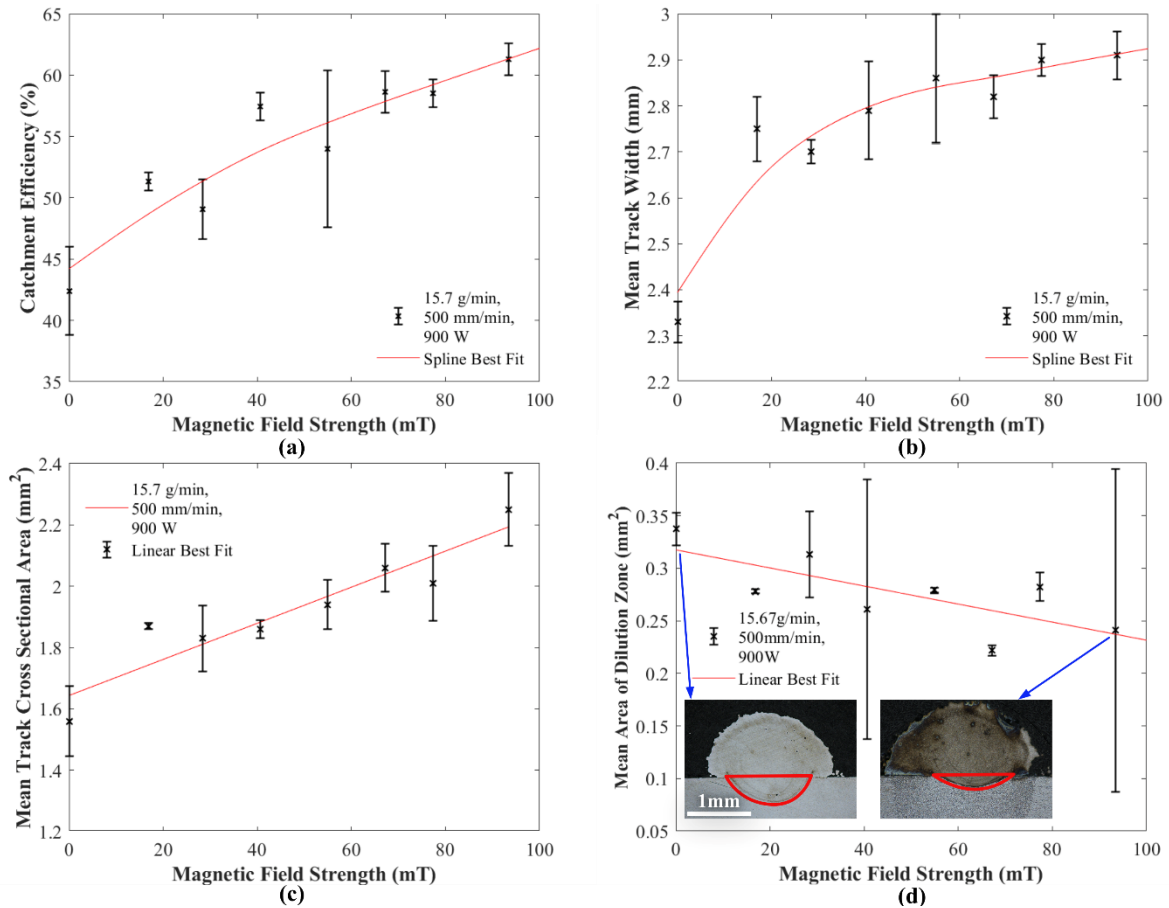


Figure 5-2 Effect of magnetic field strength on track properties, demonstrating that increased magnetic field strength leads to improved catchment efficiencies, whilst dilution is reduced. (a) Catchment efficiency (b) track width (c) cross sectional area (d) dilution is reduced. (a) Catchment efficiency (b) track width (c) cross sectional area (d) dilution area. Error bars indicate standard deviation.

Overall, an increase in magnetic field strength causes a proportional increase in the catchment efficiency and the cross-sectional area of tracks, whilst a proportional decrease occurs in the case of dilution area. A significant increase in the width of tracks occurs when the magnetic field is used even at low field strength, this is followed by a proportional increase in track width with field strength. The cross-sectional area above the substrate, Figure 5-2(c), validates the improvement in catchment efficiency, as this was measured in the stable region of the track, meaning start and stop powder build up was not included.

5.3.2 Role of laser power with magnetic assistance

In this experiment, laser power was varied to determine whether the changes caused by magnetic assistance depended on the laser power present, also investigating if the changes to dimensions could be replicated across a range of laser powers.

An increase in laser power is shown to increase track cross sectional area (Figure 5-3), track height, width, and dilution. The larger cross-sectional area shown in Figure 5-3(a) is in agreement with literature, where laser power is correlated with increased track width [71]. In Figure 5-3(b) a consistent and significant reduction in the size of the dilution zone is shown when magnetic assistance is applied at 800 and 900 W. Significant deviation at 1000 W means effective comparison here is less meaningful. Notably deviation in the dilution zone area is reduced with magnetic assistance.

Figure 5-3 (c) shows that the height of tracks is slightly reduced when magnetic assistance is applied, despite changes to the laser power. The deviation in height is similar to the difference in height between the magnetically assisted and control conditions, suggesting that this correlation is not strong. The effect of magnetic assistance on height appears to be greatest at low laser powers.

In Figure 5-3(d) it is shown that there is a consistent increase in the width of tracks when magnetic assistance is applied at all powers tested. This increase in width appears to be consistent even as power increases, which also increases the width of tracks. An increase in catchment efficiency was also demonstrated at all powers when applying magnetic assistance, from 56% to 60% at 1000 W.

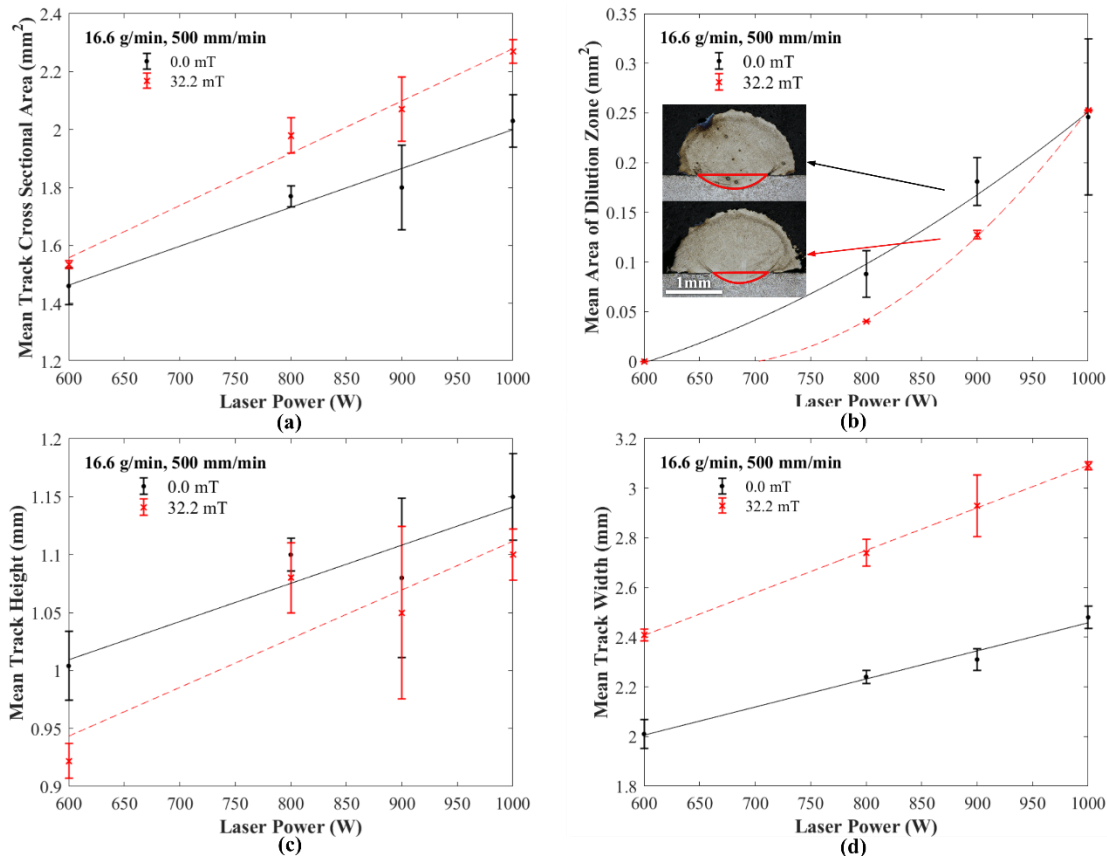


Figure 5-3 Effect of laser power and magnetic assistance on (a) cross sectional track area (b) track width (c) height and (d) area of dilution zone. Cross-sectional area increases due to magnetic assistance whilst height and the area of the dilution zone decrease. Error bars indicate standard deviation.

Magnetic assistance increases the powder catchment efficiency and track width even when power is varied by up to 400 W. In this case magnetic assistance of 32.2 mT reduced the dilution zone size and height of tracks compared to the control.

5.3.3 Powder flow rate and traverse speed in the presence of a magnetic field

Here powder flow rate was varied to determine whether magnetic assistance has a similar effect to increasing the powder flow rate, or whether the effect is independent of the change in the available powder. Scan speed is generally not considered to dominate track morphology [71]. By varying this parameter, the authors sought to determine whether this is still the case with magnetic assistance.

Magnetic assistance is shown to increase cross-sectional area and track width, despite variation in either flow rate or traverse speed. In Figure 5-4(a) the increase in cross-sectional area is shown to be reduced at lower powder flow rates, rising towards a maximum area increase at higher flow rates around 19 g/min. For track width, Figure 5-4(b), there is an

immediate jump at 13.7 g/min which appears to peak in the case of magnetic assistance, whereas a more consistent increase in width is shown when no magnetic assistance is present.

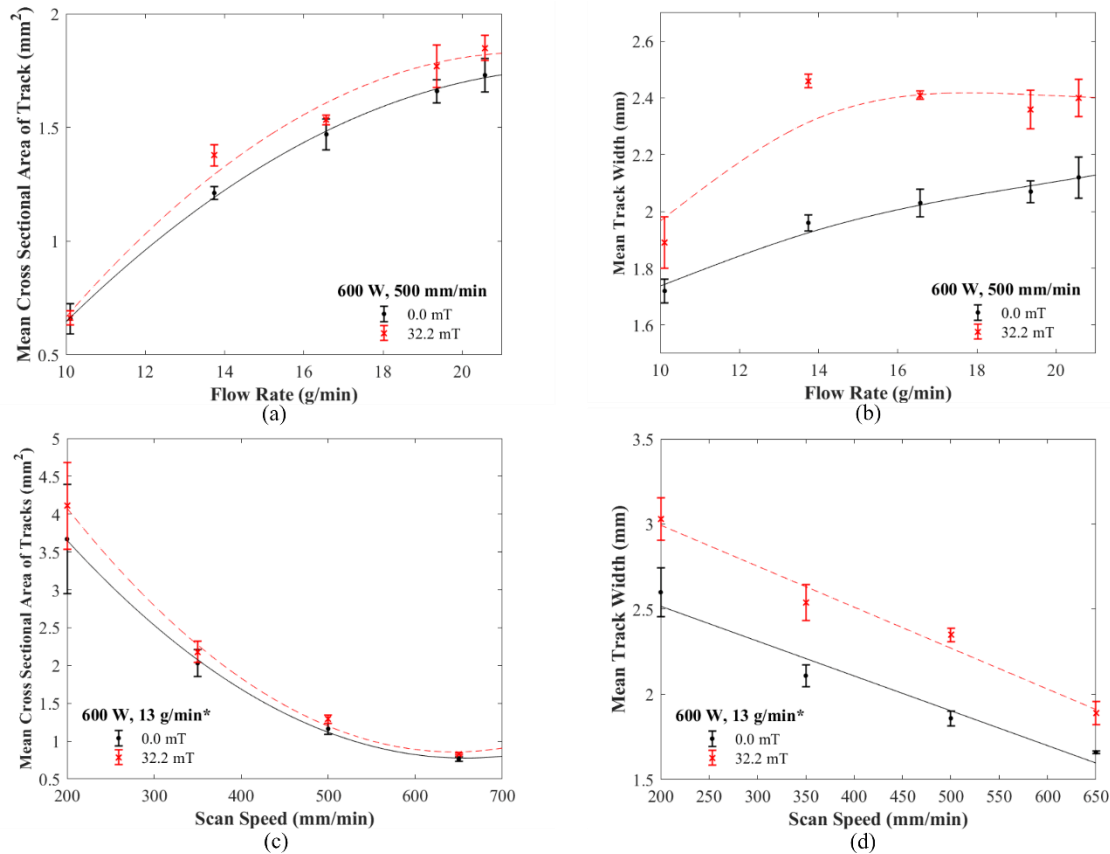


Figure 5-4 Effect of powder flow rate and scan speed on (a), (c), cross-sectional area and (b), (d) track width. The effects of magnetic assistance are consistent with regard to scan speed, but vary with flow rate. Asterisk (*) indicates powder flow rate calculated from mass of control tracks. Error bars indicate standard deviations.

In Figure 5-4(c) and (d) the effects of traverse speed are shown to be inconsequential, with a consistent change in the size of tracks being observed when traverse speed is varied.

Catchment efficiency follows the trends of cross-sectional area in both the cases shown in Figure 5-4. Cross-sectional area is a more accurate, though indirect measure of catchment efficiency. As catchment efficiency is determined by mass, inconsistencies in the deposition at the beginning and end of tracks show in the deviation of catchment efficiency, whereas cross-sectional area taken across a long section is independent of start and end fluctuations. Hence, catchment efficiency is omitted from Figure 5-4. Magnetic assistance caused an increase in catchment efficiency from 36% to 41% at 20.6 g/min in powder flow rate experiments and from 37% to 41% at 650 mm/min in traverse speed experiments.

5.3.4 Solenoid position

By using the same magnetic field in both a coaxially aligned and static (magnetic preloading) case the mechanism of magnetic assistance can be explained more comprehensively than has been done previously. The experiments here are designed to determine whether this is the case. Allowing the deposited powder to magnetically preload in certain positions over the smaller fixed solenoid may also be an effective measure to change track dimensions in specific locations, with magnetic preloading experiments helping to determine whether this is possible.

The results here are based on the solenoid positioning experiment shown schematically in Figure 5-1(c). In this experiment the cross-sections were measured where the position over which the static solenoid was placed. Figure 5-5(a) shows that magnetic preloading caused a greater increase in track cross-sectional area than when the magnet was aligned to the laser and preloading was eliminated. FVM profile measurements show that the cross-sectional area of tracks increased by 83% when comparing tracks magnetically preloaded in the centre of the track to the equivalent with no magnetic field. When the magnetic field was coaxially aligned the cross-sectional area increased by 23% compared to the control condition.

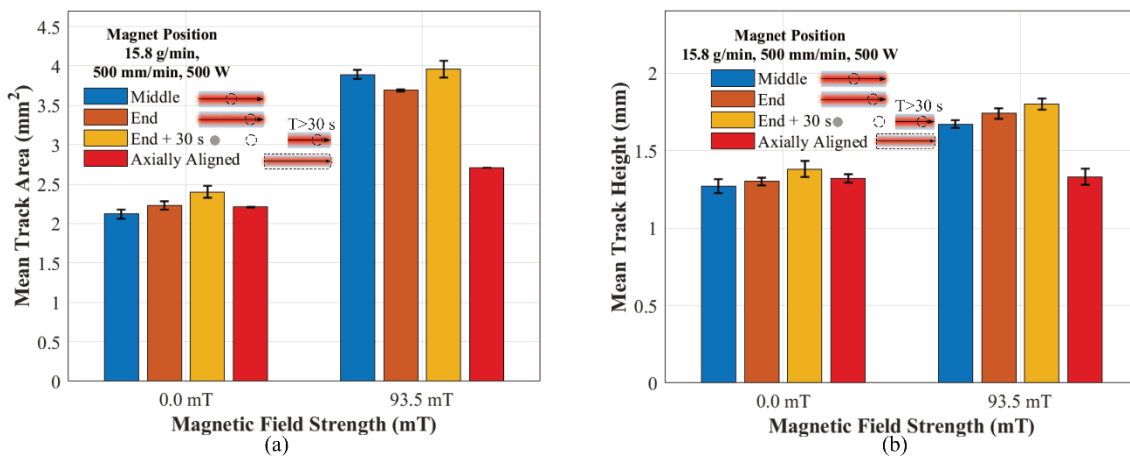


Figure 5-5 Effect of magnetic preloading on track geometry, (a) cross-sectional area, (b) track height at the preloading positions. A significant increase in track cross-sectional area and height occurs when using magnetic assistance in the preloading condition compared to where the solenoid is coaxially aligned to the laser.

Figure 5-5 (b) shows that the height of tracks is also increased due to magnetic preloading, with a mean track height increase of 31% when preloading in the centre of the track, with only a 1% increase when the solenoid was coaxially aligned with the laser. The width of tracks also increased, by 52% in the case of central preloading compared to 49% when

coaxially aligned. There is some variation in both the cross-sectional area and height of tracks when the magnetic field is off and on depending on the position. Although height appears to increase with distance from the track start, this effect is not significant given the deviation in results.

5.3.5 Hardness

The hardness of tracks produced in the magnetic field strength experiment was assessed using a Vickers microhardness testing machine as described in Section 3.2.2. A total of 72 measurements were used to quantify how magnetic field strength affects the hardness of track manufactured using this method. Two samples were used in each condition to quantify the hardness of the tracks and measurements were taken in similar locations in both samples. The data gathered from these samples is shown in Figure 5-6.

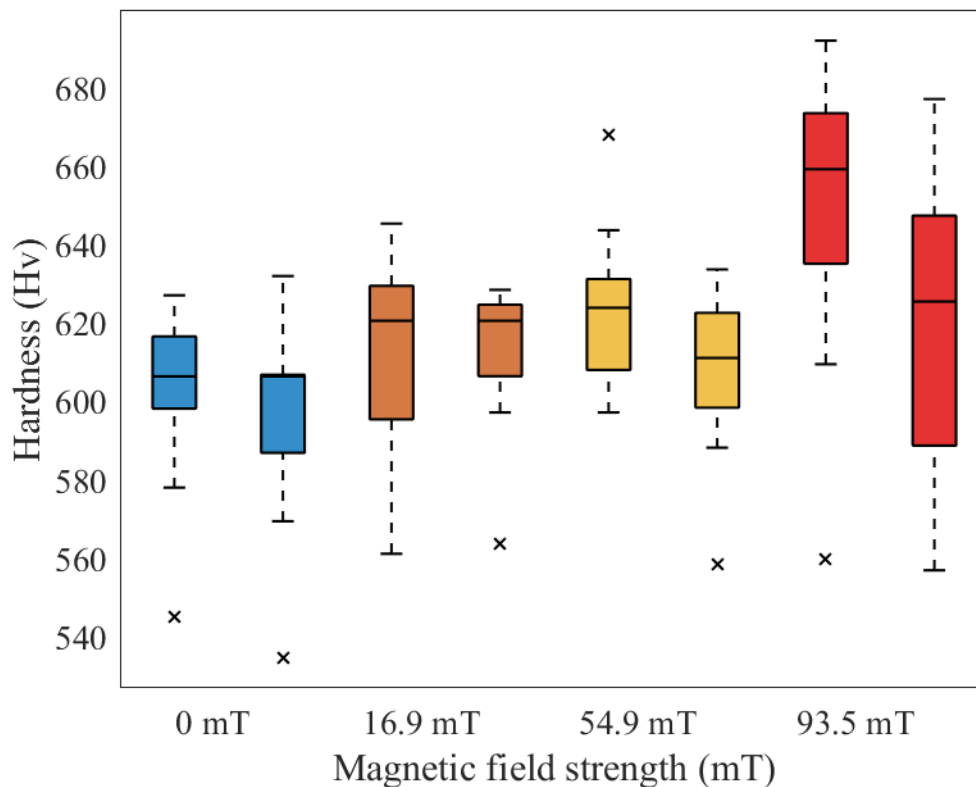


Figure 5-6 Hardness of cross-sections produced at different magnetic field strengths with the magnetic field coaxially aligned.

The significant deviation in the results means no firm conclusions can be drawn on whether , an increase in magnetic field strength leads to an increase in the microhardness of the track cross-sections. An overall increase in magnetic field strength may have a slight effect on the

hardness of tracks, but more work is required to confirm this. There may be slight increase in hardness when applying a stronger magnetic field compared to not using one at all.

5.4 Discussion

Critically, this work has shown that magnetic assistance can increase powder catchment efficiency by up to 25.0% with a magnetic field coaxially aligned to the laser, and up to 74.2% using only a small magnetic field of 109.1 mT produced by a 12 V solenoid. The mean cross-sectional area was also increased by up to 83% via magnetic preloading. As powder catchment efficiency has been shown to be proportional to the magnetic field strength, this suggests that there is a strong case for further development of magnetic assistance in DED systems. Figure 5-7 shows the effect of the magnetic field on the powder stream without the laser. Turbulent and rebounding particles are constrained onto the substrate even without a melt pool. This is demonstrated in Figure 5-7(e) by the high baseline of brightness close to the substrate which is not present when the magnetic field is active. The angle of illumination explains why the brightness is consistently greater on the left-hand side. Figure 5-7(c)-(e) show that the powder concentration trends towards a gaussian shape at the powder focal distance close to the melt substrate. In the area measured (0 – 7 mm from the nozzle tip) the only difference observed in concentration was due to the powder rebounding, although measurement could not be taken very close to the substrate (<3 mm away) due to the noise created from rebounding powder and that which is attracted to the substrate. Reduced rebounding and deflection are therefore likely at least part of the causes of increase powder catchment efficiency. However, whether the powder stream is also reduced in diameter was not measured here.

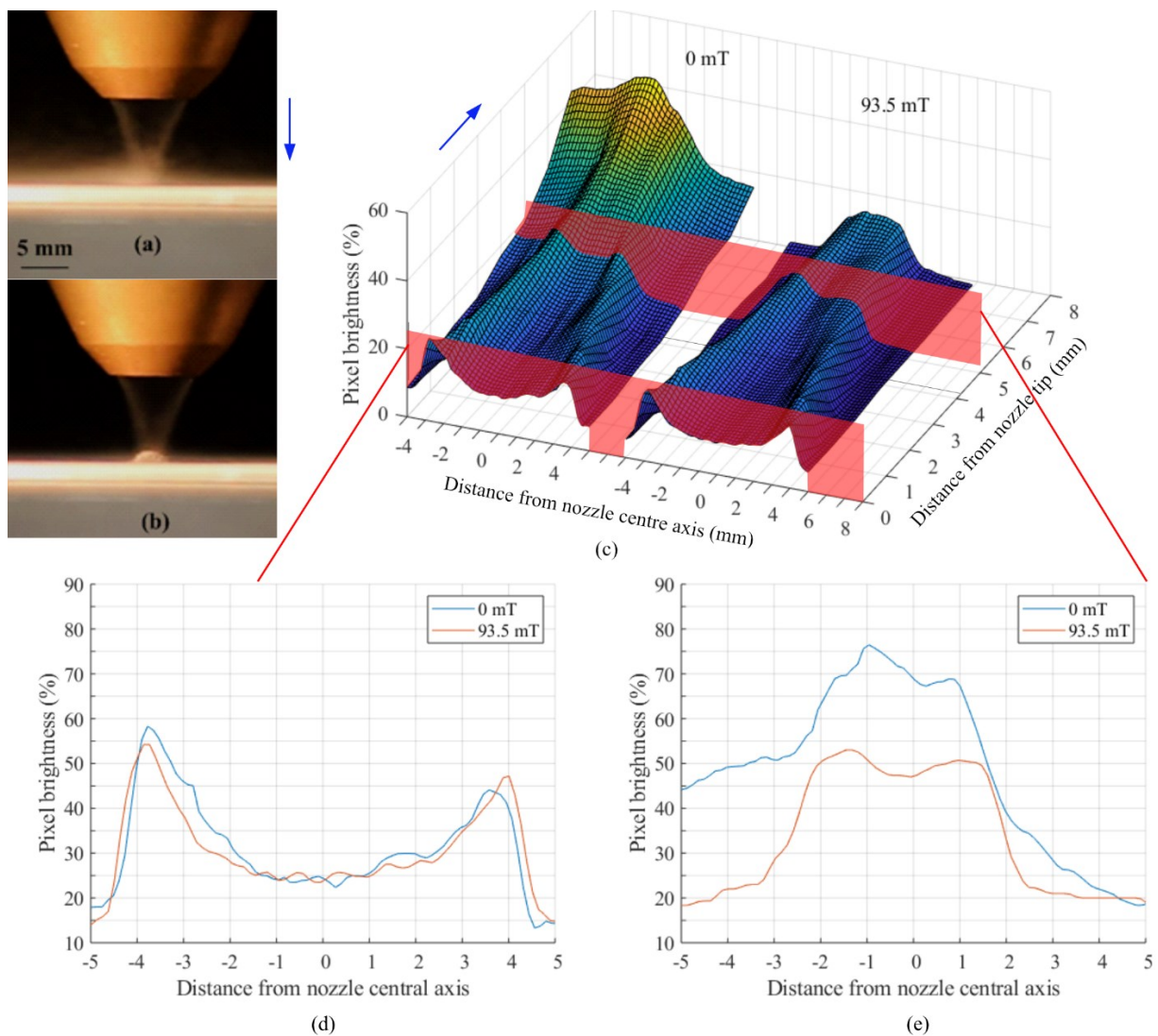


Figure 5-7 Images of the powder stream exiting the nozzle without an incident laser; (a) shows with no magnetic assistance, (b) shows with 93.5 mT magnetic assistance after the magnet had been switched on for 0.12 s. The brightness of these images was measured across the nozzle width to generate (c)-(e). The 3d plot of pixel brightness (c) demonstrates that the powder converges from a bimodal to a gaussian distribution, whilst (d) shows a slice of the distributions at the orifice as the powder exits the nozzle and (e) shows the distributions 5mm after exiting the nozzle.

The catchment efficiency increases as more powder is consolidated at the edges of the tracks, also making the track wider in MADED. This is clear because the height of tracks remained more stable, and a slight reduction, of 50 μm or 5% of the total height, could sometimes be observed (Figure 5-3(c)). In contrast, increasing powder feed rate is normally associated with an increase in track height. An increase in track height was sometimes observed. When magnetic preloading is allowed this becomes significant as shown in Figure 5-5(b). A specific combination of parameters (such as high powder feed rate and low power) may cause the relationship with height to change in the case of a coaxial magnet, this is likely related to the

powder feed rate, as height is more greatly affected by powder feed rate when deposition rates are high, though further work is required to determine this.

Increased powder feed rate is normally associated most strongly with an increase in track height. Because increasing magnetic assistance is more closely linked to an increase in width, sometimes with a slight reduction in height, the mechanism of magnetic assistance on track geometry is different to simply increasing powder feed rate. This is demonstrated in Figure 5-2 & Figure 5-4, as track width increases much more significantly than catchment efficiency or area.

Magnetic field strength is inversely proportional to the square of distance, so the magnetic field strength is greatest at the substrate surface, closer to the source. The highest change in magnetic field strength will also occur at the substrate surface, as the substrate is magnetised. Ferromagnetic particles will experience the greatest force due to the magnetic field where this gradient is greatest [158]. This means the particles are preferentially attracted across the width of the magnetised part of the substrate rather than increasing the concentration directly in the centre of the magnet. This could explain an increase in the width of the track rather than the height. With the particles further from the centre of the field (but still close enough to experience it) experiencing the greatest displacement towards the centre. Although the gradient of magnetic field strength will also be greatest at the edge of the field, the field is much wider than the melt pool (at 4 mm diameter compared to track width ~2 mm), so no powder is melted here. Powder which is not immediately melted will also be retained due to the field, meaning there is more time for powder which does not melt immediately on impact to be consolidated by conduction, this could also be the cause of the increase in width. More investigation, such as melt pool and powder imaging is required to fully understand why width increases more than other dimensions.

An increase in the peak height, which appeared in the switching experiment, could be expected if either more powder is attracted evenly to the whole of the melt pool, or more powder is attracted to the centre. Direct imaging of the powder flow is required to determine why width is increased preferentially. If powder is attracted to the centre, fields narrower than the melt pool could be used to reduce the width of tracks and thereby manufacture finer features, providing surface tension can be overcome.

Figure 5-4 suggests that the effects of magnetic assistance on the increase in size of tracks is largely independent of both scan speed and powder feed rate. This is not true of the track

width, at a feed rate threshold around 13.7 g/min the track width increases substantially and then largely levels off, this is likely due to the limited energy available to the powder, as power has been closely linked to melt pool diameter and track width. This supports the theory that the powder distribution on the substrate is increased across the powder stream. It is likely that an equivalent increase in laser power would allow the track to expand further, as suggested by the positive linear correlation between width and power, in Figure 5-3(d).

The area of the dilution zone also appears to be reduced with magnetic assistance. Increasing powder feed rate has been shown to attenuate laser energy both at the melt pool and on the track surface, [176] and hence the increase in powder due to magnetic assistance would be expected to reduce the energy available to melt the substrate, as has been previously suggested. Magnetic assistance therefore has an equivalent effect to increasing powder feed rate on dilution. In Figure 5-3 additional power was shown to increase the dilution, and so to retain consistent dilution power should be increased when using magnetic assistance. Or instead, magnetic assistance could be used to reduce dilution intentionally.

This work has shown that improvements to catchment efficiency are not limited to the preloading condition. As shown schematically in Figure 5-8 below, this could not be determined by previous work. This finding is important to the practical implementation of magnetic assistance, as the potential time dependence of preloading means that magnetic assistance would result in unstable deposition if this were the only mechanism present. In Figure 5-5 preloading is shown to lead to a much greater increase in catchment efficiency and deposition height than coaxially aligned magnetic assistance, but a significant increase is still present using a coaxially aligned magnetic field.

Preloading may not be completely eliminated in this setup, as the magnetic field radius (2 mm) could not be made as small as the laser spot (0.7 mm). However, the magnetic field only extends 1.3 mm ahead of the edge of the laser spot (with the melt pool being even bigger than this), so there is only 0.15 s before the laser reaches the edge of the magnetic field. Hence the mechanism must be negligible compared to the 37.2 s delay time in the fixed position solenoid, delayed laser condition.

Whether the amount of magnetic preloading is dependent on the previous deposition time remains unclear, as the increase in area with time is small and close to the deviation. If a relationship is present, it is likely to be weak.

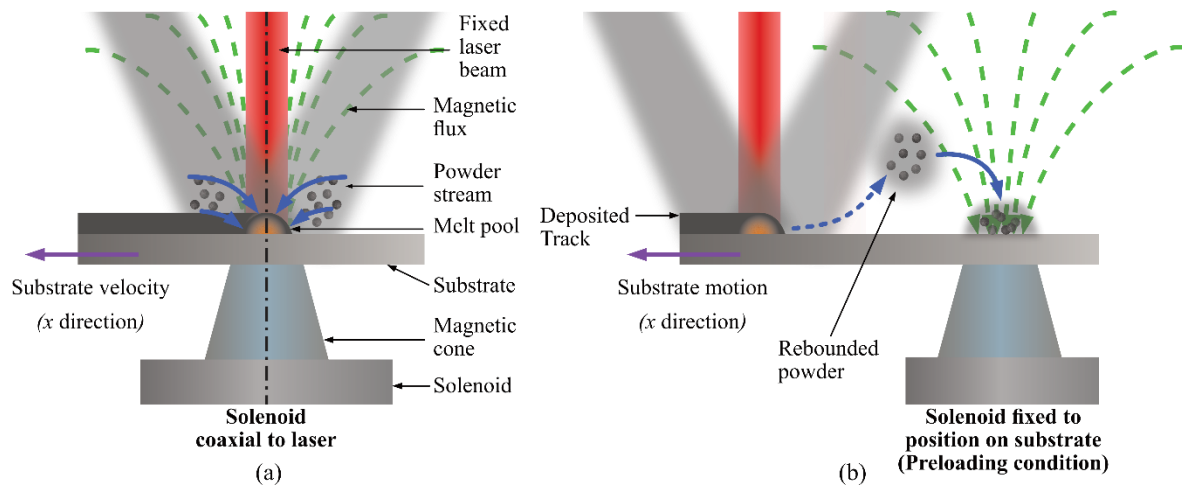


Figure 5-8 Mechanisms of powder capture via magnetic assistance, (a) where preloading is eliminated via a coaxial aligned solenoid. (b) Where preloading is encouraged using a solenoid in a fixed position relative to the substrate. Both have been shown to increase the dimensions of tracks.

The slight change in hardness and particularly the increase in hardness variation when applying increasing magnetic field strengths suggests that the magnetic field strength has an effect on the cooling of depositions. In steel cooled from molten under these conditions an increase in hardness is most commonly associated with an increase in the cooling rate. Lu et al. conducted a similar experiment using paramagnetic steel to determine the effects on cooling rate and hardness [165] and suggested that use of a static magnetic field increased the cooling time of the melt pool by restricting the size of the plasma plume, they suggest that this can cause the cooling rate to decrease and encourage larger grains to form by prolonging the time of solid-state transformation. The magnetic field decelerating fluid flow in the melt pool via Lorentz forces is also suggested as a reason for a reduced cooling rate as less fluid motion means convection would be reduced. A decrease in the cooling time would be expected to reduce the hardness as it is likely to increase grain size and reduce martensite formation. They suggest that this is because there is an increase in compressive residual and a reduction in tensile residual stress in the samples where static magnetic fields were applied, because the longer cooling time allows tensile stress through the track to dissipate. Validation of the Lu et al.'s findings on hardness means more work is required to confirm that the mechanism they have suggested is correct. The similarity of the peaks in XRD analysis suggested that there is little difference in phase between the samples produced with and without magnetic assistance, implying that any small change in hardness is not due to a difference in phase. Overall, the hardness results in this work are inconclusive and more work is required to confirm any changes in this property.

5.5 Conclusions

Magnetically assisted directed energy deposition has proved to be an effective method for modifying and deliberately varying track geometry by altering powder behaviour beyond the nozzle tip, at the melt pool. The relationships between magnetic field strength, scanning speed, laser power, powder feed rate and track geometry have been explained. A solenoid coaxially aligned with the laser has been used to demonstrate magnetic assistance, manipulating track dimensions in a ferromagnetic steel. The key conclusions can be summarised as the following.

- Coaxially aligned magnetic assistance may be used to increase powder catchment efficiency by up to 25%.
- There is a positive linear relationship between the magnetic field strength at the substrate surface and both the catchment efficiency and track width.
- Using a solenoid fixed to a specific location along the toolpath can be used to increase the cross-sectional area of tracks by up to 83% in specific positions.
- An increase in hardness of 20 – 40 Hv occurs when a 93.5 mT magnetic fields are applied compared to without one.

Further work beyond this thesis should determine whether more advanced electromagnets can be used with similar effects, without constraining the deposition to a single layer as is done by placing the magnet below the substrate. Building on the experiments in this chapter, the following work will investigate the effect of using alternate materials, to expand the process beyond only steel. Furthermore, more advanced uses of magnetic assistance will be studied, including whether overlapping tracks may be created, whilst retaining the improvements to catchment efficiency. The use of a dynamic magnetic field will also be investigated, towards the development of magnetic assistance as an adaptive control technique.

6 Expanding the Applications of Magnetic Assistance

6.1 Introduction

Adaptive control techniques have sought to improve track geometry and consistency by monitoring parameters and products and altering inputs to modify this in real time. On-line monitoring can be used to actively feed models based on the dimensions, grain structure and distortion of components, allowing parameters to be altered in real time to improve these properties. Because of the high level of responsiveness required, laser power and scanning speed are normally the parameters which are controlled in this manner rather than controlling powder feed rate, [10] though powder feed rate has been shown to significantly affect track height and consistency, [71] meaning this is an area of growing interest. Arrizubieta et al. tested a system using a fast response solenoid valve to stabilise the powder feed rate, showing that this method could be used to make track height more consistent when used in straight line tests and when changing direction, [57] crucially allowing flow rate to be controlled closer to the nozzle tip. As identified in Section 5.5 magnetic assistance is a potential method to do this, the concept will be investigated here.

In Section 2.2.5 adaptive control techniques are discussed for LDED, and a lack of control over the powder feeding was identified. Controlling powder catchment directly at the melt pools is a potential approach for enhancing efficiency. This would be beneficial in reducing inconsistencies in flow which can occur between the nozzle tip and the melt pool, particularly due to the effects of the laser on the path of powder flow in-flight and irregular vibration caused by the CNC movement. Laser-powder interaction has been observed, in high-speed x-ray imaging, to both increase and reduce powder catchment depending on the mechanisms at play; either increasing powder velocity towards the melt pool via partial vaporisation, or shadowing the laser and reducing consolidation at the melt pool [26]. Having direct control over the geometry of the mass addition would also allow new deposition strategies to be used, where track geometry and powder catchment are more closely controlled so that they may be changed based on the specific features of components, granting the ability to vary track dimensions and shape without altering the powder feed rate. No work has so far attempted to adaptively control the powder catchment at the melt pool itself. The previous chapter showed that increasing the magnetic field strength of a solenoid allows more powder to be captured and increases the size of tracks whilst reducing dilution. In combination with this knowledge switching the solenoid dynamically has potential for dynamic control over track geometry.

As discussed in Section 2.5.2, many works have also investigated the manufacture of nickel alloys in LDED. The field has therefore become quite well developed and has been investigated through every manufacturing stage. Bax et al. created process maps for Inconel 718 with predictive capabilities [71]. Gradl & Protz demonstrated that the materials were useful to make state-of-the-art components, showing that LDED rocket nozzles allowed integration of features and improved upon existing manufacturing techniques [11]. This demonstrates the industrial need for the process in these materials. As has been previously demonstrated here, magnetic assistance improves powder catchment efficiency, reducing waste and therefore saving costs. If this can be achieved in nickel alloys this would open the process up more widely. Therefore, in this chapter nickel is used as a powder feedstock to provide the foundation for later experiments using nickel alloys.

In this chapter several other techniques are tested which build upon the results demonstrated in the setup in the previous chapter. To evaluate the use of magnetic assistance as an adaptive control technique, the magnetic field was switched from full strength (93.5 mT) to 0 mT midway along the track. This has potential to be used to change the track geometry dynamically throughout a build, using a toolpath algorithm with varying magnetic field strength. Furthermore, to assess whether magnetic assistance could be used in more complex manufacturing scenarios, meandering toolpaths were used. This also allows examination of whether meandering toolpaths can still be used to improve powder catchment (as has been previously shown by Soshi et al. [140]) when magnetic assistance is also employed. Thick wall experiments, using overlapping tracks was also investigated, as this may be expected to affect the magnetic flux density and therefore track geometry. It is vital that magnetic assistance be applicable to thicker depositions as single thickness walls are rarely manufactured via LDED. To expand the applications of the process, experiments were also conducted using ferromagnetic elemental nickel powder to determine whether the process may be used in non-ferrous ferromagnetic materials.

6.2 Experimental

The experiments in this chapter develop upon the ideas examined on the apparatus used in Chapter 5. The same configuration was used here, with the solenoid being coaxial to the laser underneath the substrate as shown in Figure 6-1. In this chapter more complex toolpaths and different materials are used. The compositions of the different feedstock and substrate materials are shown in Table 6-1.

Table 6-1 Composition of materials used in Chapter 6 (wt. %).

Material	Ni	Cr	Mn	C	Mo	Si	P	S	Co	Cu	Fe
4340 powder	2.0	0.92	0.79	0.38	0.29	0.23	-	-	-	-	Bal
Ni powder	99.9	-	-	<0.01	-	-	-	0.03	0.08	<0.01	<0.01
Ni substrate	>99.0	-	-	-	-	-	-	-	-	-	-
MS substrates	0.20	0.15	0.50	0.10	0.06	0.10	<0.040	0.05	-	-	Bal

Some magnetic and thermal properties are shown in Table 6-2 to aid the reader with comparison throughout this chapter. It should be noted that permeability depends on the applied magnetic field strength, therefore the values shown in the table may not precisely predict that magnetic field strengths measured.

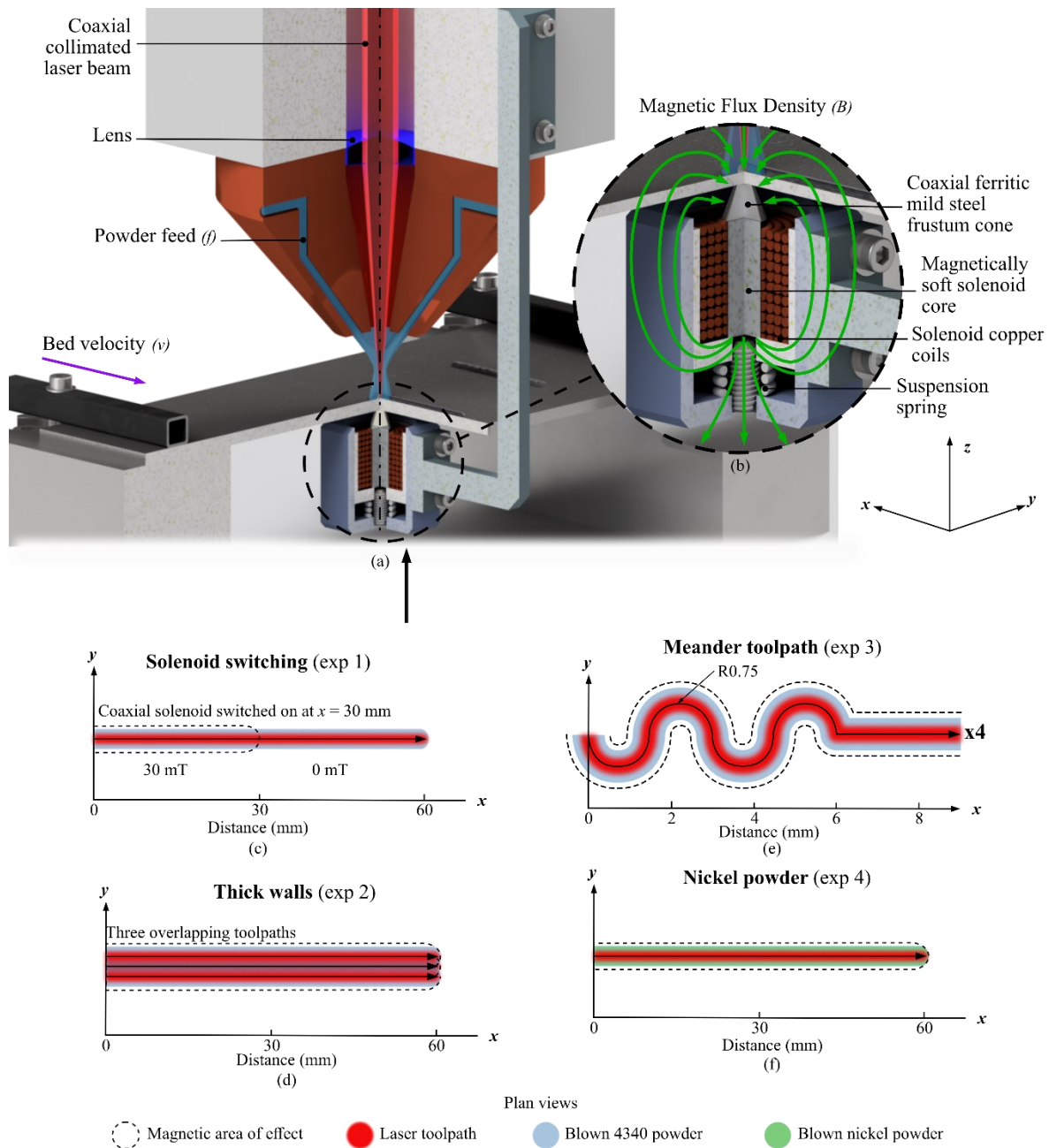


Figure 6-1 Setup of experiments used in this chapter. (a) shows the physical setup, (b) shows the magnetic field, whilst (c) - (f) show the toolpaths, magnetic and feedstock parameters used.

During the magnetic switching experiment the magnet was initially switched on, before being automatically switched off after 3.5 s, at the centre of the track length (Figure 6-1(c)). In the thick wall experiment (Figure 6-1(d)), 3 tracks were deposited successively, with each track beginning at the same end of the substrate. A stepover distance of 1.2 mm was used between the centre of each track in both magnetically assisted and the control condition. For the tracks where meandering toolpaths were demonstrated (Figure 6-1(e)), 4 sections of 4 arcs were

separated by 3 mm of straight path. The radius of each bend was 0.75 mm. This meandering path was then followed by a 24 mm straight path. The parameters used in each experiment are elucidated in Table 6-3. Commercially pure nickel powder (Alfa Aesar) was used to examine whether non-ferrous ferromagnetic materials behaved similarly, with a view to using more advanced alloys in future.

Table 6-2 Magnetic and material properties of materials used in this study [148,177]. The magnetic field strength, measured at the substrate surface, is shown for comparison.

Material	Curie Temperature (°C)	Melting point ($\times 10^3$ °C)	Thermal Conductivity (W/m.°C)	Relative permeability - μr (unitless)	Magnetic field strength through substrate (mT)
4340 Powder	770	1.43 – 1.51	35 – 50	600 – 1100	-
Nickel Powder	360	1.44 – 1.45	73 – 91	600	-
0.5mm Nickel Substrate	360	1.44 – 1.45	73 – 91	600	79.6
0.8mm MS Substrate	770	1.49 – 1.53	50 – 54	2420 – 3800	101.1
0.6mm MS Substrate	770	1.49 – 1.53	50 – 54	2420 – 3800	109.1

In the nickel powder experiment (exp 4), the substrates were sanded with P120 grit abrasive to reduce the reflectivity of the nickel substrates, as grit blasting caused the substrates to warp. MS substrates were also prepared in this way in this experiment.

Table 6-3 LDED parameters used in each experiment conducted in this chapter (Chapter 6).

#	Investigated Variable	Solenoid Placement	Flow Rates (g/min)	Laser Powers (W)	Field Strengths (mT)	Scan Speeds (mm/min)	Powder Material	Substrate Material
1	Solenoid switching	Coaxially aligned to laser	19.4	600	0 & 32.2	500	AISI 4340	0.8mm ± 0.09 0 Mild Steel
2	Thick wall	“	16.2	600	“	500	“	“
3	Meander toolpath	“	19.4	900	0 & 93.5	500	“	“
4	Nickel powder	“	15.75	500	0, 79.6 (nickel) & 109.1 (MS)	500	Commercially pure nickel	0.5 mm ± 0.07 0 nickel & 0.6 mm ± 0.07 0 MS

6.3 Results

To demonstrate the applicability of the technology, some potential novel applications of using a programmable solenoid in MADED were explored. By changing the solenoid position, it was determined that the using a preloading solenoid (where the solenoid is fixed to a position on the substrate) could be used to increase powder capture in those positions. Solenoid switching demonstrated that magnetic assistance could be used as an adaptive control technique to dynamically change the powder capture in-process. The use of meandering toolpaths and thick walls also demonstrated that magnetic assistance was effective not only in single line tracks, but also where toolpaths were more complex. The use of nickel powder also expands the potential magnetic assistance to much wider applications, including to the manufacture of nickel superalloys.

6.3.1 Solenoid switching

In the solenoid switching experiment, the magnetic field was reduced to zero approximately halfway along the track (3.5 s after deposition began). This was done to determine whether

magnetic assistance could be used as an adaptive control technique, potentially with the ability to control the volume of powder entering the melt pool independently of the powder feed rate or at specific locations along the toolpath. Switching the solenoid off resulted in tracks becoming narrower, shorter and with a smaller cross-sectional area as shown in Figure 6-2.

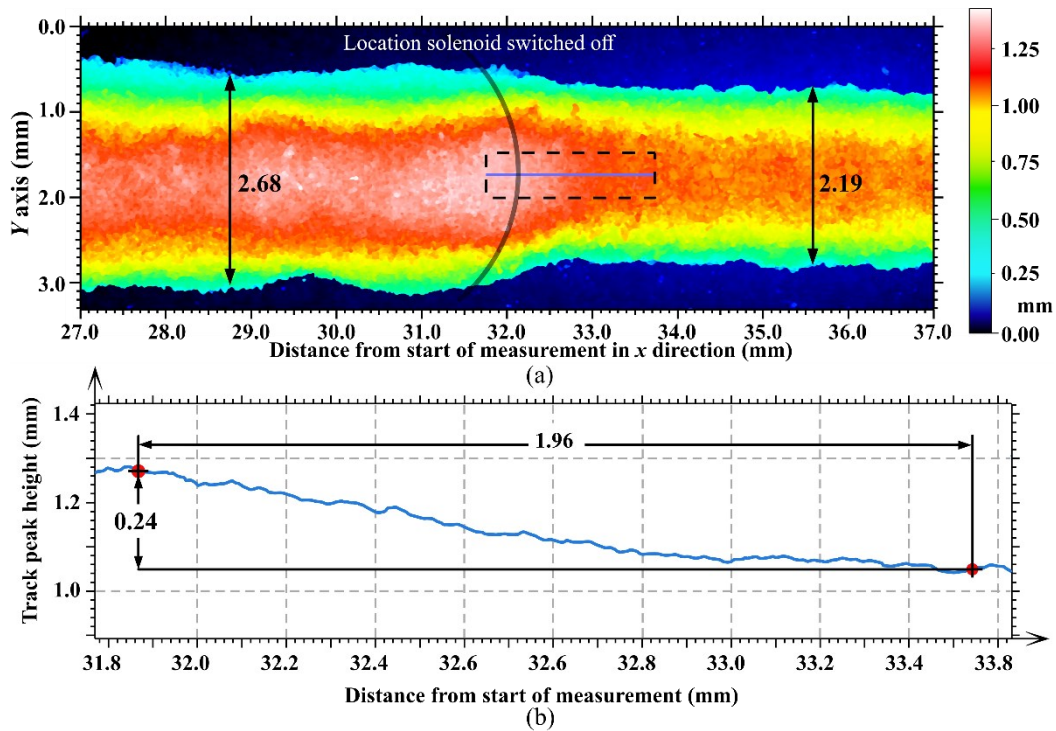


Figure 6-2 Effect of dynamic magnetic switching on track morphology. The magnetic field was reduced to zero halfway along the track; starting with 32.2 mT of magnetic assistance (left), before being switched to 0 mT (right). The mean (averaged in the y direction) cross-section of the box indicated in (a) is shown in (b), this shows how the peak height changed in one example across the transition. All dimensions are taken from the mean profiles in FVM measurements. Experiment conducted at 600 W, 500 mm/min, 19.4 g/min.

When compared to a control track without any magnetic assistance the sections of track with the magnet switched off have similar dimensions. The mean cross-sectional area with the magnet switched off was found to be within 2.4% of an equivalent track and the mean of the area (1.70 mm^2) fell within the margin of error for the mean area of the non-switched track ($1.66 \text{ mm}^2 \pm 0.051$). The mean width and height of the sections increased by 5.8% and 2.8% respectively. Although this is outside the standard deviation for width and height of the equivalent track, this level of variation in height is common among tracks produced in similar conditions, despite the width still being larger than the expected range. The cross-sectional area and height of the track are therefore close to the nominal of around 1.96 mm after the magnetic field is switched off. Whilst operating at 500 mm/min this suggests that the effects of the

magnetic field took 0.24 s to entirely recede. Distortion of the substrates may also explain the difference between dimensions in the “off” section of the switched tracks and the control tracks without magnetic assistance. As the substrates deformed by a few millimetres close to the ends of the tracks, possibly causing a change to the laser focus and hence the geometry there. This area was only measured in switched tracks, so may explain the discrepancy between the dimensions in the control track and the off section in the switched track.

The region where the magnetic field was present was larger than the equivalent control track. This control track (with coaxial magnetic assistance along the whole length) had an area of 1.77 mm², width of 2.36 mm and height of 1.09 mm. The dimensions of the magnetically assisted region of the switched track are outside the expected deviation of the equivalent magnetically assisted tracks.

6.3.2 Thick walls & meandering toolpaths

The experiments in this section were conducted in order to determine whether magnetic assistance is suitable for applications beyond straight, single line tracks. Case studies were used to examine whether complex toolpaths and overlapping tracks inhibit the efficacy of magnetic assistance.

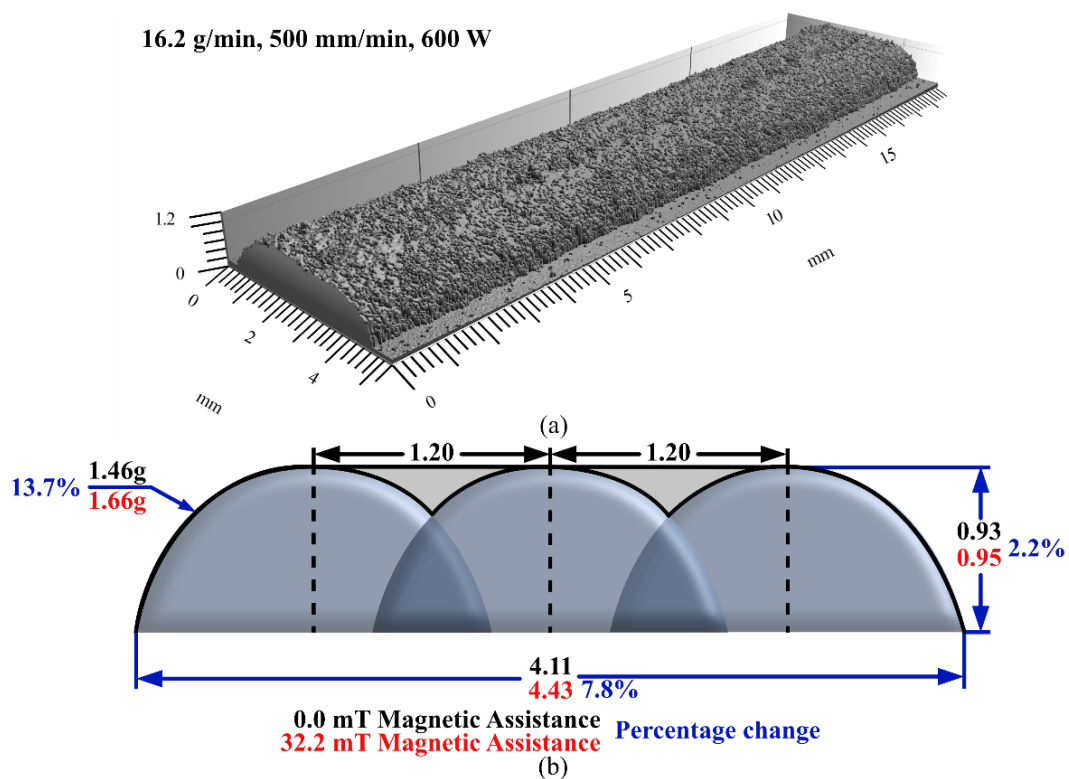


Figure 6-3 Dimensional changes in bulk depositions due to magnetic assistance. (a) shows an FVM render of the sample with magnetic assistance, in (b) the effect on dimensions are shown. Both samples were produced with 1.20 mm stepover.

The mass and dimensions of tracks produced in experiment 2 are shown schematically in Figure 6-3. The powder catchment efficiency measured was 25.1% without magnetic assistance, increasing to 28.5% with magnetic assistance applied. The mean catchment efficiency for equivalent single-track depositions were 40.0% and 45.9% without and with 32.2 mT of magnetic assistance respectively. The equivalent single tracks without magnetic assistance had a width of 2.01 mm and a height of 1.00 mm whilst with magnetic assistance width was increased to 2.41 mm and height was reduced to 0.92 mm.

These results suggest that magnetic assistance increases the dimensions and catchment efficiency for thin walls more than in thick walls, though using the same stepover distance is uncommon when producing tracks of different widths.

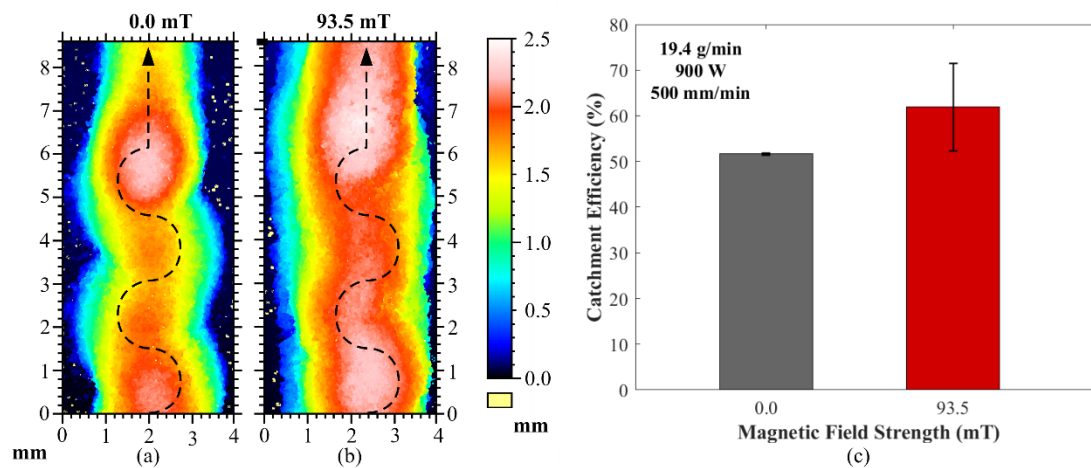


Figure 6-4 Meandering toolpaths with magnetic assistance. FVM height colour map (a) without magnetic assistance and (b) with 93.5 mT magnetic assistance, (c) shows the difference in catchment efficiency. The meandering toolpath is overlaid on (a) and (b).

The use of 93.5 mT magnetic assistance with the toolpath shown in Figure 6-1(c) increased catchment efficiency from 51.7% to 61.9%, compared to when using a linear toolpath with equivalent parameters where catchment efficiency increased from 42.4% to 61.3%. Once again, the efficiency improvement was reduced in this practical application as compared to the purely experimental one, though in this case the magnetically assisted catchment efficiencies are similar.

6.3.3 Nickel powder

This work ultimately aims to prove magnetically assisted DED as a generically applicable adaptation to enhance deposition of magnetic materials. To reach this goal it is important to understand the behaviour of different ferromagnetic feedstock materials, and different substrate types. Here the deposition of nickel powder onto both nickel and mild steel

substrates was conducted. While magnetic assistance was applied, the track in Figure 6-5(a) underwent fluctuations in track height from 0.99 mm to 2.08 mm, whilst width varied from 2.41 mm to only 2.51 mm. In comparison, the mean dimensions of a tracks produced without magnetic assistance, but otherwise equivalent conditions, were consistently close to 0.92 mm high and 1.66 mm wide. This variation was only apparent in some tracks using nickel powder on both nickel and mild steel substrates. It should be noted that the width along the whole length of the inconsistent track is significantly greater than the equivalent without magnetic assistance, though the height deviated from a similar number to approximately double.

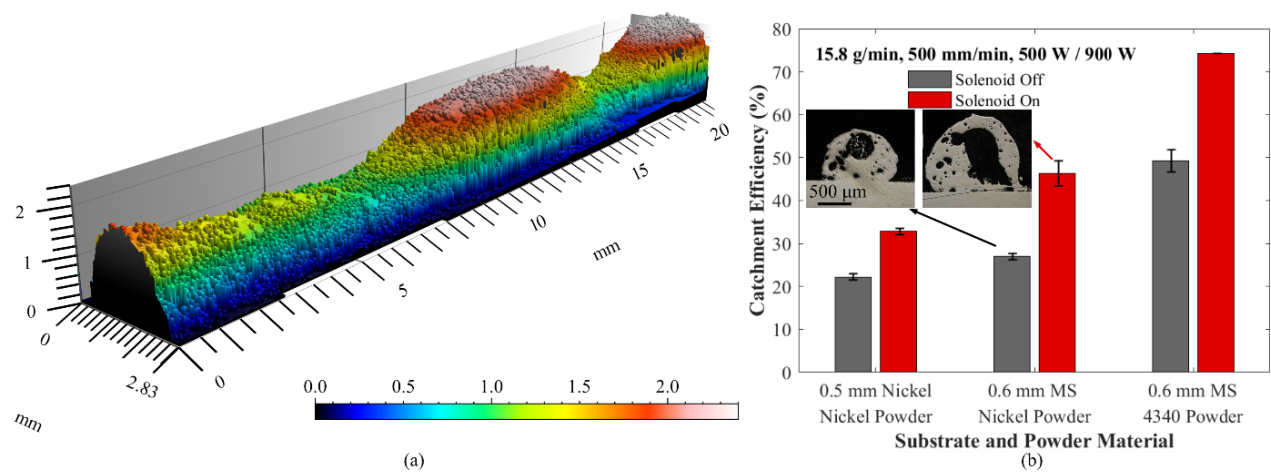


Figure 6-5 The role of magnetic assistance when using pure nickel powder on different substrate materials. (a) shows an image of a nickel track with an inconsistent surface, produced on a mild steel substrate, (b) catchment efficiency with magnetic assistance using different substrates. The magnetic field was measured as 79.6 mT whilst through the MS substrate this was measured as 109.1 mT. 500 W laser power was used for the nickel powder and 900 W for the 4340 powder.

Figure 6-5(b) demonstrates that magnetic assistance is effective in increasing catchment efficiency of pure nickel on both nickel and mild steel substrates. On the nickel substrate the catchment efficiency increased from 22.2% to 32.8%, whilst with nickel powder on mild steel the catchment efficiency improved from 27.0% to 46.4%. Macroscale pores were seen in the sections of all nickel tracks (examples shown in Figure 6-5(b)), though the pores were found to be larger in tracks where the magnetic field was used. For the tracks produced from nickel powder and on nickel substrates, pores occupied a mean area of 19.9% of the cross-sectional area without magnetic assistance and of 32.8% of the area of the tall sections on magnetically assisted tracks. Porosity was reduced on the shorter sections in magnetically assisted nickel tracks. In general, porosity is an expected phenomenon when laser welding pure nickel, [126]

even in inert atmospheres [178]. Alloying with chromium, titanium or aluminium reduces porosity [126] but this would reduce the magnetic permeability of the material significantly. It is important to note that catchment efficiency is calculated via mass, therefore the effects of porosity are inconsequential to the graph displayed above. Overall, the catchment efficiencies using nickel powder were significantly reduced compared to those using 4340 powder on a 0.6 mm mild steel substrate (49.2% catchment efficiency rising to 74.2% with magnetic assistance).

6.4 Discussion

The experiments in this chapter are aimed at moving magnetic assistance to a higher technology readiness level, whilst also demonstrating the breadth and capability of the technique. The switching of magnetic fields has the potential for implementation in practical and novel settings, given the increase in the catchment efficiency and track width, accompanied by the reduction in size of dilution zones. In this simple setup, and under the conditions used here, the magnetic field was shown to cease its effects ~ 1.96 mm (or 0.24 s) after being switched off. This delay in changes to dimensions was expected given the large radius of the magnetic field compared to the laser spot (shown in Figure 6-2). Given that powder is attracted across the width of the magnetic field, more powder will be concentrated on the substrate as the axis of deposition approaches, meaning even after the magnetic field is switched off there will be marginally more powder concentrated on the substrate ahead of the laser. Use of a smaller diameter field could therefore reduce the size of the transition zone significantly. Magnetic hysteresis may also cause this; although the current has ceased to flow, the core and magnetic focusing cone are both imperfect magnetically soft materials, remaining magnetised for a short time after the solenoid is not. Therefore, there may be some residual magnetism still present in the substrate even after the coil is de-energised. The effect of this is shown in Figure 6-6. This could be solved by using a more sophisticated setup, using magnetically soft materials for the focusing cone or more advanced magnetic control, including the use of air-core solenoids. These results indicate that unless the effect can be negated more quickly, manipulating the magnetic field over a discrete range (as in the magnetic field strength experiment) and using magnetic assistance as an adaptive control technique may not be possible except when long duration fluctuations are present. If the delay in eliminating the effects of magnetic assistance can be reduced, magnetic assistance could be used to stabilise or alter tracks adaptively. The use case depends on whether more consistent deposition, or a change in feature size is required.

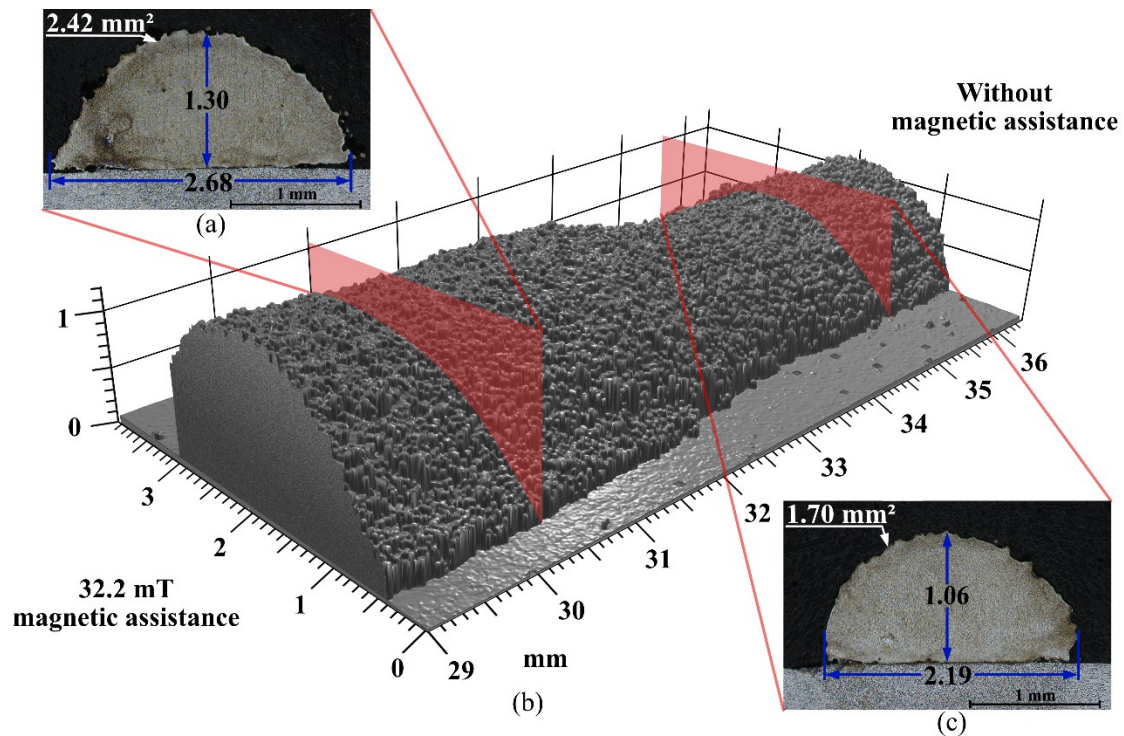


Figure 6-6 Demonstration of switching magnetic assistance, showing cross-sections of while magnetic assistance was applied (a) and when this was switched off (c). A render of the centre section of a switched track is shown in (b).

In the thick-wall case study, magnetic assistance also led to an improvement in catchment efficiency and an increase in track width in the example tracks. The catchment efficiency of both the control and magnetically assisted walls was reduced compared to single track depositions. This is expected when performing overlapping tracks. The increase in catchment efficiency due to the magnetic field was also reduced (from a 5.9% improvement down to a 3.4% improvement using 32.2 mT) due to the effect of the first track on the magnetic field. Where there is already a track present, the effect of the magnetic field is reduced. This is because the existing track would be expected to distort the magnetic field in an undesirable manner, reducing localisation of the magnetic flux. The use of the same stepover distance in the control and magnetically assisted deposition is necessary for direct comparison, but stepover would be expected to increase with the width of the tracks produced, hence marginally larger increases in efficiency are likely when using an optimised stepover distance.

The use of a meandering toolpath has previously been shown to improve catchment efficiency significantly, [140] hence the baseline improvement in catchment efficiency was an intended consequence of using a meandering path. This case study demonstrated that magnetic assistance remained effective when using meander toolpaths. The catchment

efficiency increased to a value which is close to that achieved in linear toolpaths (61.9% compared to 61.3% respectively). This suggests that using complex toolpaths has little effect on the overall catchment efficiency. Therefore, this should simplify the design of toolpaths intended for use with magnetic assistance.

The improvement in catchment efficiency is most pronounced in a coaxially aligned solenoid in the case of 4340 powder deposited on a thinner mild steel substrate. The efficiency in this case increased from 49.2% to 74.2%, an increase of 25.0%. This significant improvement is due to the combination of a high strength solenoid and a thin substrate, leading to the greatest magnetic field strength on the substrate surface (these values can be compared in Table 6-2). This result is an expected outcome based on the field strength experiment in Chapter 5. The smaller permeability of nickel (values are described in context in Table 6-3) means that the induced magnetic field is not as strong, both around the nickel substrate and powder, meaning the effect of magnetic field strength is reduced in this material, as shown in Figure 6-5.

High porosity (up to 32.8%) was observed in both sets of samples manufactured in high purity nickel. This porosity is common when welding commercially pure nickel and is caused by contaminants of either nitrogen or oxygen [126]. The pores cause unstable deposition to occur only when the magnetic field was applied. Within the taller regions of the tracks, larger pores are present. Large bubbles of gas forming in the magnetically assisted clad therefore explain the height variability. When these bubbles become too large, they reach the outside of the melt pool and are expelled, hence the tall track sections being followed by shorter sections. The consistently increased width of the magnetically assisted nickel depositions shows the resilience of the magnetic assistance. Because a change in width similar to when the magnet is switched off (as in Figure 6-6) did not occur.

As the proportion of the track cross-sectional area consisting of pores increases (from 19.9% without magnetic assistance to 32.8% on the taller sections with magnetic assistance) this suggests that the larger pores are not simply as a result of a larger deposition volume. Lu et al. have shown that magnetic fields can manipulate the plasma plume in the deposition of paramagnetic austenitic steel, causing it to be compressed and short [165]. In this case the magnetic field appears to be trapping plasma inside the melt pool, disrupting the usual behaviour of gas expulsion, and causing pores to grow. This is similar to previous work showing that electrostatic fields vary porosity [130]. No difference in macroscale porosity was observed in sections of the steel deposits, therefore it is likely that the magnetic field is exacerbating pores rather than explicitly causing them. In Zhang et al.'s work an Ampere

force was applied using the combination of magnetic and electrostatic fields which then acted on the plasma plume. For the same mechanism to apply here the plasma must be charged, such as by friction with the powder/apparatus. An increase in porosity could also be caused by an increase in the velocity of particles meaning more gas is trapped, but this would also be expected in the steel depositions. More work examining electrostatic forces and gas entrapment is required to validate either of these theories. With a nickel-based alloy composition which does not encourage porosity the effect is likely to be less pronounced. The aluminium, titanium and chromium which are normally added to nickel alloys are effective in reducing porosity through oxide and nitride formation, [126] but these additions would reduce the magnetic permeability of the material and inhibit magnetic powder control. Therefore, if magnetic assistance is to be used when manufacturing alloys via DED a new method of alloying is required.

In summary, the ability to alter track dimensions dynamically over the course of a build opens new possibilities in DED. The possibility to do this in both ferrous and nickel-based alloys makes magnetic assistance a useful addition to the LDED process. Further investigation and development is required to increase the value and intricacies of magnetic assistance. The solenoid placement used here only allows a single layer to gain the benefits of magnetic assistance, further experiments should develop this, extending the applications to multi-layer components. In its current form the process would benefit from high-speed imaging to determine the exact path divergence of particles. More sophisticated materials must also be developed for use in the process, including exploration of in-process alloying to manufacture non-magnetic materials. This is examined in the following chapter. The effects of magnetic assistance on material properties should also be considered with this new method in mind.

6.5 Conclusions

- A programmable solenoid was used to dynamically change the track dimensions even when switched during operation, suggesting magnetic assistance is a valid technique of adaptive control.
- By removing the magnetic field during deposition there is a short transition zone before the track returns to normal operation, this is due to magnetic hysteresis of the magnetic focusing cone and the large diameter of the magnetic field.

- Magnetic assistance was shown to improve powder catchment efficiency even when several track wall thicknesses were used. Although the significance of the improvement was reduced in both cases.
- This work showed for the first time that magnetic assistance could also be effective on non-ferrous ferromagnetic materials, with powder catchment efficiency being improved from 27.0% to 46.4% on a mild steel substrate.

The clear next step, after determining that nickel could be used in the magnetically assisted process, is to show that alloys of nickel can also be used. This presents a further challenge, because these alloys are only paramagnetic. A method of compositing powders in order to manufacture these alloys whilst retaining the benefits of magnetic assistance is demonstrated in the following chapter. Here it has been shown that magnetic assistance can be used dynamically, other work should also investigate the use of magnetic assistance as a fast-acting adaptive control technique to encourage stable depositions in-spite of unstable powder flow rates.

7 Manufacturing Non-Magnetic Alloys using Magnetic Assistance

7.1 Introduction

The benefit of magnetic assistance to improve powder catchment efficiency and enlarge tracks when using pure ferromagnetic powders has been documented in laser directed energy deposition. These benefits include improved powder catchment efficiency and the ability to dynamically control track size during deposition. However, so far, the magnetic assistance has only been shown to be effective in ferromagnetic materials such as ferritic steels and pure nickel. For magnetic assistance to be utilised more widely, it must be demonstrated in a greater range of materials, including the manufacture of non-magnetic alloys. This work examines the possibility of making and using composite powders via the powder satelliting process. In the powder satelliting process, smaller “satellite” particles are adhesively bonded to a larger “parent” particle, these composite powders are then melted in-situ to produce alloy materials. In order to use magnetic assistance to deposit non-magnetic alloys this work uses a ferromagnetic nickel parent particle with satellite particles of non-magnetic chromium. The hypothesis is that by adhesively bonding these particles together the trajectory of the composite powder will be altered similarly to as it is when using pre-alloyed ferromagnetic powder, meaning that the powder catchment efficiency and track width is increased. This theory is shown in Figure 7-1. This section will investigate whether use of satellited powders enables the previously demonstrated improvements to powder catchment efficiency and track geometry whilst manufacturing a non-magnetic alloy. The tracks produced using satellited powder are compared to those produced using pre-alloyed nichrome powder with the same composition which is non-magnetic.

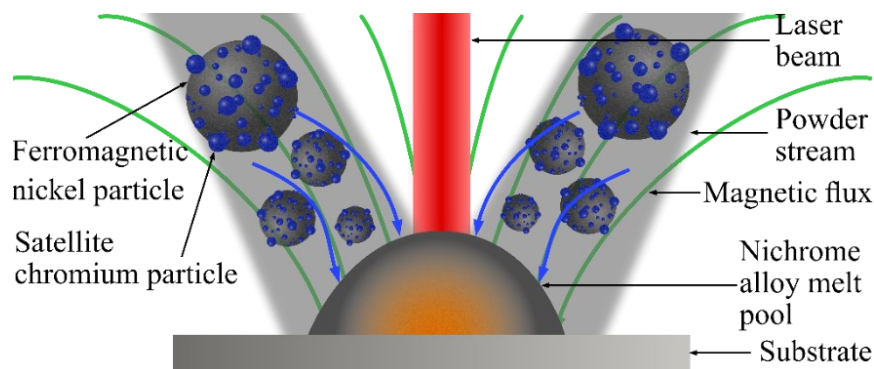


Figure 7-1 Hypothesis of magnetically assisted DED using satellited powder.

Powder satelliting has previously been examined for a small range of cases, generally these are focused towards using the method to create new alloys in small batches to develop new alloys for use in additive manufacturing processes. In principle, the satelliting process involves coating a parent particle ($\sim 100 \mu\text{m}$ for LDED) in finer satellite particles ($\sim 5 - 10 \mu\text{m}$) [179]. The particles are bonded together using an aerosolised binder solution. Metal matrix composites have been manufactured using this method for both directed energy deposition [108] and PBF, with microstructural homogeneity being observed compared to mixed feedstocks. Farayibi et al. first demonstrated the use of this method in LDED, showing that using satellite TiB_2 bonded to Ti-6Al-4V could be used to manufacture homogenous material, whereas simply mixing the powder led to microstructural segregation and the detrimental clustering of TiB_2 and Ti-6Al-4V over sections of the deposits [179]. This microstructural segregation means the material has inconsistent properties and makes qualifying it for use difficult. In contrast, satellited feedstocks can be used to create alloys which have similar microstructures to those produced using pre-alloyed feedstocks in Ti-6Al-4V in powder bed fusion. Microstructural segregation, porosity and coarse grain structures were found to be more severe in mechanically mixed powders as compared to satellited ones, due to the segregation of particles materials due to the difference in the size and density of powders being used causing the feedstock to pack poorly and absorb energy unevenly [180]. Satellited feedstocks have also begun to be used as a tool to study new alloy compositions, with iron satellites having been used to effectively refine grains in the Ti-6Al-4V [109]. This has potential to reduce anisotropy in additive manufacturing processes by reducing the size of grains and therefore reducing the effects of their directionally solidified orientation. As more than 3 % iron no longer has a refinement effect only small quantities of this were required, but because this percentage should be included homogeneously satelliting was used. This meant that costly, small-batch pre-alloyed powder did not have to be manufactured, when it has been shown, by Gasper et al., that the use of satellite powder can reduce material costs by around 40 % [48]. To date, satelliting has mainly only been used to investigate a small range of materials, either using titanium alloys or metal-ceramic composites. An example of this being, Al-Thamir et al.'s examination of satellited tungsten carbide cobalt powder, which showed that tungsten carbide could be deposited in a cobalt matrix in laser powder bed fusion [181]. With the materials palette in aerospace engine components being an important and growing area of alloy development in additive manufacturing [182] this should be studied further. By combining the cost reduction of using satellited material with

the improvement in material efficiency of using magnetic assistance there is a clear cost incentive for using this technique.

The composition of the target alloy (nichrome) has been chosen as a precursor to the more complex compositions of nickel aerospace alloys. These nickel aerospace alloys, such as Inconel 625, are commonly studied in additive manufacturing applications, [182] due to the potential for light weighting and cooling of turbine components which is enabled by the manufacturing flexibility of additive manufacturing [150,183]. This is because the layered approach of additive manufacture allows complex lattice structures to be manufactured more easily. Catchpole-Smith et al. examined the use of different infill structures and their ability to conduct heat more effectively, showing that a greater spacing between structures increased the ability of these structures to dissipate heat [183]. Improved cooling could be advantageous to increasing the efficiency of engine turbines while lattice light weighting reduces the payload. Inconel 625 has a simplified chemical composition compared to some other alloys, such as Inconel 718, therefore a proto-Inconel 625 (with only the two main elements, nickel and chromium included) has been chosen as the target material for this work because satelliting several different elements has never been examined and is beyond the scope of this work. Inconel 625 consists mainly of ferromagnetic material (nickel), so it is a good material to initialise investigation in this area, particularly as the high cost of Inconel 625 in powder form means there is a fiscal priority to improving powder catchment efficiency in this material.

In addition to determining how ferromagnetic powder bonded to non-magnetic powder reacts in magnetic assistance, an improved method of manufacturing satellited powder is determined and the effects using this method on the track geometry and composition of depositions will also be examined and quantified. This work will inform future work in this area which uses the techniques explored here to create products using functional alloys, future work will be able to then tailor powder characteristics to meet the demands of products.

7.2 Experimental

To examine the effects of using satellite powders a nickel superalloy composition is simplified to enable analysis whilst remaining relevant to the application of aerospace alloys. These alloys typically contain a significant quantity of chromium, with other elements in

smaller quantities and the bulk of the alloy being nickel. To this end, nichrome (Ni 80 wt. %: Cr 20 wt. %) was chosen as the target composition.

Table 7-1 shows the compositions of the powder materials used in this work as stated by manufacturer's analysis. Inconel 625 is also included for reference and comparison purposes.

Table 7-1 Powder compositions used in this section (wt. %).

Material	Cr	Co	Fe	Cu	C	S	Si	Mn	Mo	Nb	Ta	Ni
Inconel 625 (nominal)	20.0	-	-	-	-	-	-	-	8.0	3.15	0.05	58.0
Nichrome powder	19.4	-	0.53	-	0.02	0.004	0.97	0.03	-	-	-	79.3
Chromium powder	99.6	-	0.31	-	0.02	0.02	0.01	-	-	-	-	-
Nickel powder	-	0.08	-	-	-	0.03	-	-	-	-	-	99.9

In this section the same experimental setup was used as in Chapters 5 and 6 with two changes. A 400 μm fibre was used to carry the laser, meaning the laser spot diameter was 0.6 mm, this is due to damage to the 600 μm fibre in unrelated work. The same solenoid and magnetic field strength were used as in Chapter 6, leading to a magnetic field strength of 79.6 mT at the substrate surface.

Table 7-2 shows the parameters which were used for experiments in this chapter.

Table 7-2 Experimental parameters used for satellited powder experiments.

Powder material	Solenoid Placement	Flow Rates (g/min)	Laser Powers (W)	Field Strength (mT)	Scan Speeds (mm/min)	Substrate Material
Satellited nickel with chromium (80:20)	Coaxially aligned to laser	15.9	500	79.6	500	0.5 mm nickel
Pre-alloyed nichrome (80:20)	Coaxially aligned to laser	15.7	500	79.6	500	0.5 mm nickel

In this chapter simple straight tracks of 60 mm length were deposited onto the substrates. Depositions were made using the satellited feedstock and the nichrome control feedstock onto a 0.5 mm pure nickel substrate. This was done with the solenoid coaxially aligned to the laser, with the solenoid switched on and with the solenoid switched off. Three tracks were produced in each condition. The mass of substrates before and after deposition was measured and 2 mm portions of the tracks were scanned via FVM. As in previous sections, the mean cross-section of this FVM scan was used to measure the above substrate dimensions of tracks. The tracks were also cross-sectioned, ground and polished, then etched using Marble’s reagent to reveal the dilution zone and pores, which were then measured using optical micrographs and the image analysis software ImageJ [171].

7.2.1 Powder manufacturing

Before using the satellited powder in additive manufacturing trials, a qualitative analysis loop was used to determine an effective powder. This process is described in Figure 7-2.

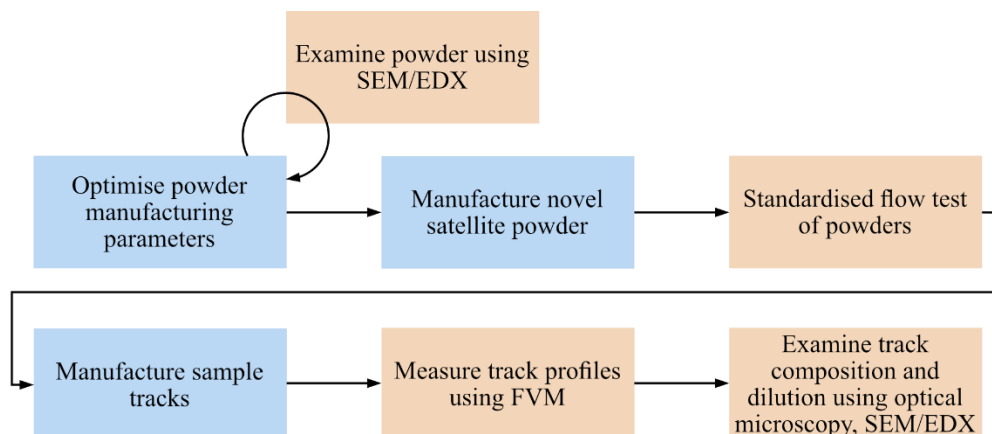


Figure 7-2 Powder manufacturing and analysis process. Initial powder composition was chosen based on a nichrome 80:20 and the powder diameters described in the literature [179].

The primary aim of this loop was to determine an optimum amount of binder to add to the mixture to adhere the two powders together adequately. The order of operations was examined to attempt to reduce powder diameter bimodality as demonstrated in previous works. This bimodality is caused by not all of the satellite powder being bonded to the parent particles which causes a second peak in powder size distribution at the smaller diameter of the satellite powder [179]. Incomplete intraparticle bonding can lead to powder segregation and so should be minimised. The order and number of mixing operations was varied to establish one which reduced the number of loose satellite particles, as determined by SEM. The improved manufacturing process flow shown in Figure 7-3 was then determined. Larger batches of powder meant that the binder was unevenly distributed and led to chromium agglomerates. Sieving was also added (compared to some processes described in literature) to ensure the powder diameter was more consistent in the final powder.

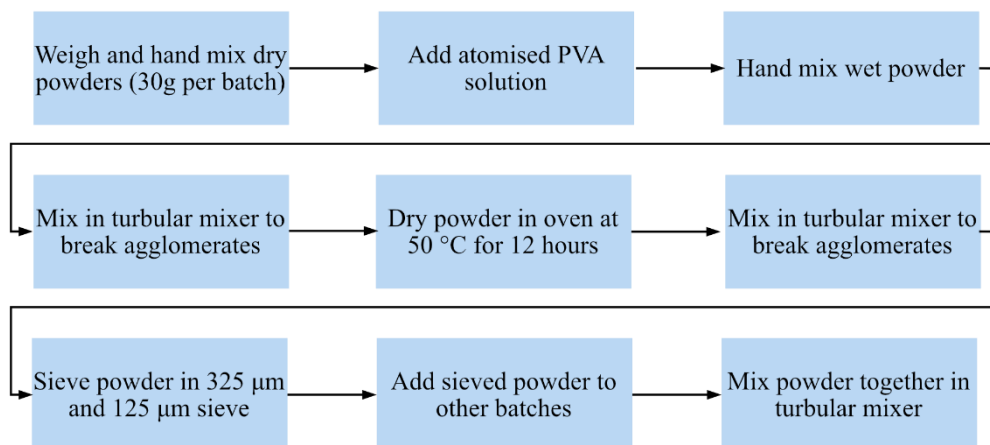


Figure 7-3 Improved powder satelliting manufacturing process flow as determined by SEM.

Once an improved process flow had been determined, the quantity of binder solution was varied incrementally to determine the desired quantity. The same binder solution which has frequently been used in literature was used here [108,179,180]. This consists of 2.7 vol. % polyvinyl alcohol (PVA) in water. This binder is then sprayed into a thin layer of powder and mixed in as described in Figure 7-3. When too little binding solution was used the powder particles were not bonded and could be observed separately, with the difference in material being identified by EDX mapping. Figure 7-4 shows the effect of using increasing quantities of binder solution. At 0.04 wt. % (1.2 g binder solution per 30 g powder) the chromium particles (blue) appear to evenly coat the nickel particles (red) and few grains of unbound powder which can be observed. Whereas, when 0.7 wt. % binder solution was used,

chromium agglomerated into irregular branched particular structures (as shown Figure 7-4 b & d), both separately and on the surface of nickel parent particles. It has been shown that spherical powders flow better and therefore these are more desirable, whilst a more even coating is likely to reduce compositional segregation. In addition, work on powder mixtures suggests that powders with significant quantities of different sizes should be avoided to improve flowability [20], therefore ideally no chromium will be present which is not bonded to a parent particle. In practice, bonding all of the the satellite particles to parent particles has not been achievable in other works, as shown by particle size measurement [181]. It should also be noted that the uneven surface (already containing satellites) of the nickel powder, as can be seen in Figure 7-4 b) and d), may improve satellite particle adhesion.

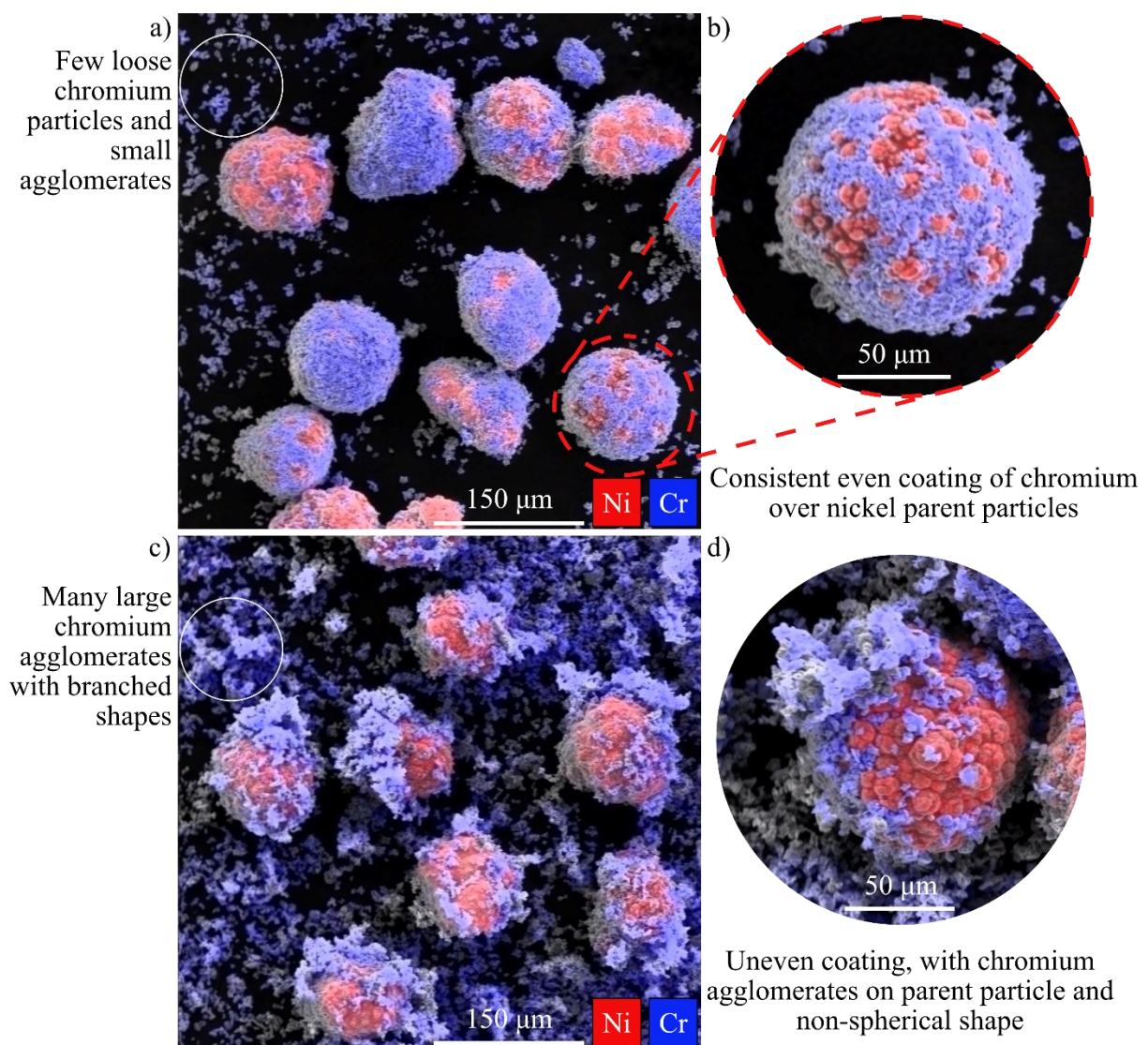


Figure 7-4 SEM/EDX images showing the effect of increasing binder quantity on satellited powder; a) and b) showing 0.04 wt. % binder solution; c) and d) showing with 0.07 wt. % binder solution.

After a desirable powder had been identified (with 0.04 wt. % binding solution) the powders were tested for their flowability in both standardised flow tests and through the disk feeder of the DED machine. Importantly, when no binder was used (with the two powders being simply mixed) the powder did not flow through the disk feeder at all. This agrees with the literature around the use of differing particle sizes [20], which suggests that when using powders of similar density the diameters should be similar, as discussed in Section 2.3.8. Clearly the difference in particle sizes when the powders were simply mixed meant that the powder jammed in the feeder. This was attempted three times, with the machine being fully cleaned each time, to confirm that the powder was completely unable to flow. The fact that this did not occur in the satellited feedstock helps to demonstrate another reason to use satellited feedstock, powders of different sizes may be used without blockage.

After 250 g of the powder had been manufactured with the improved quantity of binder solution, according to the process flow detailed in Figure 7-3, the powder was imaged again using SEM/EDX. This revealed that the powder feedstock did not appear to be as high quality as is shown in Figure 7-4(a). The powder was observed to have a drastically greater amount of loose chromium agglomerated together, with some particles having a poor and uneven coating of chromium over the parent particles, though some were still well coated. This may indicate that subsequent mixing operations may have served to remove some of the chromium from the parent particles, or that even the improved powder manufacturing process is not repeatable. Subsequent laser diffractometry shows that a small proportion of the volume of satellited powder had a diameter less than 10 μm whilst some of the powder being larger than the original nickel parent particles indicates that a significant proportion of the chromium existed as a coating over the nickel particles. The results of laser diffractometry are shown in Figure 7-5 and Table 7-3.

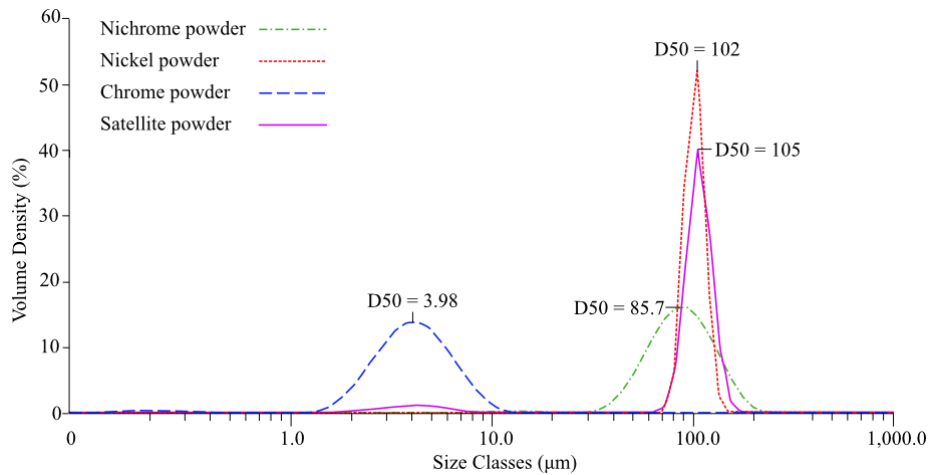


Figure 7-5 Powder size distributions of the constituent powders and the satellite powder used in LDED experiments.

Table 7-3 Powder size distribution of powders used in this section (μm) as measured by laser diffractometry [102].

Powder	D10	D50	D90
Nickel	88.4	102	117
Chromium	2.26	3.97	6.77
Satellited	82.3	105	125
Pre-alloyed nichrome	52.9	85.7	135

Hall flow measurements were used to determine the flowability of materials, though as discussed in the standard B964 [94] when powder did not flow through the Hall flow apparatus, Carney flow apparatus was used instead. The mean of three flow rates of 50 g of powder are shown in Table 7-4. It is likely that the loose small chromium particles impeded the flow of the satellited powder through the small orifice in the hall flow apparatus, causing the blockage, though satellite nodules have also been suggested to impede flow by causing the particles to mechanically interlock [92].

Table 7-4 Powder flow rates using standardised test methods.

Powder	Hall (g/min)	Carney (g/min)
Satellited	Did not flow	702.0
Pre-alloyed nichrome	84.7	618.1
Nickel	135.7	992.3

The satellited powder flowed freely through the larger orifice in the Carney flow apparatus, with the powder flowing more quickly, even faster than the pre-alloyed powder.

To enable fair comparison of results each powder flow was calibrated to 15.8 ± 0.1 g/min. The disk speed to achieve this flow rate was 2.3 rpm in the case of the pre-alloyed nichrome powder and 2.05 rpm for the satellited powder. With an increase in disk speed normally being expected to lead to a linear increase in flow rate when using the same material (shown for AISI 4340 in Figure 3-2) this confirms that the satellited powder is more free flowing in the feeding apparatus than the pre-alloyed equivalent.

The increase in Carney flow for the satellited powder as compared to the nichrome powder are likely related to the larger size of this powder and tighter distribution as shown in Figure 7-5 and Table 7-3. The satellite powder flowed more slowly than the pure nickel powder, likely as a result of the satellites and the mix of particle sizes present in the satellited powder.

7.3 Results

7.3.1 Deposition Geometry

Several satellited powder tracks showed similar trends in dimensions to those experienced by pre-alloyed ferromagnetic powder used with magnetic assistance previously. Similar to these experiments, was a 26.7 % increase in the width of tracks produced using satellited powder (a 20 - 30 % width increase was observed in previous chapters using similar setups), and an increase in powder catchment efficiency (from 18.4 % to 24.1 %). As well as a 37.8 % increase in the cross-sectional area of tracks above the substrate surface when using magnetic assistance. This contrasts with the non-magnetic pre-alloyed nichrome powder which had no significant change in dimension due to the magnetic field. The link between dilution area and magnetic field strength has also been confirmed when using satellited feedstock. As with previous experiments, the area of the dilution zone is reduced with the application of the magnetic field in satellited ferromagnetic materials. This was not true in the non-magnetic pre-alloyed nichrome. These results are shown in Figure 7-6.

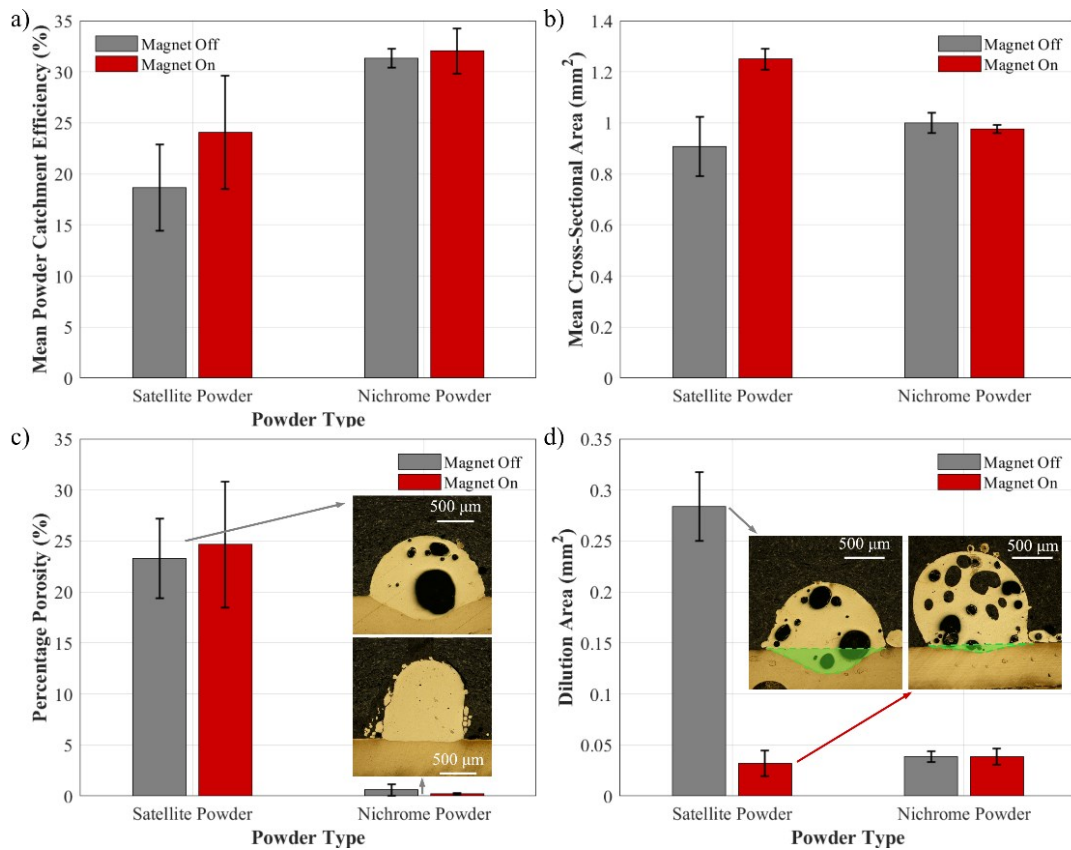


Figure 7-6 Results from satellited material experiments. showing a) powder catchment efficiency, b) cross-sectional area above the substrate, c) percentage porosity and d) the area of the cross-sectional dilution zone.

Unlike in Chapter 6, there is no clear link between porosity and the presence of the magnetic field in satellited powder, although the porosity in the tracks produced in nichrome is significantly reduced compared to the satellite powder. This indicates that the effect of chromium to reduce porosity is occurring as expected in the pre-alloyed powder, but not in the satellited powder. The effect of composition will be reviewed and discussed in the following sections.

Though the improvement in powder catchment efficiency is reduced in satellited materials compared to in previous work, this is an expected phenomenon of using a weaker magnetic field and may also be affected by the use of a smaller laser spot size. The build-up of powder at the beginning and end of tracks due to the static laser also contributes to deviation in these results. This is discussed further in Section 7.4.

7.3.2 Deposition Composition

Compositional analysis by EDX was conducted on 4 samples in each condition, with two points in each location being used for analysis. The result of this compositional analysis is shown in Figure 7-7. Most obviously, the chromium content in the tracks produced from

satellited powder only consist of 2 – 9 % chromium, whereas the pre-alloyed powder had 17 – 20 % chromium content. This suggests that much of the chromium content is lost when using satellited powders, regardless of magnetic assistance. This indicates that the intended nichrome composition of 80:20% nickel was not achieved from the satellited powder, although some of the chromium was successfully alloyed with chromium.

Chromium content is shown to be slightly elevated in all locations in tracks produced using magnetic assistance and satellited powder. This is not the case in the pre-alloyed nichrome tracks, suggesting that the effect is likely due to an effect of the magnetic field on the powder rather than one taking place within the molten pool. A slight increase in chromium content (around 1 wt. %) is also apparent at the top and edges of the tracks compared to at the centre of the clad. It is clear from Figure 7-7b & d that chromium is present throughout the track both conditions.

In some specific locations at the edge of the tracks (as shown by white mark on the track in Figure 7-7c) the chromium content was much greater than in the rest of the track. Very limited leaching of chromium into the substrate (rather than the dilution zone) was observed in all cases, with EDX suggesting that the absolute chromium content 200 μm from the clad layer was between 0.00 and 0.14 wt. %.

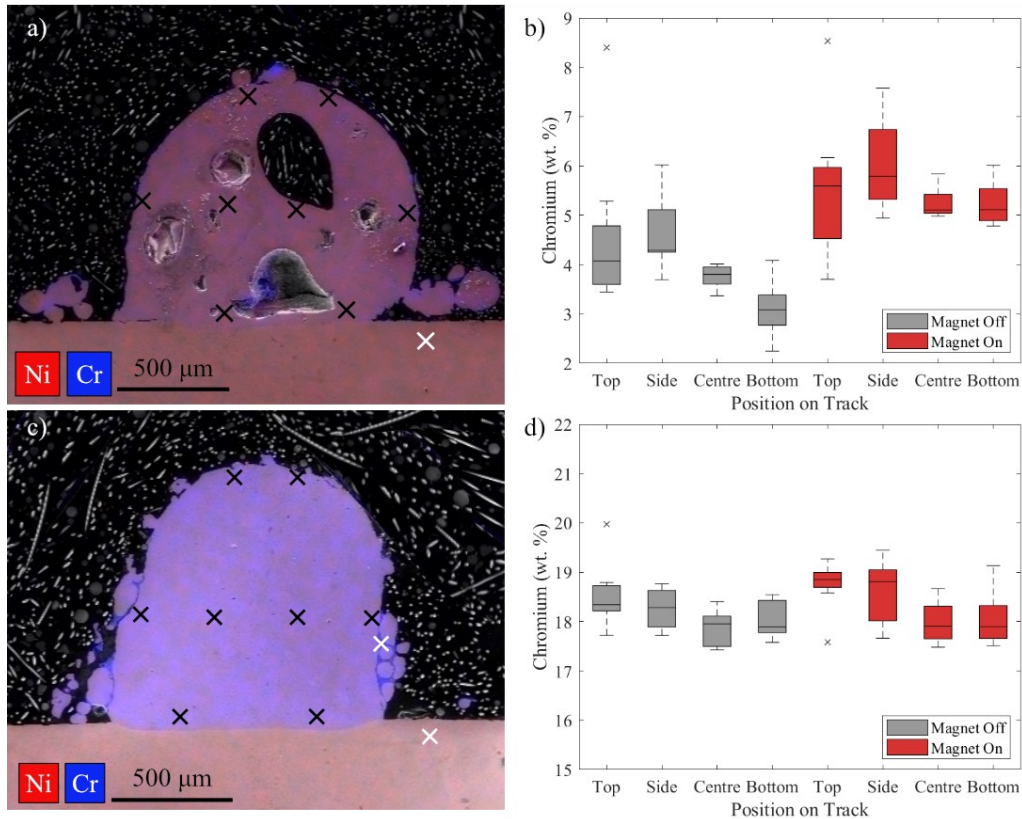


Figure 7-7 Compositions of satellited and pre-alloyed nichrome tracks. Showing EDX maps of the chromium and nickel content in tracks produced with magnetic assistance in a) a satellited powder track and d) a pre-alloyed nichrome track. Also shown is the composition of these cross-sections b) and d) at the locations marked in black. The white marks indicate additional compositional measurements. The colour strength of the nickel is reduced 50 % here compared to in Figure 7-4 to show the difference in chromium more effectively.

7.4 Discussion

Measurements of both the size (area and width) and mass of tracks produced using satellited powder and magnetic assistance indicate that magnetic assistance increases the powder catchment efficiency even when using satellited nickel-chromium feedstock. The size of the dilution zone also followed the same trend as when using non-satellited ferromagnetic feedstock, that is the size of the dilution zone was reduced when the magnetic field was on, likely due to laser attenuation from the increase in powder present, as previously discussed. These effects suggest it is possible to use composite satellited powder whilst retaining some of the benefits of magnetic assistance. The pre-alloyed nichrome powder had greater powder catchment efficiency than the satellited powder in all cases, likely as a result of the powder being more spherical and being directed towards the melt pool more effectively, or because it absorbs the laser power more efficiently. More work is required to determine if this is case

with other parameter combinations. EDX analysis also confirmed that in-situ alloying did occur in the depositions and that there was no measurable leaching of chromium into the substrate. The presence of close to 25 % porosity in tracks produced using the satellited feedstock is a limiting factor in the potential for the use of satellited feedstock. Previous work using pure nickel powder resulted in porosity up to 32.8 % under similar conditions, therefore the presence of porosity is not a result of using satellited feedstock. In comparison, only low levels of porosity were observed in the pre-alloyed nichrome tracks. The parameters used for both of these feedstocks were equivalent. This means that more optimisation of parameters may be required for satellite feedstocks compared to pre-alloyed powder, to eliminate or reduce porosity. Meaning pre-alloyed nichrome may have a larger processing window than equivalent satellited powder. However, the elemental composition of the depositions is likely to offer a better explanation of the cause of porosity. The significantly higher chromium content of tracks manufactured using pre-alloyed nichrome powder (18 – 19 % compared to 3 – 7 % in satellited depositions) likely explains the difference in porosity. Porosity occurs in pure nickel due to the insolubility of nitrogen in nickel. Though porosity also occurs due to gas entrapped in and by the powder and as a result of the rapid cooling of the material not allowing time for bubbles to escape. In welding of *commercially pure* nickel, additives are used to reduce the effects of atmospheric contaminants on the formation of pores, particularly by increasing the solubility of nitrogen in nickel [184]. Although aluminium and titanium are commonly used (up to 5 % total) [126] chromium has a similar effect, especially in much greater quantities present in the tracks manufactured from pre-alloyed nichrome powder. In future better shielding, such as using higher flow rate of shielding gas [122], or addition of small quantities of aluminium/titanium may be used to reduce porosity in satellited tracks. However an increase in gas flow rate has also been shown to increase gas entrapment in nickel alloys [185]. Hence the need for research of nickel welding in a vacuum [186] or underwater [187]. Chromium may have led to the reduced porosity here, compared to in the previous experiments using pure nickel powder (Section 6.3.3), but the difference in energy density (due to a smaller fibre being used causing the different spot size) means chromium content is not the only new factor.

No meaningful difference is noted between the porosity of tracks produced with or without magnetic assistance. This is in contrast to in the previous section (6.3.3) using pure nickel powder. The effect of chromium in reducing the pore area may be masking this phenomenon

somewhat, though in this case the large deviations make it difficult to determine whether there is a difference between the two cases.

In this work the height of tracks was also increased by around 25 % on satellited powder tracks. In previous work the link between magnetic assistance and track height has been unclear. With it being inconsistent in ferritic steel and attributed to increased pore size in pure nickel tracks. However, the smaller difference in porosity for satellited tracks with and without magnetic assistance means that a significant increase in the height of tracks produced in nickel alloy may be due to the presence of more material, not only an increase in air pockets.

The decrease in chromium content from the satellited feedstock (20 wt. % chromium) to that present in the deposition (3 – 7 wt. % approx.) is significant. This is likely due to the smaller loose chromium particles not entering the melt pool. The presence of loose satellite particles could not be eliminated by the improved powder manufacturing process used here, but the composition of satellite composition is likely to increase if better methods to adhere particles are developed. The very small loose particles are not well directed by the nozzle which is not designed for powder of this diameter. In this case they are likely to disperse at a short distance from the orifice. EDX maps suggested that consecutive violent mixing operations may have broken up the coating of satellited particles onto the parent particles. Therefore, it is likely that this continued to take place during powder feeding. The satellited powder was still able to flow through the system (unlike the simply mixed powder) which implies that not all of the chromium was separated from the nickel parent particles.

Approximately 1.5 wt. % more chromium was found in all locations of the satellited powder tracks when the solenoid was switched on, compared to when there was no magnetic field, but not in the pre-alloyed nichrome tracks. As chromium is not ferromagnetic it will not be attracted to the melt pool unless attached to a nickel particle. The ratio of nickel to chromium content on a coated particle depends on the ratio of the volume of the parent particle to the volume of the coating. Assuming there is a uniform coating of satellite particles onto a spherical parent particle (and that this coating has the same thickness regardless of the diameter of the parent particle), the volume of the coating can be estimated using Equation 7-1:

Equation 7-1 $V_c = \frac{4}{3}\pi(r^3 - (r - t)^3)$

Where V_c is the volume of the coating, r is the radius of the parent particle and t is the coating thickness. Following this, the percentage volume of each material may be calculated for a given coated particle. When plotted for the particle size distribution of the parent particles this results in a negative relationship as shown in Figure 7-8. It should be noted that this calculation assumes that only a single layer of satellite particles will cover the parent particle, so this method may be used to calculate the volume of coating comparatively (for different sized parent particles) but not to calculate an expected coating volume.

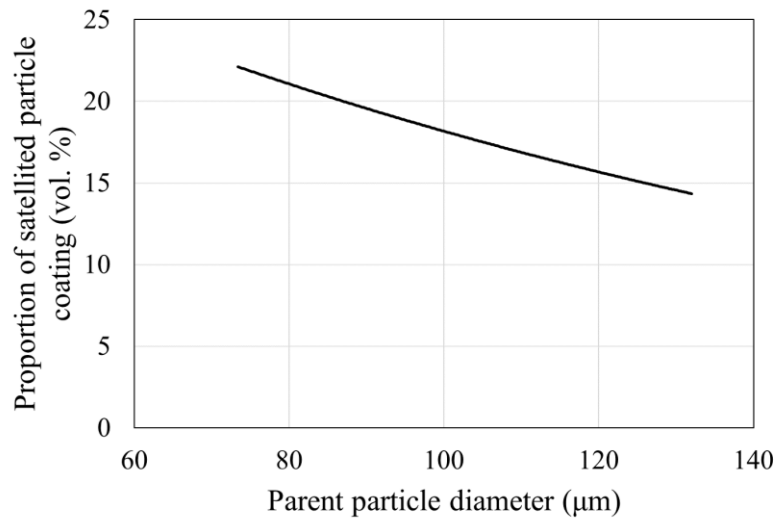


Figure 7-8 Percentage volume of chromium content with parent particle diameter. Showing that as the diameter of the parent particle increases the percentage volume of the coating material declines.

Therefore, the increase in the proportion of chromium found in the magnetically assisted satellited tracks indicates that there was a greater proportion of smaller particles (which have a greater proportion of chromium attached). Although domain theory suggests that larger particles will be attracted towards the magnetic field more strongly than smaller ones, Wolff et al. showed that smaller particles are more readily deflected by the vapour plume [26]. Therefore, it is possible that the magnetic field is reducing the number of small particles which are deflected, leading to a greater chromium content. This phenomena is shown diagrammatically in Figure 7-9, in (a) without a magnetic field the small particles are easily deflected, whereas in (b) the magnetic field provides an extra force which retains these small particles which are normally easily deflected. A reduction in the number of sparks which are expelled from around the melt pool was qualitatively observed during deposition, which supports the idea that fewer particles are deflected with the presence of a magnetic field.

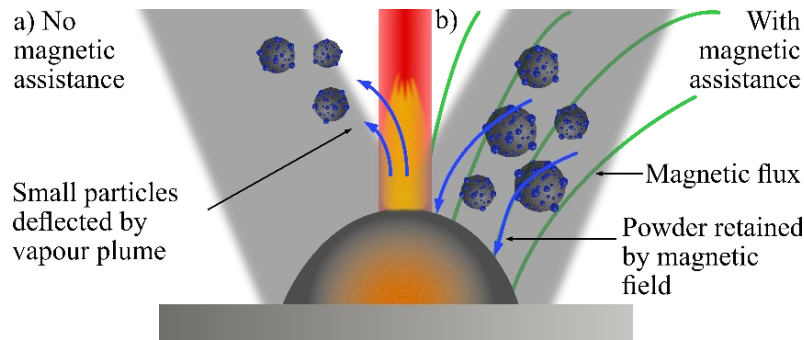


Figure 7-9 Small particles deflected by the vapour plume without magnetic assistance in a) these particles are retained by the magnetic field shown in b).

7.5 Conclusions

This work has shown for the first time that satellited composite powder can be used in magnetically assisted directed energy deposition to create alloys in-situ. It has also been shown that magnetic assistance improves powder catchment efficiency, in this case increasing the mass of tracks by 29.0 %. The following conclusions can be drawn from this work:

- Ferromagnetic powder coated in satellited particles of non-magnetic powder benefits from increased catchment efficiency when using magnetic assistance.
- Magnetic assistance can be used alongside powder satelliting to create alloys of the two powder components.
- Using magnetic assistance with this satellited powder produces similar effects to using purely ferromagnetic powder, including increasing track width by 26.7 % and reducing dilution area by 88.7 %.
- The tracks produced using satellited powder and magnetic assistance also increased in height by 33.3 %.
- Satellited powder was found to flow freely during Carney flow tests and through a directed energy deposition disk feeder and coaxial nozzle.
- The satellited chromium accounted for around 2.5 to 5 wt. % of the composition of tracks produced without magnetic assistance, but between 5 and 7 wt. % for tracks with magnetic assistance. It is therefore likely that magnetic assistance causes some small particles coated with a higher proportion of coating to be retained instead of deflected by the vapour plume.
- Chromium content was generally between 17.5 and 19 wt. % for tracks manufactured using pre-alloyed powder with the same theoretical composition (80 % Ni, 20 % Cr)

as the satellited powder. This indicates that a significant proportion of the chromium satellites did not enter the molten pool in satellited powder.

- Despite the increases in catchment efficiency introduced using magnetic assistance pre-alloyed nichrome powder had a higher catchment efficiency than the magnetically assisted satellited powder at equivalent parameters (31.3 % compared to 24.1 %).

More work is required to develop and improve upon the use of satellited powder for magnetic assistance. This work showed that the composition in the deposited track has a limited quantity of the satellite powder, which may be due to inconsistencies in the satelliting process or poor adhesion between the two powders. In particular research should be conducted which examines whether stronger adhesives may be used to join particles and whether this improves the composition of tracks. New methods of applying these adhesives should also be examined. It is also recommended that a multi-stage satelliting process be tested to examine whether this increases the proportion of satellited material in the tracks. Techniques such as subsequently partially melting the powders together could also be examined. More work could also be applied to the design of magnetic assistance systems to allow this technique to be used in three-dimensions.

8 Overall Discussion

The novel findings on the effect of magnetic assistance on powder catchment efficiency and track characteristics in LDED have a number of implications on research and industry. Although the benefits should be weighed against potential pitfalls. The findings made are consistent across the different technologies used in this work. In particular, the relationships between track geometry and the application of a magnetic field have generally shown to be dependable regardless of the shape of the magnetic field or the magnetic source. In the first study a permanent magnetic field strength of 27 mT across the whole length of the tracks was used. Using AISI 4340 powder on mild steel substrates, this resulted in an increase in the mean cross-sectional area rising 79.8% at a feed rate of approximately 16 g/min. In the same material and using similar parameters and magnetic field strength, the area increased by 17.3% when the solenoid was coaxially aligned. This indicates that magnetic preloading has a greater effect on catchment efficiency than using a coaxially aligned field, though significant increases are still observed with a coaxially aligned solenoid at higher magnetic field strengths. The magnetic preloading effect is likely reduced when crossing the areas of dense magnetic flux in Section 4.3.2 because the powder was also attracted across the whole width of the lines, rather than just over specific areas, as was ensured when placing the solenoid in specific locations. The strong effects of magnetic preloading are reinforced by the solenoid positioning experiment in Section 5.3.4, which showed that increases in area up to 83.5% when material was deliberately preloaded using a magnetic field. Here the effect of magnetic preloading can be directly compared to a coaxially aligned magnetic field of the same strength. This shows that the effect of magnetic preloading on the size and powder catchment of tracks is significantly greater than when using the instant, coaxially aligned magnetic field, which caused an equivalent increase in area of 23%. Magnetic preloading therefore successfully captures particles which would otherwise not be directed into the molten pool. Increasing the time for magnetic preloading to occur by up to 30 s was not found to increase the powder captured significantly when the powder was deposited 50 mm from the preloading area. This means that it is unlikely that this would be problematic over longer duration builds and may be used as a technique to selectively add powder in specific locations. However studies should be done which create real 2 or 3 dimensional parts to assess whether preloading is a problem over real build scenarios. An increase in area up to 83.5% shows how effective magnetic preloading can be, suggesting that even if the materials which can be used remain limited, magnetic assistance has a niche in manufacturing of

ferromagnetic coatings. It should be noted that magnetic assistance is only one method of improving powder catchment efficiency, other methods, such as parameter optimisation or improving nozzle design may lead to higher levels of efficiency and be applicable to a greater range of materials. However, compared to the time investment required in optimising parameters, this study has shown how magnetic assistance may be able to quickly improve powder catchment without having to do lengthy optimisations. There is therefore potential in the technique to reduce the effort required when conducting LDED, reducing a barrier to its wider application. However, this will come at the cost of requiring new materials which can be used and potentially having to add costly magnetic modules.

The increases in cross-sectional area above the substrate do not include powder catchment efficiency completely (as determined by mass), because dilution was shown to decrease when magnetic assistance is applied. When magnetic preloading was done when crossing over magnets in Section 4.3.2 and again in the solenoid position experiments in Section 5.3.4, the catchment could not be measured directly through mass just for those areas. Therefore improvements in total catchment efficiency cannot be quantified independently of the whole track, though the fact that small increases in the total track mass could still be observed (16.3% for the permanent magnet preloading experiment in Section 4.3.2) indicates that preloading greatly increases catchment efficiency.

The width of tracks is also consistently enlarged throughout these experiments, when using the permanent magnet in the feasibility study the width of tracks increased by up to 36.3% when producing tracks along the lines of dense magnetic flux. In comparison, when using similar parameters in the coaxial solenoid experiment the width of tracks was increased by 15.9% and up to 24.9% using a stronger magnetic field strength of 93.5 mT. Some degree of magnetic preloading still occurred in the permanent magnet experiments, hence the increase even when the field strength was greater in the coaxially aligned experiment. An increase in powder feed rate alone has not generally been associated with an increase in track width, which is limited by the power present to cause heating [71]. The increase in width is therefore not simply as a result of increased powder capture. It is likely that the magnetic field is influencing the heating and cooling in the melt pool. It has previously been suggested that static magnetic fields (as used in this work) can increase the cooling time of tracks by either reducing convective flow in the melt pool and compressing the plasma plume above the track [165]. This has even been shown to increase the melt pool diameter. Therefore, this is the likely cause of the increase in track width. In this work, where ferromagnetic particles are

used, particles which are hot (but below their Curie temperature) will also be guided towards the melt pool rather than deflected by the plasma plume when the magnetic field is present. This can be observed as a reduction in sparking around the melt pool. This would also lead to a reduction in heat loss and hence an increase in the energy present and therefore the track width. An increase in track width could also be construed as a negative effect of magnetic assistance, because it essentially reduces the resolution of the process. An application could be imagined where the magnetic field is switched in intensity depending on whether wider, more efficient tracks were required when filling between edges, or the magnet was switched off for applications which are tolerance dependant. However, such a change to the process would require significant additions to software and CNC control and therefore requires massive capital investment.

With an increase in laser power (and melt pool energy) a corresponding increase in dilution area and depth would also be expected. However, this was not observed, likely due to the increase in catchment efficiency meaning there was more thermal mass above the substrate and therefore less energy to penetrate the substrate. This work showed that an increase in the laser power could be used to remedy poor dilution due to magnetic assistance, though low dilution may be an intended outcome in coating applications.

No change in dilution zone size was observed when using paramagnetic nichrome powder in Section 7.3.1., this powder was not attracted to the magnetic field so there was no increase in thermal mass. If the magnet influenced heat loss even in paramagnetic materials as Lu et al. suggested, then the tracks would be expected to be wider and the dilution zones to be larger with the magnet on. No statistically relevant difference was observed here, in any measure of track geometry when using the magnet or not though. The rate of heat loss is more likely reduced due to a reduction in the amount of hot powder that is deflected.

The relationship between track height and magnetic assistance is less consistent throughout this work, when magnetic preloading is employed the height of tracks generally increases, by up to 52.9% when using the solenoid and 71.6% for the permanent magnet preloading. This was not the case for the coaxial solenoid, where the height of tracks was consistently around $1 \text{ mm} \pm 0.1$ when increasing the magnetic field strength from 0 mT. When the flow rate was varied with the coaxial magnet at a constant field strength no meaningful difference in height was observed either. A change in height can be readily observed when switching the magnetic field off though, as shown in Figure 6-6. It is likely that small inconsistencies in track height across different tracks masks any increase that the magnetic field is causing, or

equally that changes to the liquid flow in the melt pool caused waviness in the switched track, which is responsible for the 240 μm dip immediately after the magnet is switched off. A slight increase in height may therefore be expected, but this is unlikely to affect the vertical resolution when using LDED. Having a reliable track height is very important in LDED, if the layers are not consistent in an AM product then it will fail to be produced. Therefore the effects should be better established as this has potential to limit the process application.

Different use cases of magnetic assistance have also been demonstrated throughout this work. In Chapter 4 it was shown that magnetic assistance can be used to mitigate the decrease in powder catchment when directed energy deposition is conducted on a surface which is not horizontal, and it was also shown that the technique reduces the asymmetry of tracks in this case. In Chapter 5 results from parameter studies suggested that altering laser power may help to compensate for the reduced dilution which occurs using magnetic assistance and that placing magnetic fields in specific positions can be used as a technique to locally increase track size. More novel techniques were demonstrated in Chapter 6, this included the first demonstration of magnetic assistance being used to dynamically change track proportions during deposition, potentially leading to new control capabilities, whilst the technique was also shown to be useful when manufacturing using more complex toolpaths and nickel. In terms of substrate materials, it is demonstrated that using a more magnetically permeable substrate increases the effects of powder catchment in both Chapter 4, on stainless steel substrates, and Chapter 5 using pure nickel substrates. The use of nickel powder is also demonstrated in Chapter 6. It was shown that nickel could also be used in the process, although porosity proved to be a problem, likely as a result of the high purity nickel used and the low solubility of nitrogen in this material. Porosity is therefore a potential pitfall of magnetic assistance in LDED. This should be researched further to establish whether it will stop the process from being used.

Chapter 7 is primarily focused on a method of using magnetic assistance, by using composite feedstock to create alloys in-situ. In this case it was shown that magnetic assistance could be used to subtly change the composition of the alloy, in this case increasing the chromium content by around 2%. Therefore, there is potential for the functional grading of materials by using the previously demonstrated magnetic switching to change material composition throughout a build, if satellited materials are also used. For example, a material may be manufactured which has greater corrosion resistance closer to the surface for applications in the energy industry. It was also shown that using this kind of powder compositing method

allowed the benefits of magnetic assistance, such as on increasing track width to still be applied. However, the limits of what can be done with satellited powders has not yet been uncovered. For example, it was shown here that adding 20% chromium satellites only led to a maximum of 9% in the final product, this 9% may be a limiting factor to the process, or adding more chromium in the initial powder may have meant the desired composition was reached.

This thesis has shown for the first time that magnetic assistance can be used to enhance the geometry and powder catchment efficiency in the directed energy deposition process. The foundational relationships between parameters, magnetic assistance and deposition quality have been determined here and novel applications of magnetic assistance have been uncovered and explained. This work will inform future research on how to improve this process addition further, so that it may find practical industrial application. The addition of magnetic assistance to the LDED process has the potential to improve the controllability and performance of LDED whilst also improving the material processing efficiency. Research to advance the ability of MADED to create non-magnetic alloys, has shown that in-situ alloying could also prove to benefit from magnetic assistance, especially if this garners further attention from the research community. This research lays the foundation for this new technique.

9 Overall Conclusions & Future Work

The aim of this thesis is to demonstrate whether magnetic assistance could be used to improve powder catchment efficiency and change deposition geometry in laser directed energy deposition. This aim has been met successfully via the experimental work reported here.

- Coaxially aligned magnetic assistance may be used to increase powder catchment efficiency by up to 42% to 61%. Using a small magnetic field strength of only 93.5mT provided by a 12V solenoid.
- Using a permanent magnet to provide a field of only 27 mT can increase powder catchment efficiency of ferromagnetic powder to a value of 56% on a horizontal plane, compared to a maximum of 26% without use of magnets. This shows that considerable efficiency improvements are possible using this novel method.
- There is a positive linear relationship between the magnetic field strength at the substrate surface and both the catchment efficiency and track width.

- Magnetic assistance can mitigate the decrease in powder catchment when an inclined workpiece angle of 45° is used, from 20% to 39% at higher flow rates.
- At lower traverse speeds, and higher powder flow rates, magnetic assistance has a greater effect on powder catchment.
- The level of dilution significantly decreased when using a magnet, particularly at lower powder flow rates. This is explained by the greater divergence of laser energy when the magnetic field is present.
- A programmable solenoid was used to dynamically change the track dimensions even when switched during operation, suggesting magnetic assistance is a valid technique of adaptive control.
- By removing the magnetic field during deposition there is a short transition zone before the track returns to normal operation, this is due to magnetic hysteresis of the magnetic focusing cone and the large diameter of the magnetic field.
- Magnetic assistance can be used alongside powder satelliting to create alloys of the two powder component whilst improving powder catchment efficiency.

9.1 Future Work

The work presented in this thesis represents the beginning of a new processing adaptation, therefore there is significant scope for future work to continue building on the results and ideas presented here. Further work in this area will confirm and strengthen the findings made here, whilst widening the application and usefulness of the techniques which have been developed. The greatest limitation of the below substrate magnetic assistance technique which has been used in this work is the inability of the magnetic field to permeate through thicker substrate materials. This means that the technique will not be able to function in thicker, multi-layer component manufacture. Currently industrial use for the technique would be limited to the laser cladding and coating of thin sheet materials, though the widening of tracks and increase in powder catchment efficiency would serve to reduce powder wastage and processing time, which is a useful outcome in itself.

However, to act as intended and be used as a true three-dimensional additive manufacturing technique, development must focus on new methods of providing the magnetic field which do not depend on it permeating through thick layers. More complex magnetic sources will be required to do this whilst locating the source in an unobtrusive position. Potentially, much

stronger fields will therefore be required, but since only relatively weak fields were used here (of the order 10 – 100 mT) this is perfectly feasible. It should be determined whether using different and perhaps more well optimised equipment can be used to change the powder stream distribution in more beneficial ways. For example, it should be determined whether use of softer magnetic cores could be used to switch between the wide tracks produced using magnetic assistance and narrower ones produced without it, much more quickly than has been done here. Magnetic assistance may also be used to both widen and narrow powder stream or direct powder into a specific portion of the melt pool. Furthermore, magnetic assistance may be added to a closed loop control system, where the track size is monitored and a near instantaneous variation of the magnetic field strength allows tracks to be deposited with excellent geometric stability. Predetermined control may also be useful, for example the development of algorithms which include magnetic assistance in toolpath generation would allow magnetic assistance to be used to manufacture wide tracks to quickly fill in the centre of a shape.

More analysis of how magnetic fields change the density of the powder stream should also be conducted. For example, by focusing the magnetic field on one edge of the melt pool may allow steep sided tracks to be produced or those with built-in asymmetry. This would increase the capability of the process significantly by creating components with smoother sidewalls by. Using very narrow magnetic fields it may also be possible to reduce the width of tracks and thereby improve the resolution of the LDED process. In contrast, the use of magnetic fields which are coaxial, but extend slightly ahead of the laser may be useful to increase powder catchment using the magnetic preloading technique in a controlled manner.

The use of powder compositing and in-situ alloying as a technique to widen the materials palette which can be used in MADED is burgeoning. Future work may be used to improve the powder manufacturing process so that designed track compositions can be created. This may involve a multi-stage satelliting process, where the satellite material is added in successive steps, or an entirely different technique may be used. This work is vital for the development of magnetic assistance, because uptake of the process will otherwise be severely limited by the use of only ferromagnetic materials.

10 References

This work uses in text references in the style of the *Additive Manufacturing* journal, a leading journal on the subject of this thesis.

- [1] B. Norhafzan, S.N. Aqida, E. Chikarakara, D. Brabazon, Surface modification of AISI H13 tool steel by laser cladding with NiTi powder, *Appl. Phys. A Mater. Sci. Process.* 122 (2016) 384. <https://doi.org/10.1007/s00339-016-9937-6>.
- [2] M.A. Melia, H.D.A. Nguyen, J.M. Rodelas, E.J. Schindelholz, Corrosion properties of 304L stainless steel made by directed energy deposition additive manufacturing, *Corros. Sci.* 152 (2019) 20–30. <https://doi.org/10.1016/j.corsci.2019.02.029>.
- [3] ISO/ASTM, INTERNATIONAL STANDARD ISO / ASTM 52900 Additive manufacturing — General principles — Terminology, *Int. Organ. Stand.* 5 (2015) 1–26. <https://doi.org/10.1520/ISOASTM52900-15>.
- [4] J. Bennett, D. Garcia, M. Kendrick, T. Hartman, G. Hyatt, K. Ehmann, F. You, J. Cao, Repairing Automotive Dies with Directed Energy Deposition: Industrial Application and Life Cycle Analysis, *J. Manuf. Sci. Eng. Trans. ASME.* 141 (2019) 021019-1-02019–9. <https://doi.org/10.1115/1.4042078>.
- [5] E. Toyserkani, A. Khajepour, S. Corbin, *Laser Cladding*, CRC Press, New York, 2004.
- [6] A. Singh, S. Kapil, M. Das, A comprehensive review of the methods and mechanisms for powder feedstock handling in directed energy deposition, *Addit. Manuf.* 35 (2020) 101388. <https://doi.org/10.1016/j.addma.2020.101388>.
- [7] S. Alya, C. Vundru, B. Ankamreddy, R. Singh, Characterization and modeling of deposition geometry in directed energy deposition over inclined surfaces, *Procedia Manuf.* 34 (2019) 695–703. <https://doi.org/10.1016/j.promfg.2019.06.225>.
- [8] Y. He, J. Wei, J. Liu, X. Wang, Y. Wang, L. He, Experimental study on the fabrication profile and mechanical properties by substrate-inclined angle using laser melting deposition (LMD) integrating with the substrate of stainless steel, *Opt. Laser Technol.* 125 (2020) 106038. <https://doi.org/10.1016/j.optlastec.2019.106038>.
- [9] J. Lin, B.C. Hwang, Coaxial laser cladding on an inclined substrate, *Opt. Laser*

- Technol. 31 (1999) 571–578. [https://doi.org/10.1016/S0030-3992\(99\)00116-4](https://doi.org/10.1016/S0030-3992(99)00116-4).
- [10] A. Dass, A. Moridi, State of the art in directed energy deposition: From additive manufacturing to materials design, *Coatings*. 9 (2019) 1–26. <https://doi.org/10.3390/COATINGS9070418>.
- [11] P.R. Gradl, C.S. Protz, Technology advancements for channel wall nozzle manufacturing in liquid rocket engines, *Acta Astronaut.* 174 (2020) 148–158. <https://doi.org/10.1016/j.actaastro.2020.04.067>.
- [12] P. Urhal, A. Weightman, C. Diver, P. Bartolo, Robot assisted additive manufacturing: A review, *Robot. Comput. Integr. Manuf.* 59 (2019) 335–345. <https://doi.org/10.1016/j.rcim.2019.05.005>.
- [13] W.E. Frazier, Metal additive manufacturing: A review, *J. Mater. Eng. Perform.* 23 (2014) 1917–1928. <https://doi.org/10.1007/s11665-014-0958-z>.
- [14] Y. Chen, X. Zhang, M.M. Parvez, F. Liou, A review on metallic alloys fabrication using elemental powder blends by laser powder directed energy deposition process, *Materials (Basel)*. 13 (2020) 3562. <https://doi.org/10.3390/MA13163562>.
- [15] S.M. Yusuf, S. Cutler, N. Gao, Review: The impact of metal additive manufacturing on the aerospace industry, *Metals (Basel)*. 9 (2019) 1286. <https://doi.org/10.3390/met9121286>.
- [16] J.C. Najmon, S. Raeisi, A. Tovar, Review of additive manufacturing technologies and applications in the aerospace industry, in: *Addit. Manuf. Aerosp. Ind.*, Elsevier Inc., 2019: pp. 7–31. <https://doi.org/10.1016/B978-0-12-814062-8.00002-9>.
- [17] Y. Chew, J.H.L. Pang, G. Bi, B. Song, Effects of laser cladding on fatigue performance of AISI 4340 steel in the as-clad and machine treated conditions, *J. Mater. Process. Technol.* 243 (2017) 246–257. <https://doi.org/10.1016/j.jmatprotec.2016.12.020>.
- [18] L. Li, W.M. Steen, Sensing, modelling and closed loop control of powder feeder for laser surface modification, *Laser Cladding J. Laser Appl.* 11 (1993) 965–974. <https://doi.org/10.2351/1.5058663>.
- [19] W. Wang, L. Li, High-quality high-material-usage multiple-layer laser deposition of nickel alloys using sonic or ultrasonic vibration powder feeding, *Proc. Inst. Mech.*

- Eng. Part B J. Eng. Manuf. 225 (2011) 130–139.
<https://doi.org/10.1177/09544054JEM2128>.
- [20] W. Li, J. Zhang, X. Zhang, F. Liou, Effect of optimizing particle size on directed energy deposition of Functionally Graded Material with blown Pre-Mixed Multi-Powder, *Manuf. Lett.* 13 (2017) 39–43. <https://doi.org/10.1016/j.mfglet.2017.07.001>.
- [21] A. Saboori, A. Aversa, F. Bosio, E. Bassini, E. Librera, M. De Chirico, S. Biamino, D. Ugues, P. Fino, M. Lombardi, An investigation on the effect of powder recycling on the microstructure and mechanical properties of AISI 316L produced by Directed Energy Deposition, *Mater. Sci. Eng. A.* 766 (2019) 138360.
<https://doi.org/10.1016/j.msea.2019.138360>.
- [22] J. Whiting, A. Springer, F. Sciammarella, Real-time acoustic emission monitoring of powder mass flow rate for directed energy deposition, *Addit. Manuf.* 23 (2018) 312–318. <https://doi.org/10.1016/j.addma.2018.08.015>.
- [23] G. Tapia, A. Elwany, A Review on Process Monitoring and Control in Metal-Based Additive Manufacturing, *J. Manuf. Sci. Eng.* 136 (2014) 060801.
<https://doi.org/10.1115/1.4028540>.
- [24] L. Tang, J. Ruan, R.G. Landers, F. Liou, Variable powder flow rate control in laser metal deposition processes, *J. Manuf. Sci. Eng.* 130 (2008) 0410161.
<https://doi.org/10.1115/1.2953074>.
- [25] J.Y. Jeng, S.C. Peng, C.J. Chou, Metal rapid prototype fabrication using selective laser cladding technology, *Int. J. Adv. Manuf. Technol.* 16 (2000) 681–687.
<https://doi.org/10.1007/s001700070039>.
- [26] S.J. Wolff, H. Wu, N. Parab, C. Zhao, K.F. Ehmann, T. Sun, J. Cao, In-situ high-speed X-ray imaging of piezo-driven directed energy deposition additive manufacturing, *Sci. Rep.* 9 (2019) 1–14. <https://doi.org/10.1038/s41598-018-36678-5>.
- [27] G. Winkler, Analysing the vibrating conveyor, *Int. J. Mech. Sci.* 20 (1978) 561–570.
- [28] P. Dunst, P. Bornmann, T. Hemsel, W. Sextro, Vibration-assisted handling of dry fine powders, *Actuators.* 7 (2018) 1–11. <https://doi.org/10.3390/act7020018>.
- [29] Y. Chen, S.J. Clark, Y. Huang, L. Sinclair, C. Lun Alex Leung, S. Marussi, T. Connolley, O. V. Magdysyuk, R.C. Atwood, G.J. Baxter, M.A. Jones, I. Todd, P.D.

- Lee, In situ X-ray quantification of melt pool behaviour during directed energy deposition additive manufacturing of stainless steel, *Mater. Lett.* 286 (2021) 129205. <https://doi.org/10.1016/j.matlet.2020.129205>.
- [30] D.M. Goodarzi, J. Pekkarinen, A. Salminen, Effect of process parameters in laser cladding on substrate melted areas and the substrate melted shape, *J. Laser Appl.* 27 (2015) S29201. <https://doi.org/10.2351/1.4906376>.
- [31] M. Dias Da Silva, K. Partes, T. Seefeld, F. Vollertsen, Comparison of coaxial and off-axis nozzle configurations in one step process laser cladding on aluminum substrate, *J. Mater. Process. Technol.* 212 (2012) 2514–2519. <https://doi.org/10.1016/j.jmatprotec.2012.06.011>.
- [32] A. Lamikiz, I. Taberner, E. Ukar, S. Martinez, L. N. Lopez de Lacalle, Current Designs of Coaxial Nozzles for Laser Cladding, *Recent Patents Mech. Eng.* 4 (2012) 29–36. <https://doi.org/10.2174/2212797611104010029>.
- [33] P. Ramiro-Castro, M. Ortiz, A. Alberdi, A. Lamikiz, Effects of gravity and non-perpendicularity during powder-fed directed energy deposition of ni-based alloy 718 through two types of coaxial nozzle, *Metals (Basel)*. 10 (2020) 560. <https://doi.org/10.3390/met10050560>.
- [34] A.J. Pinkerton, L. Lin, Modelling powder concentration distribution from a coaxial deposition nozzle for laser-based rapid tooling, *J. Manuf. Sci. Eng. Trans. ASME*. 126 (2004) 33–41. <https://doi.org/10.1115/1.1643748>.
- [35] A.J. Pinkerton, L. Li, Modelling the geometry of a moving laser melt pool and deposition track via energy and mass balances, 37 (2004) 1885. <https://doi.org/10.1088/0022-3727/37/14/003>.
- [36] D. Eisenbarth, P.M. Borges Esteves, F. Wirth, K. Wegener, Spatial powder flow measurement and efficiency prediction for laser direct metal deposition, *Surf. Coatings Technol.* 362 (2019) 397–408. <https://doi.org/10.1016/j.surfcoat.2019.02.009>.
- [37] S. Zekovic, R. Dwivedi, R. Kovacevic, Numerical simulation and experimental investigation of gas–powder flow from radially symmetrical nozzles in laser-based direct metal deposition, *Int. J. Mach. Tools Manuf.* 47 (2007) 112–123. <https://doi.org/10.1016/j.ijmachtools.2006.02.004>.

- [38] A. Kuznetsov, A. Jeromen, G. Levy, M. Fujishima, E. Govekar, Annular laser beam cladding process feasibility study, *Phys. Procedia*. 83 (2016) 647–656. <https://doi.org/10.1016/j.phpro.2016.08.067>.
- [39] E. Govekar, A. Jeromen, A. Kuznetsov, G. Levy, M. Fujishima, Study of an annular laser beam based axially-fed powder cladding process, *CIRP Ann. - Manuf. Technol.* 67 (2018) 241–244. <https://doi.org/10.1016/j.cirp.2018.04.082>.
- [40] D. Ding, Z. Pan, D. Cuiuri, H. Li, Wire-feed additive manufacturing of metal components: technologies, developments and future interests, *Int. J. Adv. Manuf. Technol.* 81 (2015) 465–481. <https://doi.org/10.1007/s00170-015-7077-3>.
- [41] C.K. Kim, J. Il Jeong, S.G. Choi, J.H. Kim, Y.T. Cho, High-throughput directed energy deposition process with an optimized scanning nozzle, *J. Mater. Process. Technol.* 295 (2021) 117165. <https://doi.org/10.1016/j.jmatprotec.2021.117165>.
- [42] M. Rombouts, G. Maes, W. Hendrix, E. Delarbre, F. Motmans, Surface finish after laser metal deposition, in: *Phys. Procedia*, Elsevier Srl, 2013: pp. 810–814. <https://doi.org/10.1016/j.phpro.2013.03.152>.
- [43] J.K. Watson, K.M. Taminger, R.A. Hafley, D.D. Petersen, Development of a Prototype Low-Voltage Electron Beam Freeform Fabrication system, *Solid Free. Fabr. Proc.* (2002) 458–465.
- [44] A.G. Demir, Micro laser metal wire deposition for additive manufacturing of thin-walled structures, *Opt. Lasers Eng.* 100 (2018) 9–17. <https://doi.org/10.1016/j.optlaseng.2017.07.003>.
- [45] D.G. Ahn, Directed Energy Deposition (DED) Process: State of the Art, *Int. J. Precis. Eng. Manuf.* 8 (2021) 703–742. <https://doi.org/10.1007/s40684-020-00302-7>.
- [46] J. Kelbassa, A. Gasser, J. Bremer, O. Pütsch, R. Poprawe, J. Henrich Schleifenbaum, Equipment and process windows for laser metal deposition with coaxial wire feeding, *J. Laser Appl.* 31 (2019) 022320. <https://doi.org/10.2351/1.5096112>.
- [47] J.M. Flynn, A. Shokrani, S.T. Newman, V. Dhokia, Hybrid additive and subtractive machine tools - Research and industrial developments, *Int. J. Mach. Tools Manuf.* 101 (2016) 79–101. <https://doi.org/10.1016/j.ijmachtools.2015.11.007>.
- [48] A.N.D. Gasper, S. Catchpole-Smith, A.T. Clare, In-situ synthesis of titanium

- aluminides by direct metal deposition, *J. Mater. Process. Technol.* 239 (2017) 230–239. <https://doi.org/10.1016/j.jmatprotec.2016.08.031>.
- [49] S.W. Williams, F. Martina, A.C. Addison, J. Ding, G. Pardal, P. Colegrove, *Wire + Arc additive manufacturing, Mater. Sci. Technol. (United Kingdom)*. 32 (2016) 641–647. <https://doi.org/10.1179/1743284715Y.00000000073>.
- [50] H. Wang, W. Liu, Z. Tang, Y. Wang, X. Mei, K.M. Saleheen, Z. Wang, H. Zhang, Review on adaptive control of laser-directed energy deposition, *Opt. Eng.* 59 (2020) 070901. <https://doi.org/10.1117/1.oe.59.7.070901>.
- [51] M. Miyagi, T. Tsukamoto, H. Kawanaka, Adaptive shape control of laser-deposited metal structures by adjusting weld pool size, *J. Laser Appl.* 26 (2014) 032003. <https://doi.org/10.2351/1.4869499>.
- [52] A. Fathi, A. Khajepour, E. Toyserkani, M. Durali, Clad height control in laser solid freeform fabrication using a feedforward PID controller, *Int. J. Adv. Manuf. Technol.* 35 (2007) 280–292. <https://doi.org/10.1007/s00170-006-0721-1>.
- [53] L. Song, J. Mazumder, Feedback control of melt pool temperature during laser cladding process, *IEEE Trans. Control Syst. Technol.* 19 (2011) 1349–1356. <https://doi.org/10.1109/TCST.2010.2093901>.
- [54] J.C. Haley, B. Zheng, U.S. Bertoli, A.D. Dupuy, J.M. Schoenung, E.J. Lavernia, Working distance passive stability in laser directed energy deposition additive manufacturing, *Mater. Des.* 161 (2019) 86–94. <https://doi.org/10.1016/j.matdes.2018.11.021>.
- [55] Y. Ding, J. Warton, R. Kovacevic, Development of sensing and control system for robotized laser-based direct metal addition system, *Addit. Manuf.* 10 (2016) 24–35. <https://doi.org/10.1016/j.addma.2016.01.002>.
- [56] H. Qi, M. Azer, P. Singh, Adaptive toolpath deposition method for laser net shape manufacturing and repair of turbine compressor airfoils, *Int. J. Adv. Manuf. Technol.* 48 (2010) 121–131. <https://doi.org/10.1007/s00170-009-2265-7>.
- [57] J.I. Arrizubieta, S. Martínez, A. Lamikiz, E. Ukar, K. Arntz, F. Klocke, Instantaneous powder flux regulation system for Laser Metal Deposition, *J. Manuf. Process.* 29 (2017) 242–251. <https://doi.org/10.1016/j.jmapro.2017.07.018>.

- [58] Y.S. Lee, M. Nordin, S.S. Babu, D.F. Farson, Influence of fluid convection on weld pool formation in laser cladding, *Weld. J.* 93 (2014) 292–300.
- [59] A.G. Grigoryants, Thermal Processes in Laser-Metal Interaction Zones, in: P.S. Ivanov (Ed.), *Basics Laser Mater. Process.*, Mir Publishers, Moscow, 1994: pp. 69–116.
- [60] J. Trapp, A.M. Rubenchik, G. Guss, M.J. Matthews, In situ absorptivity measurements of metallic powders during laser powder-bed fusion additive manufacturing, *Appl. Mater. Today.* 9 (2017) 341–349. <https://doi.org/10.1016/j.apmt.2017.08.006>.
- [61] A.T. Clare, W.J. Reynolds, J.W. Murray, N.T. Aboulkhair, M. Simonelli, M. Hardy, D.M. Grant, C. Tuck, Laser calorimetry for assessment of melting behaviour in multi-walled carbon nanotube decorated aluminium by laser powder bed fusion, *CIRP Ann.* 69 (2020) 197–200. <https://doi.org/10.1016/j.cirp.2020.04.053>.
- [62] X. He, J.T. Norris, P.W. Fuerschbach, T. Debroy, Liquid metal expulsion during laser spot welding of 304 stainless steel, *J. Phys. D Appl. Phys.* 39 (2006) 525–534. <https://doi.org/10.1088/0022-3727/39/3/016>.
- [63] S. Sreekanth, E. Ghassemali, K. Hurtig, S. Joshi, Effect of Direct Energy Deposition Process Parameters, *Metals (Basel).* 10 (2020) 96. <https://doi.org/https://doi.org/10.3390/met10010096>.
- [64] H. Gedda, J. Powell, G. Wahlström, W.-B. Li, H. Engström, C. Magnusson, Energy redistribution during CO2 laser cladding, *J. Laser Appl.* 549 (2001) 549–558. <https://doi.org/10.2351/1.5059908>.
- [65] N.K. Tolochko, T. Laoui, Y. V Khlopkov, S.E. Mozzharov, V.I. Titov, M.B. Ignatiev, Absorptance of powder materials suitable for laser sintering, *Rapid Prototyp. J.* 6 (2000) 155–161. <https://doi.org/https://doi.org/10.1108/13552540010337029>.
- [66] A.J. Pinkerton, L. Li, An analytical model of energy distribution in laser direct metal deposition, *Proc. Inst. Mech. Eng. Part B J. Eng. Manuf.* 218 (2004) 363–374. <https://doi.org/10.1243/095440504323055498>.
- [67] J. Xie, A. Kar, Laser Welding of Thin Sheet Steel with Surface Oxidation, *Weld. J.* 78 (1999) 343–348.
- [68] M.F. Gouge, J.C. Heigel, P. Michaleris, T.A. Palmer, Modeling forced convection in the thermal simulation of laser cladding processes, *Int. J. Adv. Manuf. Technol.* 79

- (2015) 307–320. <https://doi.org/10.1007/s00170-015-6831-x>.
- [69] I. Gibson, D.W. Rosen, B. Stucker, Additive manufacturing technologies: Rapid prototyping to direct digital manufacturing, *Addit. Manuf. Technol. Rapid Prototyp. to Direct Digit. Manuf.* (2010) 1–459. <https://doi.org/10.1007/978-1-4419-1120-9>.
- [70] G.F. Sun, S. Bhattacharya, G.P. Dinda, A. Dasgupta, J. Mazumder, Influence of processing parameters on lattice parameters in laser deposited tool alloy steel, *Mater. Sci. Eng. A.* 528 (2011) 5141–5145. <https://doi.org/10.1016/j.msea.2011.03.003>.
- [71] B. Bax, R. Rajput, R. Kellet, M. Reisacher, Systematic evaluation of process parameter maps for laser cladding and directed energy deposition, *Addit. Manuf.* 21 (2018) 487–494. <https://doi.org/10.1016/j.addma.2018.04.002>.
- [72] M. Gibson, J. Tyrer, R. Higginson, Direct metal deposition melt pool temperature distribution control through novel holographic beam shaping, allowing improved mechanical and corrosion properties, *ICALEO 2009 - 28th Int. Congr. Appl. Lasers Electro-Optics, Congr. Proc.* 102 (2009) 545–551. <https://doi.org/10.2351/1.5061608>.
- [73] ASTM International, Standard Guide for Directed Energy Deposition of Metals, *ASTM Stand.* (2016) 1–22. <https://doi.org/10.1520/F3187>.
- [74] H. Liu, X. Qin, S. Huang, Z. Hu, M. Ni, Geometry modeling of single track cladding deposited by high power diode laser with rectangular beam spot, *Opt. Lasers Eng.* 100 (2018) 38–46. <https://doi.org/10.1016/j.optlaseng.2017.07.008>.
- [75] K. Partes, Analytical model of the catchment efficiency in high speed laser cladding, *Surf. Coatings Technol.* 204 (2009) 366–371. <https://doi.org/10.1016/j.surfcoat.2009.07.041>.
- [76] E. Fearon, K.G. Watkins, Optimisation of layer height control in direct laser deposition, *ICALEO 2004 - 23rd Int. Congr. Appl. Laser Electro-Optics, Congr. Proc.* (2004) 1708. <https://doi.org/10.2351/1.5060232>.
- [77] J. Lin, Simple model of powder catchment in coaxial laser cladding, *Opt. Laser Technol.* 31 (1999) 233–238. [https://doi.org/10.1016/S0030-3992\(99\)00046-8](https://doi.org/10.1016/S0030-3992(99)00046-8).
- [78] J.L. Arrizubieta, I. Tabernero, J. Exequiel Ruiz, A. Lamikiz, S. Martinez, E. Ukar, Continuous coaxial nozzle design for LMD based on numerical simulation, *Phys. Procedia.* 56 (2014) 429–438. <https://doi.org/10.1016/j.phpro.2014.08.146>.

- [79] J. Ibarra-medina, A.J. Pinkerton, A CFD model of the laser, coaxial powder stream and substrate interaction in laser cladding, *Phys. Procedia*. 5 (2010) 337–346. <https://doi.org/10.1016/j.phpro.2010.08.060>.
- [80] D.F. De Lange, J.T. Hofman, J. Meijer, Influence of intensity distribution on the melt pool and clad shape for laser cladding, *Proc. Third Int. WLT-Conference Lasers Manuf. 2005*. (2005) 1–5.
- [81] B. He, D. Li, A. Zhang, J. Ge, X. Do, H. Xie, H. Yang, Influence of powder flow on sidewall quality of solid parts in laser metal direct forming, *Int. J. Adv. Manuf. Technol.* 68 (2013) 2703–2711. <https://doi.org/10.1007/s00170-013-4805-4>.
- [82] J. Dowden, *The Theory of Laser Materials Processing: Heat and Mass Transfer in Modern Technology*, 2009.
- [83] H.S. Prasad, F. Brueckner, A.F.H. Kaplan, Powder catchment in laser metal deposition, *J. Laser Appl.* 31 (2019) 022308. <https://doi.org/10.2351/1.5096130>.
- [84] H. Qi, J. Mazumder, H. Ki, Numerical simulation of heat transfer and fluid flow in coaxial laser cladding process for direct metal deposition, *J. Appl. Phys.* 100 (2006) 024903. <https://doi.org/10.1063/1.2209807>.
- [85] V. Kovalenko, J. Yao, Q. Zhang, M. Anyakin, X. Hu, R. Zhuk, Development of Multichannel Gas-powder Feeding System Coaxial with Laser Beam, in: *Procedia CIRP*, Elsevier B.V., 2016: pp. 96–100. <https://doi.org/10.1016/j.procir.2016.02.197>.
- [86] F. Brueckner, M. Riede, M. Müller, F. Marquardt, R. Willner, A. Seidel, E. López, C. Leyens, E. Beyer, Enhanced manufacturing possibilities using multi-materials in laser metal deposition, *J. Laser Appl.* 30 (2018) 32308. <https://doi.org/10.2351/1.5040639>.
- [87] B.A.B. Khamidullin, I.V.I. Tsvil'skiy, A.I.A. Gorunov, Ak.K. Gilmudinov, Modeling of the effect of powder parameters on laser cladding using coaxial nozzle, *Surf. Coatings Technol.* 364 (2019) 430–443. <https://doi.org/10.1016/j.surfcoat.2018.12.002>.
- [88] Z. Gan, G. Yu, X. He, S. Li, Surface-active element transport and its effect on liquid metal flow in laser-assisted additive manufacturing, *Int. Commun. Heat Mass Transf.* 86 (2017) 206–214. <https://doi.org/10.1016/j.icheatmasstransfer.2017.06.007>.
- [89] D. Du, A. Dong, D. Shu, D. Wang, G. Zhu, B. Sun, E.J. Lavernia, Influence of Static Magnetic Field on the Microstructure of Nickel-Based Superalloy by Laser-Directed

- Energy Deposition, *Metall. Mater. Trans. A Phys. Metall. Mater. Sci.* 51 (2020) 3354–3359. <https://doi.org/10.1007/s11661-020-05783-4>.
- [90] M. Bachmann, V. Avilov, A. Gumenyuk, M. Rethmeier, About the influence of a steady magnetic field on weld pool dynamics in partial penetration high power laser beam welding of thick aluminium parts, *Int. J. Heat Mass Transf.* 60 (2013) 309–321. <https://doi.org/10.1016/j.ijheatmasstransfer.2013.01.015>.
- [91] I.E. Anderson, E.M.H. White, R. Dehoff, Feedstock powder processing research needs for additive manufacturing development, *Curr. Opin. Solid State Mater. Sci.* 22 (2018) 8–15. <https://doi.org/10.1016/j.cossms.2018.01.002>.
- [92] E. Fereiduni, A. Ghasemi, M. Elbestawi, Characterization of composite powder feedstock from powder bed fusion additive manufacturing perspective, *Materials (Basel)*. 12 (2019) 3673. <https://doi.org/10.3390/ma12223673>.
- [93] P. Mellin, O. Lyckfeldt, P. Harlin, H. Brodin, H. Blom, A. Strondl, Evaluating flowability of additive manufacturing powders, using the Gustavsson flow meter, *Met. Powder Rep.* 72 (2017) 322–326. <https://doi.org/10.1016/j.mprp.2017.06.003>.
- [94] B964, Standard Test Methods for Flow Rate of Metal Powders Using the Carney Funnel, *ASTM Stand.* (2016) 4–6. <https://doi.org/10.1520/B0213-17.2>.
- [95] A.J. Pinkerton, L. Li, Rapid prototyping using direct laser deposition - The effect of powder atomization type and flowrate, *Proc. Inst. Mech. Eng. Part B J. Eng. Manuf.* 217 (2003) 741–752. <https://doi.org/10.1243/09544050360673134>.
- [96] Y. Kakinuma, M. Mori, Y. Oda, T. Mori, M. Kashihara, A. Hansel, M. Fujishima, Influence of metal powder characteristics on product quality with directed energy deposition of Inconel 625, *CIRP Ann. - Manuf. Technol.* 65 (2016) 209–212. <https://doi.org/10.1016/j.cirp.2016.04.058>.
- [97] K.L. Terrassa, J.C. Haley, B.E. MacDonald, J.M. Schoenung, Reuse of powder feedstock for directed energy deposition, *Powder Technol.* 338 (2018) 819–829. <https://doi.org/10.1016/j.powtec.2018.07.065>.
- [98] P.A. Carroll, A.J. Pinkerton, J. Allen, W.U.H. Syed, H.K. Sezer, P. Brown, G. Ng, R. Scudamore, L. Li, The effect of powder recycling in direct metal laser deposition on powder and manufactured part characteristics, *Proc. AVT-139 Spec. Meet. Cost Eff.*

- Manuf. via Net Shape Process. NATO Res. Technol. Organ. (2006) 1–8.
- [99] N.E. Gorji, R. O'Connor, A. Mussatto, M. Snelgrove, P.G.M. González, D. Brabazon, Recyclability of stainless steel (316 L) powder within the additive manufacturing process, *Materialia*. 8 (2019) 100489. <https://doi.org/10.1016/j.mtla.2019.100489>.
- [100] K. Ma, T. Smith, E.J. Lavernia, J.M. Schoenung, Environmental Sustainability of Laser Metal Deposition: The Role of Feedstock Powder and Feedstock Utilization Factor, *Procedia Manuf.* 7 (2017) 198–204. <https://doi.org/10.1016/j.promfg.2016.12.049>.
- [101] M. Meisnar, S. Baker, C. Fowler, L. Pambaguian, T. Ghidini, Lessons learnt through the development of an application-specific methodology for metal powder characterisation for additive manufacturing, *Proc. Euro PM 2017 Int. Powder Metall. Congr. Exhib.* (2017) 3–9.
- [102] BS EN ISO 8130-13 Coating powders. Particle size analysis by laser diffraction, 2019.
- [103] BS EN ISO 4497 Metallic Powders. Determination of particle size by dry sieving., 2020.
- [104] BS 3406-4:1963 Methods for determination of particle size distribution. Optical microscopy method., 1963.
- [105] Y. Liu, C. Liu, W. Liu, Y. Ma, C. Zhang, Q. Cai, B. Liu, Microstructure and properties of Ti/Al lightweight graded material by direct laser deposition, *Mater. Sci. Technol.* (United Kingdom). 34 (2018) 945–951. <https://doi.org/10.1080/02670836.2017.1412042>.
- [106] J.M. Waller, R.L. Saulsberry, B.H. Parker, K.L. Hodges, E.R. Burke, K.M. Taminger, Summary of NDE of additive manufacturing efforts in NASA, (2015) 51–62. <https://doi.org/10.1063/1.4914594>.
- [107] X.P. Li, K.M. O'Donnell, T.B. Sercombe, Selective laser melting of Al-12Si alloy: Enhanced densification via powder drying, *Addit. Manuf.* 10 (2016) 10–14. <https://doi.org/10.1016/j.addma.2016.01.003>.
- [108] H. Tan, D. Hao, K. Al-Hamdani, F. Zhang, Z. Xu, A.T. Clare, Direct metal deposition of TiB₂/AlSi10Mg composites using satellited powders, *Mater. Lett.* 214 (2018) 123–126. <https://doi.org/10.1016/j.matlet.2017.11.121>.

- [109] M. Simonelli, D.G. McCartney, P. Barriobero-Vila, N.T. Aboulkhair, Y.Y. Tse, A. Clare, R. Hague, The Influence of Iron in Minimizing the Microstructural Anisotropy of Ti-6Al-4V Produced by Laser Powder-Bed Fusion, *Metall. Mater. Trans. A Phys. Metall. Mater. Sci.* 51 (2020) 2444–2459. <https://doi.org/10.1007/s11661-020-05692-6>.
- [110] C. Zhong, T. Biermann, A. Gasser, R. Poprawe, Experimental study of effects of main process parameters on porosity, track geometry, deposition rate, and powder efficiency for high deposition rate laser metal deposition, *J. Laser Appl.* 27 (2015) 042003. <https://doi.org/10.2351/1.4923335>.
- [111] S. Sreekanth, E. Ghassemali, K. Hurtig, S. Joshi, J. Andersson, Effect of Direct Energy Deposition Process Parameters on Single-Track Deposits of Alloy 718, *Metals (Basel)*. 10 (2020) 96. <https://doi.org/10.3390/met10010096>.
- [112] K. Zhang, W. Liu, X. Shang, Research on the processing experiments of laser metal deposition shaping, *Opt. Laser Technol.* 39 (2007) 549–557. <https://doi.org/10.1016/j.optlastec.2005.10.009>.
- [113] D.J. Corbin, A.R. Nassar, E.W. Reutzel, A.M. Beese, N.A. Kistler, Effect of directed energy deposition processing parameters on laser deposited Inconel ® 718: External morphology, *J. Laser Appl.* 29 (2017) 022001. <https://doi.org/10.2351/1.4977476>.
- [114] A.N. Jinoop, C.P. Paul, S.K. Mishra, K.S. Bindra, Laser Additive Manufacturing using directed energy deposition of Inconel-718 wall structures with tailored characteristics, *Vacuum*. 166 (2019) 270–278. <https://doi.org/10.1016/j.vacuum.2019.05.027>.
- [115] M. Ansari, R. Shoja Razavi, M. Barekat, An empirical-statistical model for coaxial laser cladding of NiCrAlY powder on Inconel 738 superalloy, *Opt. Laser Technol.* 86 (2016) 136–144. <https://doi.org/10.1016/j.optlastec.2016.06.014>.
- [116] S. Webster, K. Ehmann, J. Cao, Energy density comparison via highspeed, in-situ imaging of directed energy deposition, *Procedia Manuf.* 48 (2020) 691–696. <https://doi.org/10.1016/j.promfg.2020.05.101>.
- [117] Q. Wang, J. Li, M. Gouge, A.R. Nassar, P. Michaleris, E.W. Reutzel, Physics-Based Multivariable Modeling and Feedback Linearization Control of Melt-Pool Geometry and Temperature in Directed Energy Deposition, *J. Manuf. Sci. Eng. Trans. ASME*.

- 139 (2017) 021013. <https://doi.org/10.1115/1.4034304>.
- [118] A. Calleja, I. Taberero, A. Fernández, A. Celaya, A. Lamikiz, L.N. López De Lacalle, Improvement of strategies and parameters for multi-axis laser cladding operations, *Opt. Lasers Eng.* 56 (2014) 113–120. <https://doi.org/10.1016/j.optlaseng.2013.12.017>.
- [119] G. Zhu, S. Shi, G. Fu, J. Shi, S. Yang, W. Meng, F. Jiang, The influence of the substrate-inclined angle on the section size of laser cladding layers based on robot with the inside-beam powder feeding, *Int. J. Adv. Manuf. Technol.* 88 (2017) 2163–2168. <https://doi.org/10.1007/s00170-016-8950-4>.
- [120] C.P. Paul, S.K. Mishra, A. Kumar, L.M. Kukreja, Laser rapid manufacturing on vertical surfaces: Analytical and experimental studies, *Surf. Coatings Technol.* 224 (2013) 18–28. <https://doi.org/10.1016/j.surfcoat.2013.02.044>.
- [121] U. de Oliveira, V. Ocelík, J.T.M. De Hosson, Analysis of coaxial laser cladding processing conditions, *Surf. Coatings Technol.* 197 (2005) 127–136. <https://doi.org/10.1016/j.surfcoat.2004.06.029>.
- [122] M. Fujishima, Y. Oda, R. Ashida, K. Takezawa, M. Kondo, Study on factors for pores and cladding shape in the deposition processes of Inconel 625 by the directed energy deposition (DED) method, *CIRP J. Manuf. Sci. Technol.* 19 (2017) 200–204. <https://doi.org/10.1016/j.cirpj.2017.04.003>.
- [123] T. Kuriya, R. Koike, T. Mori, Y. Kakinuma, Relationship between solidification time and porosity with directed energy deposition of Inconel 718, *J. Adv. Mech. Des. Syst. Manuf.* 12 (2018). <https://doi.org/10.1299/jamdsm.2018jamdsm0104>.
- [124] S. Webster, S. Wolff, J. Bennett, T. Sun, J. Cao, K. Ehmman, Porosity Formation and Meltpool Geometry Analysis Using High-speed, in situ Imaging of Directed Energy Deposition, *Microsc. Microanal.* 25 (2019) 2556–2557. <https://doi.org/10.1017/S1431927619013515>.
- [125] Z.E. Tan, J.H.L. Pang, J. Kaminski, H. Pepin, Characterisation of porosity, density, and microstructure of directed energy deposited stainless steel AISI 316L, *Addit. Manuf.* 25 (2019) 286–296. <https://doi.org/10.1016/j.addma.2018.11.014>.
- [126] J.C. Lippold, S.D. Kiser, J.N. DuPont, Commercially Pure Nickel Alloys, in: *Weld. Metall. Weldability Nickel-Based Alloy.*, John Wiley & Sons, 2009: p. 2.

- [127] S. Bhattacharya, G.P. Dinda, A.K. Dasgupta, J. Mazumder, Microstructural evolution of AISI 4340 steel during Direct Metal Deposition process, *Mater. Sci. Eng. A.* 528 (2011) 2309–2318. <https://doi.org/10.1016/j.msea.2010.11.036>.
- [128] M. Khanzadeh, S. Chowdhury, M.A. Tschopp, H.R. Doude, M. Marufuzzaman, L. Bian, In-situ monitoring of melt pool images for porosity prediction in directed energy deposition processes, *IISE Trans.* 51 (2019) 437–455. <https://doi.org/10.1080/24725854.2017.1417656>.
- [129] V.A. Hosseini, S.G. Shabestari, R. Gholizadeh, Study on the effect of cooling rate on the solidification parameters, microstructure, and mechanical properties of LM13 alloy using cooling curve thermal analysis technique, *Mater. Des.* 50 (2013) 7–14. <https://doi.org/10.1016/j.matdes.2013.02.088>.
- [130] N. Zhang, W. Liu, D. Deng, Z. Tang, X. Liu, Z. Yan, H. Zhang, Effect of electric-magnetic compound field on the pore distribution in laser cladding process, *Opt. Laser Technol.* 108 (2018) 247–254. <https://doi.org/10.1016/j.optlastec.2018.06.037>.
- [131] A. Saboori, G. Piscopo, M. Lai, A. Salmi, S. Biamino, An investigation on the effect of deposition pattern on the microstructure, mechanical properties and residual stress of 316L produced by Directed Energy Deposition, *Mater. Sci. Eng. A.* 780 (2020) 139179. <https://doi.org/10.1016/j.msea.2020.139179>.
- [132] V. Ocelík, O. Nenadl, A. Palavra, J.T.M. De Hosson, On the geometry of coating layers formed by overlap, *Surf. Coatings Technol.* 242 (2014) 54–61. <https://doi.org/10.1016/j.surfcoat.2014.01.018>.
- [133] F. Cabanettes, A. Joubert, G. Chardon, V. Dumas, J. Rech, C. Grosjean, Z. Dimkovski, Topography of as built surfaces generated in metal additive manufacturing: A multi scale analysis from form to roughness, *Precis. Eng.* 52 (2018) 249–265. <https://doi.org/10.1016/j.precisioneng.2018.01.002>.
- [134] P.Y. Lin, F.C. Shen, K.T. Wu, S.J. Hwang, H.H. Lee, Process optimization for directed energy deposition of SS316L components, *Int. J. Adv. Manuf. Technol.* 111 (2020) 1387–1400. <https://doi.org/10.1007/s00170-020-06113-z>.
- [135] J. Lin, W.M. Steen, Design characteristics and development of a nozzle for coaxial laser cladding, *J. Laser Appl.* 10 (1998) 55–63. <https://doi.org/10.2351/1.521821>.

- [136] S. Takemura, R. Koike, Y. Kakinuma, Y. Sato, Y. Oda, Design of powder nozzle for high resource efficiency in directed energy deposition based on computational fluid dynamics simulation, *Int. J. Adv. Manuf. Technol.* 105 (2019) 4107–4121. <https://doi.org/10.1007/s00170-019-03552-1>.
- [137] K.Y. Nagulin, F.R. Iskhakov, A.I. Shpilev, A.K. Gilmutdinov, Optical diagnostics and optimization of the gas-powder flow in the nozzles for laser cladding, *Opt. Laser Technol.* 108 (2018) 310–320. <https://doi.org/10.1016/j.optlastec.2018.07.001>.
- [138] H.K. Lee, Effects of the cladding parameters on the deposition efficiency in pulsed Nd:YAG laser cladding, *J. Mater. Process. Technol.* 202 (2008) 321–327. <https://doi.org/10.1016/j.jmatprotec.2007.09.024>.
- [139] N. Qaud, Additive manufacturing technologies at Sulzer, *Sulzer Tech. Rev.* 100 (2018) 4–7.
- [140] M. Soshi, K. Odum, G. Li, Investigation of novel trochoidal toolpath strategies for productive and efficient directed energy deposition processes, *CIRP Ann.* 68 (2019) 241–244. <https://doi.org/10.1016/j.cirp.2019.04.112>.
- [141] Y. Huang, M.B. Khamesee, E. Toyserkani, A comprehensive analytical model for laser powder-fed additive manufacturing, *Addit. Manuf.* 12 (2016) 90–99. <https://doi.org/10.1016/j.addma.2016.07.001>.
- [142] G. Sun, R. Zhou, J. Lu, J. Mazumder, Evaluation of defect density, microstructure, residual stress, elastic modulus, hardness and strength of laser-deposited AISI 4340 steel, *Acta Mater.* 84 (2015) 172–189. <https://doi.org/10.1016/j.actamat.2014.09.028>.
- [143] C. Ajus, S.S.M. Tavares, M.R. Silva, R.R.A. Corte, Magnetic properties and retained austenite quantification in SAE 4340 steel, *Rev. Matéria.* 14 (2009) 993–999. <https://doi.org/10.1590/S1517-70762009000300011>.
- [144] S. Sun, Q. Liu, M. Brandt, V. Luzin, R. Cottam, M. Janardhana, G. Clark, Effect of laser clad repair on the fatigue behaviour of ultra-high strength AISI 4340 steel, *Mater. Sci. Eng. A.* 606 (2014) 46–57. <https://doi.org/10.1016/j.msea.2014.03.077>.
- [145] S. Da Sun, S. Da Sun, Q. Liu, M. Brandt, M. Janardhana, G. Clark, Microstructure and mechanical properties of laser cladding repair of AISI 4340 steel, in: *28th Congr. Int. Counc. Aeronaut. Sci.*, 2012: pp. 5127–5135.

- [146] V. Fallah, M. Alimardani, S.F. Corbin, A. Khajepour, Impact of localized surface preheating on the microstructure and crack formation in laser direct deposition of Stellite 1 on AISI 4340 steel, *Appl. Surf. Sci.* 257 (2010) 1716–1723. <https://doi.org/10.1016/j.apsusc.2010.09.003>.
- [147] H. Bhadeshia, R. Honeycombe, *Steels microstructure and properties*, 3rd ed., Butterworth-Heinemann, 2017.
- [148] C. Moosbrugger, F. Cverna, G. Kaufman, J. S. Crosby, P. Sikorsky, H. Sizek, Magnetically Soft Materials, in: C. Moosbrugger (Ed.), *ASM Ready Ref. - Electr. Magn. Prop. Met.*, ASM International, Ohio, 2000: pp. 197–207.
- [149] R.M. Bozorth, Factors Affecting Magnetic Quality, in: *Ferromagnetism*, Wiley-IEEE, 1978: pp. 14–47.
- [150] C.P. Paul, P. Ganesh, S.K. Mishra, P. Bhargava, J. Negi, A.K. Nath, Investigating laser rapid manufacturing for Inconel-625 components, *Opt. Laser Technol.* 39 (2007) 800–805. <https://doi.org/10.1016/j.optlastec.2006.01.008>.
- [151] F. Lia, J.Z. Park, J.S. Keist, S. Joshi, R.P. Martukanitz, Thermal and microstructural analysis of laser-based directed energy deposition for Ti-6Al-4V and Inconel 625 deposits, *Mater. Sci. Eng. A.* 717 (2018) 1–10. <https://doi.org/10.1016/j.msea.2018.01.060>.
- [152] D.A. Woodford, J.J. Frawley, The effect of grain boundary orientation on creep and rupture of IN-738 and nichrome, *Metall. Trans.* 5 (1974) 2005–2013.
- [153] M.S. Knieps, W.J. Reynolds, J. Dejaune, A.T. Clare, A. Evirgen, In-situ alloying in powder bed fusion: The role of powder morphology, *Mater. Sci. Eng. A.* 807 (2021) 140849. <https://doi.org/10.1016/j.msea.2021.140849>.
- [154] F. Fiorillo, M. Küpferling, C. Appino, Magnetic hysteresis and barkausen noise in plastically deformed steel sheets, *Metals (Basel)*. 8 (2018). <https://doi.org/10.3390/met8010015>.
- [155] R.M. Bozorth, The magnetization curve and the domain theory, in: *Ferromagnetism*, 1978: pp. 476–554.
- [156] D.E. Laughlin, *Magnetic Transformations and Phase Diagrams*, *Metall. Mater. Trans. A Phys. Metall. Mater. Sci.* 50 (2019) 2555–2569. <https://doi.org/10.1007/s11661-019->

05214-z.

- [157] N.A. Torres, D.O. Popa, Cooperative control of multiple untethered magnetic microrobots using a single magnetic field source, *IEEE Int. Conf. Autom. Sci. Eng.* 2015-October (2015) 1608–1613. <https://doi.org/10.1109/CoASE.2015.7294330>.
- [158] J.J. Abbott, O. Ergeneman, M.P. Kummer, A.M. Hirt, B.J. Nelson, Modeling magnetic torque and force for controlled manipulation of soft-magnetic bodies, *IEEE/ASME Int. Conf. Adv. Intell. Mechatronics, AIM.* 23 (2007) 1247–1252. <https://doi.org/10.1109/AIM.2007.4412546>.
- [159] M.A. Espy, H. Sandin, C. Carr, C.J. Hanson, M.D. Ward, R.H. Kraus, An instrument for sorting of magnetic microparticles in a magnetic field gradient, *Cytom. Part A.* 69 (2006) 1132–1142. <https://doi.org/10.1002/cyto.a.20337>.
- [160] M. Adachi, H. Moroka, H. Kawamoto, S. Wakabayashi, T. Hoshino, Particle-size sorting system of lunar regolith using electrostatic traveling wave, *J. Electrostat.* 89 (2017) 69–76. <https://doi.org/10.1016/j.elstat.2017.08.002>.
- [161] Y. Han, J. Dong, High-resolution direct printing of molten-metal using electrohydrodynamic jet plotting, *Manuf. Lett.* 12 (2017) 6–9. <https://doi.org/10.1016/j.mfglet.2017.04.001>.
- [162] C. Lotz, Y. Wessargues, J. Hermsdorf, W. Ertmer, L. Overmeyer, Novel active driven drop tower facility for microgravity experiments investigating production technologies on the example of substrate-free additive manufacturing, *Adv. Sp. Res.* 61 (2018) 1967–1974. <https://doi.org/10.1016/j.asr.2018.01.010>.
- [163] P. Kumar, Y. Huang, E. Toyserkani, M.B. Khamesee, Development of a Magnetic Levitation System for Additive Manufacturing: Simulation Analyses, *IEEE Trans. Magn.* 56 (2020). <https://doi.org/10.1109/TMAG.2020.2997759>.
- [164] V.S. Kovalenko, A.M. Lutay, M.S. Anyakin, Z. Mounir, Gas-powder laser cladding with electro-magnetic agitation, 21 (1997) F21–F26. <https://doi.org/10.2351/1.5059701>.
- [165] Y. Lu, G. Sun, Z. Wang, Y. Zhang, B. Su, A. Feng, Z. Ni, Effects of electromagnetic field on the laser direct metal deposition of austenitic stainless steel, *Opt. Laser Technol.* 119 (2019). <https://doi.org/10.1016/j.optlastec.2019.105586>.

- [166] Y. Huang, *Comprehensive Analytical Modeling of Laser Powder-Bed/Fed Additive Manufacturing Processes and an Associated Magnetic Focusing Module*, University of Waterloo, 2019. <http://hdl.handle.net/10012/14650>.
- [167] D.M.B. Dombroski, *Feasibility Study of Ferromagnetic Particulate Path Diversion in Additive Manufacturing*, University of Waterloo, 2018. <http://hdl.handle.net/10012/13209>.
- [168] Digital Surf., *MountainsMap Premium*, (2015). <https://www.digitalsurf.com/>.
- [169] ISO 25178 *Geometric product specification - Surface texture: Areal*, (2012).
- [170] ASTM International, *Standard Guide for Preparation of Metallographic Specimens, E0003-11R1* (2017). <https://doi.org/DOI: 10.1520/E0003-11R17>.
- [171] C.T. Rueden, J. Schindelin, M.C. Hiner, B.E. DeZonia, A.E. Walter, E.T. Arena, K.W. Eliceiri, *ImageJ2: ImageJ for the next generation of scientific image data*, *BMC Bioinformatics*. 18 (2017) 1–26. <https://doi.org/10.1186/s12859-017-1934-z>.
- [172] AISI 4340 Alloy Steel (UNS G43400), (n.d.). <https://www.azom.com/article.aspx?ArticleID=6772> (accessed 26 June 2020).
- [173] V.J. Popov, A. Katz-Demyanetz, A. Garkun, M. Bamberger, *The effect of powder recycling on the mechanical properties and microstructure of electron beam melted Ti-6Al-4 V specimens*, *Addit. Manuf.* 22 (2018) 834–843. <https://doi.org/10.1016/j.addma.2018.06.003>.
- [174] N.A. Wahab, A. Bin, M. Saleh, A. Khahar, B. Nordin, N. Fauzi, B. Tamin, M. Azimin, B. Ibrahim, S. Ahmad, D. Binti, A. Hadi, *Development of Portable Clamping for Lathe Machine*, *ARN J. Eng. Appl. Sci.* 13 (2018) 902–906.
- [175] J. Zhou, J. Xu, S. Huang, Z. Hu, X. Meng, X. Feng, *Effect of laser surface melting with alternating magnetic field on wear and corrosion resistance of magnesium alloy*, *Surf. Coatings Technol.* 309 (2017) 212–219. <https://doi.org/10.1016/j.surfcoat.2016.11.077>.
- [176] F. Lia, J. Park, J. Tressler, R. Martukanitz, *Partitioning of laser energy during directed energy deposition*, *Addit. Manuf.* 18 (2017) 31–39. <https://doi.org/10.1016/j.addma.2017.08.012>.

- [177] Granta Design Limited, Cambridge Engineering Selector Software, (2009).
- [178] J.W. Elmer, J. Vaja, H.D. Carlton, R. Pong, The effect of Ar and N₂ shielding gas on laser weld porosity in steel, stainless steels, and nickel, *Weld. J.* 94 (2015) 313s-325s.
- [179] P.K. Farayibi, T.E. Abioye, A. Kennedy, A.T. Clare, Development of metal matrix composites by direct energy deposition of ‘satellited’ powders, *J. Manuf. Process.* 45 (2019) 429–437. <https://doi.org/10.1016/j.jmapro.2019.07.029>.
- [180] M. Simonelli, N.T. Aboulkhair, P. Cohen, J.W. Murray, A.T. Clare, C. Tuck, R.J.M. Hague, A comparison of Ti-6Al-4V in-situ alloying in Selective Laser Melting using simply-mixed and satellited powder blend feedstocks, *Mater. Charact.* 143 (2018) 118–126. <https://doi.org/10.1016/j.matchar.2018.05.039>.
- [181] M. Al-Thamir, D.G. McCartney, M. Simonelli, R. Hague, A. Clare, Processability of atypical WC-Co composite feedstock by laser powder-bed fusion, *Materials (Basel)*. 13 (2020) 1–12. <https://doi.org/10.3390/ma13010050>.
- [182] S. Sanchez, P. Smith, Z. Xu, G. Gaspard, C.J. Hyde, W.W. Wits, I.A. Ashcroft, H. Chen, A.T. Clare, Powder Bed Fusion of nickel-based superalloys: A review, *Int. J. Mach. Tools Manuf.* 165 (2021) 103729. <https://doi.org/10.1016/j.ijmachtools.2021.103729>.
- [183] S. Catchpole-Smith, R.R.J. Sélo, A.W. Davis, I.A. Ashcroft, C.J. Tuck, A. Clare, Thermal conductivity of TPMS lattice structures manufactured via laser powder bed fusion, *Addit. Manuf.* 30 (2019) 100846. <https://doi.org/10.1016/j.addma.2019.100846>.
- [184] L. Sorokin, Z. Sidlin, Evaluation of the effect of alloying elements on pore formation when welding nickel-chromium alloys, *Weld. Int.* 12 (1998) 229–232.
- [185] A.N. Jinoop, C.P. Paul, K.S. Bindra, Laser-assisted directed energy deposition of nickel super alloys: A review, *Proc. Inst. Mech. Eng. Part L J. Mater. Des. Appl.* 233 (2019) 2376–2400. <https://doi.org/10.1177/1464420719852658>.
- [186] J.W. Elmer, J. Vaja, H.D. Carlton, The effect of reduced pressure on laser keyhole weld porosity and weld geometry in commercially pure titanium and nickel, *Weld. J.* 95 (2016) 419–430.
- [187] V. Kumar, M. Hussain, M.S. Raza, A.K. Das, N.K. Singh, Fiber Laser Welding of

Thin Nickel Sheets in Air and Water Medium, Arab. J. Sci. Eng. 42 (2017) 1765–1773. <https://doi.org/10.1007/s13369-016-2305-1>.